論文 / 著書情報
Article / Book Information

題目(和文)	
Title(English)	Seismic Performance of Lightly Reinforced Concrete Walls
著者(和文)	YuniarsyahEko
Author(English)	Eko Yuniarsyah
出典(和文)	学位:博士(工学), 学位授与機関:東京工業大学, 報告番号:甲第10839号, 授与年月日:2018年3月26日, 学位の種別:課程博士, 審査員:河野 進,坂田 弘安,山田 哲,吉敷 祥一,佐藤 大樹
Citation(English)	Degree:Doctor (Engineering), Conferring organization: Tokyo Institute of Technology, Report number:甲第10839号, Conferred date:2018/3/26, Degree Type:Course doctor, Examiner:,,,,
学位種別(和文)	博士論文
Type(English)	Doctoral Thesis

Tokyo Institute of Technology

Seismic Performance of Lightly Reinforced Concrete Walls

by

Eko Yuniarsyah

Supervisor: Prof. Susumu Kono

A dissertation submitted in partial fulfillment of the requirements for the Doctor of Engineering Degree

ABSTRACT

This research focuses on both experimental and analytical investigation of the seismic behavior of lightly reinforced concrete (RC) walls. The main objective of this research is to develop a performance based backbone model for lightly RC walls to predict their seismic behavior and to achieve a variety of seismic performance level for both new and existing lightly RC walls. The approach is the result of experimental investigations and analytical modeling.

The effects of axial force, amount of shear reinforcement, and shear span to wall length ratio on seismic behaviors of lightly RC walls were investigated by testing four real-scale lightly RC wall specimens. The parameters of this experiment were axial load, amount of shear reinforcement, and shear span to wall length ratio. The experimental results showed that axial load ratio, shear span to wall length ratio, and amount of horizontal reinforcement affected damage process and failure mode. An experimental test was also carried out on three upgraded lightly RC walls. The goal of the upgrading was to improve the seismic behavior of lightly RC walls by enhancing both shear and ultimate drift capacities. Two specimens were upgraded by placing an additional wall panel and the other specimen was upgraded by improving the reinforcement details. It was concluded that adding RC and UFC panels improved the seismic behavior of lightly RC walls and prevented crack formation at the central part of the wall panel. Increasing the amount of horizontal reinforcement and providing confinement in the boundary regions controlled the opening of crack width and made structure more ductile.

A finite element (FE) analysis was conducted to simulate the hysteretic characteristics of lateral load – drift relations with damage process of tested specimens. Four tested specimens were modeled using hexahedral elements and beam elements with bond links. Some constitutive models were evaluated in order to find a suitable material model for lightly RC walls. The finite element analysis simulated the maximum lateral load capacities and hysteresis loops with reasonably accurate. The damage progress and the crack propagation also reasonably agreed with experimental observations. Additional finite element analysis with 210 case studies by combining seven axial load levels, six shear reinforcement ratios, and five shear span ratio was also conducted. It was concluded that case with axial load tends to fail in brittle manner. Case with large shear span to length ratio are less susceptible to brittle shear failure than case with smaller shear span to wall length ratio.

A performance based backbone model was developed to predict the seismic behavior of lightly RC walls. The selected tri-linear model is associated with three limit state: diagonal cracking, peak shear strength, and ultimate deformation was proposed. The proposed shear strength model was

formulated using an experimental database of rectangular walls and combined with parametric study using finite element analysis by modifying revised UCSD shear model for RC walls considering the ductility of lightly RC walls. By evaluating experimental data of 39 walls that failed in shear, the proposed shear formula resulted in significant improvement in the calculated shear capacity of lightly RC walls. The proposed shear strength was used to develop performance based backbone curve by modifying ASCE/SEI 41-13 and Wallace's backbone curve. The modification provided a good estimate to the force-drift response in the lightly RC wall database. The proposed backbone curve could become an essential tool for performance-based assessment and design of lightly RC walls

ACKNOWLEDGEMENTS

First of all, I would like to express my sincere appreciation and deep gratitude to my supervisor Prof. Susumu Kono for his continuous advice supporting my research and his invaluable guidance during my study at Tokyo Institute of Technology.

I would like to express my deep appreciation to the examiners of my dissertation, Prof. Hiroyasu Sakata, Prof. Satoshi Yamada, Dr. Yasuji Shinohara, Dr. Shoichi Kishiki, and Dr. Daiki Sato for taking time from their busy schedule to read and give constructive feedback to my thesis. Their helpful comments and suggestions significantly contributed to improve the work and my understanding of the subject.

I would like to thank to JICA-ITB for their scholarship and I also would like to thank to Asia SEED staff that support me from the first time came to Japan until going back to my country.

My special thanks to Prof. Iswandi Imran and Prof. Bambang Budiono of Bandung Institute of Technology (ITB) who always encourage and support me and also introduce me to the research world. I also would like to thank Dr. Hidekazu Watanabe of Building Research Institute (BRI), Dr. Masanori Tani of Kyoto University, and Dr. Kuniyoshi Sugimoto of Yokohama National University for their discussions and invaluable suggestions which have significantly helped me in advancing the research.

Thanks to Dr. Aris Aryanto, Mr. Rafik Taleb, Mr. Masaya Ogura, Mr. Taku Obara, Mr. Kou Miyamoto, Mr. Hiroki Maruyama, Mr. Fuhito Kitamura, Mrs. Yuki Hayakawa, fellow students and friends at Kono and Shinohara Laboratory who helped me and support me during my research work especially during experimental work and who provide a pleasant atmosphere in the Labs. I greatly appreciate what all those people have done for me. My thanks also go to PPI Tokodai, my colleagues and friends in Tokyo Tech.

Finally, my sincerest gratitude goes out to my families, especially my parents, Syarifudin Syafei and Zaleha Karim who always support and encourage me to pursue my dream.

List of Publications

Journal Papers

1) *Yuniarsyah, E.*, Kono, S., Tani, M., Taleb, R., Watanabe, H., Obara, T., Mukai, T., "Experimental Study of Lightly Reinforced Concrete Walls Upgraded with Various Schemes under Seismic Loading", Engineering Structures, 2017, Vol. 138, pp. 131-145
2) *Yuniarsyah, E.*, Kono, S., Tani, M., Taleb, R., Sugimoto, K., Mukai, T., "Damage Evaluation of Lightly RC Walls in Moment Resisting Frames under Seismic Loading", Engineering Structures, 2017, Vol. 132, pp. 349-371.

Conference Papers

1) Kono, S., Kitamura, F., *Yuniarsyah, E.*, Watanabe, H., Mukai, T., Mukai, D. J., "Efforts to Develop Resilient Reinforced Concrete Building Structures in Japan", Proceedings of the Fourth Conference on Smart Monitoring, Assessment and Rehabilitation of Civil Structures, Zurich, Switzerland, Sept 13-15, 2017.
2) Kitamura, F., Kuwabara, R., *Yuniarsyah, E.*, Watanabe, H., Kono, S., Mukai, T., Maeda, M., Kinugasa, H., "Damage Evaluation of the Five Story Building Tested at BRI in 2014 with A Nonlinear Finite Element Analysis – Part 1 Comparison Between Test and Analytical Results", Summaries of Technical Papers of Annual Meeting, Architectural Institute of Japan, Hiroshima, Japan, August, 2017. (In Japanese)
3) *Yuniarsyah, E.*, Kitamura, F., Watanabe, H., Endo, K., Mukai, T., Sakashita, M., Kono, S., Maeda, M., Kinugasa, H., Tani, M., "Static Loading Test on A Full Scale Five Story Reinforced Concrete Resilient Building Utilizing Walls – Part 8 Investigation of Damage States for the Beam with walls at 2nd Floor", Summaries of Technical Papers of Annual Meeting, Architectural Institute of Japan, Fukuoka, Japan, August, 2016. (In Japanese)
4) Watanabe, H., Kitamura, F., *Yuniarsyah, E.*, Mukai, T., Tani, M., Kono, S., Maeda, M., Kinugasa, H., "Static Loading Test on A Full Scale Five Story Reinforced Concrete Building Utilizing Wing Walls for Damage Reduction: Damage Evaluation of the 2nd Floor Beam with Secondary Walls and RC Slab", The Japan-Korea-Taiwan Joint Seminar on Earthquake Engineering for Building structures (SEEBUS), Yokohama, Japan, Sept 18-19, 2015.
5) Taleb, R., *Yuniarsyah, E.*, Watanabe, H., Kono, S., Tani, M., Mukai, T., "Experimental Study on Residual Damage of Full-scale RC Non-structural Wall Specimens – Part 4 Experimental Results for Improved Specimens", Summaries of Technical Papers of Annual Meeting, Architectural Institute of Japan, Kanagawa, Japan, Sept, 2015.

6) *Yuniarsyah, E.*, Taleb, R., Watanabe, H., Kono, S., Tani, M., Mukai, T., "Experimental Study on Residual Damage of Full-scale RC Non-structural Wall Specimens – Part 3 Experimental Program for Improved Specimens", Summaries of Technical Papers of Annual Meeting, Architectural Institute of Japan, Kanagawa, Japan, Sept, 2015.
7) Watanabe, H., *Yuniarsyah, E.*, Mukai, T., Tani, M., Kono, S., Kitamura, F., Maeda, M., Kinugasa, H., "Static Loading Test on A Full Scale Five Story Reinforced Concrete Building Utilizing Wing Walls for Damage Reduction – Part 12 Damage Analysis of the 2nd Floor Slab", Summaries of Technical Papers of Annual Meeting, Architectural Institute of Japan, Kanagawa, Japan, Sept, 2015. (In Japanese)
8) Kitamura, F., *Yuniarsyah, E.*, Mukai, T., Tani, M., Kono, S., Watanabe, H., Maeda, M., Kinugasa, H., "Static Loading Test on A Full Scale Five Story Reinforced Concrete Building Utilizing Wing Walls for Damage Reduction – Part 9 Damage Analysis of the 2nd Story Beam with Secondary Walls", Summaries of Technical Papers of Annual Meeting, Architectural Institute of Japan, Kanagawa, Japan, Sept, 2015. (In Japanese)
9) Tani, M., *Yuniarsyah, E.*, Mukai, T., Kono, S., "Full Scale Experiment of RC Non-Structural Walls Focused on Damage Reduction and Seismic Behavior Improvement", JCI Annual Convention, Chiba, Japan, July, 2015. (In Japanese)
10) Kono, S., Arai, M. Watanabe, H., Taleb, R., *Yuniarsyah, E.*, Obara, T., "Seismic Performance and Its Assessment of RC Structural Walls", Structural Engineering Frontier Conference (SEFC), Tokyo Institute of Technology, Yokohama, Japan, March 18-19, 2015.
11) Kono, S., Taleb, R., *Yuniarsyah, E.*, Tani, M., Watanabe, H., Sakashita, M., "Ultimate Drift Capacity of Reinforced Concrete Walls", Conference for Civil Engineering Research Networks (ConCERN), Institut Teknologi Bandung, Bandung, Indonesia, November 4-5, 2014.
12) *Yuniarsyah, E.*, Taleb, R., Kono, S., Tani, M., "An Experimental Study on Confined RC Wall Boundary Regions under Uniaxial Monotonic and Cyclic Reversal Loadings", The Japan-Korea-Taiwan Joint Seminar on Earthquake Engineering for Building structures (SEEBUS), Seoul, South Korea, Sept 19-20, 2014.
13) Taleb, R., *Yuniarsyah, E.*, Ogura, M., Kono, S., Tani, M., "Performance of Confined RC Rectangular Wall Boundary Regions under Cyclic Loadings – Part 2 Experimental Results and Discussion", Summaries of Technical Papers of Annual Meeting, Architectural Institute of Japan, Kobe, Japan, Sept 12-14, 2014.
14) *Yuniarsyah, E.*, Taleb, R., Ogura, M., Kono, S., Tani, M., "Performance of Confined RC Rectangular Wall Boundary Regions under Cyclic Loadings – Part 1 Experimental Program", Summaries of Technical Papers of Annual Meeting, Architectural Institute of Japan, Kobe, Japan, Sept 12-14, 2014.

Contents

List of Figure

List of Table

1 INTRODUCTION

1.1 Background

Reinforced concrete shear walls have been widely used as the primary lateral-load resisting systems for both wind and earthquake loading in multi-story buildings throughout the world. Observations from previous earthquakes have shown that well-designed shear walls can be used to control both structural and nonstructural damage in the buildings. Wall systems may take a variety of forms according to the building configuration and designers' intentions. Many walls may also form part of a mixed system (comprising combinations of walls and lateral force resisting frames). General forms of walls are described below in Figure 1-1. Most wall configurations will conform to one or the other of these general arrangements, noting that often the behavior will be significantly modified by the foundation system. In particular, rocking foundation systems will often act to preclude some of the less desirable failure modes, and will substantially influence the overall building response.

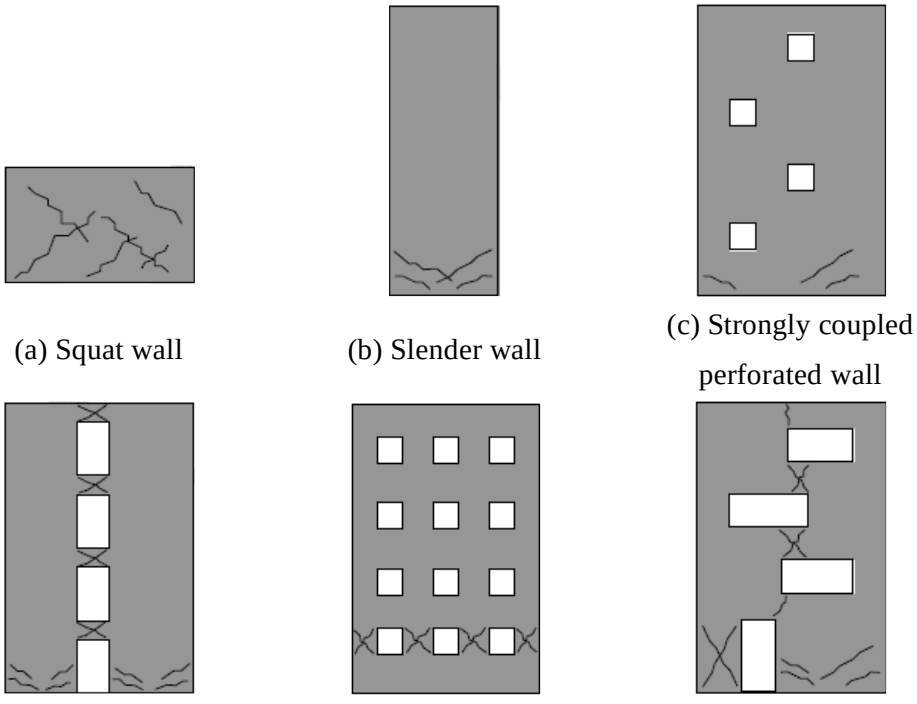

(a) Squat wall (b) Slender wall (c) Strongly coupled perforated wall

(d) Strong pier/weak spandrel coupled wall (e) Weak pier/strong spandrel perforated wall (f) Weakly coupled perforated wall

Figure 1-1 Typical wall systems [1]

In Japan, reinforced concrete (RC) moment resisting-frames are usually constructed monolithically with lightly reinforced infill walls with opening (spandrels, wall piers, and wing walls). Although such walls are connected rigidly to the surrounding frame, they are often treated as a secondary structural component which attract less attention in design. In an ordinary Japanese

design practice, lightly RC walls are design with no axial load. It is highly desirable that they are designed to exhibit a ductile behavior. However, the National Institute for Land and Infrastructure Management (NILIM) and the Building Research Institute (BRI) reported that many perimeter lightly RC walls with opening (spandrels, wall piers, and wing walls) in residential and government office buildings had experienced severe damage during both the 2011 off the Pacific coast of Tohoku Earthquake [2] and the 2016 Kumamoto Earthquake [3] as shown in Figure 1-2. Most damages to these walls were due to brittle shear failure. It was considered that the shear failure occurred as the flexure capacity increased due to axial compression force exerted by surrounding frames under seismic loading. Although it did not jeopardize safety, their damage often impaired functions of buildings after earthquakes and caused economic losses.

(a) Shear failure of lightly RC wall

(b) Shear failure of wing wall

(c) Shear failure of wall pier

Figure 1-2 Damage of Lightly RC walls after the 2011 Tohoku and the 2016 Kumamoto Earthquakes [2][3]

Lightly RC walls are typically 120 – 200 mm thick, and have a single curtain of reinforcement in two directions with additional boundary vertical reinforcing bars at section ends. In many cases, horizontal reinforcement has no hook anchorage and boundary region has no confinement. Hence,

the current design practice makes lightly RC walls intrinsically vulnerable to earthquake damages. Therefore, it is necessary to develop a performance based design for lightly RC walls to predict their seismic behavior. The performance based design aims to improve structural engineering by providing engineers with the capability of designing structures to achieve a variety of seismic performance levels as shown in Figure 1-3 and Figure 1-4 [4], and it allows structures to experience damage to a certain extent during earthquakes, which makes it necessary to define the damage levels corresponding to the different performance levels of structures. However, there are several issues regarding lightly RC wall structures as follows:

1) In terms of performance based design, it is required to develop a backbone model for lightly RC walls to predict their seismic behavior and to achieve a variety of seismic performance levels for both new and existing lightly RC walls.
2) An accurate prediction procedure of shear strength of lightly RC walls is required not only for new structures but also for existing structures. An accurate prediction of shear strength helps to identify the failure mode of structure walls with limited ductility. In addition, it is needed as an analysis tool for strengthening strategy in order to have proper upgrading schemes to improve the seismic performance of existing lightly RC walls and avoid unnecessary retrofits.
3) It is required to develop a post-earthquake seismic evaluation method for lightly RC walls to help the inspector in estimating the current limit state or performance level of the wall and to help engineer to develop repair strategies.

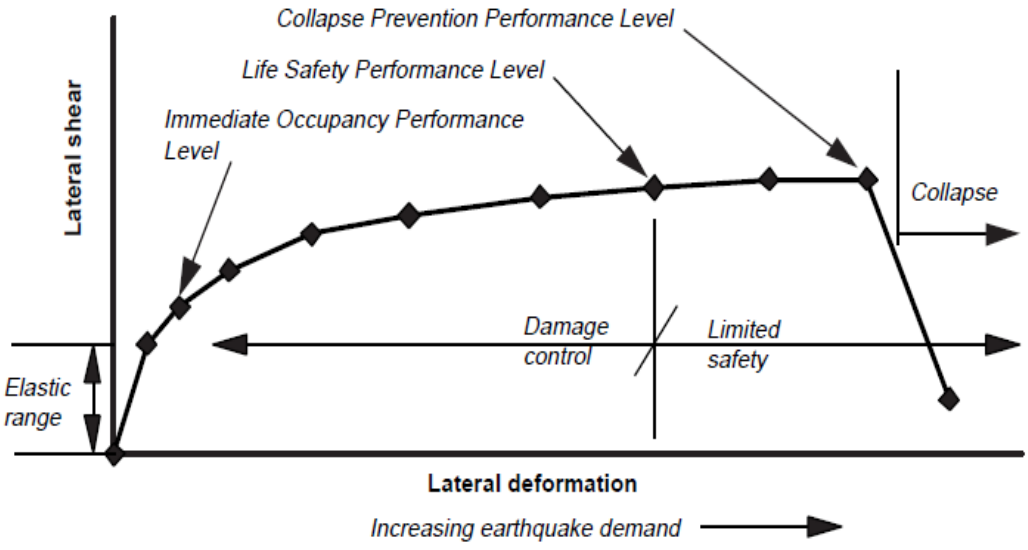

Figure 1-3 Performance and structural deformation demand for ductile structures [4]

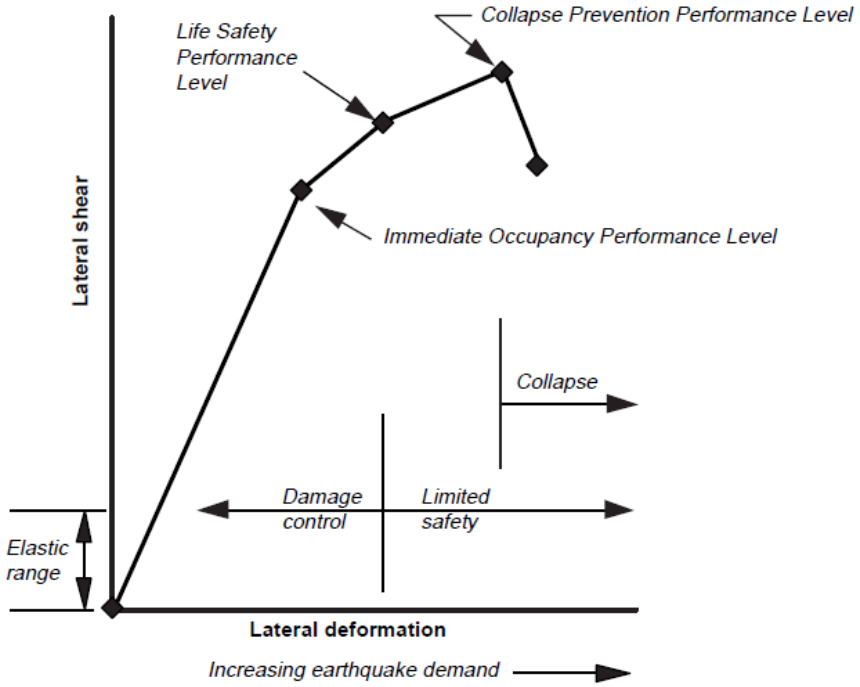

Figure 1-4 Performance and structural deformation demand for non-ductile structures [4]

Several studies have been conducted to investigate seismic behaviors of lightly RC walls [5][6][7] including the seismic performance of frames with lightly RC walls [8][9][10]. However, no general method has been established to evaluate their seismic damages quantitatively. Therefore, further research is necessary to understand the behavior of lightly RC walls, in particular focusing on their damage processes including failure modes to develop a performance based backbone model.

1.2 Objective and Scope of the Study

This study focuses on both experimental and analytical investigation of the seismic behavior of lightly RC walls to develop a performance based backbone model. A quantitative seismic damage evaluation in terms of crack width, crack length, and concrete spalling area was carried out to investigate the correlation between seismic damage and lateral drift. A finite element analysis model for lightly RC wall has been developed to simulate the hysteretic characteristics of lateral load - drift relations with damage process. The main objectives of this study are to:

1. Develop a performance based backbone model for lightly RC walls to predict their seismic behavior and to achieve a variety of seismic performance levels for both new and existing lightly RC walls.
2. Develop shear strength formula considering wall ductility for predicting failure mode.
3. Investigate the effects of axial force, amount of shear reinforcement, and shear span to wall length ratio on seismic behaviors of lightly RC walls, such as load and displacement capacities, damage progress, and failure modes through experimental test.

4. Develop a post-earthquake seismic evaluation criteria for lightly RC walls by conducting a quantitative damage evaluation in term of crack width, crack length, and concrete spalling area.
5. Investigate and evaluate the effectiveness of various upgrading schemes of lightly RC walls.
6. Simulate the hysteretic characteristics of lateral load – drift relations with damage process through finite element analysis (FEA).

The scope of this study was limited to lightly RC wall piers. Wing walls and spandrel walls are not included in this study since they have different boundary conditions. In addition, the effects of lightly RC walls and the upgrading schemes to the frame are not analyzed and evaluated.

1.3 Outline of Thesis

The thesis comprises into seven chapters. In the following, each chapter is briefly described.

Chapter 1 "Introduction" briefly describes the challenges involved in designing lightly RC walls. It also identifies research needs and clarify objectives. The outline of the thesis is also described in this chapter.

Chapter 2 "Literature Review" addresses the available literatures on previous studies on the seismic performance of lightly RC walls. Various shear strength models and analysis techniques are also summarized.

Chapter 3 "Development of Backbone Curve for Lightly Reinforced Concrete Walls" introduces a proposed performance based backbone model for lightly RC walls. The selected trilinear model is associated with three limit states: diagonal cracking, peak shear capacity, and ultimate deformation. The proposed shear capacity model was formulated to include the ductility by modifying revised UCSD shear model for RC walls [11]. It was validated using 39 experimental specimens of rectangular walls combined with 210 FEM rectangular wall cases, which are explained in Chapter 6. The proposed shear formula resulted in significant improvement in computing the shear capacity of lightly RC walls. The proposed shear capacity was used to develop backbone curves by modifying ASCE/SEI 41-13 [12] and Wallace's [13] backbone curves. The proposed backbone curve provides a good estimate to the force-drift response in lightly RC wall database.

Chapter 4 "Experiment 1: Seismic Behavior of As-Built Lightly Reinforced Concrete Walls" states the effects of axial force, amount of shear reinforcement, and shear span to wall length ratio on seismic behaviors of lightly RC walls through an experiment. The experiment included four real-scale lightly RC walls focusing on damage processes and failure modes. The experimental results showed that axial load ratio, shear span to wall length ratio, and amount of horizontal reinforcement affected damage process and failure mode. In addition, a quantitative damage evaluation in terms of crack width, crack length, and concrete spalling area was carried out to investigate the correlation between seismic damage and drift. The damage level of walls was

assessed using “Guidelines for Performance Evaluation of Earthquake Resistant Reinforced Concrete Buildings (Draft)” (Architectural Institute of Japan, 2004), which takes into account damage level such as residual crack width or stress level of concrete and reinforcement. Considering the total damage (crack length and spalling area) of concrete, the criteria of the guidelines well captured damage level of lightly RC walls. The limit stress level was proposed to be raided from 67% to 80% of the compressive strength to better estimate the drift of serviceability limit state of concrete. In addition, the ratio of concrete spalling area was proposed as one of damage state index to determine the limit state.

Chapter 5 “Experiment 2: Seismic Behavior of Retrofitted Lightly Reinforced Concrete Walls” presents the experimental study on three upgraded lightly RC walls to improve the seismic behavior by enhancing both shear and ultimate drift capacities. Two specimens were upgraded by placing an additional wall panel and the other specimen was upgraded by improving the reinforcement details. It was concluded that adding RC and UFC panels improved the seismic behavior of lightly RC walls and prevented crack formation of the wall panel. Increasing the amount of horizontal reinforcement and providing confinement in the boundary regions decreased the opening of crack width and increased ductility.

Chapter 6 “Parametric Study of Lightly Reinforced Concrete Walls using FEM Analysis” explains the finite element analysis to simulate the hysteretic characteristics and damage process of specimens tested in Chapter 4. lightly RC walls specimens were modeled using hexahedral and beam elements with bond links. The finite element analysis well simulated the maximum lateral load capacities and hysteresis loops. The damage progress reasonably agreed with experimental observations. Additional finite element analysis with 210 cases were conducted combining seven axial load levels, six shear reinforcement ratios, and five shear span to wall length ratio to validated the proposed shear capacity equation in Chapter 3.

Finally, Chapter 7 “Conclusions” summarizes the main findings of this study and further research needs related to the design of lightly RC walls.

2 LITERATURE REVIEW

2.1 Introduction

This research was initiated following observations on the seismic performance of lightly reinforced concrete (RC) walls in recent earthquake that have clarified the weakness of lightly RC walls with opening (spandrel, wall pier, wing wall) in residential and government office building in Japan. The research was undertaken to develop a performance based backbone model to predict the seismic behavior of lightly RC walls. In this chapter, a literature review on topics related to this research study is presented. This chapter is organized into the following parts: (1) Review of performance based design of lightly RC walls, (2) review of several shear strength models, (3) review of experimental testing on lightly RC walls both as-built and retrofitted walls, and (4) review of finite element (FE) analysis studies. Prior research is presented and discussed with focuses on performance based design of lightly RC walls. The objective of this review is to ensure that the experimental research program does not duplicate existing tests, and to identify gaps in the literature.

2.2 What is "Performance Based Design for Lightly Reinforced Concrete Walls"

Based on FEMA 454 [14], performance based design is a design approach that meets the life safety and building performance intents of the code, while providing designers and building officials with a more systematic way to get at the alternative design option currently available in codes. Performance based seismic design allows building owners to define performance levels to meet the specific requirements for the building and its contents. Performance based seismic design will also allow lenders, insurers, and government response and recovery agencies to help reduce the impact and cost of future earthquakes.

In order to implement a performance based design, it is necessary to select one or more performance objectives. A performance objective is simply a statement of the desired building behavior; given that it experiences earthquake demands of specified severity. Both the Guidelines and Commentary for Seismic Rehabilitation [15] and Vision 2000 [16] projects have identified similar series of standard behavior state definitions, albeit with slightly different designations as described in Table 2-1. Figure 2-1 illustrates the behavior of a ductile structure as it responds with increasing lateral deformation. The figure is a schematic plot of the lateral force induced in the structure as a function of lateral deformation. Three discrete points are indicated, representing the discrete Performance Levels: Immediate Occupancy, Life Safety, and Collapse Prevention. Figure 2-2 is a similar curve, representative of the behavior of a non-ductile, or brittle, structure. Note that for such a structure, there may be relatively little margin in the response that respectively defines the three performance levels.

Table 2-1 Standard performance level definitions

Designation		Description
ATC-33	Vision 2000	
Operational	Fully operational	Only very minor structural or non-structural damage has occurred. The building retains its original stiffness and strength. Non-structural components operate and the building is available for normal use. Repairs, if required, may be instituted at the convenience of the building users. The risk of life threatening injury during the earthquake is negligible.
Immediate occupancy	Functional	Only minor structural damage has occurred. The building structure retains nearly all its original stiffness and strength. Non-structural components are secured and if utilities are available, most would function. Life safety systems are operable. Repairs may be instituted at the convenience of the building users. The risk of life threatening injury during the earthquake is very low.
Life safety	Life safe	Significant structural and non-structural damage has occurred. The building has lost a significant amount of its original stiffness, but retains some lateral strength and margin against collapse. Non-structural components are secure, but may not operate. The building may not be safe to occupy until repaired. The risk of life threatening injury during the earthquake is low.
Collapse prevention	Near collapse	A limiting damage state in which substantial damages has occurred. The building has lost most of its original stiffness and strength and has little margin against collapse. Non-structural components may become dislodged and present a falling hazard. Repair is probably not practical.

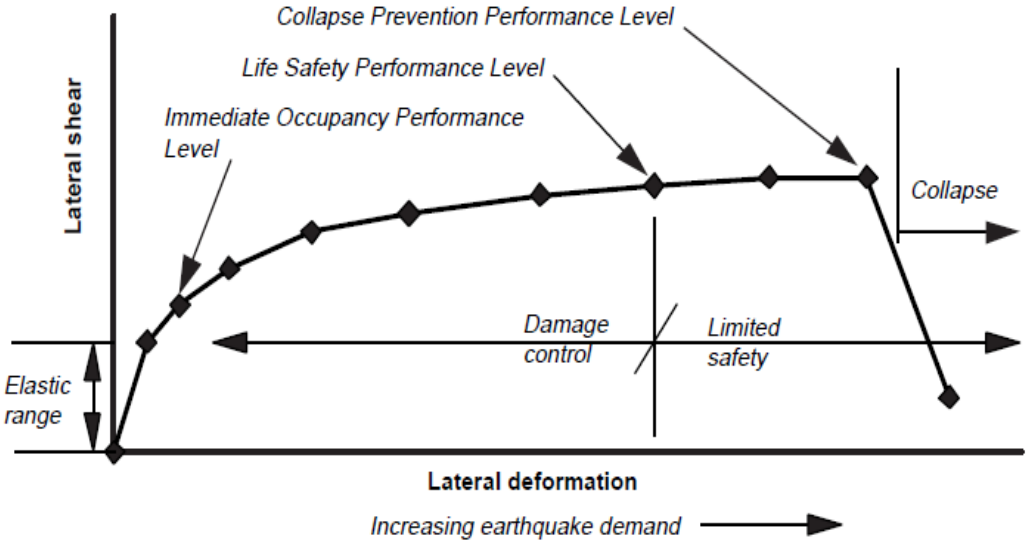

Figure 2-1 Performance and structural deformation demand for ductile structures [4]

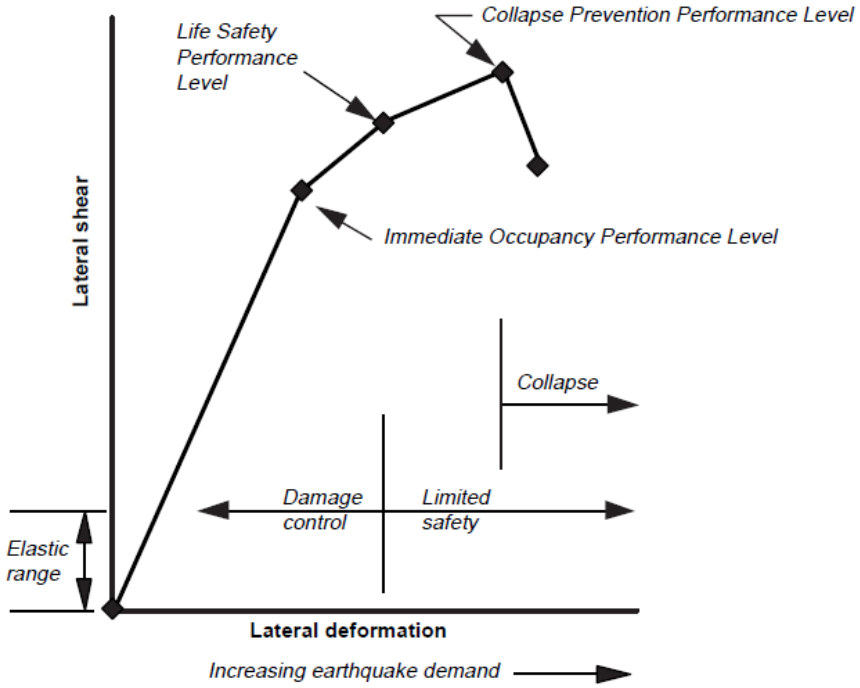

Figure 2-2 Performance and structural deformation demand for non-ductile structures [4]

In order to ensure the desirable performance of buildings at different design levels, the strength, stiffness, and deformability of the structures should be reasonably proportioned. To achieve this goal, it should be clearly understood which one of these structural characteristics primarily governs the design at different performance levels. The Performance-Based Seismic Design (PBSD) approach involves not only the analysis and design of the structure for sustaining the seismic demands but also comprises the seismic behavior in terms of the displacement capacity and its residual performance.

Basically, performance based design of lightly RC walls is similar with RC building as explained above. However, since many of lightly RC walls failed in shear during recent earthquakes [2][3], an accurate prediction procedure of shear strength of lightly RC walls is essential to develop performance based backbone curve and to identify the failure mode of structure walls with limited ductility.

2.3 Shear Capacity

2.3.1 Introduction

The ultimate shear strength of shear walls and the design criteria to adequately resist shear has been the focus of many experimental and analytical studies. Two different approaches have been used by researchers for predicting the ultimate shear strength of shear walls: the derivation of empirical expressions based on test results [17][18][19][20], and the application of shear models based on structural mechanics through the use of equilibrium, compatibility and material constitutive relationships [21][22]. Most of the seismic design provisions found in modern building codes, such as the ACI Code provisions [23], use empirical or semi-empirical equations to estimate the ultimate shear strength of shear walls. In this section, three equations, i.e. Arakawa's Equation, ACI 318, and UCSD's Formula are introduced.

2.3.2 Arakawa's Equation

Arakawa's Equation [24] is the most familiar empirical equation derived through a lot of experimental results and is now widely used for practical design in Japan for the evaluation of RC beams and columns in existing buildings as well as new designed buildings. One of the main merits of this equation might be its simplicity and its incorporation of the main variables in a clear manner including the effect of the axial load. The Arakawa's Equation is shown in Eq. (2-1).

$$Q_{su} = \left\{ \frac{0.068\, p_{te}{}^{0.23} \left(f'_c + 18 \right)}{\sqrt{M/(QD) + 0.12}} + 0.85\sqrt{f_{wh}\, p_{wh}} + 0.1\sigma_0 \right\} t_e\, j \qquad (2\text{-}1)$$

where, p_{te} is equivalent tensile reinforcement ratio (%) (=100a_t/$t_e d$), a_t is area longitudinal reinforcement in the wall boundary area, t_e is equivalent wall thickness, d is effective length of wall (=0.95D), D is wall length, f'_c is concrete compressive strength, M/(QD) is shear span to wall length ratio ($1 \le M/(QD) \le 3$), f_{wh} is yield strength of horizontal web reinforcement, p_{wh} is horizontal web reinforcement ratio, σ_0 is average axial stress for gross cross-sectional area, and j is lever arm length (=7/8d).

2.3.3 ACI 318

Except for minor changes in format, the ACI 318 equation for wall nominal shear strength has not changed since it was introduced in the ACI 318-83. In ACI 318-14 [23], the corresponding equation is in the form of

$$V_n = A_{cv}(\alpha_c \lambda \sqrt{f'_c} + \rho_t f_y) \tag{2-2}$$

where the coefficient α_c is 0.25 for height-to-length ratios (h_w/l_w) $\leq$ 1.5, is 0.17 for $h_w/l_w \geq$ 2.0, varies linearly between 0.25 and 0.17 for h_w/l_w between 1.5 and 2.0. In this equation, A_{cv} is the cross-sectional web area of a wall, ρ_t is transverse reinforcement ratio, f_y is the yield strength of transverse reinforcement, and f'_c is the compressive strength of concrete. The variation of α_c for h_w/l_w between 1.5 and 2.0 accounts for the observed increase contribution of concrete in low *h/l* walls.

2.3.4 Original UCSD Shear Model

Priestley et al. [25] examined in detail both code provisions and available models in order to assess the seismic strength of reinforced concrete columns. The proposed shear strength of column is considered to consist of three independent components: a concrete component V_c whose magnitude depends on the level of ductility, an axial load component V_p whose magnitude depends on the column aspect ratio, and a truss component V_s whose magnitude depends on the transverse reinforcement content. Thus

$$V_n = V_c + V_p + V_s \tag{2-3}$$

Concrete Component, V_c

The concrete component for both circular and rectangular columns reduces with increasing ductility in accordance with the form of Figure 2-3, and given by

$$V_n = k\sqrt{f'_c}A_e \tag{2-4}$$

where *k* depends on the member displacement ductility level and the system of units chosen (megapascals or pounds per square inch); as well as on whether the column is expected to be subjected to uniaxial or biaxial ductility demand. The effective shear area is taken as $A_e = 0.8A_g$ for both circular and rectangular columns.

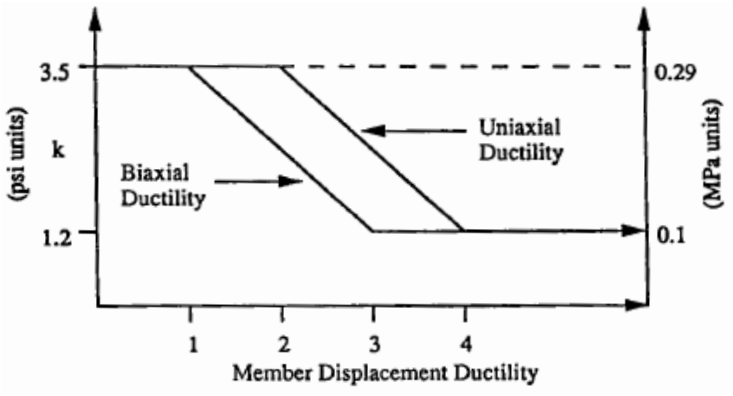

Figure 2-3 Degradation of concrete shear strength with ductility

Axial Load Component, V_p

It is considered that the column axial force enhances the shear strength by arch action forming an inclined strut as shown in Figure 2-4. The enhancement to shear strength is the horizontal component of the diagonal compression strut, since this component directly resists the applied shear force. Thus

$$V_p = P \tan \alpha = \frac{D - c}{2a} P \tag{2-5}$$

where D is the overall section depth or diameter, c is the depth of the compression zone, and $a = L$ for a cantilever column and $L/2$ for a column in reversed bending. V_p does not degrade with increasing ductility.

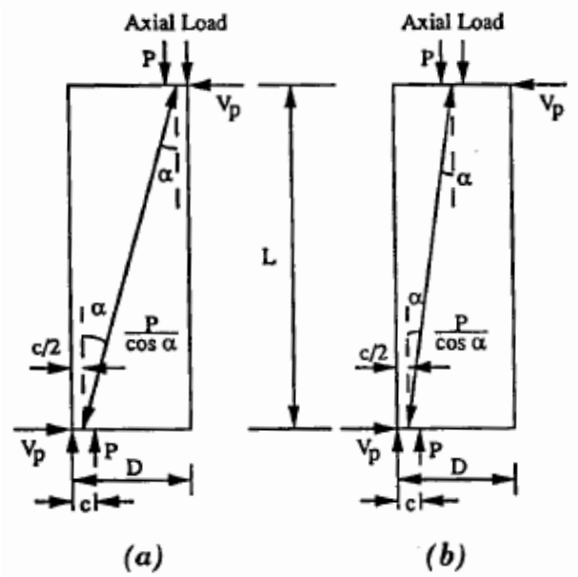

Figure 2-4 Contribution of axial force to column shear strength;
(a) double curvature and (b) cantilever

Truss Mechanism Component, V_s

The contribution of transverse reinforcement to shear strength is based on a truss mechanism using a 30° angle between the compression diagonals (i.e., crack pattern) and the column axis or the corner-to-corner inclination, whichever is larger. Thus both initial and residual strength of the truss mechanism are given by, for circular columns:

$$V_s = \frac{\pi}{2}\frac{A_{sh} f_{yh} D'}{s}\cot 30° \tag{2-6}$$

and for rectangular columns:

$$V_s = \frac{A_v f_{yh} D'}{s}\cot 30° \tag{2-7}$$

where A_v is total transverse reinforcement area per layer, D' is the distance between centers of the peripheral hoop or spiral, f_{yh} is yield strength of transverse reinforcement, and s is spacing of transverse reinforcement along member axis.

2.3.5 Revised UCSD Shear Model

The model which was published by Kowalsky and Priestley [26] addressed the assessment of shear strength of circular columns. Three revisions to the UCSD model are proposed as follows: (1) Effect of concrete compression zone on steel truss mechanism, (2) effect of aspect ratio on the concrete shear resisting mechanism, and (3) effect of longitudinal steel ratio on the concrete shear resisting mechanism.

$$V_D = 0.85(V_s + V_p + V_c) \tag{2-8}$$

The factor 0.85 was introduced to correlate the model to experimental data in order to use it for design purpose.

Truss Mechanism, V_s

The truss mechanism accounted only for transversal reinforcement that transferred shear across cracks. Therefore, spiral reinforcement in the compressive zone was assumed to be not effective since there are no open cracks in this part of the cross-section. The inclination of crack plane was suggested to be equal to 30°. A simplified relationship for the truss component is shown in Eq. (2-9).

$$V_s = \frac{\pi}{2} A_{sp} f_y \frac{D - c - \text{cov}}{s} \cot\theta \tag{2-9}$$

where A_{sp} is spiral area, D is column depth, c is depth of compression zone, cov is cover concrete thickness, s is spiral spacing, and θ is inclination of crack plane.

Concrete Mechanism, V_c

A smaller longitudinal steel ratio will result in a decrease in the strength of the concrete shear resisting mechanism. This is due to three aspects. First, dowel action from the longitudinal reinforcement will be smaller if there are fewer numbers of small diameter bars. Second, crack distribution will be more concentrated resulting in fewer, more widely spaced cracks, which, in turn, results in a decrease in the strength of the concrete aggregate interlock mechanism. Third, the smaller compression zone resulting from the reduced longitudinal steel ratio will, in turn, reduce the compression zone shear transfer. This variable was also ignored in the original UCSD model. On the basis of these considerations, the concrete mechanism strength was revised to give

$$V_c = \alpha\beta\gamma\sqrt{f'_c}(0.8A_g) \tag{2-10}$$

$$1 \le \alpha = 3 - \frac{M}{VD} \le 1.5 \tag{2-11}$$

$$\beta = 0.5 + 20\rho_l \le 1 \tag{2-12}$$

where the factor α accounts for the column aspect ratio, and is given by Eq. (2-11). The variable M/VD, where M = moment and V = shear at the critical section, is equivalent to the aspect ratio L/D, where L = distance from critical section to the point of contra flexure. Note that it is probable that the value for α continues to increase for $M/VD < 1.5$, but no data are currently available to confirm this. The factor β is a modifier that accounts for the longitudinal steel ratio, and is given by Eq. (2-12). Parameter γ, which represents the reduction in strength of the concrete shear resisting mechanism with increasing ductility. The revised relationship is shown in Figure 2-5 by re-examination of the test data.

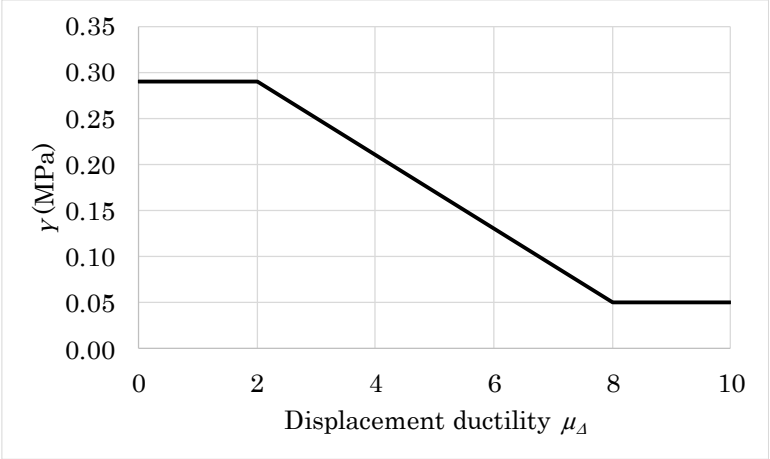

Figure 2-5 Revised parameter γ

Axial Load Mechanism, V_p

The axial load mechanism is given by Eq. (4-13) is unchanged from the Original UCSD Shear Model, where P is the axial load including seismic effects, D is the column diameter, L is the length of column from the critical section to the point of contra-flexure, and c is the neutral axis depth.

$$V_p = \frac{D-c}{2L} P \tag{2-13}$$

2.3.6 Krolicki et al. (2011)

Krolicki et al. [11] proposed a new shear strength formula for RC wall by evaluating revised UCSD shear model by Kowalsky and Priestley [26] using 26 RC wall specimens (18 walls failed in shear and 8 specimens failed in flexure-shear) in database. The revised UCSD shear model was, however, developed for calculating the shear resistance of columns based on cyclic loaded column tests. The shear resistance of columns and walls, and how it is calculated, is somewhat different and worthy of comparison. Based on Krolicki et al. [11], some differences that affect the calculation of shear resistance of walls and columns include the following: (1) Walls are more likely to be squat than columns, (2) walls have proportionally better development of reinforcement, (3) walls may have distributed flexural reinforcement, (4) walls are typically designed for uniaxial bending, where columns are subjected to biaxial demands, and (5) there has been more testing of columns than walls.

The form of the proposed shear strength equation is unchanged from the revised UCSD shear model by Kowalsky and Priestley [26] given as:

$$V_n = V_c + V_s + V_p \tag{2-14}$$

where V_c is concrete shear-resisting mechanism, V_s is horizontal reinforcement truss shear-resisting mechanism, and V_p is axial load component.

Concrete Component, V_c

The contribution of the concrete to the shear resistance is calculated by Eq (2-15). This formula is unchanged from the revised UCSD shear model. However, the limit of parameter α and γ was changed as given in Eqs. (2-16) - (2-18).

$$V_c = \alpha\beta\gamma\sqrt{f'_c}(0.8A_g) \tag{2-15}$$

$$\alpha = 3 - \frac{M}{Vl_w} \geq 1.0 \tag{2-16}$$

$$\gamma = 0.29 \text{, for } \mu_\Delta \leq 2 \tag{2-17}$$

$$\gamma = 0.05 \text{, for } \mu_\Delta \geq 6 \tag{2-18}$$

where μ_Δ is displacement ductility. The limit of parameter α was changed to fit the experimental database. The limit of parameter γ was modified since a section with a low shear span ratio would less likely reach high displacement ductility before the shear failure occurs.

The coefficient β accounts for the increase in shear resistance proportional to increasing volumetric ratio of longitudinal reinforcement and is unchanged from the USCD shear model. The coefficient β is calculated as:

$$\beta = 0.5 + 20\rho_v \leq 1 \tag{2-19}$$

where ρ_v is the ratio of total vertical reinforcement over the gross cross-sectional area of the member.

Horizontal Reinforcement Component, V_s

Krolicki et al. [11] compared the measured horizontal reinforcement contribution to shear resistant of Hidalgo et al. [27] wall specimens with calculated horizontal reinforcement contribution using the revised UCSD shear model. It was reported that as the specimen shear span ratio reduces, the over-prediction of the calculated contribution horizontal reinforcement increases. This over-prediction may result from overestimation of the cracking angle. Walls with the lower shear span ratios result in shallower compression struts and a larger angle of concrete cracking, θ. Krolicki et al. [11] proposed the contribution of horizontal reinforcement as given in Eqs. (2-20) – (2-22).

$$V_s = \rho_h f_{yh} t_w h_{cr} \tag{2-20}$$

$$h_{cr} = \frac{(l_w - c - \text{cov})}{\tan\theta_{cr}} \le h_w \tag{2-21}$$

$$\theta_{cr} = \left(\frac{30° - 45°}{2}\right)\left(\frac{M}{Vl_w}\right) + 45° \ge 30° \tag{2-22}$$

where h_{cr} is vertical crack height and θ_{cr} is average cracking angle. The compression zone c can be calculated through moment curvature analysis or reasonably assumed for walls as $0.2l_w$.

Axial Load Component, V_p

The axial load component V_p was used directly in the proposed model as originally formulated in UCSD shear model. For cantilever walls tests:

$$V_p = \frac{l_w - c}{2h_w} P \tag{2-23}$$

For wall test loaded in double curvature, the equation becomes:

$$V_p = \frac{l_w - c}{h_w} P \tag{2-24}$$

2.4 Experimental Studies on Lightly Reinforced Concrete Walls

2.4.1 As-built walls

Many experimental tests have been conducted on RC shear walls [28][29], however, few tests have been performed to investigate seismic behaviors of lightly RC walls. Greifenhagen and Lestuzzi [5] carried out an experiment on one-third scale of four lightly RC walls by varying horizontal reinforcement, axial load, and concrete compressive strength to investigate their lateral load carrying capacities and deformation capacities. It was observed that lightly RC walls had large drift capacity, which was greater than or equal to 0.8%. They reported that the drift capacity was not affected by the ratio of horizontal reinforcement. The flexure strength governed the observed strength in the tests while ultimate drift was limited by shear failure. Two lightly RC walls were also tested by Gebreyohaness et al. [6] with plain round bars and no boundary elements with varying wall thickness and axial load of $0.05f'_cA_g$ (where f'_c is concrete compressive strength and A_g is gross cross-sectional area of wall). It was found that the walls did not develop distributed flexure cracks but rather exhibited a predominantly rocking response about a single crack located

at the foundation-wall interface. Orakcal et al. [7] evaluated the shear strength of lightly RC wall piers and spandrel by conducting an experiment on 3/4-scale of six wall piers and eight wall spandrel specimens. The test variables of this study were axial load (no axial force, $0.05f'_cA_g$, $0.10f'_cA_g$), shear span to wall length ratio (0.44 and 0.50), amount of longitudinal web reinforcement (0.227 – 0.428), and presence of end hooks on the transverse reinforcement. All specimens were tested under double curvature to represent the boundary conditions of an actual wall segment in a building. Lateral displacement of the wall piers was governed by shear deformations associated with diagonal cracking, followed by widening of and sliding along the diagonal cracks. Shear capacity of walls were compared with FEMA 356 and ACI 318-05. It was found that both FEMA 356 and ACI 318-05 gave a conservative shear capacity, especially for specimens with axial load of $0.05f'_cA_g$ and $0.10f'_cA_g$ since the formula does not consider the axial load.

Some researchers reported the effect of lightly RC walls on the seismic performance of RC moment resisting-frames in Japan. Sugiyama at al. [8] conducted an experiment on eight one-third scale one-story one-span RC frame with cast-in-place lightly RC walls. The test parameters were types of openings in the lightly RC walls (two specimens) and strengthening methods with carbon fiber sheets on the lightly RC walls (six specimens). The axial load ($1/6f'_cA_g$) was kept constant during the test for all specimens. Both unstrengthened specimens had higher initial stiffness and maximum lateral load capacity compared to frames without lightly RC walls. However, at 4 % drift, their capacities were similar to those of specimens with wall failure. An experiment on three 1/2.5 scale RC frames with one story and one bay was carried out by Yoon et al. [9]. Two of the specimens had a lightly RC wall, which are monolithically constructed and structurally isolated by structural slits. Axial compression load of $0.1f'_cA_g$ was applied to all specimens and maintained constant during the experiment. It was reported that lightly RC walls significantly affected the seismic performance of the overall frame, such as initial stiffness and maximum lateral load capacity. Furthermore, Sanada and Ojio [10] conducted 2D finite element (FE) analysis on an 11-story steel reinforced concrete residential building in Sendai which was damaged at the 2011 off the Pacific coast of Tohoku Earthquake. The building was modeled with and without lightly RC walls to clarify their effects on the seismic performance of the building. It was concluded that typical lightly RC walls did not significantly affect seismic performance of a steel reinforced concrete building since lightly RC wall was damaged in early stage.

Although several studies have been conducted on the seismic performance of frames with lightly RC walls, no general method has been established to evaluate their seismic damages quantitatively. Since seismic performance of lightly RC wall is not clear yet, the damage level of building is often overestimated when the 2004 AIJ Guidelines [30] is used for assessment [10]. Therefore, further research is necessary to understand the behavior of lightly RC walls, in particularly focusing on their damage processes including failure modes.

2.4.2 Retrofitted walls

Many researchers have conducted experimental studies on upgraded RC walls using different techniques and materials. These retrofitting techniques aim to improve the wall strength, stiffness, ductility, or a combination of them. One of the most frequently used methods for strengthening of RC members is RC jacketing. The effect of strengthening brick and block masonry walls by RC jacketing has been experimentally investigated in many cases [31][32][33][34]. The experiments showed that RC jacketing improves the lateral capacity. However, only few experimental works have been performed using this technique for RC walls. Marini and Meda [35] carried out an experiment on a one-third scale of RC shear wall retrofitted using high performance concrete jacket to improve its seismic behavior. The specimen represented a typical RC wall of an existing three-story building designed only for gravity load. The wall was 3.2 meters high and its cross section was 100mm x 800mm. A 15 mm thick concrete jacket with $\phi 2$ high strength steel mesh embedded was used as retrofitting materials. It was observed that the structural behavior was governed by flexure up to collapse with no appreciable influence of the shear effects. The strengthened wall failed due to crushing of concrete jacket at the base, exhibiting high ultimate strength and deformation capacities. In order to investigate the hysteresis behavior of shear deficient RC walls strengthened by bonding of steel strips, Altin et al. [36] tested four half-scale shear walls. The specimens consisted of one reference wall and three strengthened walls using externally bonded steel strips with different configurations. To prevent debonding and delay premature buckling of steel strips, an epoxy adhesive was applied to the surface of the wall with some anchor rods. All strip combinations improved the hysteresis behavior of the shear deficient RC walls significantly under cyclic loads. Strengthened specimens developed their nominal flexure strength, and hence, the observed maximum shear was controlled by flexure. The diagonal tension shear capacity of the wall was significantly enhanced by this strengthening technique. The strengthened wall exhibited 65% higher maximum strength than the reference wall, with improved initial stiffness and ductility. Liao et al. [37] conducted an experimental test on three low-rise shear walls with shape memory alloy (SMA) bars as a kind of structural bracing system to improve the seismic behavior of low-rise shear walls. The height, width, and thickness of the specimens were 1000 mm, 2000 mm, and 120 mm, respectively. The SMA bars were inclined at an angle 27 degrees. The retrofitting scheme was successful in increasing strength, however, energy dissipation and re-centering capabilities of SMA bars were not completely utilized mostly due to the length of the bars. Khalil and Ghobarah [38] tested three RC shear walls, which included one control wall and two RC walls strengthened using fiber-reinforced polymer (FRP) sheets to increase shear capacity and ductility of walls. The control wall was deficient in shear and ductility. The strengthened walls were wrapped with bi-directional sheets in the wall region and unidirectional sheets on the boundary regions. The boundary regions had FRP anchors in the upgraded walls. The control wall panel failed before reaching the yield displacement while the two strengthened walls

achieved displacement ductility of 3 and 4 before failure started. The strengthened walls sustained on average 50% more lateral load capacity and 60% more lateral drift than the control wall. Other researchers [39][40] also reported the effectiveness of using FRP to improve seismic performance (such as shear capacity, ductility, and energy dissipation capacity) of RC walls. However, it is noted that the anchoring system is the critical part of the FRP strengthening scheme [41].

Although several studies have been conducted on strengthening of RC walls using different materials and techniques, Galal and El-Sokkary [42] pointed out five factors that control the choice of retrofitting techniques for RC walls: (1) the deficiency in the existing wall and its expected failure mode, (2) the goal of retrofit (e.g. increased stiffness, strength, ductility, etc.), (3) consequences of wall rehabilitation (e.g. increased demand on foundation, etc.), (4) the allocated budget for retrofit, (5) physical constraints (e.g. architecture requirements, accessibility of the building during the retrofitting process, etc.). In addition, it is important that the retrofitting construction does not interrupt the occupancy for residential and government office buildings. In this case, retrofitting works may be allowed only on the external side of rooms or buildings to use the internal space during construction.

2.5 FEM Analysis Studies on Lightly Reinforced Concrete Walls

The finite element method is a powerful structural analysis tool that has been widely used in many different types of problems. The strength of the finite element method is based primarily on its fundamental concept of discretization, which models a structure as an assemblage of several finite elements. The concept simplifies the modelling of complex structures and allows the formulation of the problem to be written in a matrix form, which is appropriate to be incorporated into computer programs. The concept of discretization is also useful for the study of problems with material and geometric nonlinearities, because it allows a variety of material and element models to be installed at the element level. With the proper material and element models for concrete and reinforcing steel, the finite element method can be a very powerful analytical tool for studying the behavior of reinforced concrete structures.

Research in the finite element analysis of reinforced concrete shear walls in Japan is much more active than that in the U.S. Most of the shear wall research in Japan deals with the behavior of stocky shear walls (height/length less than 1.0), which represent the reinforced concrete walls used in nuclear power plants. Yamaguchi and Nomura [43] used the finite element method based on the plastic-fracture theory proposed by Bazant and Kim [44] to analyze four reinforced concrete shear walls subjected to monotonic and cyclic loadings. Ueda and Kawai [45] used a finite element model which consisted of rigid elements and spring elements to model the monotonic response of shear walls. Sotomura and Murazumi [46] analyzed a series of reinforced concrete shear walls with openings by using a simple smeared crack model for concrete and an elastoplastic model for reinforcing steel. Inoue et al. [47] developed a reinforced concrete material model based on the

results from Vecchio and Collins' panel tests [48], where thirty reinforced concrete panels subjected to different uniform stress conditions were tested, and used the model in the analysis of several shear walls that had different reinforcement ratios and different shear span ratios. In all these previous analyses of reinforced concrete walls, most of the reinforced concrete models were simple, and, regardless of differences in the material and element models, most of the analytical results agreed with the experimental results.

3 DEVELOPMENT OF BACKBONE CURVE FOR LIGHTLY REINFORCED CONCRETE WALLS

3.1 Introduction

In Japan, reinforced concrete (RC) moment resisting frames are usually constructed monolithically with lightly reinforced infill walls with opening (spandrels, wall piers, and wing walls). Lightly RC walls are typically 120-200 mm thick, and have a single curtain of reinforcement in two directions with a few additional boundary vertical reinforcing bars at section ends. In many cases, horizontal reinforcement has no hook anchorage and boundary region has no confinement. The 2011 Tohoku [2] and the 2016 Kumamoto Earthquakes [3] clarified the weakness of lightly RC walls in residential and government office buildings. Many of them suffered severe damage mostly due to shear failures and impaired the building functions after the earthquakes.

A current focus of earthquake engineering research and practice is the development of performance-based seismic design (PBSD). As accepted generally by researchers in earthquake and structural engineering, the PBSD method provides a promising solution for the design of earthquake-resistant engineering structures [16][49][50]. The PBSD aims to improve structural engineering by providing engineers with the capability of designing structures to achieve a variety of seismic performance levels, and it allows structures to experience damage to a certain extent during earthquakes, which makes it necessary to define the damage levels corresponding to the different performance levels of structures. In this section, a performance based backbone model was developed to predict the seismic behavior of lightly RC walls. The selected tri-linear model is associated with three limit states: diagonal cracking, peak shear strength, and ultimate deformation capacity was proposed.

Basically, it is expected that RC walls have ductile response during an earthquake. To achieve this behavior, the design must ensure that the shear capacity exceeds the flexural capacity. Thus, our ability to calculate both the shear and flexural capacity is critical. The latter is now increasingly well understood. Research has given us tools, such as moment-curvature analysis based on fiber models to model and calculate the flexure behavior of concrete elements. However, the manner in which shear failures can occur varies widely with the dimensions, geometry, loading, and properties of the walls. For these reasons, the current design relies on conservative benchmarks rather than precise models with physical meaning. In addition, for lightly RC walls, the impact on the shear strength calculation using single curtain of distributed reinforcement and the lack of hooks on horizontal reinforcement are not explicitly considered in the current shear strength design.

In order to develop a performance based backbone curve of lightly RC walls, the prediction of shear strength is essential. Therefore, in this research, an improved shear strength model for lightly RC walls was also proposed to help engineers develop a reliable seismic design and better

understand the ultimate behavior of RC wall structures. The proposed model based on modification to the revised UCSD shear model by Krolicki et al. [11] for RC walls. An experimental database of 39 rectangular walls is used in the formulation of the proposed shear model and to test the accuracy of the model. By meeting these objectives, the proposed shear model could become an essential tool for performance-based assessment and design of lightly RC walls.

3.2 Backbone Curve Formulation

The prediction of shear strength is essential in developing a performance based backbone curve of lightly RC walls. To determine the shear strength of a lightly RC wall using the proposed shear model, the calculation of the shear capacity envelop and the force-displacement response is required. In addition, the shear strength calculated by ductility dependent shear models rely on calculation of the displacement ductility factor, μ_Δ. The level of refinement in the flexural model used for predicting the yield displacement can affect the accuracy of the shear capacity calculation, especially the estimate of ultimate displacements. The force-displacement response maybe calculated using the results from a moment curvature analysis. However, for walls with low shear-span ratios, the effect of shear deformations and loss of stiffness resulting from shear cracking can contribute significantly to the ultimate displacements of the element. It is therefore recommended to include the additional displacements from shear deformations in the total force-displacement response. In this study, a simple fiber-type section analysis was conducted to obtain the force-displacement response by using the procedure proposed by Kono et al. [51].

3.2.1 Basic concept of backbone curve modelling

To determine obtain a backbone curve of load (Q) – drift ratio (R) relation, R is simulated by summing the flexural drift component, R_f, and shear drift component, R_s, as shown in Eq (3-1).

$$R = R_f + R_s \tag{3-1}$$

Although, a drift component due to pullout from the stub, $R_{pullout}$, is not negligible, it is not modelled explicitly but included in R_f for simplicity. Aaleti et al. [52] modelled $R_f + R_{pullout}$ together assuming that the yield penetration depth is as large as the surface plastic hinge length. With this assumption, the drift components, R_f and $R_{pullout}$, are comparable in magnitude but the experimental results by Kono et al. [53] shows that penetration depth is not that large and the drift due to pullout from the stub ranges from 10 to 20% of the total drift. In strict sense, it is important to model each of R_f and $R_{pullout}$ from experimental measurement as Beyer et al. [54] indicated.

3.2.2 Flexure Drift Component

The flexure drift component, R_f, is assumed to consist of elastic component, R_{fe}, and plastic

component, R_{fp}, as shown in Figure 3-1(a). Two components are computed based on the idealized curvature distribution in Figure 3-1(b) and their summation makes R_f as Eq. (3-2).

$$R_f = R_{fe} + R_{fp} = \frac{1}{H}(\Delta_{fe} + \Delta_{fp}) \tag{3-2}$$

where Δ_{fe} and Δ_{fp} are elastic and plastic flexural displacement, respectively. The drift component, $R_{fe} = \Delta_{fe}/H$, is computed from a linear elastic curvature distribution, ϕ_{fe}, over the height. The plastic drift component, $R_{fp} = \Delta_{fp}/H$, is computed from a uniform plastic curvature distribution, ϕ_{fp} , over the equivalent plastic hinge height, l_p. The plastic rotation is supposed to take place after the flexural yielding in reality but assumed to start from the beginning of loading for simplicity.

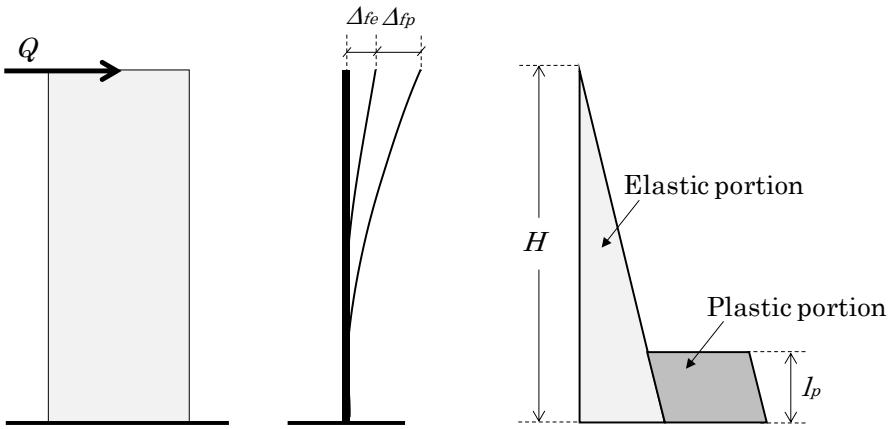

(a) Flexural deformation (b) Idealized curvature distribution

Figure 3-1 Decomposition of flexural drift component

A fiber-type section analysis is used to compute plastic flexural displacement component, Δ_{fp}. Different fibers represent elements for either plain concrete, confined concrete and vertical reinforcing bars. The concrete wall is modeled with Kent and Park Model [55] as shown in Figure 3-2. The stress-strain relations for vertical reinforcing bars were modeled with bilinear curves with strain hardening 0.01. The plastic flexural displacement component, Δ_{fp}, can be calculated as:

$$\Delta_{fp} = l_p \phi_{fp}(H - 0.5 l_p) \tag{3-3}$$

Once a set of shear force, Q, and plastic flexural displacement, Δ_{fp}, is obtained, corresponding Δ_{fe} can be computed using a basic elastic theory as:

$$\Delta_{fe} = \frac{QH^3}{3EI}, \text{ for cantilever walls} \tag{3-4}$$

$$\Delta_{fe} = \frac{QH^3}{12EI}, \text{ for wall tests loaded in double curvature} \quad (3\text{-}5)$$

where l_p is the effective plastic hinge length and in this study is assumed $0.2l_w$, ϕ_{fp} is the plastic curvature over the plastic hinge, Q is the shear force corresponding to the plastic curvature (ϕ_{fp}), H is wall height, and EI is the flexural stiffness of the wall.

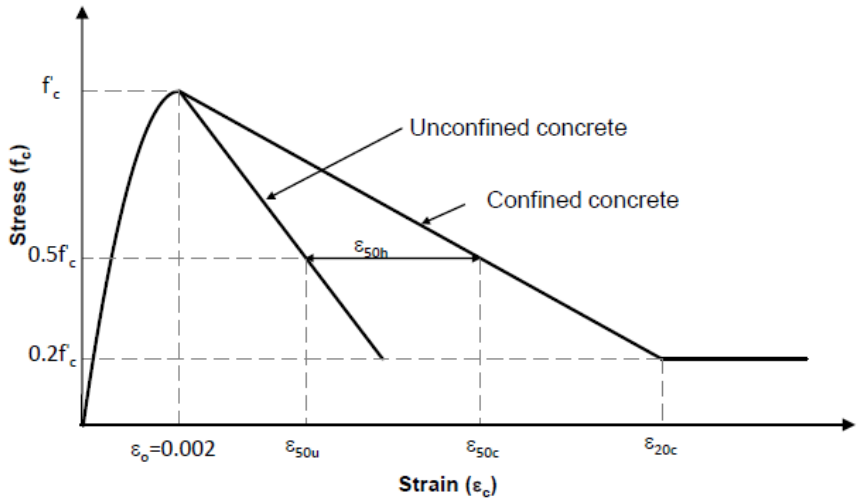

Figure 3-2 Kent and Park stress-strain model for confined and unconfined concrete

3.2.3 Shear Drift Component

Beyer et al.'s model [54] is used to simulate the shear drift component. This model allows the estimation of the ratio of shear-to-flexural deformations for shear walls whose shear-transfer mechanism is not significantly deteriorating. The model assumes that the ratio of shear-to-flexural drifts remains approximately constant over the entire range of imposed displacement ductility. However, the model does not function for walls whose shear transfer mechanism significantly degrades since the ratio of shear-to-flexural deformations increases. The ratio of shear drift, *Rs*, to flexural drift, R_f, is expressed as Eq. (3-6).

$$\frac{R_s}{R_f} = 1.5\frac{\varepsilon_m}{\phi \tan\beta}\frac{1}{H} \quad (3\text{-}6)$$

$$\beta = \tan^{-1}\left[\frac{jd}{V}\left(f_l b_w + \frac{A_{sw} f_{yw}}{s}\right)\right] < 90° \quad (3\text{-}7)$$

where ε_m and ϕ are the axial strain at the center of the wall sections and the curvature, respectively, and are derived from the moment-curvature analysis. Variable H is the shear span, and β is the cracking angle measured against the element axis and assumed 45 degrees in this study, which is

suggested by Beyer et al. [54] for simplification. With this equation, the shear drift component can be obtained with an easy and stable manner once the flexural drift component is computed.

3.2.4 Simulation Procedures

The following procedures are taken to simulate backbone curves.

1) Calculate the moment-curvature flexure response using the model that explained in Sec. 3.2.2 for concrete wall and reinforcing bars.
2) By assuming the effective plastic hinge length, $l_p = 0.2l_w$, calculate the plastic and elastic displacement using Eq. (3-3) and Eqs. (3-4) or (3-5), then superimpose the plastic and elastic displacement and calculate the flexure drift component using Eq. (3-2).
3) Calculate shear drift component using Eq. (3-6) by assuming the cracking angle $\beta = 45°$.
4) Superimpose the flexural and shear drift component to calculate the total load (Q) – drift ratio (R) response as Eq. (3-1).

3.3 Proposed Shear Capacity Equation

A new shear model is proposed for lightly RC walls by extending the revised UCSD shear model by Krolicki et al. [11]. Krolicki's model is selected for the development of the new shear model of lightly RC walls for several reasons, including: (1) The model included the most significant parameters known to relate to shear strength, (2) the model was developed for RC walls, (3) each of the identified components of shear resistance is intended to relate to physical phenomenon, not just empirical equations best fit to data, (4) the model to have good agreement in predicting RC wall shear strength.

An experimental database of 39 rectangular walls listed in Table 3-6 is used in the formulation of the proposed shear model and to test the accuracy of the model. The shear strength equation calculates the capacity as the sum of three components: (1) V_c: concrete shear-resisting mechanism, (2) V_s: horizontal reinforcement truss shear-resisting mechanism, and (3) V_p: axial load component as shown in Eq. (3-8)

$$V_n = V_c + V_s + V_p \tag{3-8}$$

The proposed changes to each component of shear resistance are discussed in detail in the following sections.

3.3.1 Proposed concrete component

The Proposed concrete shear-resisting mechanism maintains the same variables as given in the revised UCSD shear model. The contribution of the concrete to the shear resistance is calculated as:

$$V_c = \alpha\beta\gamma\sqrt{f_c'}\,0.8A_g \tag{3-9}$$

The effective shear area is the gross area of the wall excluding the compression zone. Assuming the compression zone is $0.2l_w$, the area is estimated as $0.8A_g$. The parameter α accounts for the effect of shear span ratio. The parameter β accounts for the increase in shear resistance proportional to increasing ratio of vertical reinforcement. The parameter γ represents the reduction in strength of the concrete shear resisting mechanism with increasing ductility.

Krolicki et al. [11] proposed the parameter α as Eq. (3-10), while for the parameter β is unchanged from the revised UCSD shear model as Eq. (3-11).

$$\alpha = 3 - \frac{M}{Vl_w} \geq 1.0 \tag{3-10}$$

$$\beta = 0.5 + 20\rho_l \leq 1.0 \tag{3-11}$$

Since this study focuses on lightly RC walls, where the structure has single curtain of reinforcement, the parameter α and β need to be re-evaluated. Twenty-eight lightly RC walls which failed in shear (in order to be independent from ductility) and tested with no axial force were selected from the database in Table 3-6 to evaluate those two parameters. The experimental value of concrete contribution to shear resistance, $V_{c\text{-}EXP}$, is estimated by subtracting the calculated contribution of transverse reinforcement mechanism V_s using Eq. (2-20) and the contribution of axial loads, V_p, from the measured experimental shear capacity, $V_{n\text{-}EXP}$, as given in Eq. (3-12).

$$V_{c-EXP} = V_{n-EXP} - (V_s + V_p) \tag{3-12}$$

To solve the experimental data value of α and β, the experimental concrete contribution, $V_{c\text{-}exp}$, is divided by the remaining factors of Eq. (3-9) as given in Eq. (3-13).

$$\alpha\beta_{EXP} = \frac{V_{c-EXP}}{\gamma\sqrt{f'_c}\,0.8A_g} \tag{3-13}$$

Figure 3-3 shows the correlation between ρ_v and M/Vl_w with $\alpha\beta_{EXP}$. It is clear that ratio of vertical reinforcement and shear span ratio affect to parameter $\alpha\beta$. The parameter α and β then calculated using Eqs. (3-10) and (3-11), respectively and plotted in Figure 3-4. The calculated parameter $\alpha\beta_{CAL}$ does not have a good agreement with that of experiment $\alpha\beta_{EXP}$ as shown in Figure 3-5. Therefore, both parameters α and β need to be modified. It is logical that the shear strength be greater for walls with smaller aspect ratios, as the confinement effect of the adjacent members is

greater in these situations. On the basis of these considerations, the parameter α is modified as:

$$\alpha = \frac{1}{\sqrt{\frac{M}{Vl_w}}} \tag{3-14}$$

The correlation between ρ_v and M/Vl_w with proposed parameter α and β are shown in Figure 3-6. The parameter α has a good agreement with M/Vl_w. Based on Kowalsky and Priestley [26], a smaller longitudinal steel ratio results in a decrease in the strength of the concrete shear resisting mechanism because of: (1) Reduced dowel action, (2) more concentrated crack distribution, increased crack width, reduction of aggregate interlock, and (3) smaller compression zone, smaller contribution of compression zone to shear strength. However, in author opinion, for point (2) and (3) have been accommodated in parameter γ. In addition, from Figure 3-6(a), the distribution of parameter β is spread randomly and there is no data for $\rho_v < 0.86\%$. Therefore, the parameter β is modified as β=1.25, which is the average value from 28 walls.

Table 3-1 Properties of lightly RC wall database for evaluating $\alpha\beta$

No	Code	t_w	l_w	h_w	M/Vl_w	f'_c	f_{yh}	ρ_h	ρ_v	V_{EXP}	V_s	V_c	$a\beta_{EXP}$
		(mm)	(mm)	(mm)		(MPa)	(MPa)			(kN)	(MPa)	(MPa)	
1	WS-T1-S1	152	1520	1520	0.50	25.5	424	0.0029	0.0104	633	245	388	1.43
2	WS-T1-S2	152	1520	1520	0.50	43.7	424	0.0029	0.0104	749	245	504	1.42
3	1	120	1000	2000	1.00	19.4	392	0.0013	0.0186	198	60	138	1.13
4	2	120	1000	2000	1.00	19.6	402	0.0025	0.0186	270	119	151	1.23
5	4	120	1000	2000	1.00	19.5	402	0.0038	0.0228	324	178	146	1.19
6	6	120	1300	1800	0.69	17.6	314	0.0013	0.0150	309	59	250	1.65
7	7	120	1300	1800	0.69	18.1	471	0.0026	0.0150	364	172	192	1.25
8	8	120	1300	1800	0.69	15.7	471	0.0026	0.0150	374	172	202	1.41
9	9	100	1300	1800	0.69	17.6	366	0.0027	0.0160	258	116	142	1.12
10	10	80	1300	1800	0.69	16.4	367	0.0026	0.0166	187	89	98	1.00
11	11	100	1400	1400	0.50	16.3	362	0.0014	0.0135	235	62	173	1.32
12	12	100	1400	1400	0.50	17.0	366	0.0026	0.0125	304	117	187	1.39
13	13	100	1400	1400	0.50	18.1	370	0.0026	0.0135	289	119	170	1.23
14	14	80	1700	1200	0.35	17.1	366	0.0015	0.0109	255	52	203	1.56
15	15	80	1700	1200	0.35	19.0	366	0.0027	0.0099	368	93	275	2.00
16	16	80	1700	1200	0.35	18.8	366	0.0027	0.0109	362	93	269	1.97
17	21	100	1300	1800	0.69	24.2	366	0.0000	0.0093	258	0	258	1.74
18	22	100	1300	1800	0.69	17.2	366	0.0000	0.0093	222	0	222	1.77
19	23	100	1300	1800	0.69	24.2	431	0.0025	0.0171	333	129	204	1.38
20	24	100	1300	1800	0.69	23.9	431	0.0000	0.0112	323	0	323	2.19
21	25	100	1400	1400	0.50	23.9	431	0.0000	0.0086	352	0	352	2.22
22	26	100	1400	1400	0.50	17.7	431	0.0000	0.0086	262	0	262	1.92
23	27	100	1400	1400	0.50	23.9	431	0.0026	0.0130	491	138	353	2.22
24	28	100	1400	1400	0.50	23.3	431	0.0000	0.0106	258	0	258	1.65
25	29	80	1500	1050	0.35	23.2	431	0.0000	0.0101	400	0	400	2.98
26	30	80	1500	1050	0.35	17.9	431	0.0000	0.0101	356	0	356	3.02
27	31	80	1500	1050	0.35	23.1	431	0.0027	0.0134	391	97	294	2.19
28	32	80	1500	1050	0.35	23.3	431	0.0000	0.0122	344	0	344	2.56

To simulate the parameter β with $\rho_v < 0.86\%$, a parametric study of 30 wall cases was conducted using finite element analyses. To ensure the shear failure, all wall cases had no

horizontal reinforcement. The properties of parametric study is shown in Table 3-2 and the constitutive models for concrete and steel followed models explained in Section 6.3. By conducting the similar procedure with that of experiment, the correlation between ρ_v and M/Vl_w with the combination of $\alpha\beta_{EXP}$ and $\alpha\beta_{FEM}$ are plotted in Figure 3-7. The parameter α then calculated using Eq. (3-14) and parameter β is determined as:

$$\beta = 0.6 + 100\rho_v \leq 1.25 \tag{3-15}$$

The correlation between ρ_v and M/Vl_w with proposed parameter α and β for combination of experiment and FE analysis are shown in Figure 3-8. The proposed α and β has a good agreement with ρ_v and M/Vl_w, respectively, for both experiment and FE analysis (parametric study). It is also confirmed by Figure 3-9 that shows a good correlation between $\alpha\beta_{CAL}$ with both $\alpha\beta_{EXP}$ and $\alpha\beta_{FEM}$.

The shear resistance of concrete is known to degrade during cyclic loading with increasing ductility demands. As displacement increases, the cracks widen, reducing the effectiveness of the aggregate interlock shear resistance along the crack surface. If vertical reinforcement in the center of the wall or horizontal reinforcement yields, cracks may not fully close. The parameter γ attempts to model this complex phenomenon. Since lightly RC walls have single curtain of reinforcement, they are unlikely to reach high displacement ductility before the shear failure occurs. Therefore, the displacement ductility limit of parameter γ was modified as Eqs. (3-16) and (3-17) as recommendation from ASCE/SEI 41-13 [12] for nonlinear procedures of concrete structures.

$$\gamma = 0.29 \text{, for } \mu_\Delta \leq 2 \tag{3-16}$$

$$\gamma = 0.05 \text{, for } \mu_\Delta \geq 4 \tag{3-17}$$

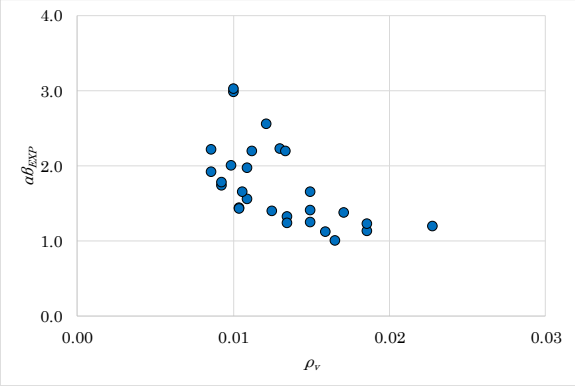

(a) ρ_v vs $\alpha\beta_{EXP}$

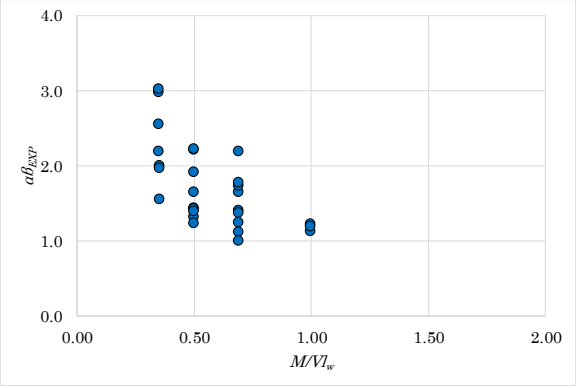

(a) M/Vl_w vs $\alpha\beta_{EXP}$

Figure 3-3 ρ_v and M/Vl_w – $\alpha\beta_{EXP}$ relations

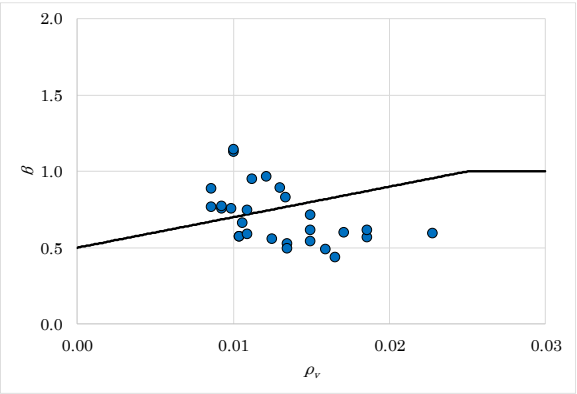

(a) Parameter β

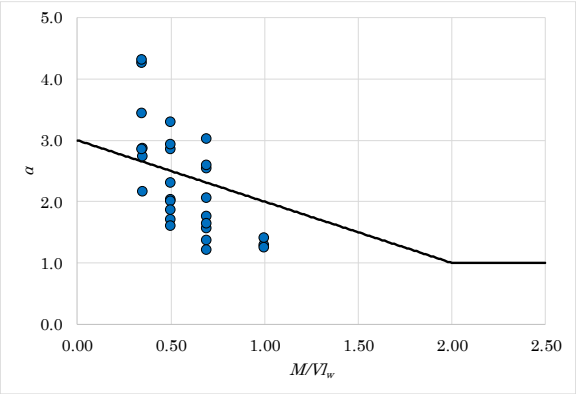

(b) Parameter α

Figure 3-4 Parameter α and β based on Krolicki et al. [10]

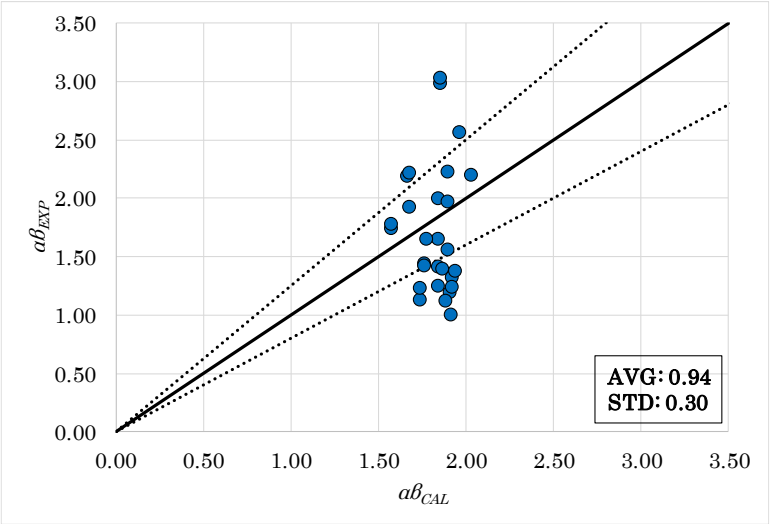

Figure 3-5 $\alpha\beta_{CAL}$ vs $\alpha\beta_{EXP}$

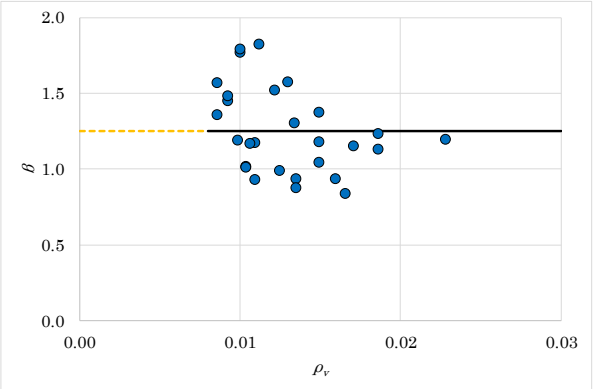

(a) Parameter β

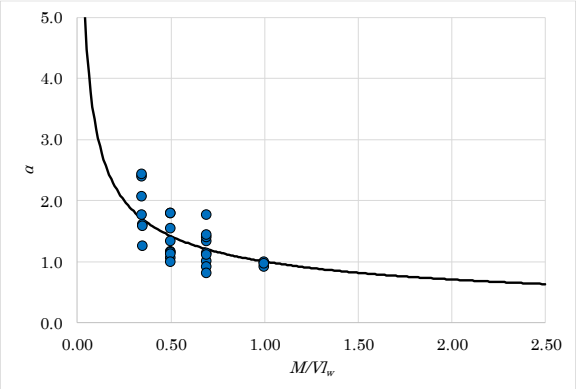

(b) Parameter α

Figure 3-6 Proposed parameter α and β

Table 3-2 Properties of parametric study for evaluating $\alpha\beta$

No	Code	t_w (mm)	l_w (mm)	h_w (mm)	M/Vl_w	f'_c (MPa)	f_{yh} (MPa)	ρ_h	ρ_v	V_{FEM} (kN)	V_s (MPa)	V_c (MPa)	$\alpha\beta_{FEM}$
1	αβ-01	120	1050	600	0.29	24.2	347	0.0000	0.0063	415.8	0	416	2.89
2	αβ-02	120	1050	600	0.29	24.2	347	0.0000	0.0045	290.1	0	290	2.02
3	αβ-03	120	1050	600	0.29	24.2	347	0.0000	0.0033	261.3	0	261	1.82
4	αβ-04	120	1050	600	0.29	24.2	347	0.0000	0.0020	260.6	0	261	1.81
5	αβ-05	120	1050	600	0.29	24.2	347	0.0000	0.0010	260.5	0	261	1.81
6	αβ-06	120	1050	600	0.29	24.2	347	0.0000	0.0000	259.8	0	260	1.81
7	αβ-07	120	1050	1100	0.52	24.2	347	0.0000	0.0063	310.0	0	310	2.16
8	αβ-08	120	1050	1100	0.52	24.2	347	0.0000	0.0045	175.9	0	176	1.22
9	αβ-09	120	1050	1100	0.52	24.2	347	0.0000	0.0033	175.5	0	176	1.22
10	αβ-10	120	1050	1100	0.52	24.2	347	0.0000	0.0020	174.1	0	174	1.21
11	αβ-11	120	1050	1100	0.52	24.2	347	0.0000	0.0010	173.8	0	174	1.21
12	αβ-12	120	1050	1100	0.52	24.2	347	0.0000	0.0000	172.6	0	173	1.20
13	αβ-13	120	1050	1600	0.76	24.2	347	0.0000	0.0063	214.3	0	214	1.49
14	αβ-14	120	1050	1600	0.76	24.2	347	0.0000	0.0045	187.2	0	187	1.30
15	αβ-15	120	1050	1600	0.76	24.2	347	0.0000	0.0033	157.2	0	157	1.09
16	αβ-16	120	1050	1600	0.76	24.2	347	0.0000	0.0020	137.4	0	137	0.96
17	αβ-17	120	1050	1600	0.76	24.2	347	0.0000	0.0010	115.9	0	116	0.81
18	αβ-18	120	1050	1600	0.76	24.2	347	0.0000	0.0000	110.0	0	110	0.76
19	αβ-19	120	1050	2100	1.00	24.2	347	0.0000	0.0063	152.0	0	152	1.06
20	αβ-20	120	1050	2100	1.00	24.2	347	0.0000	0.0045	140.9	0	141	0.98
21	αβ-21	120	1050	2100	1.00	24.2	347	0.0000	0.0033	123.9	0	124	0.86
22	αβ-22	120	1050	2100	1.00	24.2	347	0.0000	0.0020	102.4	0	102	0.71
23	αβ-23	120	1050	2100	1.00	24.2	347	0.0000	0.0010	78.8	0	79	0.55
24	αβ-24	120	1050	2100	1.00	24.2	347	0.0000	0.0000	73.3	0	73	0.51
25	αβ-25	120	1050	3100	1.48	24.2	347	0.0000	0.0063	119.5	0	120	0.83
26	αβ-26	120	1050	3100	1.48	24.2	347	0.0000	0.0045	95.5	0	95	0.66
27	αβ-27	120	1050	3100	1.48	24.2	347	0.0000	0.0033	77.1	0	77	0.54
28	αβ-28	120	1050	3100	1.48	24.2	347	0.0000	0.0020	62.4	0	62	0.43
29	αβ-29	120	1050	3100	1.48	24.2	347	0.0000	0.0010	48.8	0	49	0.34
30	αβ-30	120	1050	3100	1.48	24.2	347	0.0000	0.0000	47.7	0	48	0.33

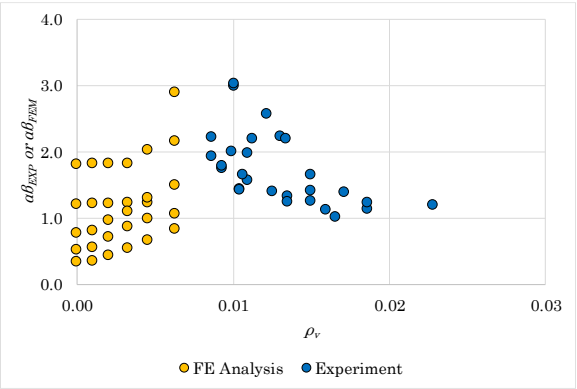

(a) ρ_v vs $\alpha\beta_{EXP}$ and $\alpha\beta_{FEM}$

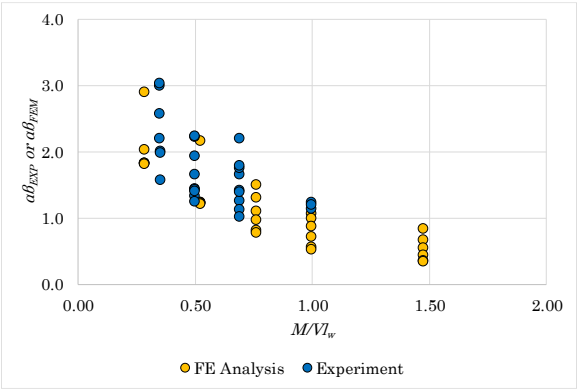

(a) M/Vl_w vs $\alpha\beta_{EXP}$ and $\alpha\beta_{FEM}$

Figure 3-7 ρ_v and M/Vl_w – $\alpha\beta_{EXP}$ and $\alpha\beta_{FEM}$ relations

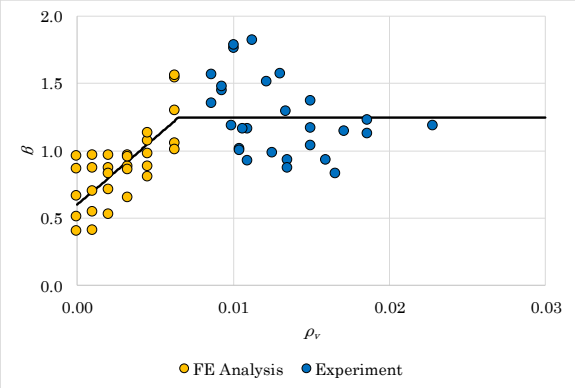

(a) Parameter β

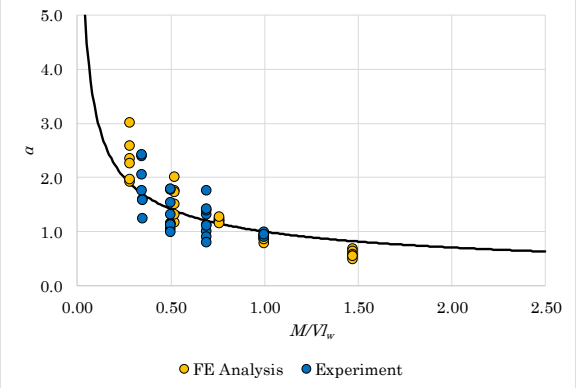

(b) Parameter α

Figure 3-8 Proposed α and β for combination experiment and FE analysis

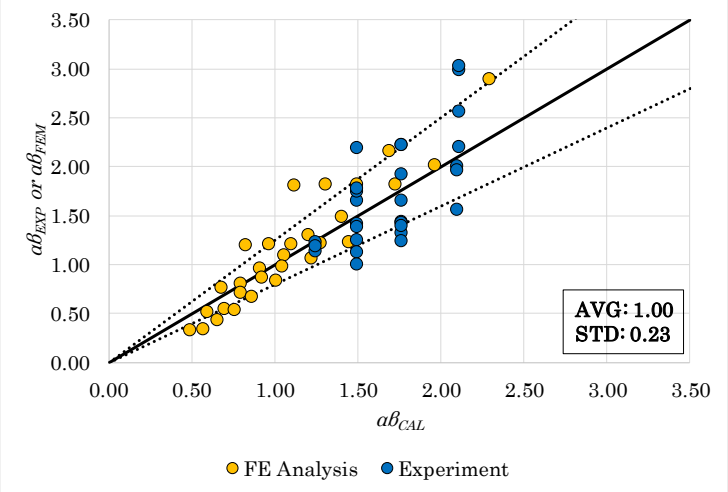

Figure 3-9 Proposed $\alpha\beta_{CAL}$ vs $\alpha\beta_{EXP}$ and $\alpha\beta_{FEM}$

3.3.2 Horizontal reinforcement component

The wall section illustrated in Figure 3-10 demonstrates the shear strength developed by the horizontal reinforcement truss mechanism, as suggested by Kowalsky and Priestley [26]. The critical inclined flexure-shear crack is shown crossing the section at an angle θ to the vertical axis. The horizontal reinforcement crossing the crack acts to transfer shear forces. The maximum shear force that can be resisted by the horizontal reinforcement equals the area of steel crossing the crack times the yield strength.

The average cracking angle θ= 30° is recommended by Priestley et al. [25] for assessment of existing structures. For design, a more conservative value of θ= 35° is recommended. However, based on Krolicki et al. [11], it is apparent that walls with the lower shear span ratios result in shallower compression struts and a larger angle of concrete cracking, θ. Therefore, to account for this change in walls with low shear span ratios, Krolicki et al. [11] proposed that the average critical cracking angle varies as a factor of shear span ratio (M/Vl_w). In addition, the maximum vertical height of the inclined crack that can develop regardless of the cracking angle is limited to

the height of the wall.

The horizontal reinforcement component, V_s, was used directly in the proposed model as formulated in Krolicki et al. [11].

$$V_s = \rho_h f_{yh} t_w h_{cr} \tag{3-18}$$

$$h_{cr} = \frac{(l_w - c - \text{cov})}{\tan\theta_{cr}} \le h_w \tag{3-19}$$

$$\theta_{cr} = \left(\frac{30° - 45°}{2}\right)\left(\frac{M}{Vl_w}\right) + 45° \ge 30° \tag{3-20}$$

where h_{cr} is vertical crack height and θ_{cr} is average cracking angle. The compression zone c can be calculated through moment curvature analysis or reasonably assumed for walls as $0.2l_w$.

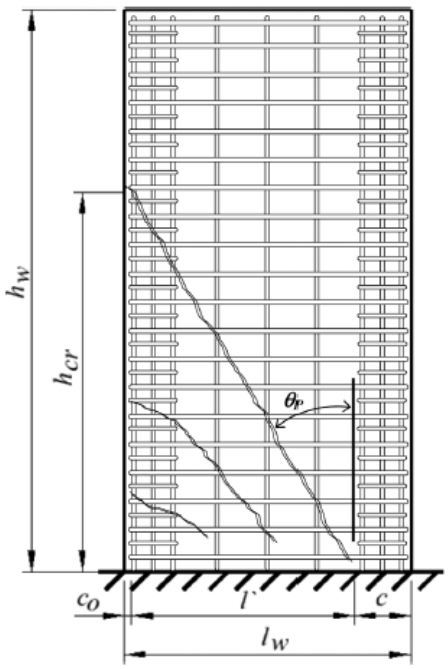

Figure 3-10 Average crack angle θ [11]

3.3.3 Proposed axial load component

The axial load component accounts for the enhancement of shear strength with increased axial compression. In Eq. 2-1, the contribution of axial load to shear strength is taken as 10% of its axial load, while for ACI 318, the influence of axial load on the shear strength of concrete is not considered in the nominal shear strength calculation.

The axial load component is based on a simplified assumption of a linear compression strut

[25]. The actual behavior is a combination of applied axial compression force and flexural compression force. As shown in Figure 3-11 for a member in double curvature, the end regions of the curved compression strut have higher magnitudes, but acting at a lower angle to the member than the middle section. Priestley et al. [25] suggested that the difference of magnitude and inclination have a similar effect on shear resistance over the member height and that the simple linear assumption of this complex behavior appears to provide a reasonable fit to test data.

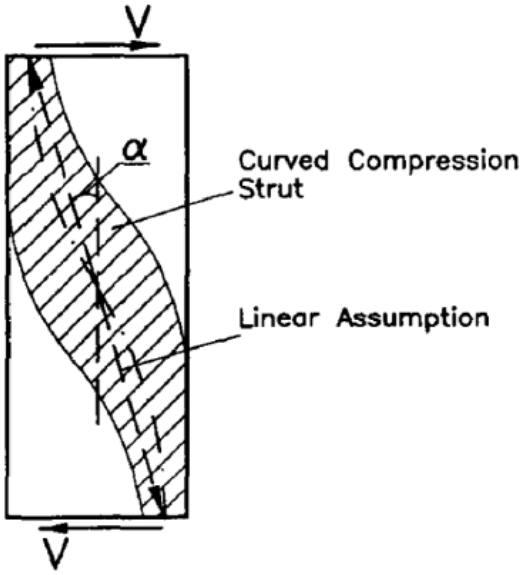

Figure 3-11 Linear representation of curved compression strut [25]

The axial load contribution to shear resistance from the simplified linear compression strut is show in Figure 3-12 [56] for wall loaded in single curvature and double curvature. The applied shear force is resisted by the horizontal component of the compression strut. The axial load contribution to shear resistance is as:

$$V_p = P\tan\zeta \tag{3-21}$$

$$\tan\zeta = \frac{l_w - c}{2h_w}\text{, for cantilever wall} \tag{3-22}$$

$$\tan\zeta = \frac{l_w - c}{h_w}\text{, for wall tests loaded in double curvature} \tag{3-23}$$

where l_w and h_w is length and height of wall, respectively, c is depth of compression zone. The compression zone c can be calculated through moment curvature analysis or reasonably assumed for walls as $0.2l_w$.

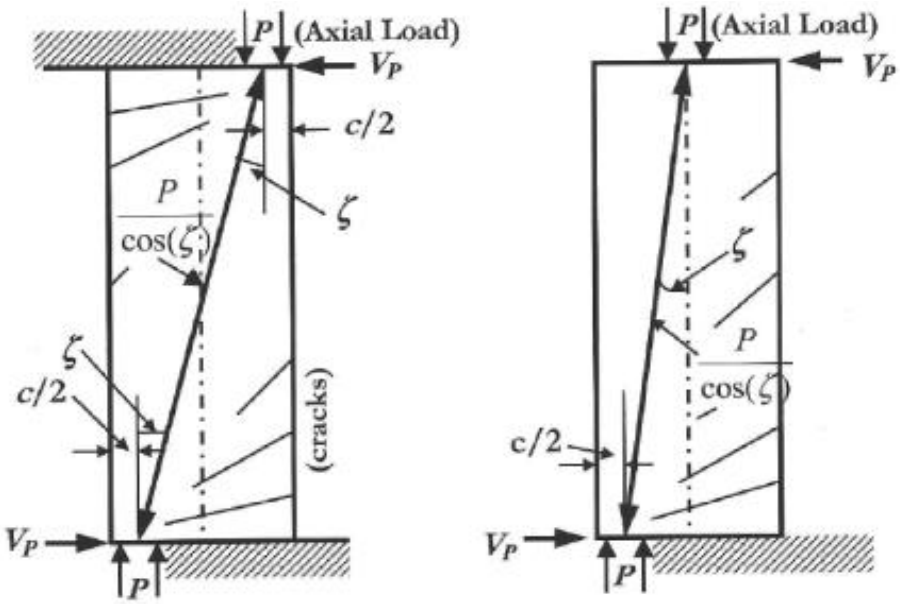

Figure 3-12 Axial load contribution V_p for walls loaded in double and single curvature [10]

The axial load contribution to shear resistance, V_p, does not degrade with increasing ductility. Eq. (3-21) implies that as the aspect ratio of the wall decreases, the axial load contribution to shear strength will increase, and that for very slender walls, the axial load contribution may be minimal. Since shear force is likely to be low in such cases, this may not be significant. However, for walls with low aspect ratio, the inclined strut angle, ζ, becomes larger, leads to overestimate the axial load contribution to shear resistance. Eq. (3-21) also implies that as the axial load increases, the effectiveness of the axial load contribution to wall shear strength decreases since the depth of the compression zone c increases. However, for simplicity, the compression zone, c, can be reasonably assumed for walls as $0.2l_w$. This assumption leads to underestimate the depth of the compression zone as the axial load increases. Therefore, Eq. (3-21) needs to be re-evaluated.

Experimental database in Table 3-6, there are only five specimens that tested under axial force. Since limited data are currently available for lightly RC walls to evaluate the axial load contribution to shear resistance, a parametric study of 30 wall cases (excluding 5 cases with no axial load) was conducted using finite element analysis. For all cases, ratio of horizontal and vertical reinforcement is constant, ρ_h= 0.24% and ρ_v= 0.63%, respectively, similar to that of NSW1 and NSW2 (Author's specimen in Chapter 4). The variables of parametric study are shear span ratio (M/Vl_w) and ratio of axial load (P/f'_cA_g). The properties of wall database and parametric study for evaluating V_p are shown in Table 3-3 and Table 3-4, respectively. The constitutive models for finite element analysis of concrete and steel followed models explained in Section 6.2.2.

Table 3-3 Properties of lightly RC wall database for evaluating V_p

No	Code	t_w (mm)	l_w (mm)	h_w (mm)	M/Vl_w	P/f'_cA_g	f'_c (MPa)	P kN	$tan(\zeta)$	V_{EXP} (kN)	$V_{p\text{-}EXP}$ (MPa)	$V_{p\text{-}CAL}$ (MPa)	$V_{p\text{-}EXP}/V_{p\text{-}CAL}$
1	NSW1	120	1050	2100	1.00	0.00	24.2	0	0.4	155	-	-	-
2	NSW2	120	1050	2100	1.00	0.15	24.2	457	0.4	297	142	183	0.78
3	WP-T5-N0-S1	152	1370	1220	0.45	0.00	29.9	0	0.9	404	-	-	-
4	WP-T5-N5-S1	152	1370	1220	0.45	0.05	31.9	332	0.9	648	244	298	0.82
5	WP-T5-N5-S2	152	1370	1220	0.45	0.05	32.0	333	0.9	682	278	299	0.93
6	WP-T5-N10-S1	152	1370	1220	0.45	0.10	28.3	589	0.9	753	349	529	0.66
7	WP-T5-N10-S2	152	1370	1220	0.45	0.10	31.4	654	0.9	819	415	587	0.71

Table 3-4 Properties of parametric study for evaluating V_p

No	Code	t_w (mm)	l_w (mm)	h_w (mm)	M/Vl_w	P/f'_cA_g	f'_c (MPa)	P kN	$tan(\zeta)$	V_{FEM} (kN)	$V_{p\text{-}FEM}$ (MPa)	$V_{p\text{-}CAL}$ (MPa)	$V_{p\text{-}FEM}/V_{p\text{-}CAL}$
1	P-01	120	1050	3100	1.48	*0*	24.2	0	0.3	132	-	-	-
2	P-02	120	1050	3100	1.48	0.02	24.2	61	0.3	147	16	17	0.95
3	P-03	120	1050	3100	1.48	0.05	24.2	152	0.3	179	47	41	1.14
4	P-04	120	1050	3100	1.48	0.10	24.2	305	0.3	233	101	83	1.22
5	P-05	120	1050	3100	1.48	0.15	24.2	457	0.3	256	124	124	1.00
6	P-06	120	1050	3100	1.48	0.20	24.2	610	0.3	285	154	165	0.93
7	P-07	120	1050	3100	1.48	0.30	24.2	915	0.3	342	211	248	0.85
8	P-08	120	1050	2100	1.00	0.00	24.2	0	0.4	195	-	-	-
9	P-09	120	1050	2100	1.00	0.02	24.2	61	0.4	227	32	24	1.29
10	P-10	120	1050	2100	1.00	0.05	24.2	152	0.4	270	74	61	1.22
11	P-11	120	1050	2100	1.00	0.10	24.2	305	0.4	317	122	122	1.00
12	P-12	120	1050	2100	1.00	0.15	24.2	457	0.4	351	156	183	0.85
13	P-13	120	1050	2100	1.00	0.20	24.2	610	0.4	392	196	244	0.80
14	P-14	120	1050	2100	1.00	0.30	24.2	915	0.4	466	271	366	0.74
15	P-15	120	1050	1600	0.76	0.00	24.2	0	0.5	262	-	-	-
16	P-16	120	1050	1600	0.76	0.02	24.2	61	0.5	285	23	32	0.70
17	P-17	120	1050	1600	0.76	0.05	24.2	152	0.5	320	58	80	0.73
18	P-18	120	1050	1600	0.76	0.10	24.2	305	0.5	363	100	160	0.63
19	P-19	120	1050	1600	0.76	0.15	24.2	457	0.5	448	185	240	0.77
20	P-20	120	1050	1600	0.76	0.20	24.2	610	0.5	456	194	320	0.61
21	P-21	120	1050	1600	0.76	0.30	24.2	915	0.5	507	245	480	0.51
22	P-22	120	1050	1100	0.52	0.00	24.2	0	0.8	337	-	-	-
23	P-23	120	1050	1100	0.52	0.02	24.2	61	0.8	388	51	47	1.10
24	P-24	120	1050	1100	0.52	0.05	24.2	152	0.8	439	102	116	0.88
25	P-25	120	1050	1100	0.52	0.10	24.2	305	0.8	497	160	233	0.69
26	P-26	120	1050	1100	0.52	0.15	24.2	457	0.8	565	228	349	0.65
27	P-27	120	1050	1100	0.52	0.20	24.2	610	0.8	618	281	466	0.60
28	P-28	120	1050	1100	0.52	0.30	24.2	915	0.8	659	323	699	0.46
29	P-29	120	1050	600	0.29	0.00	24.2	0	1.4	450	-	-	-
30	P-30	120	1050	600	0.29	0.02	24.2	61	1.4	483	33	85	0.39
31	P-31	120	1050	600	0.29	0.05	24.2	152	1.4	519	69	213	0.32
32	P-32	120	1050	600	0.29	0.10	24.2	305	1.4	598	148	427	0.35
33	P-33	120	1050	600	0.29	0.15	24.2	457	1.4	638	188	640	0.29
34	P-34	120	1050	600	0.29	0.20	24.2	610	1.4	687	237	854	0.28
35	P-35	120	1050	600	0.29	0.30	24.2	915	1.4	799	348	1281	0.27

The experimental value of axial force contribution to shear resistance, $V_{p\text{-}EXP}$, is estimated by subtracting the measured experimental shear capacity, $V_{n\text{-}EXP}$, tested under axial load with the measured experimental shear capacity, $V_{n\text{-}EXP\text{-}0}$, tested under no axial load as given in Eq. (3-24) for each specimen with same properties except the axial load.

$$V_{p-EXP} = V_{c-EXP} - V_{c-EXP-0} \tag{3-24}$$

This $V_{p\text{-}EXP}$ then compared with the calculated value of axial force contribution to shear resistance, $V_{p\text{-}CAL}$, that calculated using Eq. (3-21) as shown in Table 3-3 and Figure 3-13. The similar

procedure with that of experiment was also conducted for finite element analysis using the following formula given in Eq. (3-25). The comparison between $V_{p\text{-}FEM}$ and $V_{p\text{-}CAL}$ is shown in Table 3-4 and Figure 3-13. It is noted that the depth of compression zone, c, was assumed as $0.2l_w$ to calculate $V_{p\text{-}CAL}$.

$$V_{p-FEM} = V_{c-FEM} - V_{c-FEM-0} \tag{3-25}$$

As shown in Figure 3-14, as the shear span ratio of the wall decreases, $V_{p\text{-}EXP}/V_{p\text{-}CAL}$ and $V_{p\text{-}FEM}/V_{p\text{-}CAL}$ also decreases. It implies that the axial load contribution to shear strength that calculated using Eq. (3-21) is overestimated. In addition, as ratio of axial load increases, $V_{p\text{-}EXP}/V_{p\text{-}CAL}$ and $V_{p\text{-}FEM}/V_{p\text{-}CAL}$ decreases. This is because the depth of compression zone c was assumed as $0.2l_w$ to calculate $V_{p\text{-}CAL}$ and also leads to overestimate of axial force contribution to shear resistance.

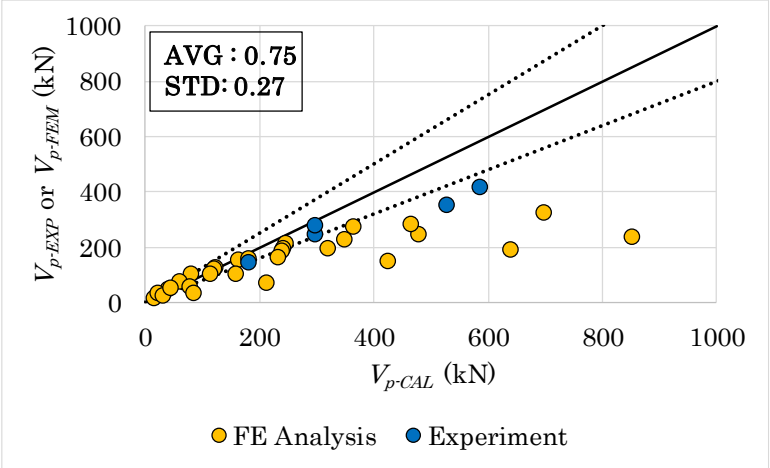

Figure 3-13 Comparison $V_{p\text{-}EXP}$ and $V_{p\text{-}FEM}$ with $V_{p\text{-}CAL}$ using Eq. (3-21)

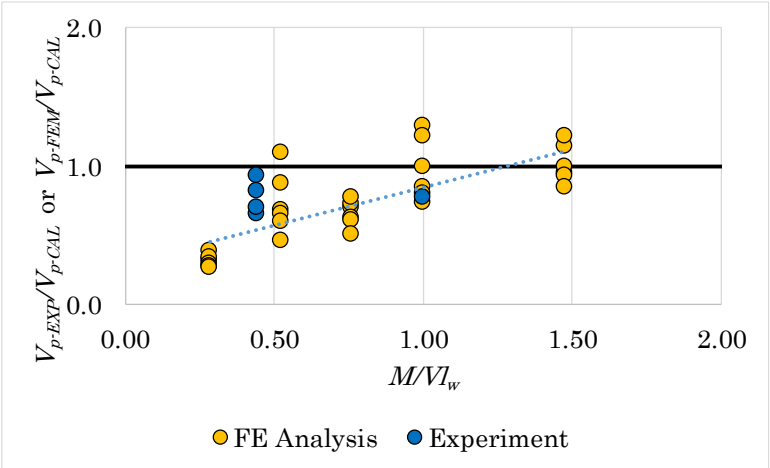

Figure 3-14 $V_{p\text{-}EXP}/V_{p\text{-}CAL}$ and $V_{p\text{-}FEM}/V_{p\text{-}CAL}$ for variation of shear span ratio

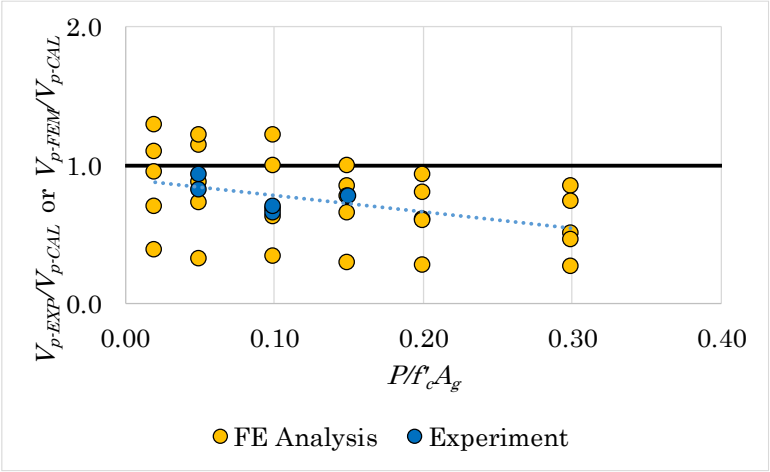

Figure 3-15 $V_{p\text{-}EXP}/V_{p\text{-}CAL}$ and $V_{p\text{-}FEM}/V_{p\text{-}CAL}$ for variation of axial load ratio

To modify the calculated axial load contribution to shear resistance $V_{p,}$ parameter λ and ω were introduced. The factor λ accounts for the shear span ratio of wall, and factor ω is a modifier that accounts for increasing the depth of compression zone due to axial load. Eq. (3-21) can be rewritten as:

$$V_p = \lambda \omega P \tan\zeta \tag{3-26}$$

The parameter λ and ω were determined by conducting regression analysis to provide a reasonable fit to test data and given as:

$$\lambda = 0.35 + 0.7\frac{M}{Vl_w} \tag{3-27}$$

$$\omega = 1.0 - 1.4\frac{P}{f'_c A_g} \tag{3-28}$$

Figure 3-16 and Figure 3-17 show the relations of parameter λ and ω with shear span ratio and axial load ratio, respectively. It shows that the formula proposed in Eqs. (3-27) and (3-28) provide a good correlation with experiment and finite element data. The axial load contribution to shear resistance of experiment and finite element are predicted well by the proposed formula in Eq. (3-26) as shown in Figure 3-18.

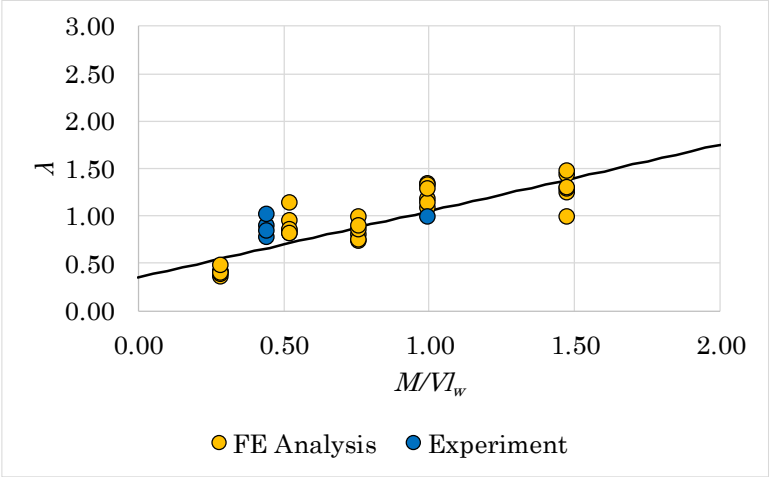

Figure 3-16 Parameter λ and shear span ratio relations

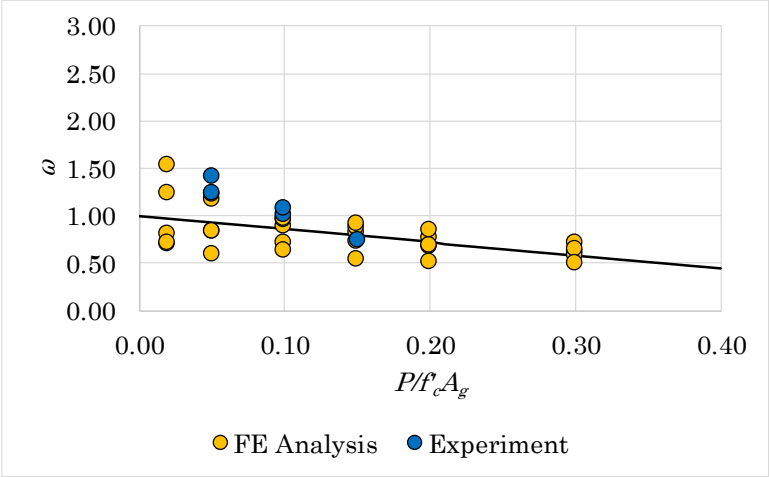

Figure 3-17 Parameter ω and ratio of axial load relations

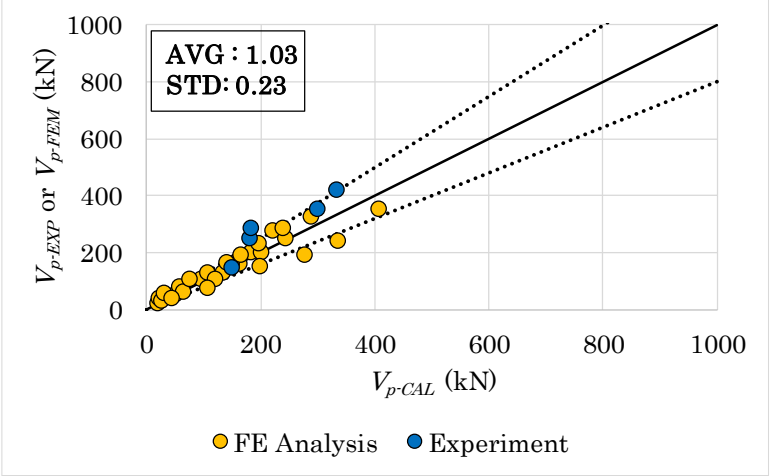

Figure 3-18 Comparison $V_{p\text{-}EXP}$ and $V_{p\text{-}FEM}$ with $V_{p\text{-}CAL}$ using Eq. (4-26)

The comparison shear strength formula between the proposed model with revised UCSD shear model for columns [26] and RC walls [11] is shown in Table 3-5.

Table 3-5 Comparison of shear strength formula

Revised UCSD (for column) Kowalsky and Priestley (2000)	Revised UCSD (for walls) Krolicki et al. (2011)	Proposed Model (for lightly RC wall)
$V_n = V_c + V_s + V_p$		
$V_c = \alpha\beta\gamma\sqrt{f_c'}\,0.8A_g$ $1 \le \alpha = 3 - \frac{M}{Vl_w} \le 1.5$ $\beta = 0.5 + 20\rho_v \le 1$ $\gamma = 0.29$, for $\mu_\Delta \le 2$ $\gamma = 0.05$, for $\mu_\Delta \ge 8$	$V_c = \alpha\beta\gamma\sqrt{f_c'}\,0.8A_g$ $\alpha = 3 - \frac{M}{Vl_w} \ge 1.0$ $\beta = 0.5 + 20\rho_v \le 1$ $\gamma = 0.29$, for $\mu_\Delta \le 2$ $\gamma = 0.05$, for $\mu_\Delta \ge 6$	$V_c = \alpha\beta\gamma\sqrt{f_c'}\,0.8A_g$ $\alpha = \frac{1}{\sqrt{\frac{M}{Vl_w}}}$ $\beta = 0.6 + 100\rho_v \le 1.25$ $\gamma = 0.29$, for $\mu_\Delta \le 2$ $\gamma = 0.05$, for $\mu_\Delta \ge 4$
$V_s = \rho_h f_{yh} t_w (l_w - c - \text{cov}) \cot\theta$ $c = 0.2 l_w$ $\theta = 30°$	$V_s = \rho_h f_{yh} t_w h_{cr}$ $h_{cr} = \frac{(l_w - c - \text{cov})}{\tan\theta_{cr}} \le h_w$ $c = 0.2 l_w$ $\theta_{cr} = \left(\frac{30° - 45°}{2}\right)\left(\frac{M}{Vl_w}\right) + 45° \ge 30°$	
$V_p = P\tan\zeta$ $\tan\zeta = \frac{l_w - c}{2h_w}$, for cantilever wall $\tan\zeta = \frac{l_w - c}{h_w}$, for wall tests loaded in double curvature		$V_p = \lambda\omega P\tan\zeta$ $\lambda = 0.35 + 0.7\frac{M}{Vl_w}$ $\omega = 1.0 - 1.4\frac{P}{f'_c A_g}$ $\tan\zeta$ is same

3.3.4 Validation with existing experimental database

The shear strength calculated by ductility dependent shear models rely on calculation of the displacement ductility factor, μ_Δ. The displacement ductility, μ_Δ, is define as the ratio of the maximum displacement, Δ_u, to the corresponding displacement at the onset of yielding, Δ_y, as follows:

$$\mu_\Delta = \frac{\Delta_u}{\Delta_y} \tag{3-29}$$

It is important to obtain yield displacement, Δ_y, in order to convert shear capacity envelope from displacement ductility to lateral drift. Priestley and Kowalsky [57] formulated the yield curvature, φ_y of rectangular walls as:

$$\phi_y = \frac{M_n}{M_y}\phi'_y \tag{3-30}$$

where M_y and φ_y are the first yield of moment and curvature, respectively, that corresponding to $\varepsilon_s = f_y/E_s$ or $\varepsilon_c = 0.002$, whichever occurs first. Nominal moment, M_n, develops when extreme compression fiber reaches 0.004 or when strain in tension reaches 0.015, whichever comes first. Eq. (3-30) can be rewritten as:

$$\Delta_y = \frac{M_n}{M_y}\Delta'_y \tag{3-31}$$

It should be noted that to obtain yield displacement, Δ_y, the summation of flexure displacement, Δ_{fy}, and shear displacement Δ_{sy} is used as the total displacement, Δ_y. The process for calculating the shear strength is summarized in the flow chart shown in Figure 3-19. The flow chart provides an outline of the recommended procedure for calculating the shear capacity envelope and load - drift response curve.

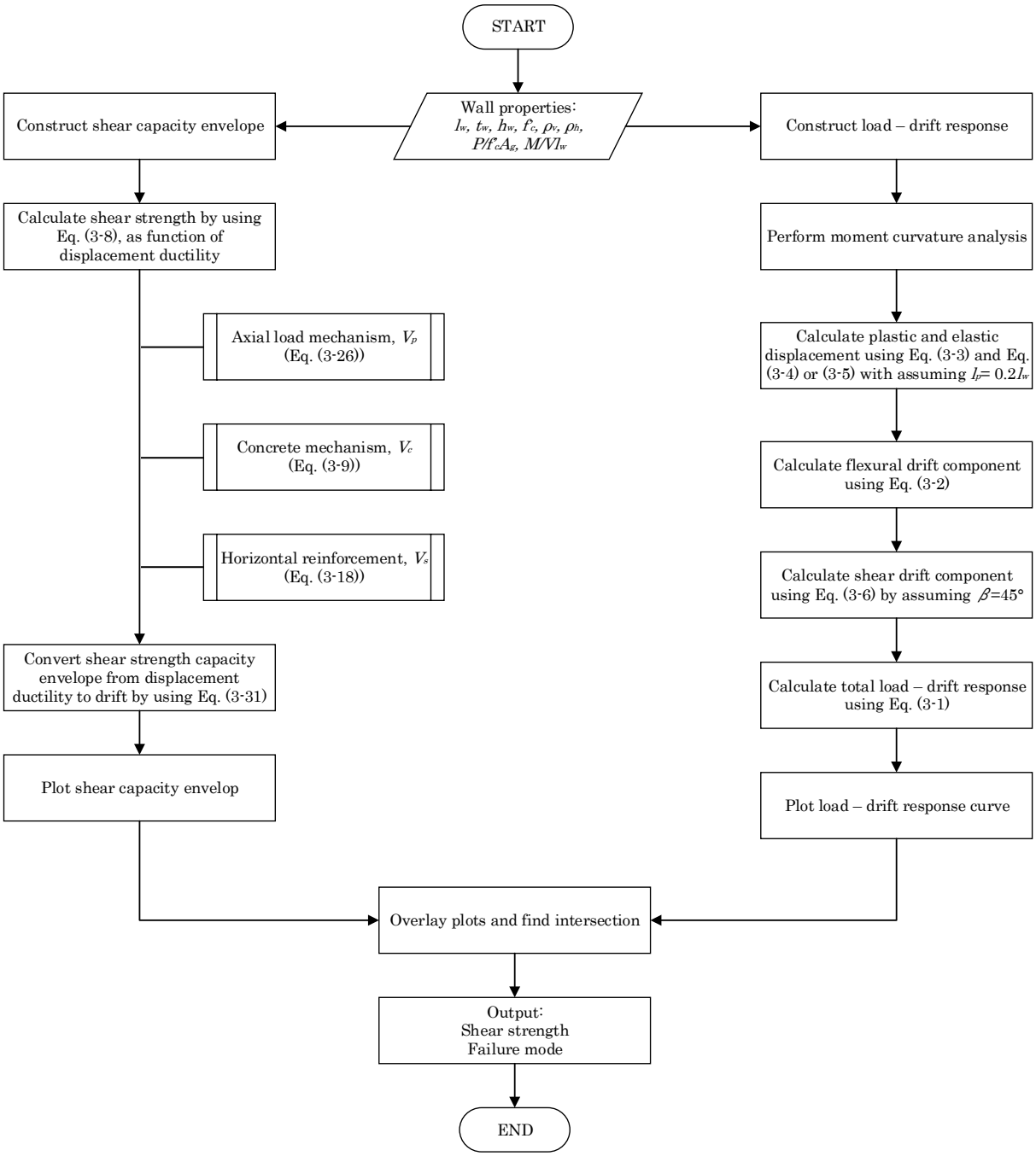

Figure 3-19 Calculation flow chart of proposed model

3.3.4.1 Experimental database

A database of relevant test results was assembled by reviewing available research to assess shear strength requirements for lightly RC walls. The available database was selected with the following criteria: (1) Rectangular wall section, (2) the specimen failed in flexure-shear or shear, (3) the wall had a single curtain of reinforcement and additional boundary vertical reinforcing bars at section ends, and (4) there was no confinement in boundary region.

The first of these is a test program of reinforced concrete walls conducted by Hidalgo et al. [27] at the Universidad Catolica de Chile in Santiago, Chile. The testing program focused on the behavior of reinforced concrete walls that exhibit shear failure through the test of 26 specimens subjected to cyclic loading in double curvature. The varying specimen parameters include the wall aspect ratio, the horizontal and vertical reinforcement ratio, and the compressive strength of concrete. The second source is from the University of California Los Angeles (UCLA) where Orakcal et al. [7] evaluated the shear strength of lightly RC wall piers and spandrel by conducting an experiment on 3/4-scale of six wall piers and eight wall spandrel specimens. The test variables of this study were axial load, shear span to wall length ratio, amount of longitudinal web reinforcement, and hooks on the transverse reinforcement. All specimens were tested under double curvature to represent the boundary conditions of an actual wall segment in a building. In addition, two wall specimens (NSW1 and NSW2) tested by the author also were included in this experimental database.

This literature review resulted in 39 experimental test specimens as shown in Table 3-6, where t_w is wall thickness, l_w is length of wall, h_w is height of wall, M/Vl_w is shear span ratio, f'_c is compressive strength of concrete, ρ_h and ρ_v are ratio of horizontal and vertical reinforcement, f_{yh} and f_{yv} are yield strength of horizontal and vertical reinforcement, respectively, and N/f'_cA_g is axial load ratio. The horizontal reinforcement ratios for the test specimens in the database were generally between 0.00 and 0.38%. All specimens had additional boundary vertical reinforcing bars at section ends. In addition, all specimens were tested under double curvature and most of the tests in the database were conducted with no axial load.

Table 3-6 Properties of lightly RC wall database

No.	Spec. No	Source	t_w	l_w	h_w	M/Vl_w	f'_c	Horizontal reinf.				Vertical reinf.			Vertical boundary reinf.	ρ_v *(%)	Axial load
			(mm)	(mm)	(mm)		(MPa)	Reinf. bar	ρ_h (%)	f_{yh} (MPa)	Hooks	Reinf. bar	f_{yv} (Mpa)	Cut bars			$(P/f'_c A_g)$
1	NSW1	Author	120	1050	2100	1.00	24.2	D10@250	0.255	347	No	D10@250	347	-	2-D13	0.629	0.00
2	NSW2	Author	120	1050	2100	1.00	24.2	D10@250	0.255	347	No	D10@250	347	-	2-D13	0.629	0.15
3	WS-T1-S1	Orakcal et al. (2009)	152	1520	1520	0.50	25.5	ϕ13@330	0.287	424	Yes	ϕ13@230	424	4 of 6	4-ϕ16	1.041	0.00
4	WS-T1-S2	Orakcal et al. (2009)	152	1520	1520	0.50	43.7	ϕ13@330	0.287	424	Yes	ϕ13@230	424	4 of 6	4-ϕ16	1.041	0.00
5	WS-T2-S1	Orakcal et al. (2009)	152	1520	1520	0.50	31.4	ϕ13@330	0.287	424	Yes	ϕ13@230	424	4 of 6	1-ϕ16 + 1-ϕ13	0.634	0.00
6	WS-T2-S2	Orakcal et al. (2009)	152	1520	1520	0.50	31.0	ϕ13@330	0.287	424	Yes	ϕ13@230	424	4 of 6	1-ϕ16 + 1-ϕ13	0.634	0.00
7	WS-T3-S1	Orakcal et al. (2009)	152	1520	1520	0.50	31.7	ϕ13@280	0.287	352	No	ϕ13@280	352	2 of 4	2-ϕ13	0.460	0.00
8	WS-T3-S2	Orakcal et al. (2009)	152	1520	1520	0.50	33.6	ϕ13@280	0.287	352	No	ϕ13@280	352	2 of 4	2-ϕ13	0.460	0.00
9	WP-T5-N0-S1	Orakcal et al. (2009)	152	1370	1220	0.45	29.9	ϕ13@305	0.286	424	No	ϕ13@330	424	-	2-ϕ13	0.446	0.00
10	WP-T5-N5-S1	Orakcal et al. (2009)	152	1370	1220	0.45	31.9	ϕ13@305	0.286	424	No	ϕ13@330	424	-	2-ϕ13	0.446	0.05
11	WP-T5-N5-S2	Orakcal et al. (2009)	152	1370	1220	0.45	32.0	ϕ13@305	0.286	424	No	ϕ13@330	424	-	2-ϕ13	0.446	0.05
12	WP-T5-N10-S1	Orakcal et al. (2009)	152	1370	1220	0.45	28.3	ϕ13@305	0.286	424	No	ϕ13@330	424	-	2-ϕ13	0.446	0.10
13	WP-T5-N10-S2	Orakcal et al. (2009)	152	1370	1220	0.45	31.4	ϕ13@305	0.286	424	No	ϕ13@330	424	-	2-ϕ13	0.446	0.10
14	1	Hidalgo et al. (2002)	120	1000	2000	1.00	19.4	ϕ6@180	0.130	392	No Data	ϕ8@167	392	-	4-ϕ18	1.864	0.00
15	2	Hidalgo et al. (2002)	120	1000	2000	1.00	19.6	ϕ8@170	0.251	402	No Data	ϕ8@167	402	-	4-ϕ18	1.864	0.00
16	4	Hidalgo et al. (2002)	120	1000	2000	1.00	19.5	ϕ8@110	0.377	402	No Data	ϕ8@167	402	-	2-ϕ22 + 2-ϕ18	2.283	0.00
17	6	Hidalgo et al. (2002)	120	1300	1800	0.69	17.6	ϕ6@180	0.131	314	No Data	ϕ8@162	314	-	4-ϕ18	1.498	0.00
18	7	Hidalgo et al. (2002)	120	1300	1800	0.69	18.1	ϕ8@170	0.256	471	No Data	ϕ8@189	471	-	4-ϕ18	1.498	0.00
19	8	Hidalgo et al. (2002)	120	1300	1800	0.69	15.7	ϕ8@170	0.256	471	No Data	ϕ8@162	471	-	4-ϕ18	1.498	0.00
20	9	Hidalgo et al. (2002)	100	1300	1800	0.69	17.6	ϕ6@110	0.267	366	No Data	ϕ6@110	366	-	2-ϕ18 + 2-ϕ16	1.597	0.00
21	10	Hidalgo et al. (2002)	80	1300	1800	0.69	16.4	ϕ6@140	0.255	367	No Data	ϕ6@140	367	-	3-ϕ18	1.658	0.00
22	11	Hidalgo et al. (2002)	100	1400	1400	0.50	16.3	ϕ6@220	0.141	362	No Data	ϕ6@110	362	-	4-ϕ16	1.351	0.00
23	12	Hidalgo et al. (2002)	100	1400	1400	0.50	17.0	ϕ6@110	0.263	366	No Data	ϕ6@220	366	-	4-ϕ16	1.250	0.00
24	13	Hidalgo et al. (2002)	100	1400	1400	0.50	18.1	ϕ6@110	0.263	370	No Data	ϕ6@110	370	-	4-ϕ16	1.351	0.00
25	14	Hidalgo et al. (2002)	80	1700	1200	0.35	17.1	ϕ6@280	0.147	366	No Data	ϕ6@140	366	-	3-ϕ16	1.095	0.00
26	15	Hidalgo et al. (2002)	80	1700	1200	0.35	19.0	ϕ6@140	0.265	366	No Data	ϕ6@280	366	-	3-ϕ16	0.991	0.00
27	16	Hidalgo et al. (2002)	80	1700	1200	0.35	18.8	ϕ6@140	0.265	366	No Data	ϕ6@140	366	-	3-ϕ16	1.095	0.00
28	21	Hidalgo et al. (2002)	100	1300	1800	0.69	24.2	-	-	-	No Data	-	-	-	3-ϕ16	0.928	0.00
29	22	Hidalgo et al. (2002)	100	1300	1800	0.69	17.2	-	-	-	No Data	-	-	-	3-ϕ16	0.928	0.00
30	23	Hidalgo et al. (2002)	100	1300	1800	0.69	24.2	ϕ6@120	0.251	431	No Data	-	-	-	3-ϕ16+ 2-ϕ18	1.711	0.00
31	24	Hidalgo et al. (2002)	100	1300	1800	0.69	23.9	-	-	-	No Data	ϕ6@110	431	-	3-ϕ16	1.124	0.00
32	25	Hidalgo et al. (2002)	100	1400	1400	0.50	23.9	-	-	-	No Data	-	-	-	3-ϕ16	0.862	0.00
33	26	Hidalgo et al. (2002)	100	1400	1400	0.50	17.7	-	-	-	No Data	-	-	-	3-ϕ16	0.862	0.00
34	27	Hidalgo et al. (2002)	100	1400	1400	0.50	23.9	ϕ6@110	0.263	431	No Data	-	-	-	2-ϕ18+ 2-ϕ16	1.302	0.00
35	28	Hidalgo et al. (2002)	100	1400	1400	0.50	23.3	-	-	-	No Data	ϕ6@110	431	-	3-ϕ16	1.064	0.00
36	29	Hidalgo et al. (2002)	80	1500	1050	0.35	23.2	-	-	-	No Data	-	-	-	3-ϕ16	1.005	0.00
37	30	Hidalgo et al. (2002)	80	1500	1050	0.35	17.9	-	-	-	No Data	-	-	-	3-ϕ16	1.005	0.00
38	31	Hidalgo et al. (2002)	80	1500	1050	0.35	23.1	ϕ6@150	0.269	431	No Data	-	-	-	4-ϕ16	1.340	0.00
39	32	Hidalgo et al. (2002)	80	1500	1050	0.35	23.3	-	-	-	No Data	ϕ6@130	431	-	3-ϕ16	1.217	0.00

*ρ_v is the ratio of total vertical reinforcement over the gross-sectional area of the member.

3.3.4.2 Shear capacity

The proposed shear model was validated using 39 lightly RC rectangular walls in database including author's specimen (NSW1 and NSW2). The shear strength of walls was obtained from the intersection between shear strength envelope and load – drift response curve. As mentioned before, this proposed model was extended from revised UCSD shear model for RC walls that was developed by Krolicki et al. [11]. The calculated shear capacity from the proposed and Krolicki et al.'s model is compared to the recorded strength of the test specimen in database.

Figure 3-20 and Figure 3-21 show the shear strength correlation between experiment and calculated shear strength using proposed model and Krolicki et al.'s model. Both models predicted well the shear capacity of lightly RC walls. However, the proposed shear model resulted in a closer average ratio of experimental to predicted shear strength and improves the dispersion of the results from Krolicki et al.'s model. In addition, Krolicki et al.'s model cannot predict shear strength NSW2 and WP-T5-N10-S2 where for both specimens were loaded under axial load 0.15 and 0.10, respectively. The load – drift response curve did not cross the shear strength envelope due to overestimate of calculated axial load contribution to shear strength. This overestimate prediction probably caused by the constant value of compression zone, c (=0.2l_w) that used in the calculation. In fact, as the axial load increases, the depth of the compression zone c increases and as a result the effectiveness of the axial load contribution to wall shear strength will decrease. However, the proposed model has considered this matter. The correlation of the proposed model against axial load ratio (N/f'_cA_g), compressive strength of concrete (f'_c), ratio of horizontal reinforcement (ρ_h), shear span ratio (M/Vl_w), and ratio of vertical reinforcement (ρ_v) is shown in Figure 3-24(a).

The shear capacity of the test specimen in database was also computed using Arakawa's Equation and ACI 318 as shown in Figure 3-22 and Figure 3-23, respectively. For Arakawa's equation, as decrease of shear span ratio (M/Vl_w), the calculated shear strength was underestimate as shown in Figure 3-24(b). This is because the formula restricts the shear span ratio should be larger than 1.0. As consequence, the concrete contribution to shear strength is constant for walls with shear span ratio less than 1.0. In addition, the shear strength of NSW1 was overestimated by Arakawa's equation. The ACI 318 provisions for calculating nominal shear strength substantially underestimates the shear strength of the lightly RC walls subjected to even under no axial loads (V_{EXP}/V_{CAL}= 1.34) as shown in Figure 3-23 and Figure 3-24(c). This finding is expected, because the influence of axial load on the shear strength of concrete is not considered in the ACI 318 nominal shear strength calculation; however, the level of conservatism is cause for concern for evaluation of existing buildings, as it may lead to erroneous prediction of soft-story failures and produce costly, unnecessary retrofits.

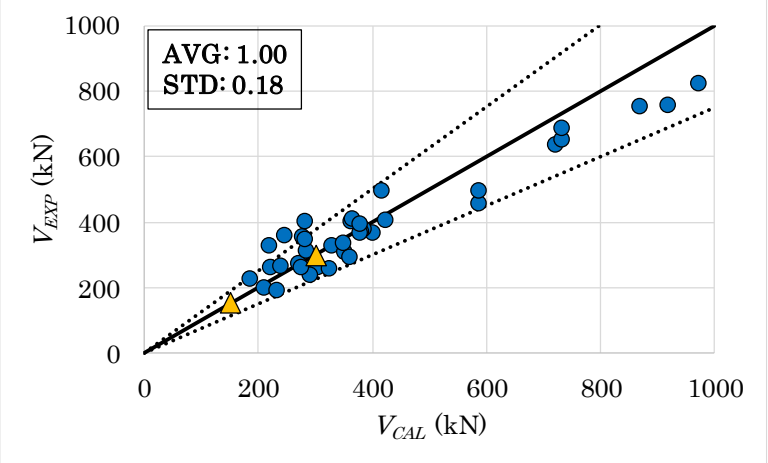

Figure 3-20 V_{EXP} vs V_{CAL} of proposed model

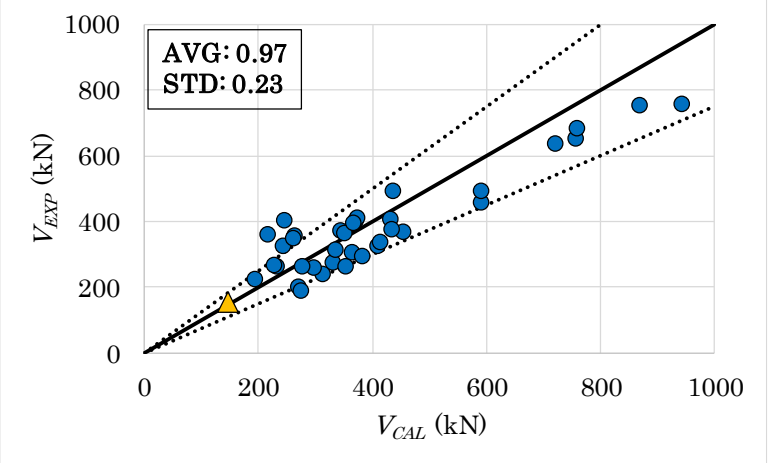

Figure 3-21 V_{EXP} vs V_{CAL} of revised UCSD model for RC walls

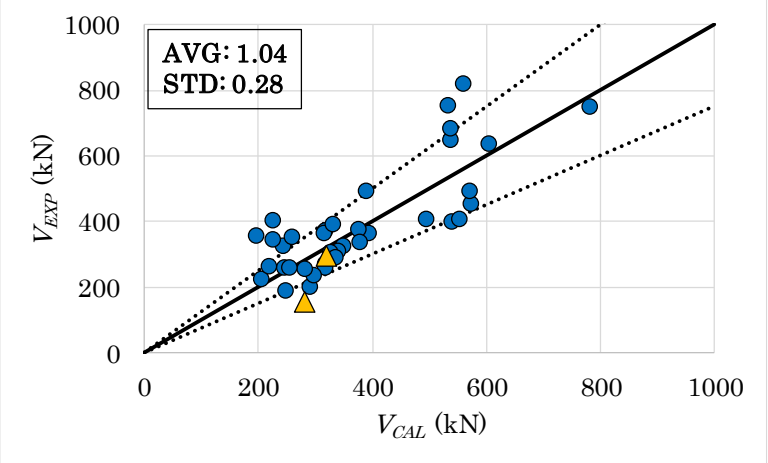

Figure 3-22 V_{EXP} vs V_{CAL} of Arakawa's equation

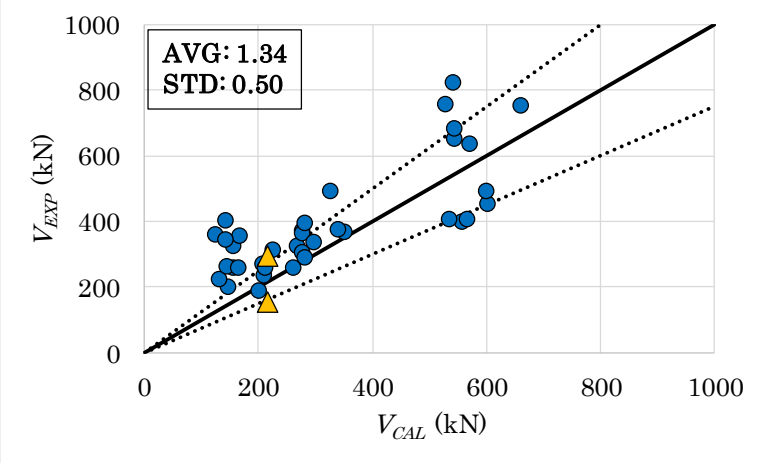

Figure 3-23 V_{EXP} vs V_{CAL} of ACI 318

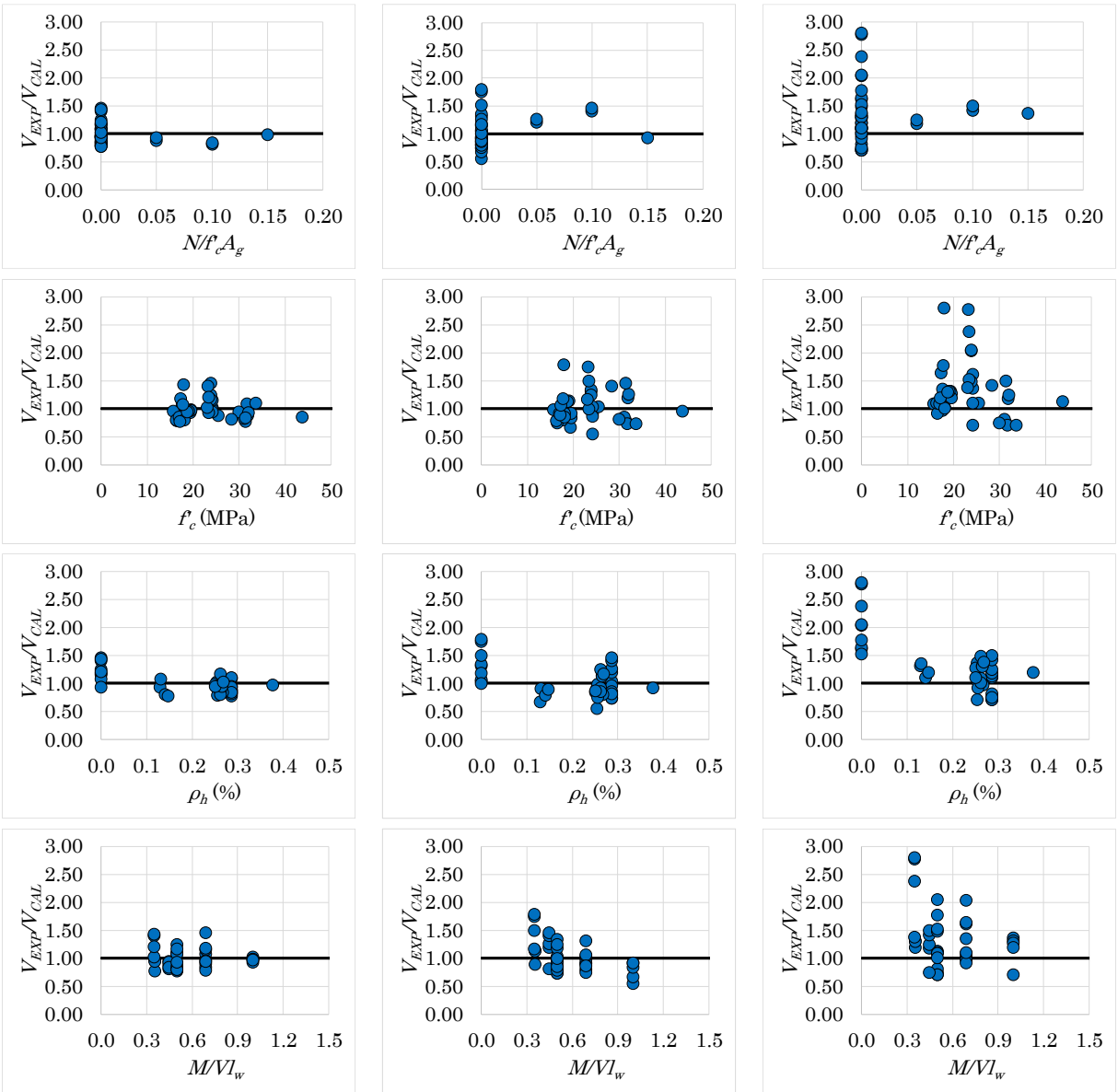

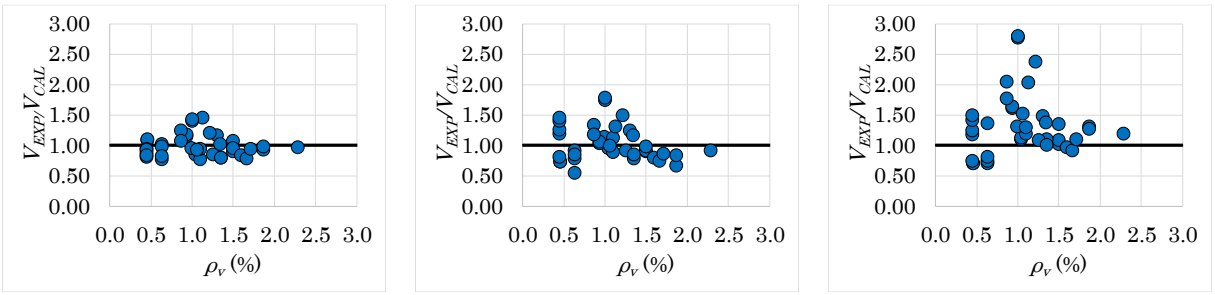

(a) Proposed model (b) Arakawa's equation (c) ACI 318

Figure 3-24 Comparison of shear strength models for different variables

3.3.4.3 Failure mode

The identification of failure mode can help engineers determine the limiting behavior of a wall or lateral system and help determine the course of action, whether it retrofit or new design. To determine the failure mode, the calculated shear strength envelopes are plotted with the load – drift response for all specimens of the collected database including Author's specimens. Based on the criteria shown in Figure 3-25, the intersection of the curves yields three possible failure modes, flexure, flexure-shear, and shear. Flexure failure is governed by concrete crushing after yielding of the reinforcing bar. Flexure-shear failure is identified by a rapid degradation of the shear resisting concrete mechanism due to cyclic loading after flexural yielding has occurred. This rapid loss of shear resistance can be seen in the hysteretic response by strength degradation on subsequent loading cycles beyond the peak strength. Therefore, members failing in flexure-shear have very limited displacement ductility. Shear failure is defined as a member loss of strength from a shear failure in diagonal tension prior to reaching flexural yield. Indications of shear failure are when the maximum experimental strength of the specimen does not reach the flexural first yield, followed by rapid strength degradation after the maximum strength is reached. The proposed shear model is used to identify the failure modes of all walls in shear and flexure-shear database. Figure 3-26 shows plotting of shear strength envelope and load drift response for all specimens to determine failure mode. The proposed shear model is found to correctly predict shear failures and flexure-shear failure for all specimens of the collected database. It should be noted that failure mode of NSW2 is classified as flexure-shear since flexural yielding has occurred before loss of strength.

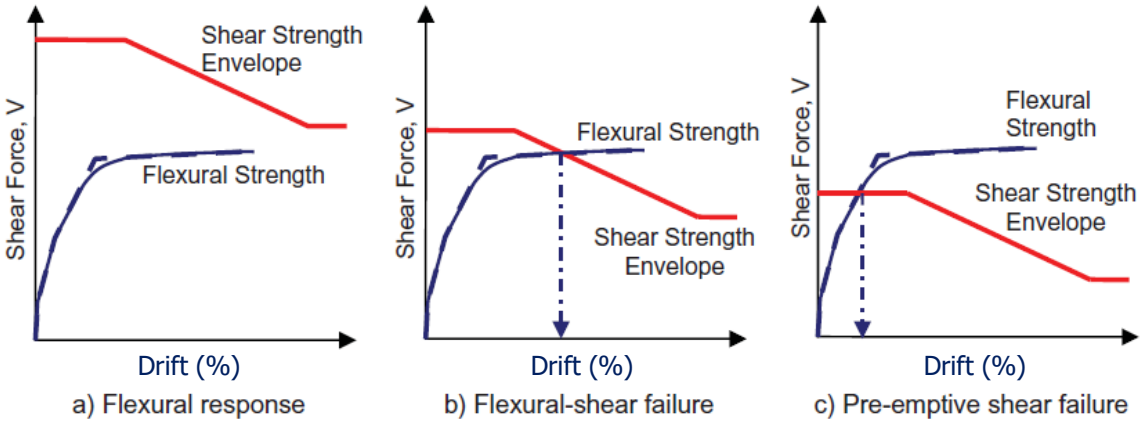

Figure 3-25 Failure modes categories of reinforced concrete walls

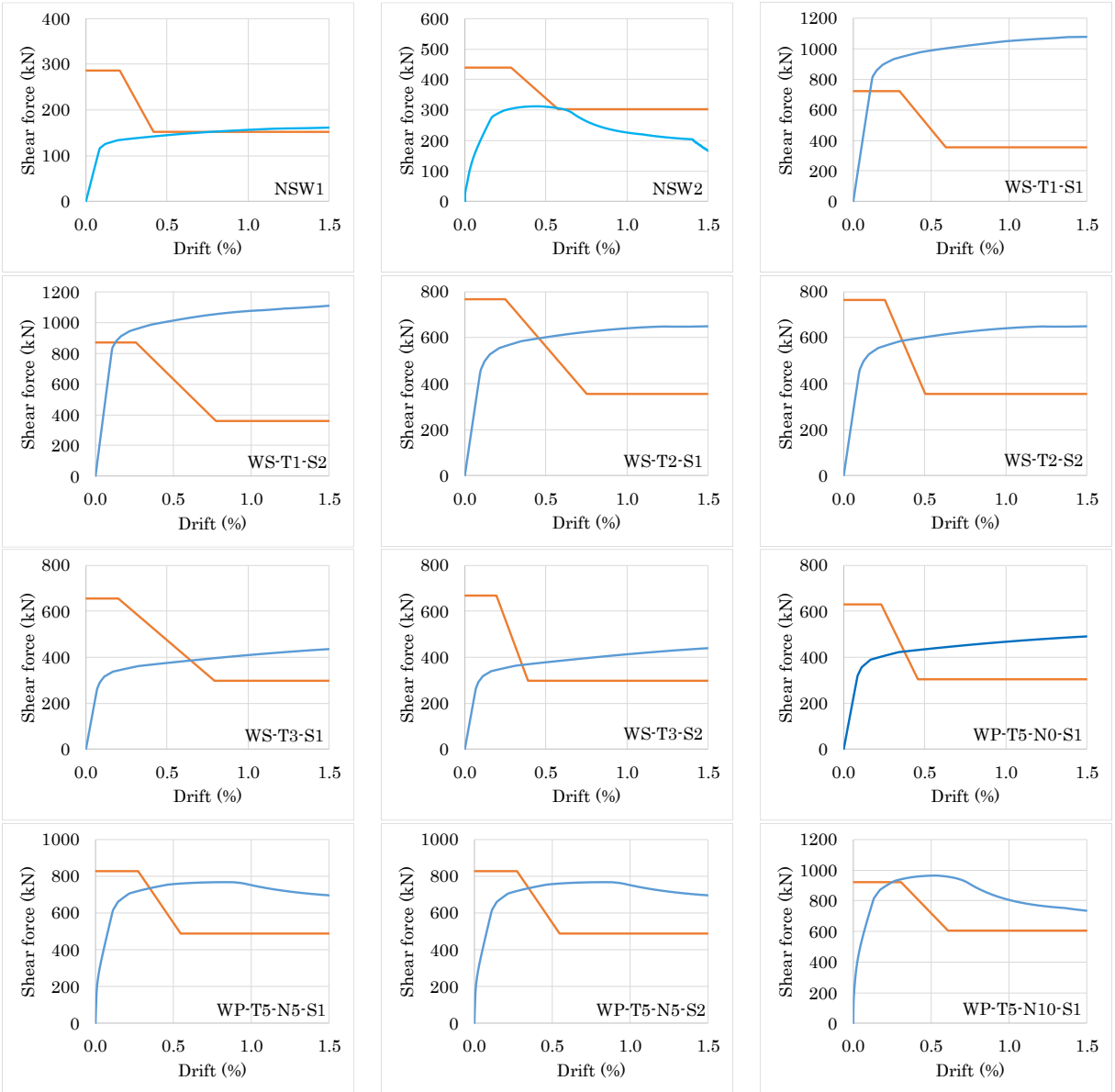

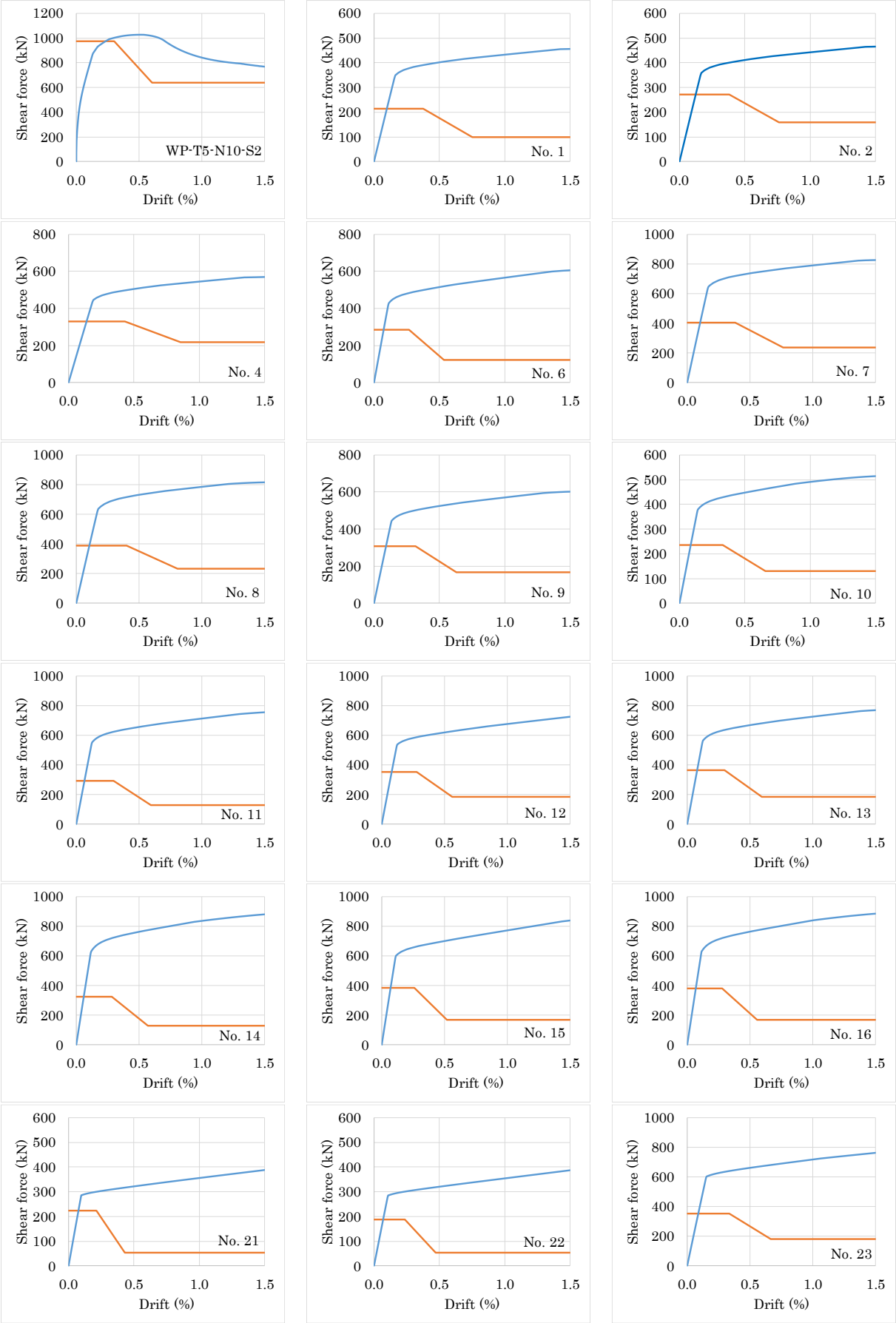
Shear force (kN)
Drift (%)
WP-T5-N10-S2
No. 1
No. 2
No. 4
No. 6
No. 7
No. 8
No. 9
No. 10
No. 11
No. 12
No. 13
No. 14
No. 15
No. 16
No. 21
No. 22
No. 23

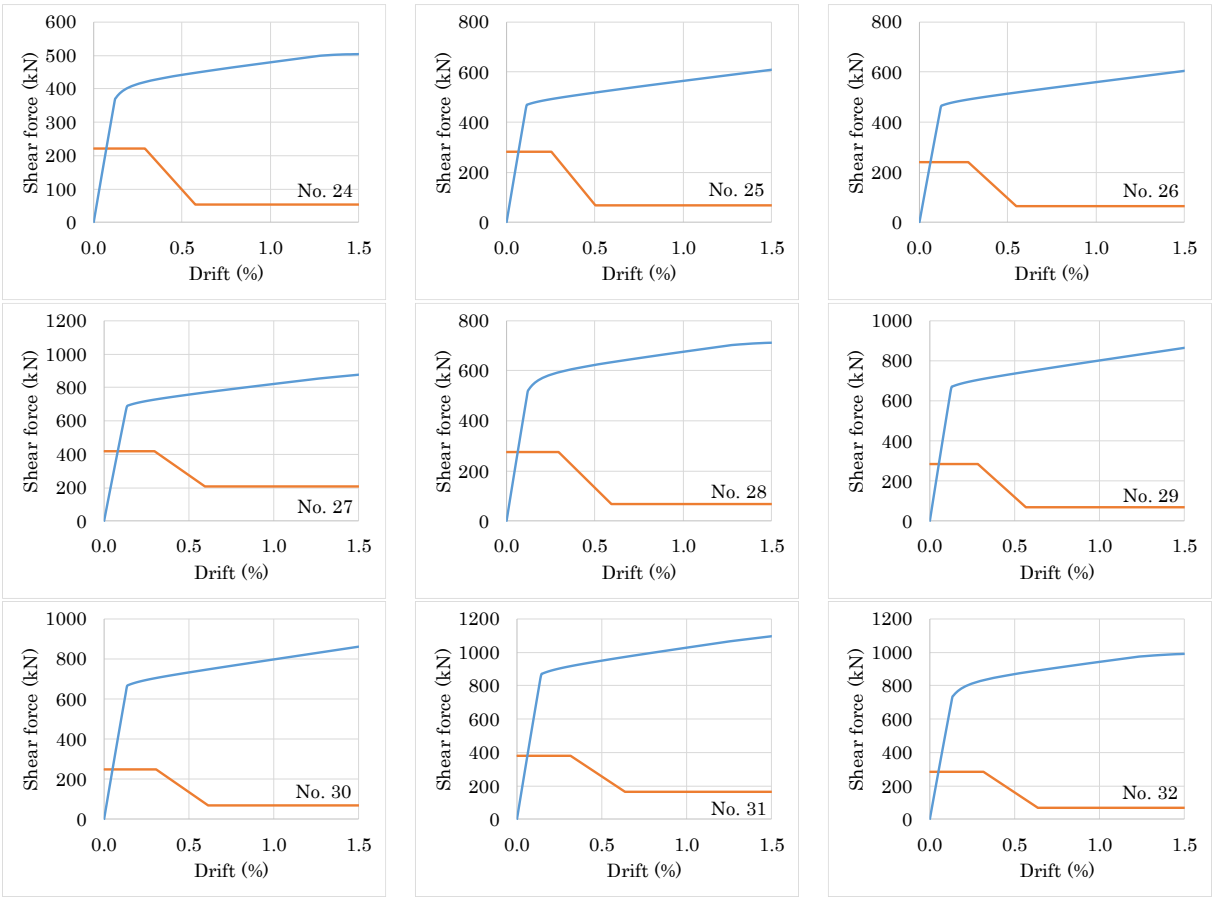

Figure 3-26 Shear strength envelope and load – drift response of all specimens

3.4 Validation of Backbone Curve

A performance-based design can be defined as a systematic method of designing structural systems to achieve a predictable and desirable performance of both structural and non-structural elements under actions the system undergoes during its lifetime. In order to ensure the desirable performance of buildings at different design levels, the strength, stiffness, and deformability of the structures should be reasonably proportioned. To achieve this goal, it should be clearly understood which one of these structural characteristics primarily governs the design at different performance levels. The Performance-Based Seismic Design (PBSD) approach involves not only the analysis and design of the structure for sustaining the seismic demands but also comprises the seismic behavior in terms of the displacement capacity and its residual performance. In the context of PBSD, performance levels are introduced as limiting values of performance indicators that can be measured in the structural response.

The ASCE/SEI 41-13 [12] includes backbone curves for creating nonlinear models. It adopts Wallace's [13] modification to the backbone curve for the behavior of RC walls governed by shear in order to include the cracking point F (shear strength ratio at cracking, V_{cr}/V_n), as shown in Figure 3-27. This curve shows the normalized shear capacity of the wall versus the drift. The strength at points B and C are both taken to be the nominal shear strength, which is calculated using Section

18.10.4 of ACI 318-14 [23]. The yield drift ratio is show as g, the drift ratio corresponding to the start of shear strength degradation is shown as d, and the maximum drift ratio is shown as e. The strength ratio for yielding is shown as f, and the strength ratio for residual strength is shown as c. The drift and strength ratio based on ASCE/SEI 41-13 [12] is presented in Table 3-7. The limit states in ASCE 41-13 are classified as immediate occupancy (IO), life safety (LS) and collapse prevention (CP).

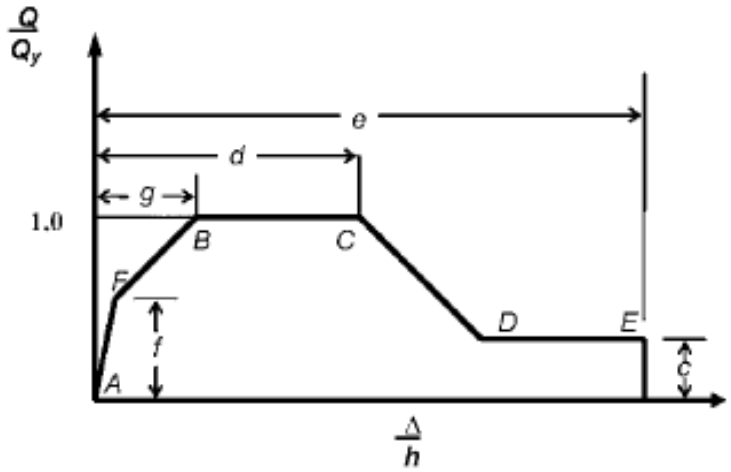

Figure 3-27 Generalized force – deformation relation for concrete elements [12]

The shear strength at cracking, V_{cr}, and the drift angle at cracking, γ_{cr}, are calculated using the following equations.

$$V_{cr} = 0.6V_n \tag{3-32}$$

$$V_n = A_{cv}(\alpha_c \lambda \sqrt{f'_c} + \rho_t f_y) \tag{3-33}$$

$$\gamma_{cr} = \frac{V_{cr}}{0.4EA} \tag{3-34}$$

where the coefficient α_c is 0.25 for height-to-length ratios (h_w/l_w) ≤ 1.5, is 0.17 for h_w/l_w ≥ 2.0, varies linearly between 0.25 and 0.17 for h_w/l_w between 1.5 and 2.0. In this equation, A_{cv} is the cross-sectional web area of a wall, ρ_t is transverse reinforcement ratio, f_y is the yield strength of transverse reinforcement, and f'_c is the compressive strength of concrete. The variation of α_c for h_w/l_w between 1.5 and 2.0 accounts for the observed increase contribution of concrete in low h/l walls. A is the wall gross area, and E is the modulus of elasticity of the concrete that is calculated based on ACI 318-14 [23].

$$E = 4700\sqrt{f'_c} \quad \text{(MPa)} \tag{3-35}$$

Table 3-7 Modeling parameters and numerical acceptance criteria for nonlinear procedures for RC walls controlled by shear

Conditions	Drift (%)			Strength ratio		Acceptable drift (%)		
						Performance level		
	d	e	g	c	f	IO	LS	CP
$\frac{(A_s - A'_s) f_y + P}{t_w l_w f'_c} \le 0.05$	1.00	2.00	0.40	0.20	0.60	0.40	1.50	2.00
$\frac{(A_s - A'_s) f_y + P}{t_w l_w f'_c} > 0.05$	0.75	1.00	0.40	0.00	0.60	0.40	0.75	1.00

Note: A_s is area of non-prestressed tension reinforcement, A'_s is area of compression reinforcement, P is axial load, f_y is yield strength of longitudinal reinforcement, f'_c is compressive strength of concrete.

Wallace's recommended backbone curve using the ACI 318-14 Section 18.10.4 equation for peak strength is plotted with the wall database force-drift response in Figure 3-28 (left side). The initial stiffness is taken as the shear stiffness, equal to $0.4E_c$, as recommended. Wallace's envelope using ACI 318-14 Section 18.10.4 for peak strength significantly overestimated the data. However, the initial stiffness recommended by Wallace was higher than that observed experimentally. Some modifications were attempted to provide a good agreement to the available data. Proposed shear strength in Section 3.3 was used for peak strength. Proposed modeling parameters and numerical acceptance criteria for nonlinear procedures for RC walls controlled by shear are presented in Table 3-8.

The additional conditions of shear span to length ratio (M/Vl_w) were added to the proposed modeling parameters as shown in Table 3-8. The shear strength at cracking, V_{cr}, was reduced to $0.5V_n$ for walls with low axial load ratio (≤ 0.05). In addition, it is logical that the stiffness be greater for walls with smaller aspect ratios, as the confinement effect of the adjacent members is greater in these situations. Therefore, the drift angle at cracking, γ_{cr}, were modified as follow.

$$\gamma_{cr} = \frac{V_{cr}}{(0.4)0.4EA}, \text{ for walls with } M/Vl_w > 0.5: \tag{3-36}$$

$$\gamma_{cr} = \frac{V_{cr}}{(0.7)0.4EA}, \text{ for walls with } M/Vl_w \le 0.5: \tag{3-37}$$

The plot from Figure 3-28 (left side) is repeated in Figure 3-28 (right side) with the modification to the initial stiffness in Wallace's backbone curve. Also, the shear strength at cracking, V_{cr}, was

reduced to $0.5V_n$ for walls with low axial load ratio (≤ 0.05). This modification provides a good estimate to the wall database force-drift response.

Table 3-8 Proposed modeling parameters and numerical acceptance criteria for nonlinear procedures for RC walls controlled by shear

Conditions	Drift (%)			Strength ratio		Acceptable drift (%) Performance level		
	d	e	g	c	f	IO	LS	CP
$\frac{(A_s - A'_s) f_y + P}{t_w l_w f'_c} \leq 0.05$ $\frac{M}{Vl_w} > 0.5$	1.00	2.00	0.40	0.20	0.50	0.40	1.50	2.00
$\frac{(A_s - A'_s) f_y + P}{t_w l_w f'_c} \leq 0.05$ $\frac{M}{Vl_w} \leq 0.5$	0.75	1.50	0.40	0.20	0.50	0.40	1.50	2.00
$\frac{(A_s - A'_s) f_y + P}{t_w l_w f'_c} > 0.05$	0.75	1.00	0.40	0.00	0.60	0.40	0.75	1.00

Note: A_s is area of non-prestressed tension reinforcement, A'_s is area of compression reinforcement, P is axial load, f_y is yield strength of longitudinal reinforcement, f'_c is compressive strength of concrete.

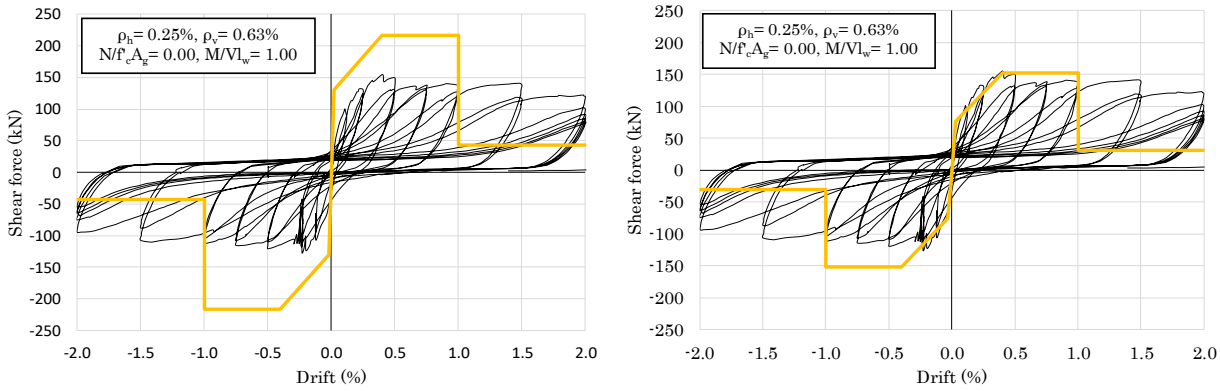

(a) NSW1 (Author's specimen)

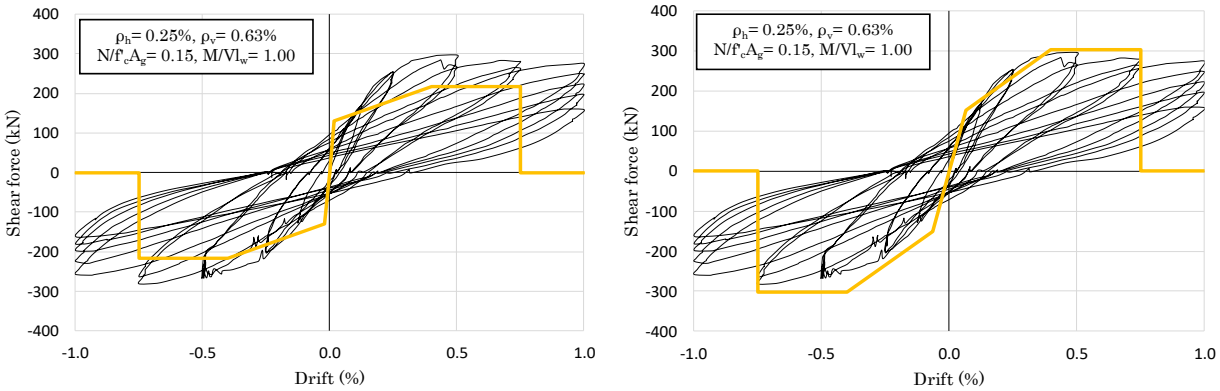

(b) NSW2 (Author's specimen)

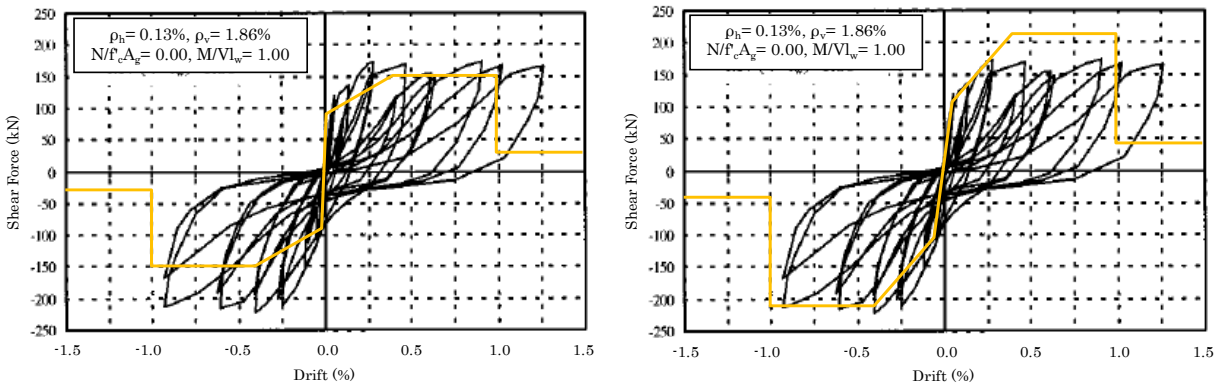

(c) No. 1 (Hidalgo et al.'s specimen [27])

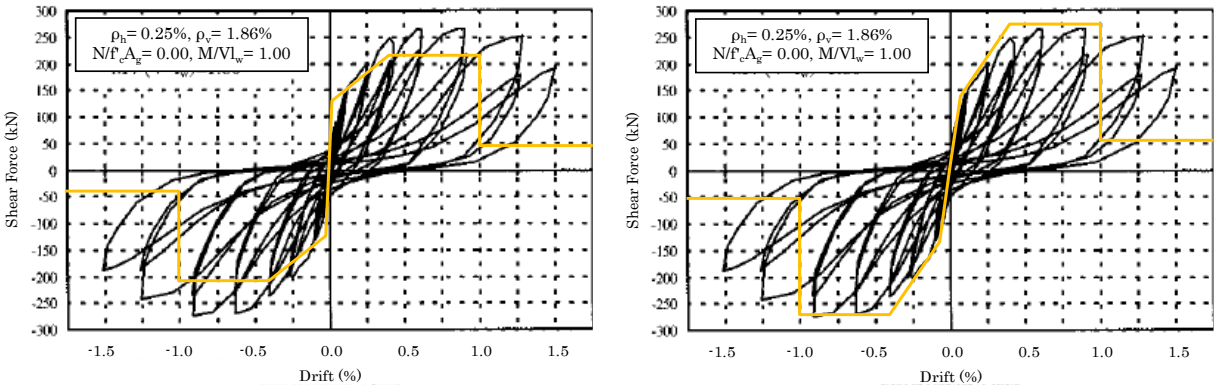

(d) No. 2 (Hidalgo et al.'s specimen [27])

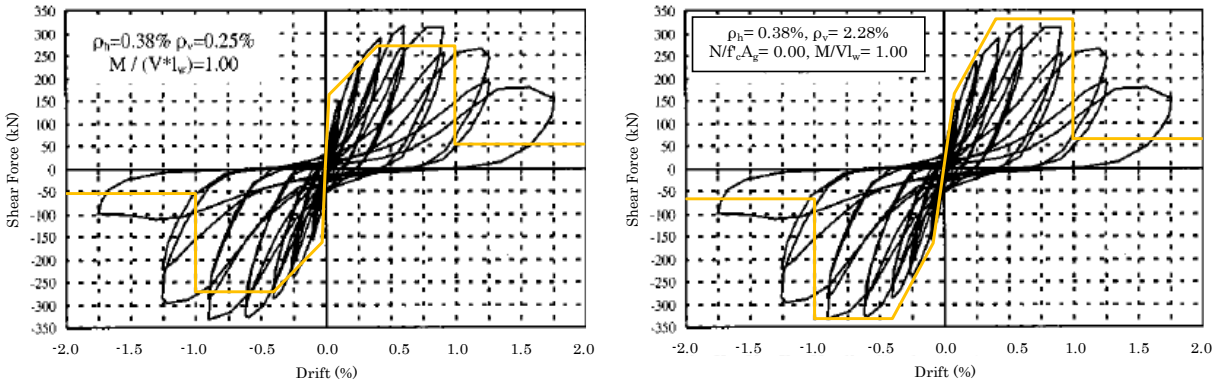

(e) No. 4 (Hidalgo et al.'s specimen [27])

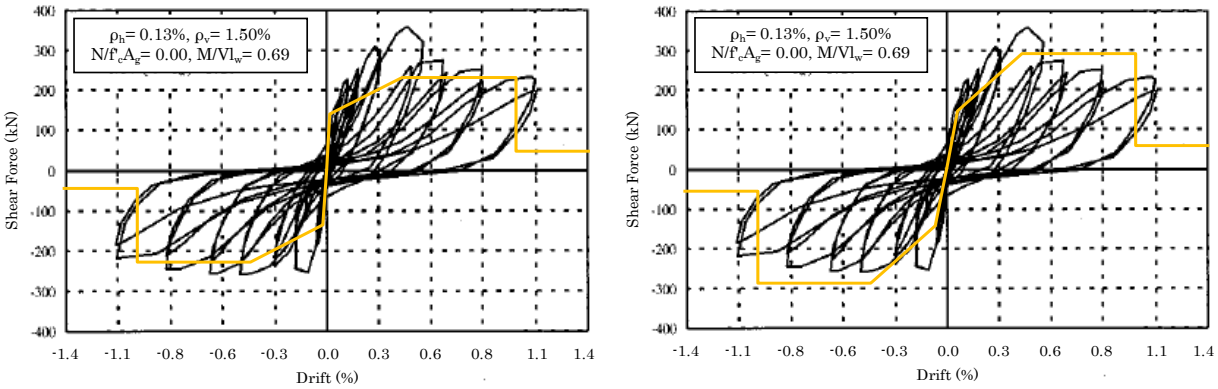

(f) No. 6 (Hidalgo et al.'s specimen [27])

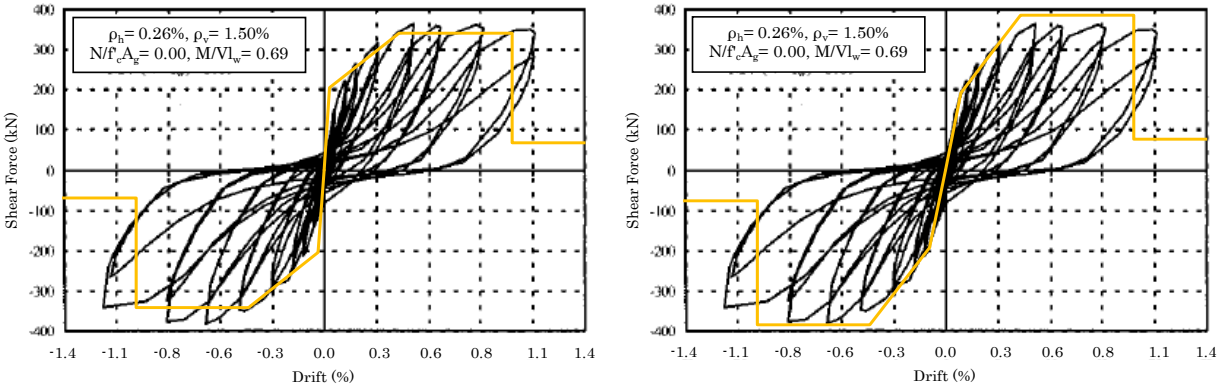

(g) No. 8 (Hidalgo et al.'s specimen [27])

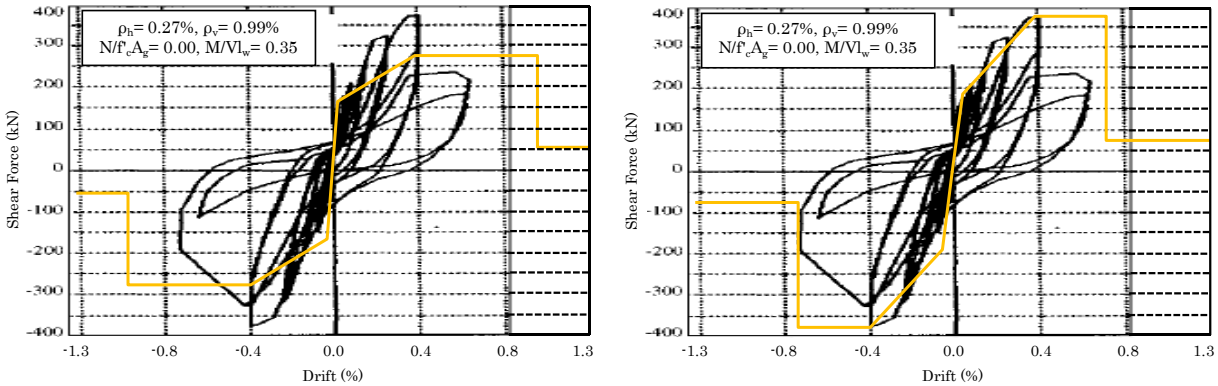

(h) No. 15 (Hidalgo et al.'s specimen [27])

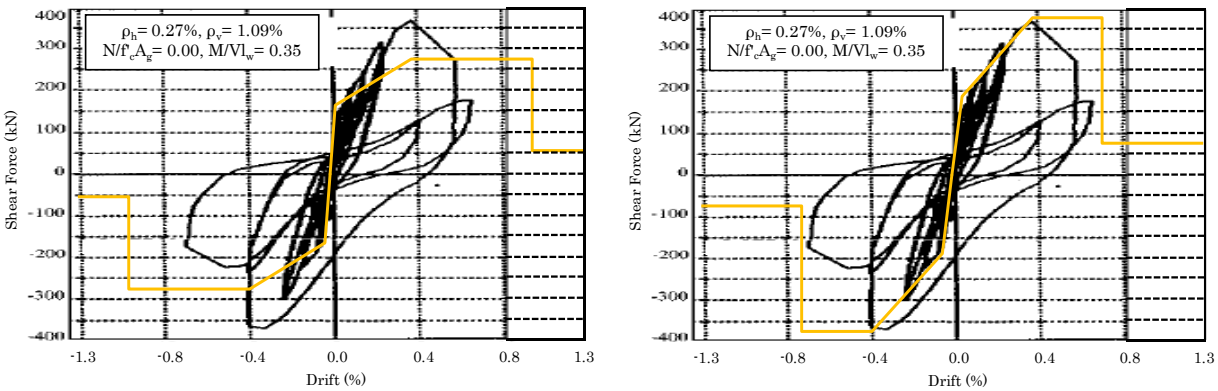

(i) No. 16 (Hidalgo et al.'s specimen [27])

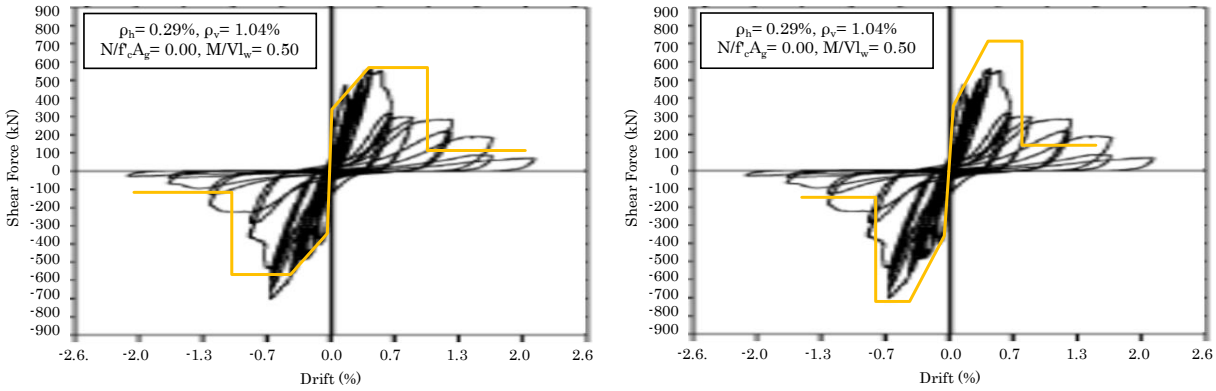

(j) WS-T1-S1 (Orakcal et al.'s specimen [7])

Figure 3-28 Comparison of ASCE-41 (left) and proposed (right) backbone curves

3.5 Conclusions

A new shear strength model was proposed by modifying revised UCSD shear model for RC walls [11]. An experimental database of 39 rectangular walls is used in the formulation of the proposed shear model. The available database was selected with the following criteria: (1) Rectangular wall, (2) the specimen failed in flexure-shear or shear, (3) the wall had a single curtain of reinforcement and additional boundary vertical reinforcing bars at section ends, and (4) there was no confinement in boundary region. Attempts have been made in the formulation of the proposed shear model to improve the calculation of the primary components contributing to the shear resistance of lightly RC walls. The focus of the proposed changes to the revised UCSD shear model for RC walls are on the contribution of the axial load and concrete shear resisting mechanisms. The recommended changes to improve the concrete contribution to shear resistance by modifying the variable α and β, reduce the upper limit of displacement ductility, introduce parameter λ and ω to modify the calculated axial load contribution to shear resistance, which the factor λ accounts for the shear span ratio of wall, and factor ω is a modifier that accounts for increasing the depth of compression zone due to axial load. The proposed model is expressed as:

$$V_n = V_c + V_s + V_p$$

The contribution of concrete, V_c:

$$V_c = \alpha\beta\gamma\sqrt{f_c'}\,0.8A_g$$

$$\alpha = \frac{1}{\sqrt{\frac{M}{Vl_w}}}$$

$$\beta = 0.6 + 100\rho_v \leq 1.25$$

$\gamma = 0.29$, for $\mu_\Delta \leq 2$

$\gamma = 0.05$, for $\mu_\Delta \geq 4$

Contribution of horizontal reinforcement, V_s:

$$V_s = \rho_h f_{yh} t_w h_{cr}$$

$$h_{cr} = \frac{(l_w - c - \text{cov})}{\tan\theta_{cr}} \leq h_w$$

$$c = 0.2 l_w$$

$$\theta_{cr} = \left(\frac{30° - 45°}{2}\right)\left(\frac{M}{Vl_w}\right) + 45° \geq 30°$$

And the contribution of axial load, V_p:

$$V_p = \lambda\omega P \tan\zeta$$

$$\lambda = 0.35 + 0.7\frac{M}{Vl_w}$$

$$\omega = 1.0 - 1.4\frac{P}{f'_c A_g}$$

$\tan\zeta = \frac{l_w - c}{2h_w}$, for cantilever wall

$\tan\zeta = \frac{l_w - c}{h_w}$, for wall tests loaded in double curvature

where parameter α accounts for the effect of shear span ratio, parameter β accounts for the increase in shear resistance proportional to increasing ratio of vertical reinforcement, parameter γ represents the reduction in strength of the concrete shear resisting mechanism with increasing ductility, f'_c is

compression strength of concrete, A_g is cross sectional area of wall, M/Vl_w is shear span ratio, ρ_v is ratio of vertical reinforcement, μ_Δ is displacement ductility, ρ_h is ratio of horizontal reinforcement, f_{yh} is yield strength of horizontal reinforcement, t_w is thickness of wall, h_{cr} is vertical crack height, l_w is length of wall, c is compression zone depth, cov is cover concrete thickness of wall, θ_{cr} is average cracking angle, h_w is height of wall, factor λ accounts for the shear span ratio of wall, factor ω is a modifier that accounts for increasing the depth of compression zone due to axial load, P is axial load, and ζ is inclined strut angle.

Based on the analysis, the proposed shear model results in a closer average ratio of experimental to predicted shear strengths and improves the dispersion of the results from Krolicki et al.'s model (revised UCSD model for RC walls). In addition, the proposed shear model is found to correctly predict shear failures and flexure-shear failure for all specimens of the collected database. Based on these results the proposed shear model is recommended for the calculation of the shear strength of lightly RC walls. It is envisioned that the proposed shear model can be used as a new tool for the assessment or design of lightly reinforced concrete walls in existing buildings or in the design of new structures.

A proposed backbone curve for performance based design were developed by modifying ASCE/SEI 41-13 and Wallace's backbone curve. The modification accounted the effects of axial load and shear span ratio to the shear strength at cracking, V_{cr}, and the drift angle at cracking, γ_{cr}. In addition, proposed shear model in Section 3.3 was used to compute the peak strength for the backbone curve. The modification provided a good estimate to the wall database force-drift response.

4 EXPERIMENTAL 1: SEISMIC BEHAVIOR OF AS-BUILT LIGHTLY REINFORCED CONCRETE WALLS

4.1 Introduction

Masonry walls are generally used as infills in reinforced concrete (RC) frames in many countries [58][59]. In Japan, however, RC moment resisting-frames are usually constructed monolithically with lightly reinforced infill walls with opening (spandrels, wall piers, and wing walls). Although such walls are connected rigidly to the surrounding frame, structural engineers do not necessarily treat them as structural components [60] due to large openings and often neglect their contributions to the lateral load carrying capacities in practical structural designs. In the 2011 off the Pacific coast of Tohoku Earthquake, many lightly RC walls in residential and government office buildings suffered severe damage as shown in Figure 4-1. Such damage may not hinder the building safety but is likely to suspend the continuity of the building functions.

(a) Building A (b) Building B (c) Building C

Figure 4-1 Damage of Lightly RC walls after the 2011 Tohoku Earthquake [61][62]

This section treats experimental studies on four lightly RC wall specimens to study the effects of axial force, amount of shear reinforcement, and shear span to wall length ratio on damage process. The main objective is to obtain fundamental data, such as damage state, load carrying capacity, and failure mode of lightly RC walls under seismic loading. The damage processes with ultimate failure mode are reported in detail.

4.2 Experimental Program

4.2.1 Specimen description and materials

The test series included four specimens focusing on damage processes and failure modes of lightly RC walls as shown in Table 4-1. Figure 4-2 shows configuration and reinforcement details of specimens. Experimental parameters were axial load, amount of shear reinforcement, and shear

span to wall length ratio. The cross section of all specimens was 120 mm x 1050 mm with height of 2100 mm.

NSW1 and NSW2 were identical except axial load level. Two D13 reinforcing bars were provided as vertical reinforcement at the either end region, while D10 bars were used at 250 mm spacing as both vertical and horizontal reinforcement. NSW3 and NSW4 were identical except shear span to wall length ratio. They had double amount of horizontal reinforcement compared to that of NSW1 and NSW2. In addition, horizontal reinforcement of NSW3 and NSW4 had 180-degree hook anchorage at both ends as recommended by Mizutani et al. [63] to increase shear capacity and improve bond performance of longitudinal reinforcement. The measured mechanical properties of concrete and reinforcing bars are shown in Table 4-2 and Table 4-3, respectively. All mechanical properties of the materials comply the specifications (f'_c= 24 MPa and JIS G 3112 [64] for concrete and reinforcement, respectively).

Table 4-1 Specification of specimens

Specimen		NSW1	NSW2	NSW3	NSW4
Configuration	Wall thickness(mm)	120	120	120	120
	Wall length (mm)	1050	1050	1050	1050
	Wall height (mm)	2100	2100	2100	2100
	Vertical bars at end regions	2-D13	2-D13	2-D13	2-D13
	Vertical bars	D10@250	D10@250	D10@250	D10@250
	Horizontal bars	D10@250	D10@250	D10@125	D10@125
	Ratio of horizontal bars (p_{wh})	0.24%	0.24%	0.48%	0.48%
	180-degree hook anchorage at horizontal bars	No	No	Yes	Yes
Loading conditions	Shear span (mm)	1050	1050	1050	2100
	Shear span to wall length ratio (M/Vl_w)	1	1	1	2
	Axial force, N (kN)	0	458	458	458
	$P/f'_c A_g$	0	0.15	0.15	0.15

f'_c: compressive strength of concrete cylinders, A_g: gross cross-sectional area of wall

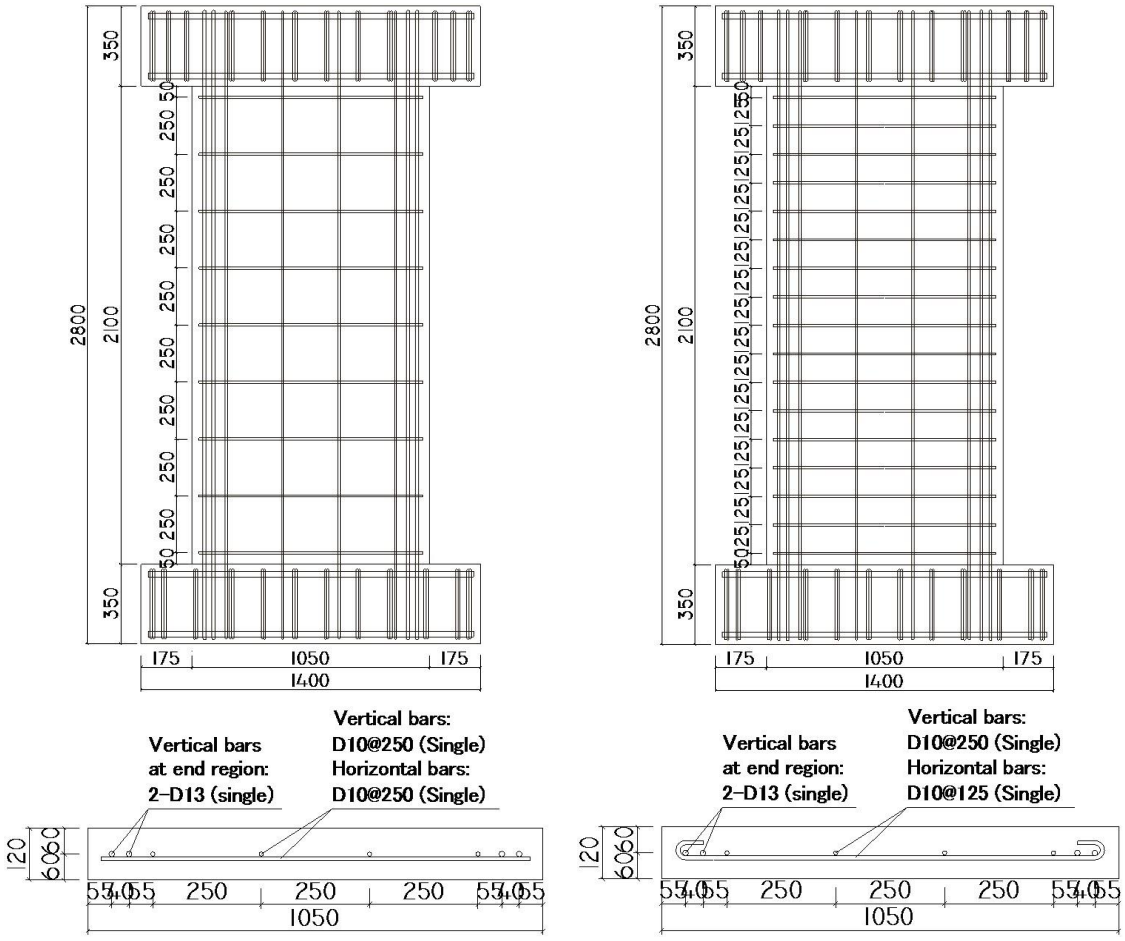

(a) NSW1 and NSW2 (b) NSW3 and NSW4

Figure 4-2 Dimensions and reinforcing details of specimens (unit in mm)

Table 4-2 Mechanical properties of concrete

f'_c (N/mm^2)	ε_c (%)	E_c (kN/mm^2)	f_t (N/mm^2)
24.2	0.182	26.3	2.46

f'_c: compressive strength of concrete cylinders,

ε_c: strain at compressive strength,

E_c: Young's modulus, f_t: splitting tensile strength

Table 4-3 Mechanical properties of steel reinforcing bars

Diameter (mm)	f_y (N/mm^2)	f_u (N/mm^2)	E_s (kN/mm^2)	ε_y (%)
D10 (SD295A)	347	484	190	0.183
D13 (SD345)	360	527	190	0.189

f_y: yield strength, f_u: tensile strength,

E_s: Young's modulus, ε_y: yield strain

4.2.2 Design of specimens (strength and damage process)

Based on Section 4.2.1, strength and damage process were studied before loading test. NSW1 is the prototype specimen, which represents a typical lightly RC wall. In an ordinary Japanese design practice, lightly RC walls are designed with no axial load. Hence, no axial force was loaded for NSW1. However, many of lightly RC walls suffered shear failure during the 2011 off the Pacific coast of Tohoku Earthquake. It was considered that the shear failure occurred as the flexural capacity increased due to axial compression force exerted by surrounding frames under seismic loading. Hence, NSW2 was designed to carry axial compression load so that it fails in shear. The same magnitude of axial compression force was applied to NSW3 and NSW4 but they were designed to fail in flexure by increasing horizontal reinforcement (NSW3) or increasing shear span to wall length ratio (NSW4).

The magnitude of axial force ratio in experiment was obtained from three lightly RC walls that experienced severe damage after the 2011 Tohoku Earthquake as showed in Figure 4-1 and Table 4-4. The flexural and shear capacities of three walls were calculated using Eq. (4-1) and Eq. (4-2), respectively. As seen in Figure 4-3, all walls should have failed in flexure under no axial force because their shear capacities exceeded their flexural capacities. However, their relation between two capacities reverses under compressive axial load. The shear capacity is smaller than the flexural capacity when the axial force ratio is larger than 15%. Hence, 15% of axial compression load is applied in experiment. In actual building, axial compression load on lightly RC wall is thought to be caused by vertical confinement from surrounding structural frame. Ojio et al. [62] conducted finite element analysis for the lightly RC wall of Building C considering the vertical confinement. They reported that the value of axial compression load rose with the increasing of wall lateral deformation and the similar failure mode with the actual wall was observed.

Actually, it is important to vary axial force level (even dynamically) to simulate the actual behaviour. However, the research community does not know the behaviour of lightly RC walls very much. In addition, it is not easy and takes time to simulate both long term and variation of axial loads separately during experiment. Therefore, it was decided to study their fundamental behaviour by loading it statically with constant axial load.

Table 4-4 Detail of damaged lightly RC walls

Name	Building A	Building B	Building C
Construction year	1969	1960	1987
Wall thickness (mm)	120	150	150
Wall reinforcement	9ϕ@200 single layer (SR24, p_{wh}=0.27%)	9ϕ@200 single layer (SR24, p_{wh}=0.21%)	D10@180 double layer*1 (SD295A, p_{wh}=0.26%)
Reinforcement for openings	1-D13 (SD35)	2-13ϕ (SR24)	2-D16 (SD295A)
Wall length (mm)	830	700	1050
Clear span length (mm)	1600	1000	2000
f'_c (N/mm^2)	18.4*2	16.2*3	21.0*3

*1 Staggered arrangement, *2 Compressive strength adopted at seismic evaluation (the value that deducts half of standard deviation from the average of core strength), *3 Design nominal strength

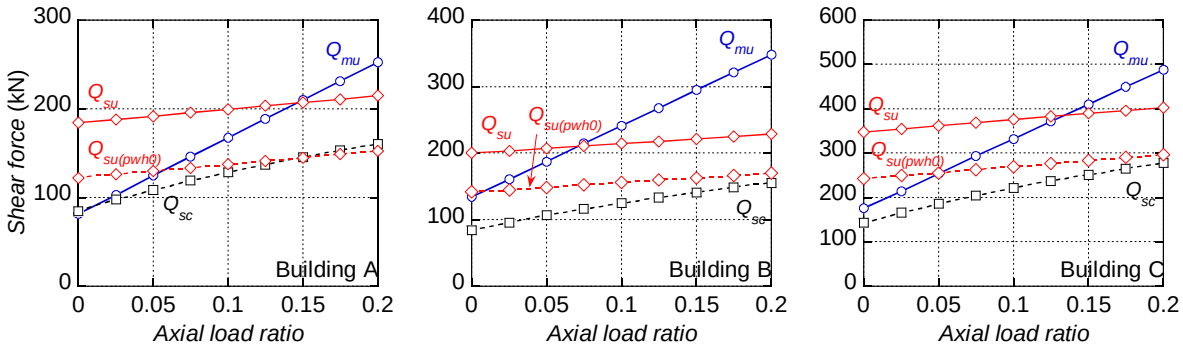

(a) Building A (b) Building B (c) Building C

Figure 4-3 Relations between calculated capacities and axial load ratio of three walls

Reference [1] provides a simplified design wall equations for ultimate flexural capacity, ${}_cQ_{mu}$, in Eq. (4-1) and Reference [65] provides an empirical equation of ultimate shear capacity, ${}_cQ_{su}$, in Eq. (4-2). In addition, the 1999 AIJ Guidelines [60] provides an equation to calculate shear cracking capacity of rectangular columns, ${}_cQ_{sc}$ as shown in Eq. (4-3).

$$ {}_cQ_{mu} = \left(a_t f_y l_w + 0.5 a_{wv} f_{wv} l_w + 0.5 N l_w\right) / a \tag{4-1} $$

$$ {}_cQ_{su} = \left\{ \frac{0.068 p_{te}^{0.23} \left(f'_c + 18\right)}{\sqrt{M/(QD) + 0.12}} + 0.85\sqrt{f_{wh} p_{wh}} + 0.1\sigma_0 \right\} t_e j \tag{4-2} $$

$$ {}_cQ_{sc} = \phi\left(\sqrt{{\sigma_T}^2 + \sigma_T\sigma_0}\right)t_e D \Big/ \kappa \qquad (4\text{-}3) $$

where, a_t, f_y: area and yield strength of longitudinal reinforcement in the wall boundary area, a_{wv}, f_{wv}: area and yield strength of longitudinal web reinforcement, l_w: length between the centers of boundary columns (0.9D for rectangular cross-section), N: axial load, a: shear span length, p_{te}: equivalent tensile reinforcement ratio (%) (=100$a_t/t_e d$), d: effective length of wall (=0.95D), f'_c: concrete compressive strength, $M/(QD)$: moment-to-shear ratio ($1 \le M/(QD) \le 3$), f_{wh}: yield strength of horizontal web reinforcement, p_{wh}: horizontal web reinforcement ratio, σ_0: average axial stress for gross cross-sectional area, t_e: equivalent wall thickness, j: lever arm length (=7/8d), ϕ: capacity reduction coefficient to consider scatter of experimental data (1.0 was used in this paper although 0.51 for practical design purpose), σ_T: concrete tensile strength ($=0.33\sqrt{f'_c}$, where f'_c is in N/mm^2), D: wall length, κ: shape coefficient (=1.5 for rectangular section).

Flexural capacity (${}_cQ_{mu}$), shear capacity (${}_cQ_{su}$) and diagonal shear failure capacity (${}_cQ_{sc}$) are shown in Table 4-5. Defining the shear safety factor, z, as ratio of shear capacity to flexural capacity, z of NSW1 was 2.22. Hence, NSW1 was expected to yield in flexure first and fail in tension controlled flexure mode. With axial compression load of 0.15f'_cA_g, z of NSW2 was 0.96. Hence, NSW2 was expected to have diagonal shear cracks first followed by shear failure. Since the horizontal reinforcement of NSW1 and NSW2 was not well anchored, the premature failure mode was likely to occur if concrete degrades due to cyclic loading. Since the amount of horizontal reinforcement of NSW3 was two times as large as that of NSW2, z of NSW3 was 1.06. Based on Eqs. (4-1) and (4-2), NSW3 was expected to yield in flexure, then fail in shear. Index z of NSW4 was 1.80 and NSW4 was expected to yield first, and fail in tension controlled flexure mode.

Table 4-5 Capacities of specimens (Q in kN and R in %)

Spec.	Cal. based on Eqs. (2-1) - (2-3)				
	${}_cQ_{mu}$	${}_cQ_{su}$	${}_cQ_{sc}$	z	Q_{CAL} *1
NSW1	127	282	136	2.22	127
NSW2	333	320	245	0.96	320
NSW3	333	352	245	1.06	333
NSW4	166	298	245	1.80	166

*1 Q_{cal} = min (${}_cQ_{mu}$, max(${}_cQ_{su}$, ${}_cQ_{sc}$)),

4.2.3 Test setup and loading method

The test setup is shown in Figure 4-4. High-strength post-tensioning rods were used to fix the upper and lower stubs to the steel reaction beams. Axial compression load of 458 kN, equivalent to $0.15f'_cA_g$ was maintained constant during the experiment for NSW2, NSW3, and NSW4 with two vertical hydraulic jacks. NSW1 was tested without axial load to simulate a common Japanese design practice, in which lightly RC walls are assumed to carry no axial load. NSW1, NSW2, and NSW3 were tested under double curvature with shear span to wall length ratio as 1.0, and the upper stub was kept parallel to the lower stub during the loading. NSW4 was tested under single curvature with shear span to wall length ratio as 2.0.

The lateral load was applied by a horizontal hydraulic jack and controlled by drift *R*, which is defined as the ratio of horizontal displacement to the clear height of the wall panel (2100 mm). The loading protocol consisted of one cycle of *R*= ±0.125% followed by two cycles of ±0.25%, ±0.50%, ±0.75%, ±1.00%, ±1.50%, and ±2.00%. It was planned that reversed cyclic loading of five full cycles were imposed at *R*= 2.00% to find the effect of cyclic loading on the capacity degradation. Since lateral load capacity of NSW2 degraded quickly after the peak, five cycles were imposed at *R*= 1.00%. NSW3 failed at the first negative excursion of *R*= 1.50% and five cycles were not imposed.

Loading system malfunctioned for NSW2 and the specimen experienced tensile axial force before the loading test. Multiple horizontal cracks appeared as shown by black lines in Figure 4-9(b) and the stiffness seems to have decreased. However, the initial crack width was smaller than 0.05mm and the test was continued as other specimens. Since NSW2 failed in shear, the initial damage due to axial tension should not have been very serious. The pre-loading procedures for all specimens is shown in Table 4.6.

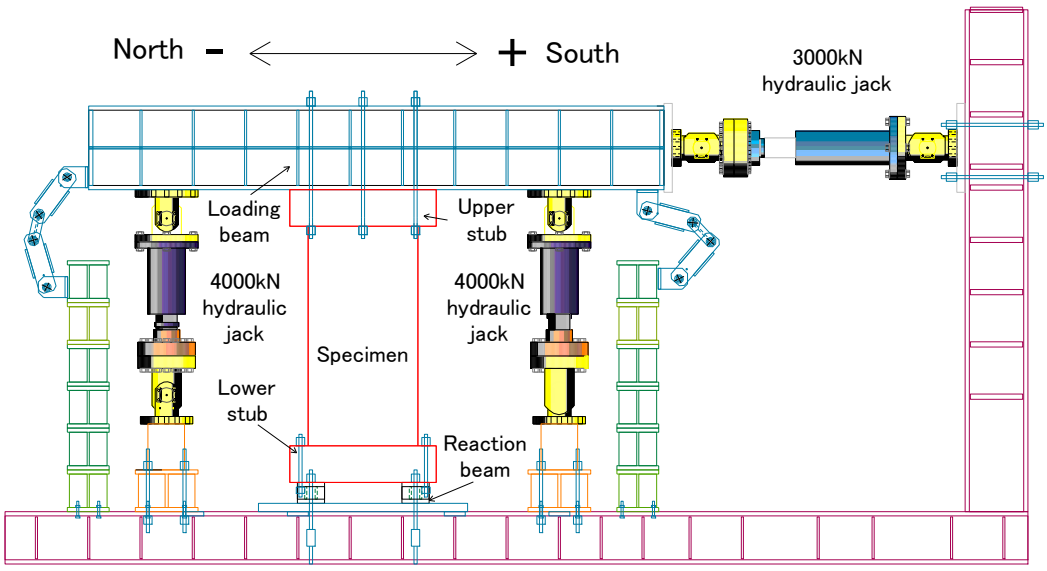

Figure 4-4 Test setup (unit in mm)

Table 4.6 Pre-loading procedures

Step	Procedure
1	The specimen was placed on the steel reaction beam as shown in Figure 4-4.
2	A mortar was applied between stub and steel reaction and loading beams to increase their friction.
3	The lower stub was fixed to the steel reaction beam by post-tensioning PS rods.
4	Before the steel loading beam touched the upper stub, all strain gauge readings were initialized.
5	Axial compression load of 100 kN was applied and the upper stub was fixed to the steel loading beam by post-tensioning PS rods.
6	The axial load was released to ZERO, then all displacement transducers were initialized.

4.2.4 Instrumentation and measurement

Figure 4-5(a) shows displacement transducer locations. Four displacement transducers were mounted vertically to measure flexure deformation at intervals 0~550 mm from lower end of the wall panel (Z1), 550-1050 mm (Z2), 1050-1550 mm (Z3), and 1550-2100 mm (Z4) for both of north and south sides. To measure shear deformation, eight displacement transducers were mounted diagonally with same intervals as the vertical transducers. The pullout and sliding of lower and upper stubs were measured using ten displacement transducers attached vertically and horizontally to the bottom and top portions of the wall panels with distance 50 mm to the stubs. Out-of-plane deformation was measured using three displacement transducers which were mounted to a reference frame as shown in Figure 4-6. The lateral drift was measured using two methods, i.e. (1) by using transducer mounted to a reference frame parallel to the upper stub of the specimen as shown in Figure 4-6 and Figure 4-7, and (2) by using transducers mounted at the wall panel. Strain gauges were placed on steel reinforcing bars at critical locations as shown in Figure 4-5(b).

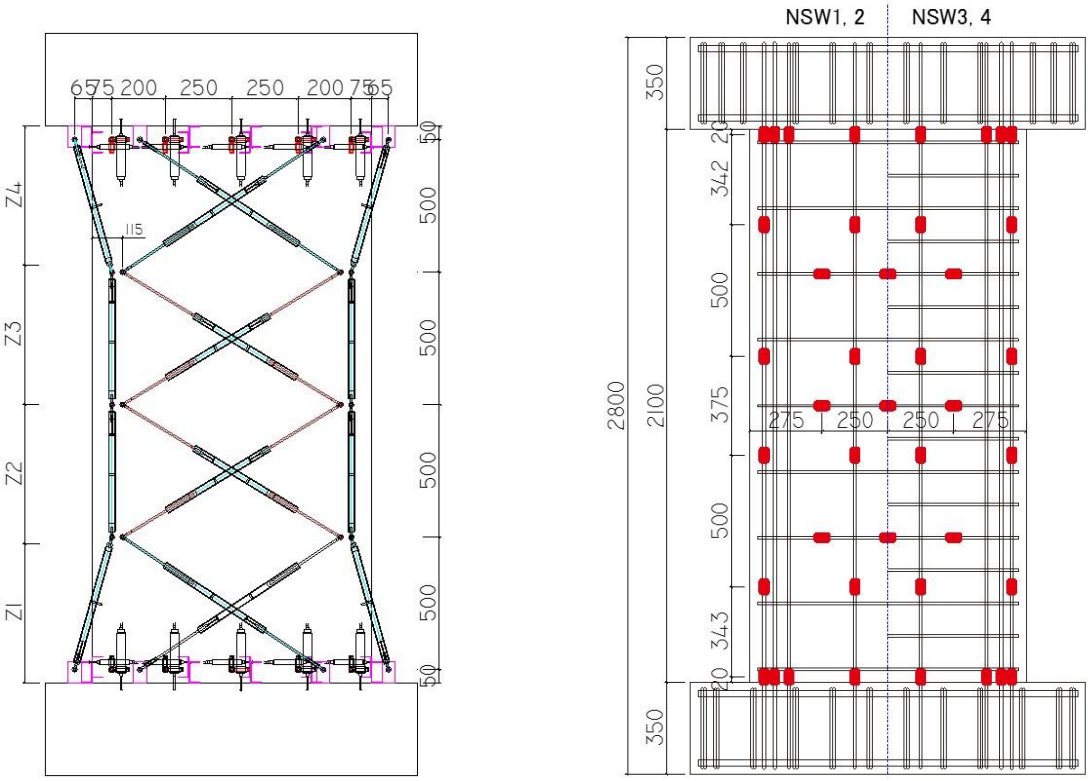

(a) Displacement gauge locations (b) Strain gauge locations

Figure 4-5 Location of stain and displacement gauges (unit in mm)

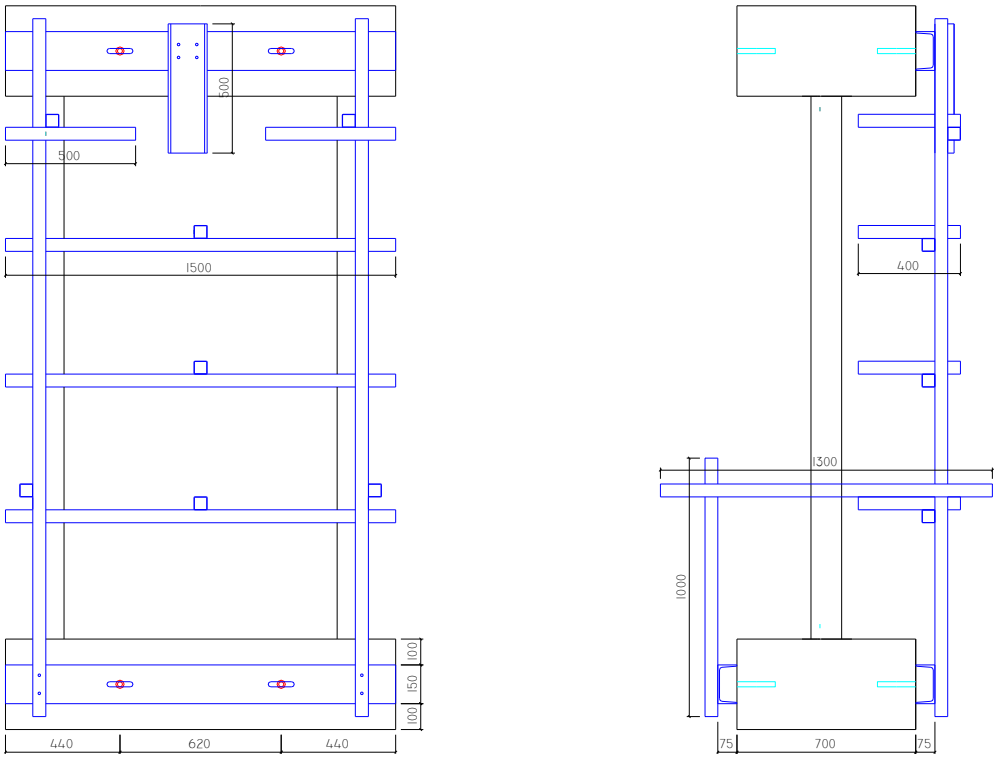

(a) Back face (b) South side

Figure 4-6 Reference frame

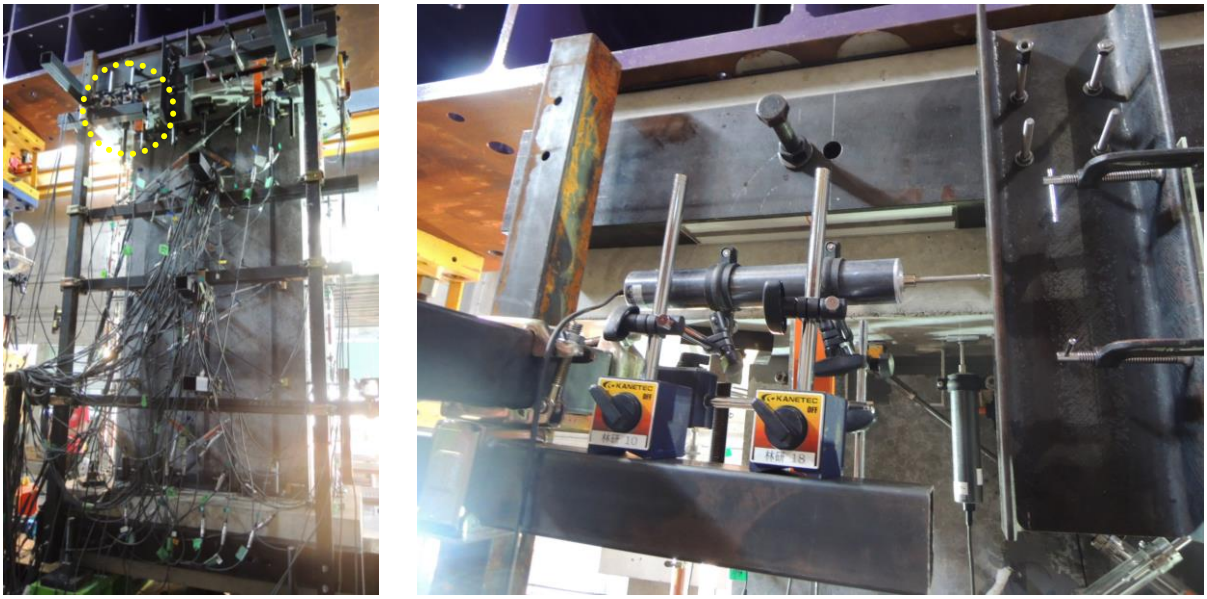

(a) Reference frame (b) displacement transducer

Figure 4-7 Displacement transducer to measure lateral drift

4.3 Experimental Results

4.3.1 Shear force – drift relations

Shear force – drift relations are shown in Figure 4-8. ${}_cQ_{mu}$ and ${}_cQ_{su}$ are computed flexure and shear capacities using Eqs. (4-1) and (4-2), respectively. Table 4-7 summarizes the maximum lateral load capacity, Q_{max}, lateral load of vertical reinforcement yielding, Q_{yv}, lateral load of horizontal reinforcement yielding, Q_{yh}, and their corresponding drifts, R.

For NSW1, yielding of vertical reinforcement occurred at R= 0.16% and R= -0.20% for positive and negative loadings, respectively. The maximum lateral load capacities were reached at 155 kN and -120 kN during the first cycle of R= ±0.50%. During unloading the second cycle of R= ±0.50%, significant sliding occurred along the stub interface to cause a pinched hysteresis loop. Horizontal reinforcement yielded at 0.61% and -1.22% drifts for positive and negative loading, respectively after the maximum lateral load capacity was reached. Lateral load capacity started to decrease significantly at the second cycle of R= ±1.50%, and then five full cycles of R= ±2.00% were imposed. After applying five full cycles of R= ±2.00%, the lateral load capacity decreased approximately 52% from its maximum capacity and the loading was terminated. This drop of lateral load capacity was caused by sliding along flexure-shear cracks at the wall top and base.

For NSW2, the first yielding of vertical reinforcement occurred at R= 0.31% and R= -0.21% for positive and negative loadings, respectively. Horizontal reinforcement was yielding when NSW2 reached its maximum capacity at R= +0.50%. The maximum lateral load capacities were reached at 297 kN and -282 kN during the first cycle of R= +0.50% and R= -0.75%, respectively. A large drop of lateral load capacity was observed during the second cycle of R= ±0.75%, and then five full cycles of R= ±1.00% were imposed before the loading was terminated. The lateral load

capacity decreased approximately 45% at the end of the fifth cycle from its maximum capacity because excessive concrete spalling occurred in the upper region.

For NSW3, the maximum lateral load capacities were observed at 321 kN and -312 kN during the first cycle of R= ±1.00%. Both vertical and horizontal reinforcement had yielded before NSW3 reached its maximum lateral load capacity. Unlike NSW2, NSW3 maintained its lateral load capacity in the post-peak region up to the first cycle of R= +1.50%. However, significant loss of lateral load capacity occurred during the first cycle of R= -1.50% due to sliding at the flexure-shear crack around the upper north corner and the loading was terminated.

For NSW4, yielding of vertical reinforcement occurred at R= 0.24% and R= -0.40% for positive and negative loading, respectively. The horizontal reinforcement yielded at 0.31% drift in the positive loading, while it did not yield in the negative loading. During the first cycle of R= ±1.50%, the maximum lateral load capacities were reached at 187 kN and -162 kN for positive and negative loading, respectively. Five full cycles of R= ±2.00% were imposed before the loading was terminated and the lateral load capacity decreased approximately 54% from its peak value at the end of cycle. Spalling of concrete and buckling of vertical reinforcement at the wall base caused drop of lateral load carrying capacity.

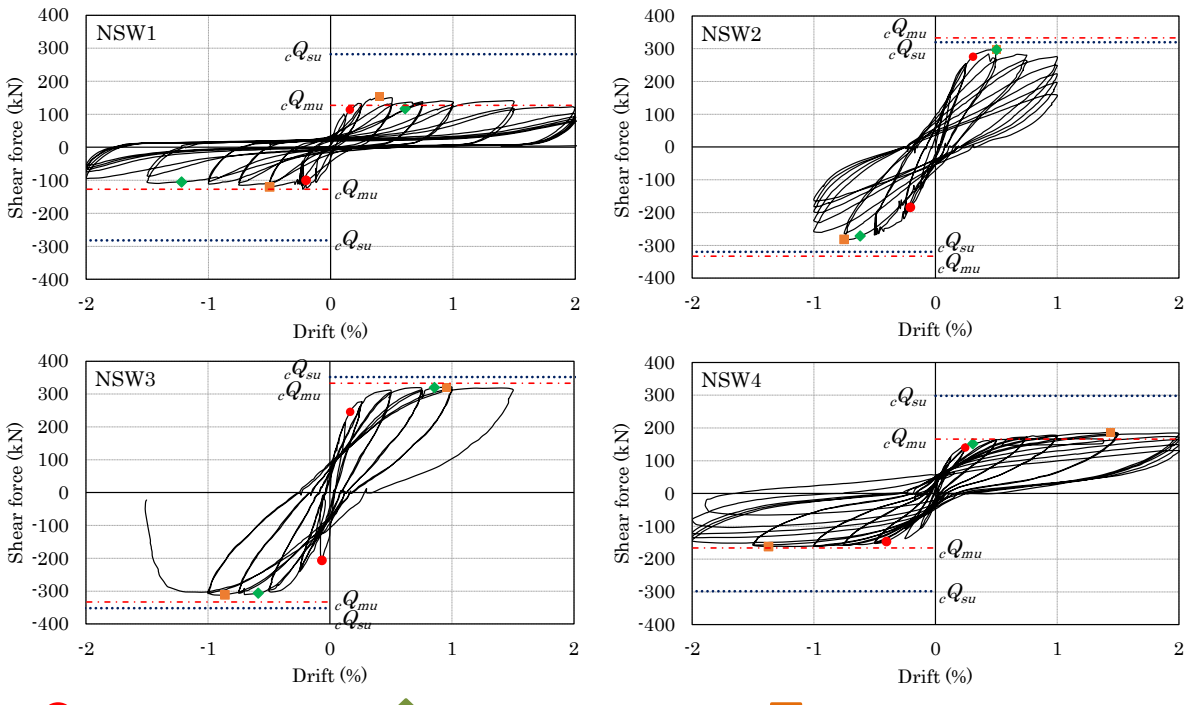

Figure 4-8 Shear force – drift relations

Table 4-7 Shear force and drift of characteristic points and failure modes

Specimen	Q_{max}, kN (R_{max}, %)		Q_{yv}, kN (R_{yv}, %)		Q_{yh}, kN (R_{yh}, %)		Overall damage process
	+	-	+	-	+	-	
NSW1	155	-120	114	-100	117	-105	Wall yielded in flexure, deformation increased accompanied by large slip at stub interface without degrading capacity, shear sliding occurred along the shear cracks, then wall failed in shear.
	(0.40)	(-0.50)	(0.16)	(-0.20)	(0.61)	(-1.22)	
NSW2	297	-282	276	-184	297	-271	Diagonal shear cracks emerged and the peak point was reached soon after. Then capacity degraded after the peak, and finally failed in shear compression.
	(0.50)	(-0.75)	(0.31)	(-0.21)	(0.50)	(-0.62)	
NSW3	321	-312	246	-207	320	-306	Wall yielded in flexure, deformation increased without degrading capacity, then finally failed with shear sliding.
	(0.96)	(-0.86)	(0.17)	(-0.07)	(0.86)	(-0.59)	
NSW4	187	-162	140	-146	152	-	Wall yielded in flexure, deformation increased without degrading capacity, then finally failed in flexure compression.
	(1.44)	(-1.37)	(0.24)	(-0.40)	(0.31)		

4.3.2 Damage process and failure modes

Figure 4-9 shows residual crack pattern of the specimens after the second cycle of each drift (except at R= 0.125% after the first cycle). Blue and red lines show cracks in positive and negative loadings, respectively. Black lines in Figure 4-9(b) and (d) indicate the cracks which occurred due to a loading system trouble. For NSW1, flexural cracks started to appear at the lower and upper parts of wall during R= ±0.125%. As increasing the drift, new cracks appeared and existing cracks extended and widened. The peak load was reached at the first cycle of R= 0.50% both in positive and negative directions. During the first cycle of R= -1.50%, the first shear crack (1-①) appeared from the upper south to the middle north of wall. Concrete spalling (1-②) was observed during the second cycle of R= ±1.50% at both lower south and north of walls. During R= ±2.00, flexure-shear cracks (1-③) at the wall top opened significantly and the area of concrete spalling at the wall base became larger. Relatively large slip took place at the upper and lower stub interfaces. Severe sliding occurred along the flexure-shear crack (1-④) and failed in shear as shown in Figure 4-10(a). Although sliding at the stub interfaces and the final shear sliding were not properly expected, flexure-governed features of damage process took place as expected. For NSW2, a web-shear crack (2-①) appeared during the first cycle of R= ±0.50%. Concrete crushed (2-②) around the intersection of shear cracks at the upper portion of the wall during R= ±0.75% and developed to the central part (2-③) of wall during R= ±1.00%. Severe spalling of concrete (2-④) occurred at the second cycle of R= 1.00% since the horizontal reinforcement was simply curtailed

at the end and not properly anchored to the concrete. During unloading of the fifth cycle of *R*= +1.00%, excessive concrete spalling (2-⑤) occurred in the upper south corner of the wall followed by buckling of vertical reinforcement (2-⑥) at the end region. The ultimate failure mode is considered as shear-compression failure as shown in Figure 4-10(b). Since the computed flexural and shear capacities are close to each other, the degradation after the peak load took place as expected due to the inadequate anchorage of horizontal reinforcement. For NSW3, shear cracks (3-①) started to appear at the central part of the wall during the second cycle of *R*= ±0.50%. Crack width at the upper part (3-②) became larger during *R*= ±0.75% and concrete crushed (3-③) at both upper south and north parts. There was no concrete spalling in the central part since the shear cracks did not develop. Sliding occurred along the flexure-shear crack (3-④) resulting in the ultimate failure just before reaching the first cycle of *R*= -1.50% as shown in Figure 4-10(c). Although the computed flexural and shear capacities are close to each other, NSW3 did not show any noticeable degradation of lateral load capacity probably because the horizontal reinforcement was properly anchored. Unlike NSW1, NSW3 did not show the sliding at the stub interfaces because NSW3 had axial force. For NSW4, during *R*= ±0.125% cycle, a flexural crack (4-①) appeared at the lower portion. As drift increased, new cracks (4-②) appeared and existing cracks extended and widened. Vertical cracks (4-③) occurred at the wall base during the first cycle of *R*= ±1.50% and cover concrete spalling (4-④) was observed at the second cycle of *R*= ±1.50%. During loading and unloading of the first cycle of *R*= -2.00%, concrete crushed (4-⑤) and vertical bars (4-⑥) buckled at the end region at the lower north and south parts. NSW4 failed in compression-controlled flexure as shown in Figure 4-10(d). Similar to NSW3, NSW4 did not show any noticeable slip along the lower stub interface since the same magnitude of axial force was applied.

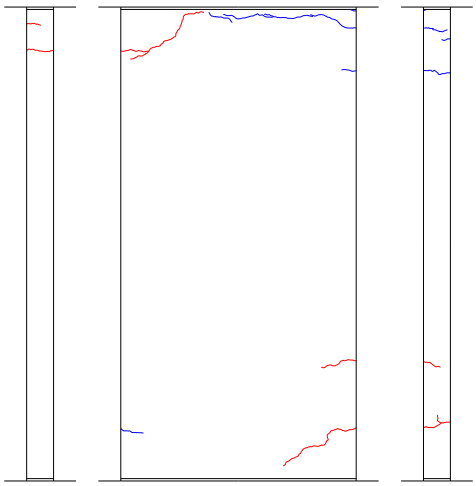

R= ±0.125%

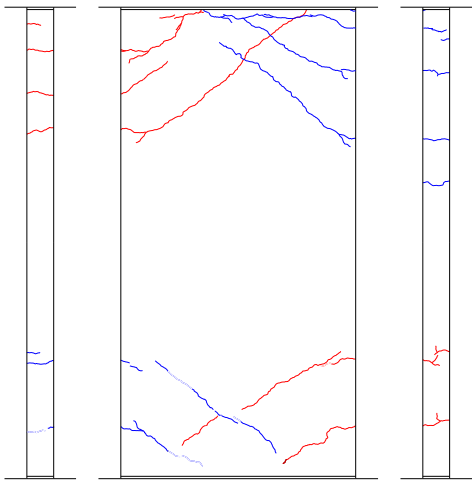

R= ±0.25%(2)

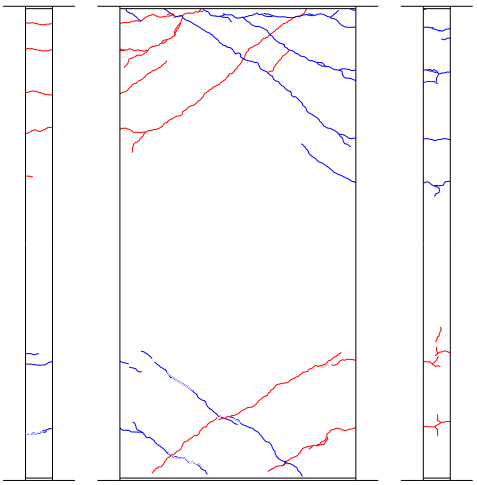

R= ±0.50%(2)

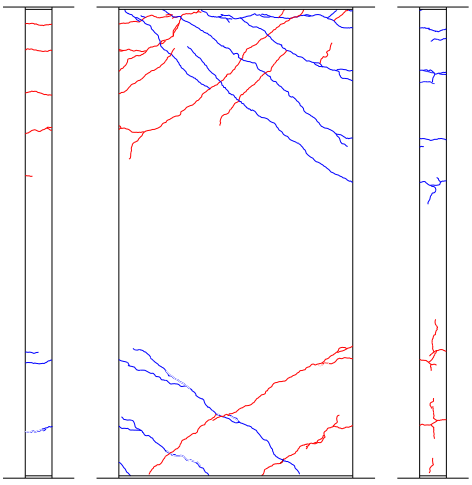

R= ±0.75%(2)

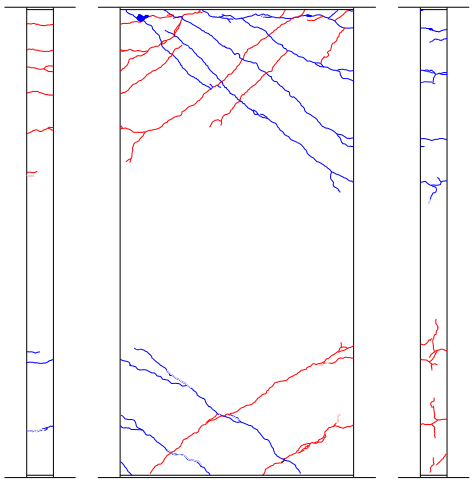

R= ±1.00%(2)

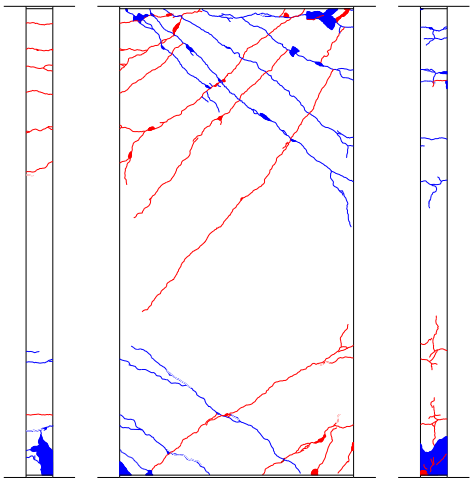

R= ±1.50%(2)

(a) NSW1

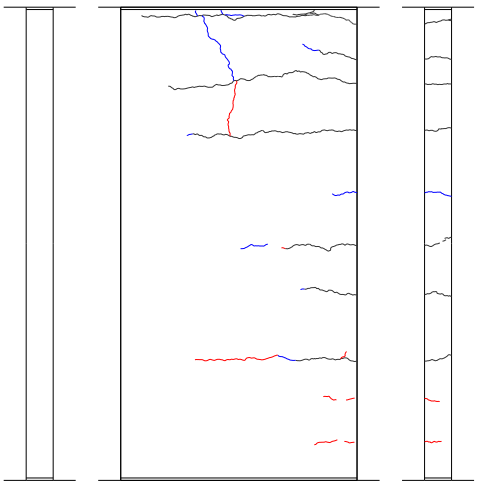

R= ±0.125%

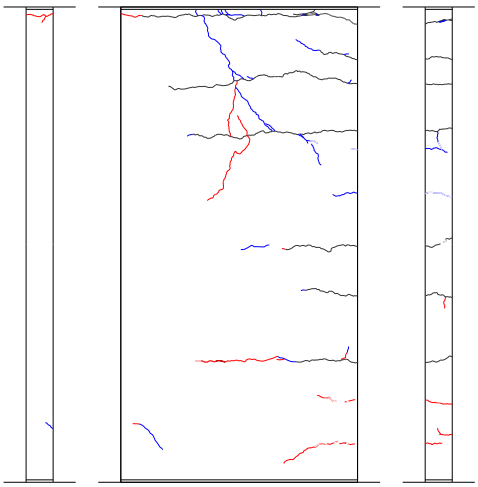

R= ±0.25%(2)

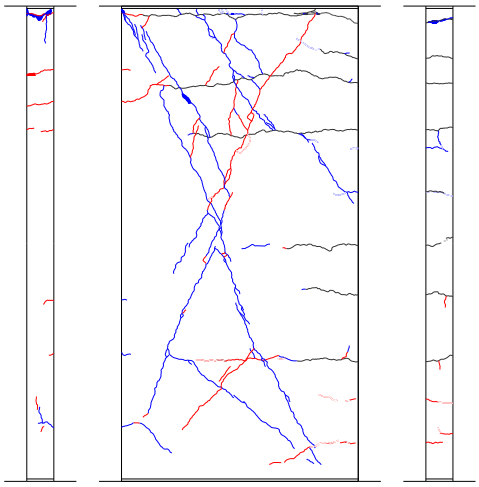

R= ±0.50%(2)

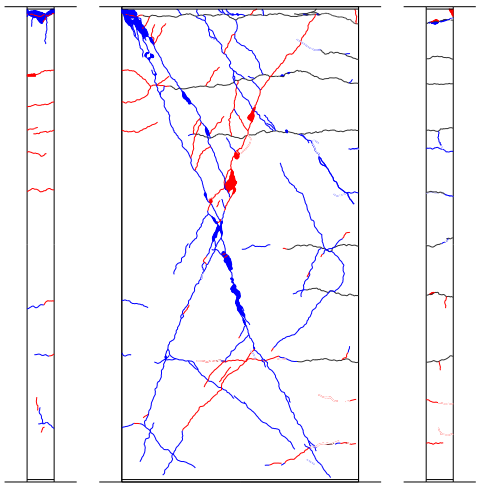

R= ±0.75%(2)

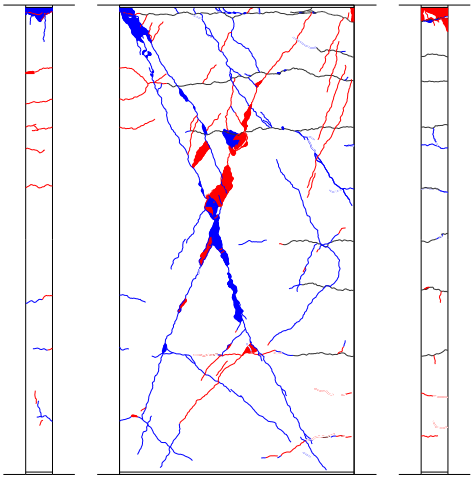

R= ±1.00% (2)

(b) NSW2

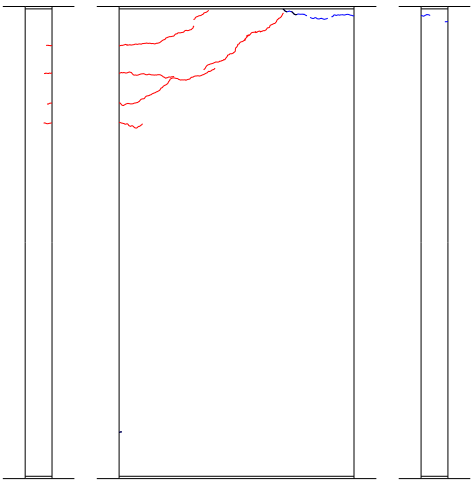

R= ±0.125%

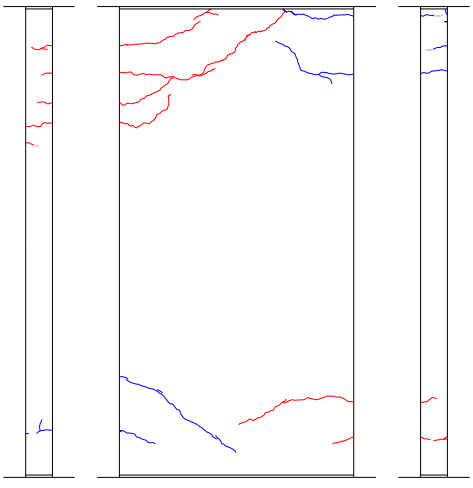

R= ±0.25%(2)

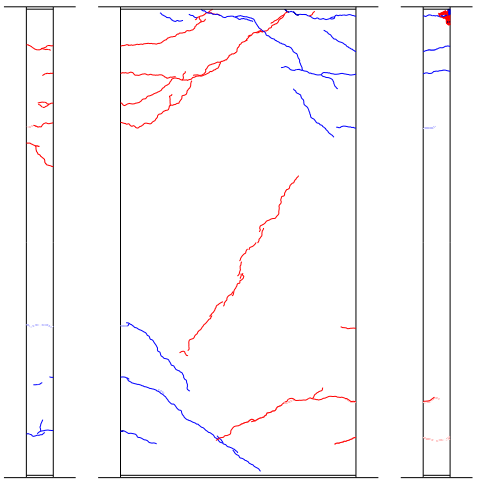

R= ±0.50%(2)

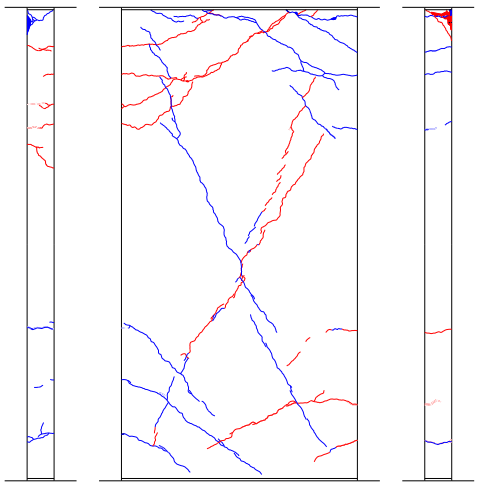

R= ±0.75%(2)

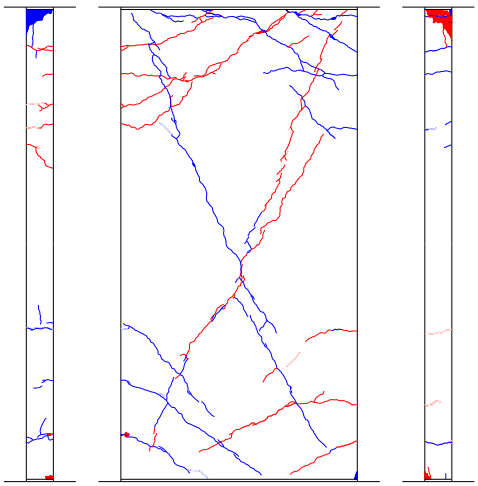

R= ±1.00%(2)

(c) NSW3

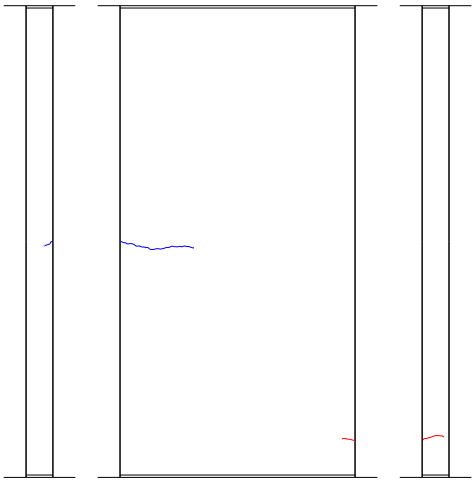

R= ±0.125%

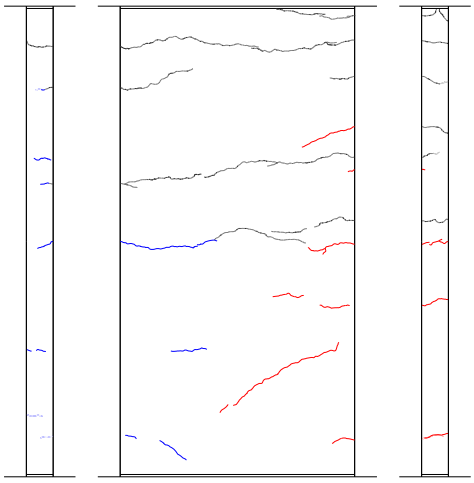

R= ±0.25%(2)

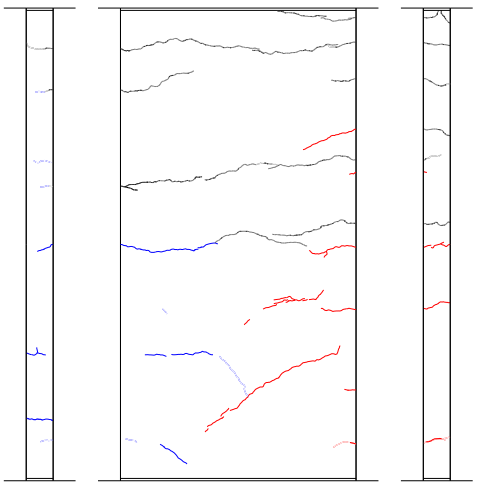

R= ±0.50%(2)

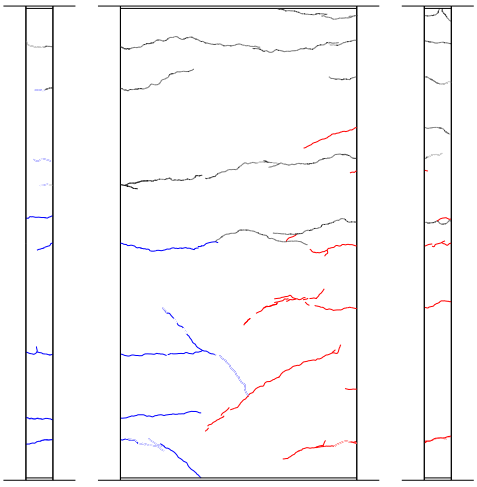

R= ±0.75%(2)

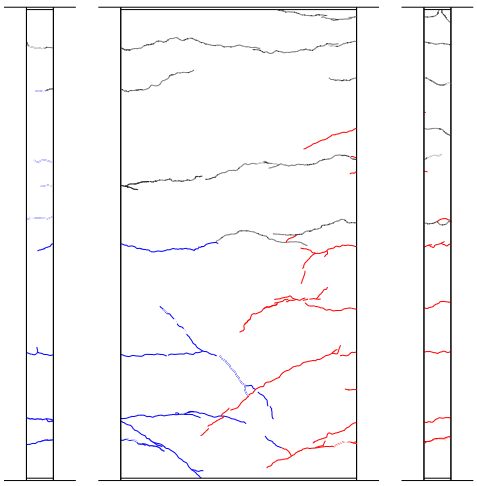

R= ±1.00%(2)

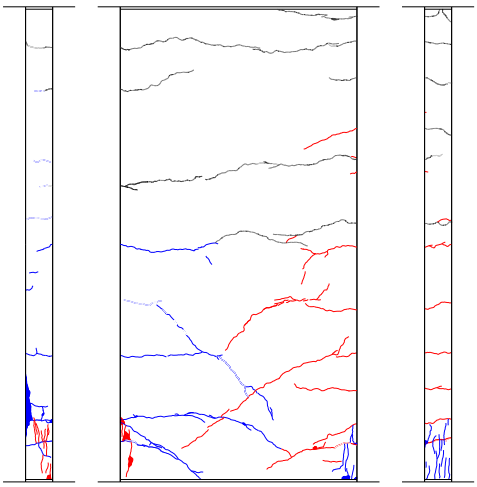

R= ±1.50%(2)

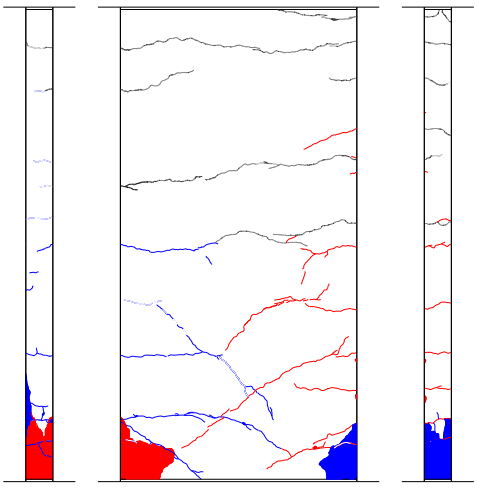

R= ±2.00%(2)

(d) NSW4

Figure 4-9 Residual cracks of all specimens

Upper North side

Upper South side

Lower North side

Front face

(a) NSW1

Lower South side

Upper North side

Upper South side

Lower North side

Front face

(b) NSW2

Lower South side

Upper North side

Lower North side

Front face

Upper South side

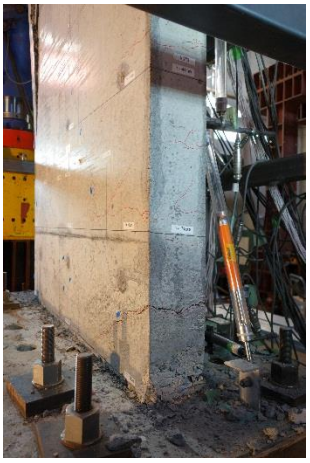

Lower South side

(c) NSW3

Upper North side

Lower North side

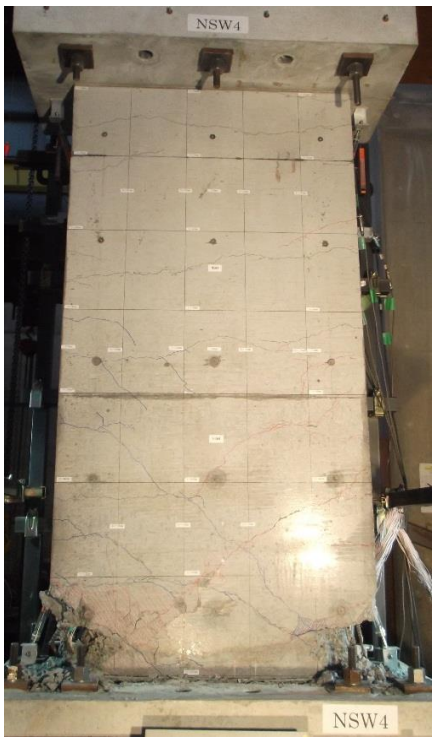

Front face

Upper South side

Lower South side

(d) NSW4

Figure 4-10 Final damage of specimens

Except for NSW4, it should be noted that the damages at the upper part of wall were intense compared to the lower part as shown in Figure 4-10. This is probably because the specimen was cast vertically in two stages: first the lower stub and then the wall and upper stub as one part with intentionally roughened surface created at lower stub wall interface to ensure adherence and mechanical interlocking. After initial placement and prior to settling, bleeding takes place. The heavier cement and aggregates tend to settle, while the air, particles of low specific gravity, and excess water tend to rise. As the air and particles rise they become trapped under horizontal bars, under the lugs of vertical bars, and under the coarse aggregate in the upper portion of the fresh concrete mass. Air voids and water pockets produces weaker concrete in the upper portion of a concrete mass relative to the lower portion. The reduction in strength can be attributed to increased porosity and increased water content. Air and lightweight particles trapped under the bars or lugs form soft, spongy pockets of very weak concrete. The air pockets reduce the area of bearing between the concrete and the lugs resulting in loss of bond strength. The "soft" concrete under the lugs is easily damaged and the bar may slip before full bearing (and strength) is developed.

4.4 Discussion of Test Results

4.4.1 Strength and stiffness of specimens

Response envelopes for all specimens are shown in Figure 4-11. As expected, the maximum lateral load capacity of NSW1 was lower than other specimens since it was loaded without axial force. However, NSW1 maintained its capacity up to R= 2.0% without significant post-peak degradation. Unlike NSW1, NSW2 experienced large drop of lateral load capacity about 10.8% and 6.4% for positive and negative loading, respectively, after reached its maximum lateral load capacity. This is because diagonal shear cracks became severe and concrete crushing occurred at the intersection of shear cracks. Since NSW3 had double amount of horizontal reinforcement, its maximum lateral load capacity was 8.0% higher than that of NSW2, and maintained its capacity up to R= 1.5%. Although NSW4 was loaded under cantilever, its capacity was higher than NSW1 since axial force was applied. However, both specimens maintained their capacity up to R= 2.0% without significant post-peak degradation.

The variation of the secant stiffness with shear force for all specimens is illustrated in Figure 4-12. NSW1 and NSW4 had similar initial and secant stiffness due to no axial load and cantilever wall, respectively. For NSW2, the initial cracking occurred due to the loading system trouble resulting in initial stiffness decreased. However, at the maximum lateral load, the secant stiffness of NSW2 was similar to NSW3 about 28.1 kN/mm. Increasing the maximum displacement of the loading cycle increases stiffness deterioration (see Figure 4-12). Furthermore, after a number of cycles, the decrease in secant stiffness is smaller than the decay occurring during the first few cycles.

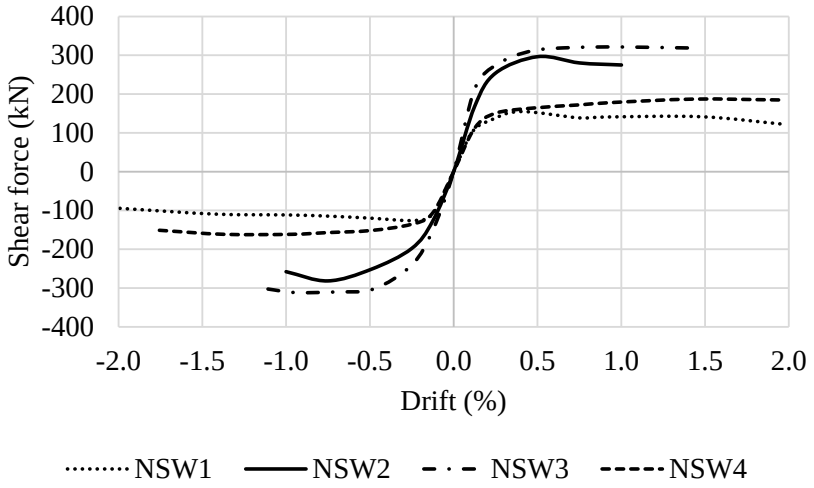

Figure 4-11 Response envelopes of specimens

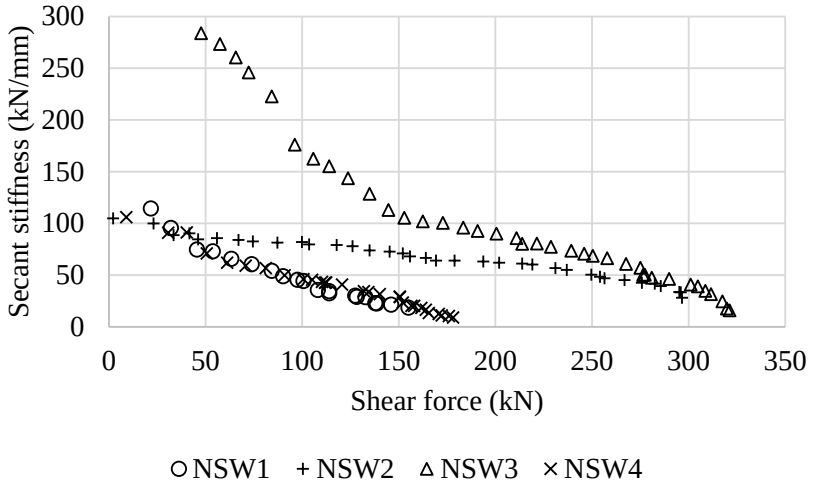

Figure 4-12 Secant stiffness variation of specimens

4.4.2 Drift capacity and energy dissipation

The ultimate drift is defined as the lateral drift corresponding to the lateral load dropped to 80% of peak value. The ultimate drift of NSW1 was reached at R= 2.0% since severe sliding occurred along the flexure-shear crack, while NSW2 was 1.0% due to excessive concrete crushing around the intersection of shear cracks at the central part. NSW3 had higher ultimate drift compared with NSW2, occurred at R=1.5%. This is probably because the horizontal reinforcement of NSW3 was properly anchored. NSW4 was loaded under single curvature and failed in flexure. As a result, NSW4 maintained its lateral load capacity with small deterioration after the peak and reached its ultimate drift at R= 2.0%.

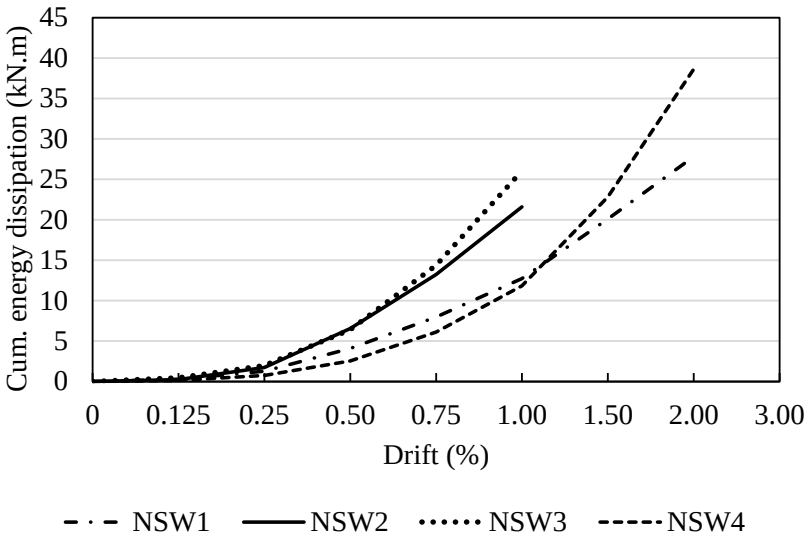

Figure 4-13 Cumulative energy dissipation of specimens

Figure 4-13 shows the cumulative energy dissipation of specimen at each level of drift. For each specimen, energy dissipation was determined by calculating the areas inside the hysteretic loops for each cycle. The cumulative energy dissipation was defined as the summation of the areas enclosed by all previous hysteresis loops. For all specimens, the energy dissipation during the first cycle was larger than the amount energy dissipated during the second cycle at the same drift level. The experimental data also show that the amount of energy dissipation increased considerably with the drift level of the cyclic loading. The cumulative energy dissipation of NSW1 was higher than NSW4 up to R= 1.0%. However, NSW1 exhibited pinched hysteresis loops due to shear slip along the joint planes between wall and blocks. As a result, NSW1 dissipated less amount of energy than that of NSW4 after R= 1.0%. NSW2 dissipated similar amount of energy with NSW3 up to R= 0.5%. Although the cumulative energy dissipation of NSW2 still increased after R= 0.5%, it was smaller than that of NSW3. This can be explained basically by lateral load capacity dropped due to shear cracks propagation at the central part. The energy dissipation of NSW2 was associated with concrete crushing and cracking, while for NSW3 dissipated energy through the yielding of tensile bars and the concrete cracking.

4.4.3 Drift components

This section provides lateral drift component measurements based on experimental result. Displacements of a shear wall subjected to a lateral load are illustrated in Figure 4-14(a). It is assumed that these displacements can be represented by two components, i.e. flexural deformation and shear deformation. The vertical displacement transducers were used to measure flexural deformation (U_f) and can be calculated as:

$$U_f = \theta h = \frac{(V_L - V_R)}{L} h \tag{4-4}$$

where θ is the rotation over the height h, V_L and V_R are the vertical displacements along the wall edge (measurements of the two vertical displacement transducers), and L is the horizontal between V_L and V_R, as shown in Figure 4-14(a). The diagonal displacement transducers were used to measure shear deformation (U_s), which was estimated from changes in their length as expressed in Eq. (4-5).

$$U_s = \frac{(d_1' - d)d - (d_2' - d)d}{2L} \tag{4-5}$$

where d_1' and d_2' are the deformed length of diagonal, d is the original diagonal length, and L is the horizontal distance between gauges, as shown in Figure 4-14(a). However, the shear deformation given by Eq. (4-5) contains flexural deformation because of the existence of a moment gradient along the height of the shear walls [66]. Therefore, the shear deformation given by Eq. (4-5) should be corrected and can be expressed as follows [67]:

$$U_{s\_corrected} = U_s - (\alpha - 0.5)\theta h \tag{4-6}$$

Hiraishi [67] suggested that the factor α is estimated based on the rotation (θ), as it is the ratio of the shaded area to the rectangular surrounded by solid lines shown in Figure 4-14(c), giving same results for α when calculated as the ratio of curvature centroid to panel height as shown in Figure 4-14(b). Massone and Wallace [68] set α to 0.67, assuming a triangle curvature distribution. By using this assumption, the drift components of wall at the first cycle for each drift level are illustrated in Figure 4-15.

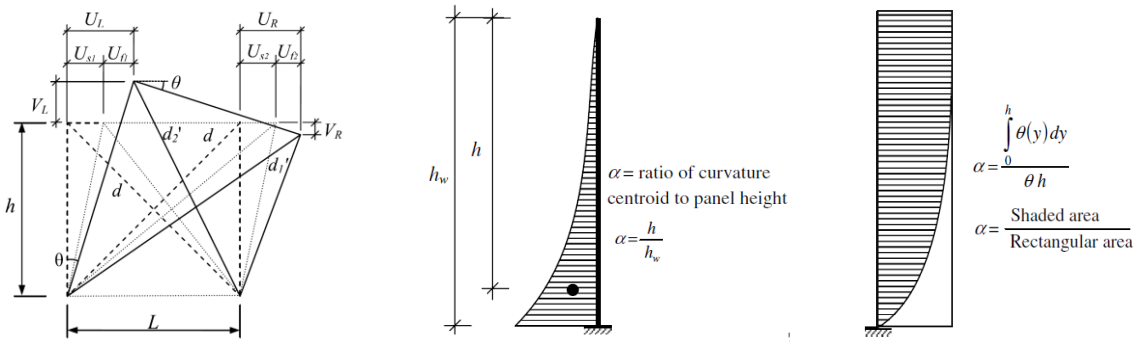

(a) Flexure and shear deformations accounting for vertical displacement

(b) Estimating α based on curvature profile

(c) Estimating α based on rotation profile

Figure 4-14 Drift components [66]

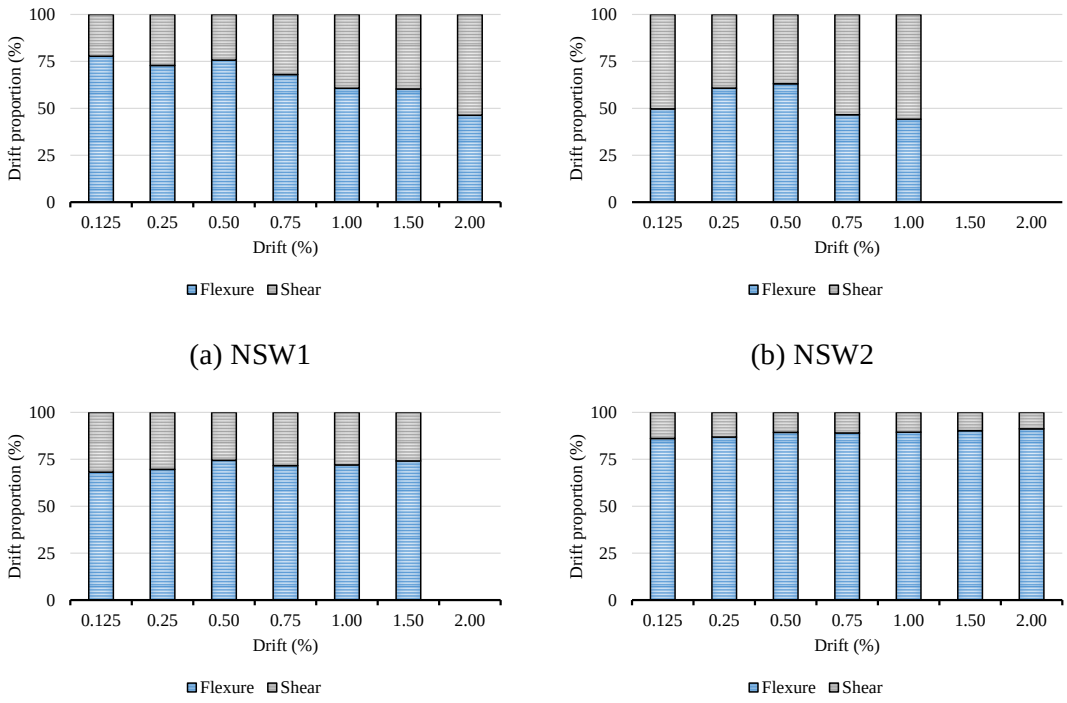

(a) NSW1 (b) NSW2

(c) NSW3 (d) NSW4

Figure 4-15 Drift components of specimens

It is clear from Figure 4-15 that the relative contribution of each mode varied with the level of lateral drift. For NSW 1, flexural deformations dominated the response (more than 60% of the total deformation) up to *R*= 1.5% and dropped to 46% at *R*= 2.0% due to diagonal shear cracks. For NSW2, flexural deformations dominated the response (more than 50% of the total deformation) up to *R*= 0.50%. However, at higher level of drift, the shear deformation became significantly pronounced and the contribution of flexural deformation decreased to 45% of the total deformation. This is corresponding to concrete crushing around the intersection of shear cracks at the central part. For NSW3 and NSW4, although the contribution of each deformation varied, the flexural deformations dominated the response for all drift levels. The flexural deformations were 71.7% and 88.9% of the total deformation in average for NSW3 and NSW4, respectively. This is consistent with envelope curve of both specimens that showed ductile behavior.

4.5 Damage Assessment

Post-earthquake assessment of damaged structures is a critical and complex problem. In the immediate aftermath of an earthquake, it is the engineer's responsibility to judge, if a structure is safe enough to keep using. In the subsequent phase, the responsibility to identify the most cost effective repair actions for the damaged structure belongs to the engineer. Evaluating the effects of the damage on the structural properties and expected future seismic performance is pivotal in this respect.

The objective of this study is to develop a post-earthquake seismic evaluation method for lightly reinforced concrete (RC) walls. For this purpose, damage evaluation in terms of crack width, crack length, and concrete spalling area was carried out at different drift levels to see damage progress of lightly RC walls. Then, the damage level was assessed using the 2004 AIJ Guidelines [30] to study its validity for lightly RC walls. Some modifications have been proposed and the recommendations of this study can help the inspector in estimating the current limit state or performance level of the wall.

4.5.1 Concrete cracking and spalling area

The crack width is accepted as an important index for evaluating the damage level of structural components affected by earthquakes. The residual crack width, closely related to the retrofit method and cost, has been used as a damage indicator in some standards [30][69]. In this study, the intensity of observed damage of specimens was evaluated in terms of crack width, crack length, and concrete spalling area. The measurement was carried out on three faces of the wall; front face and both north and south side faces. Crack width was measured using an imprinted crack scale card with 0.05 mm intervals as shown in Figure 4-16(a). The crack width measurement was conducted at peak drift and unloading for each cycle. Each visible residual crack at the first cycle of R= -0.125% and the second cycle of -0.25%, -0.50%, -0.75%, -1.00%, -1.50%, and -2.00% was traced on transparencies (overhead projector sheets) as shown in Figure 4-16(b). The numbering system on the transparencies and the wall panel is shown in Figure 4-17. Each individual crack was labeled and the maximum width along its length was measured. In this measurement, if the crack was visible but the crack width was less than 0.05 mm (minimum measurable crack width with the crack scale), the crack width was expressed as 0.00 mm. These transparencies were scanned and all cracks were traced digitally on a computer CAD program so that location and length of cracks were digitalized later. Each residual crack was classified based on the maximum width along the crack. In this study, the residual crack width, $_rW_{cr}$ was classified as $_rW_{cr} < 0.2$ mm, $0.2 \text{ mm} \leq {}_rW_{cr} < 1.0$ mm, $1.0 \text{ mm} \leq {}_rW_{cr} < 2.0$ mm, $2.0 \text{ mm} \leq {}_rW_{cr} < 5.0$ mm, $_rW_{cr} \geq 5.0$ mm.

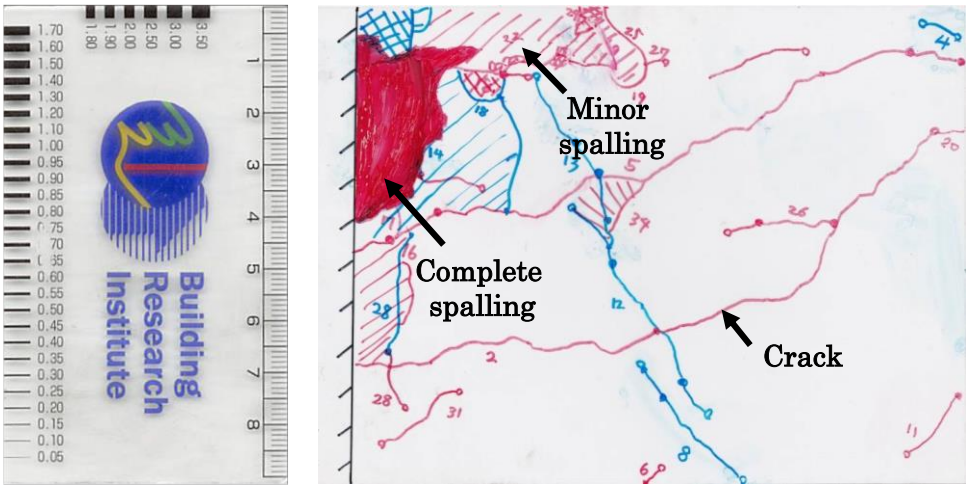

(a) Crack gauge card (b) Sample of transparency

Figure 4-16 Tracing cracking and spalling on a transparency

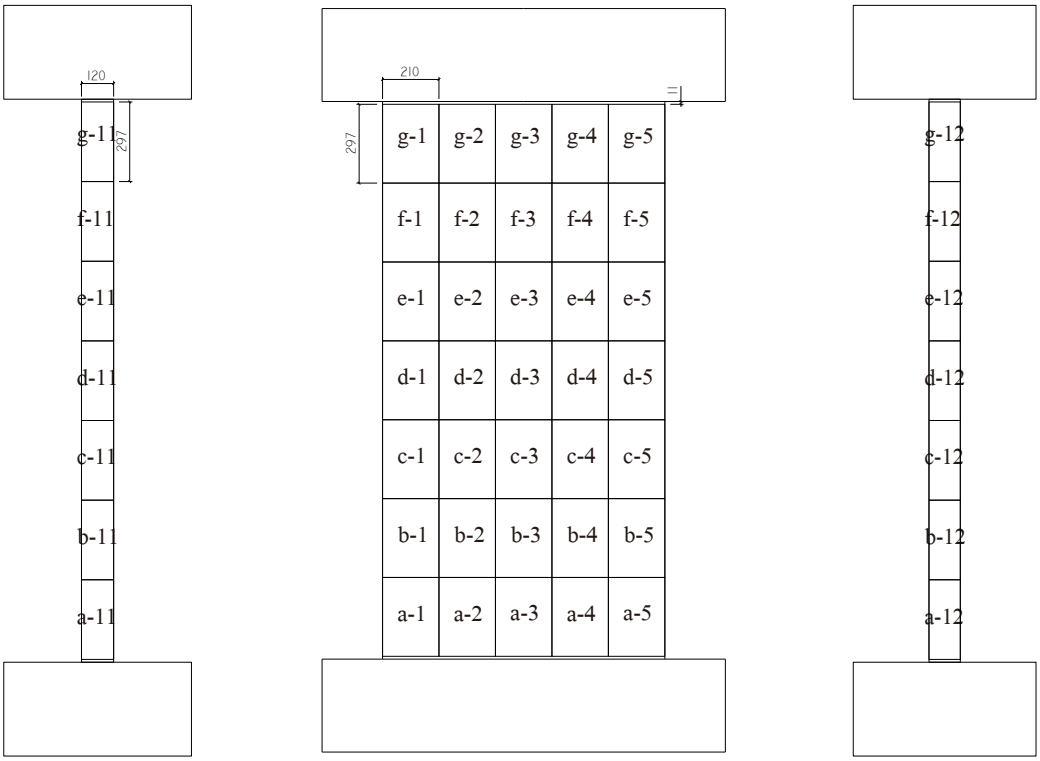

(a) North side (b) Front face (c) South side

Figure 4-17 Numbering system of crack measurement

4.5.1.1 Maximum crack width

Transitions of maximum peak and residual crack widths are shown in Figure 4-18. The maximum peak crack width ($_pW_{cr\text{-}max}$) is defined as the maximum width of all visible cracks at the peak point of the cycle. The maximum residual crack width ($_rW_{cr\text{-}max}$) is defined as the maximum width of all visible cracks when the lateral load is completely removed from the peak point. It is

noted that ${}_pW_{cr\text{-}max}$ and ${}_rW_{cr\text{-}max}$ were not necessarily measured at the same point. In actual earthquake condition, smaller earthquake shakings after the maximum shaking make the residual drift smaller. Therefore, this study considers the worst scenario for residual crack width. ${}_rW_{cr\text{-}max}$ of NSW1 and NSW2 was as large as ${}_pW_{cr\text{-}max}$ but that of NSW3 and NSW4 was less than half of ${}_pW_{cr\text{-}max}$. The reason is explained as follows. Flexure-shear cracks were dominant in NSW1 and shear cracks were dominant in NSW2. These shear cracks did not close when unloaded probably because the sliding accompanied to opening and cracked concrete surface was not able to return to the original position. However, flexural cracks were dominant in NSW3 and NSW4. Flexural cracks are able to return to the original position relatively easily since sliding does not accompany. It should be noted that diagonal shear cracks in NSW3 emerged at R= 0.50% and did not affect the plot in Figure 4-18 since flexural cracks were wider than that of diagonal shear cracks.

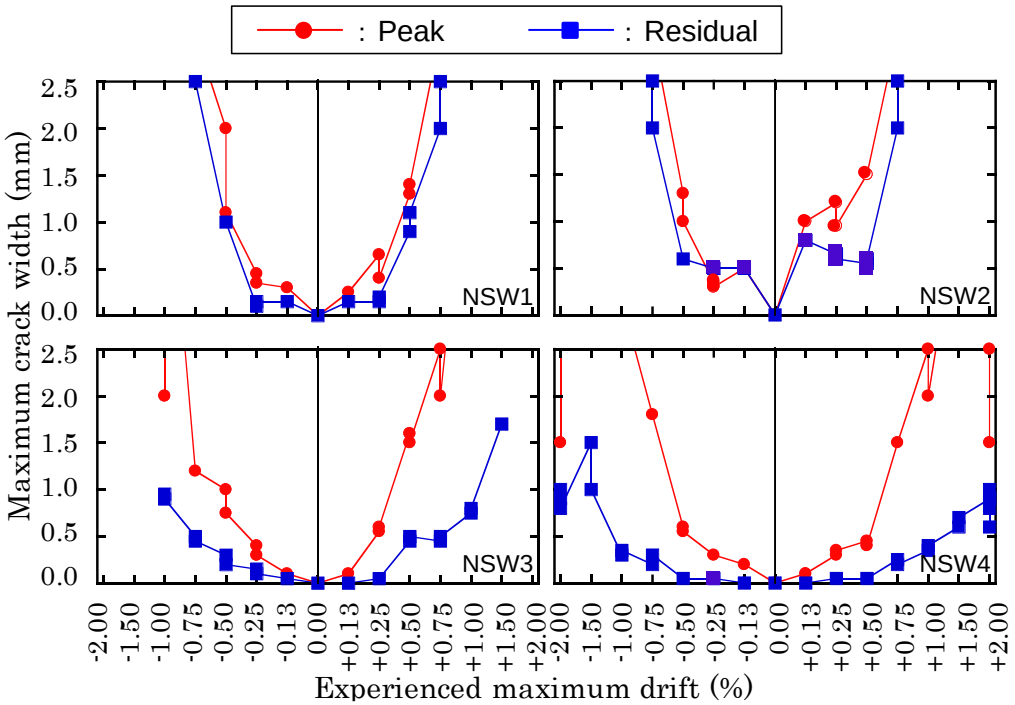

Figure 4-18 Maximum peak and residual crack widths

4.5.1.2 Residual crack density

Figure 4-19 shows the variation of residual crack density after the second cycle of negative loading. The residual crack density is defined as the total residual crack length per square root area. Each labeled crack was classified depending on its representative crack width and its length was summed to obtain the total length of that classification. The total length was divided by the square root area of front surface. The total residual crack density basically increased by increasing the drift. The residual crack density of NSW1 with ${}_rW_{cr} < 0.2$ mm decreased after R= 0.25% and the wider cracks increased. For NSW2, the total residual crack density was less than NSW1 up to R=

0.25%. However, it started to increase rapidly after R= 0.25% and exceeded NSW1 after R= 0.50%. Although NSW3 had larger total residual crack density than NSW2 up to R= 0.25%, NSW2 and NSW3 had similar total residual crack density at R= 0.75%. Unlike NSW2, NSW3 had no residual crack wider than 1.0 mm until R= 1.00%. It indicates that increasing the amount of horizontal reinforcement with anchorage suppressed the opening of crack width. NSW4 had less total residual crack density compared to the other specimens since flexural cracks concentrated in the lower portion of wall due to the cantilever type loading.

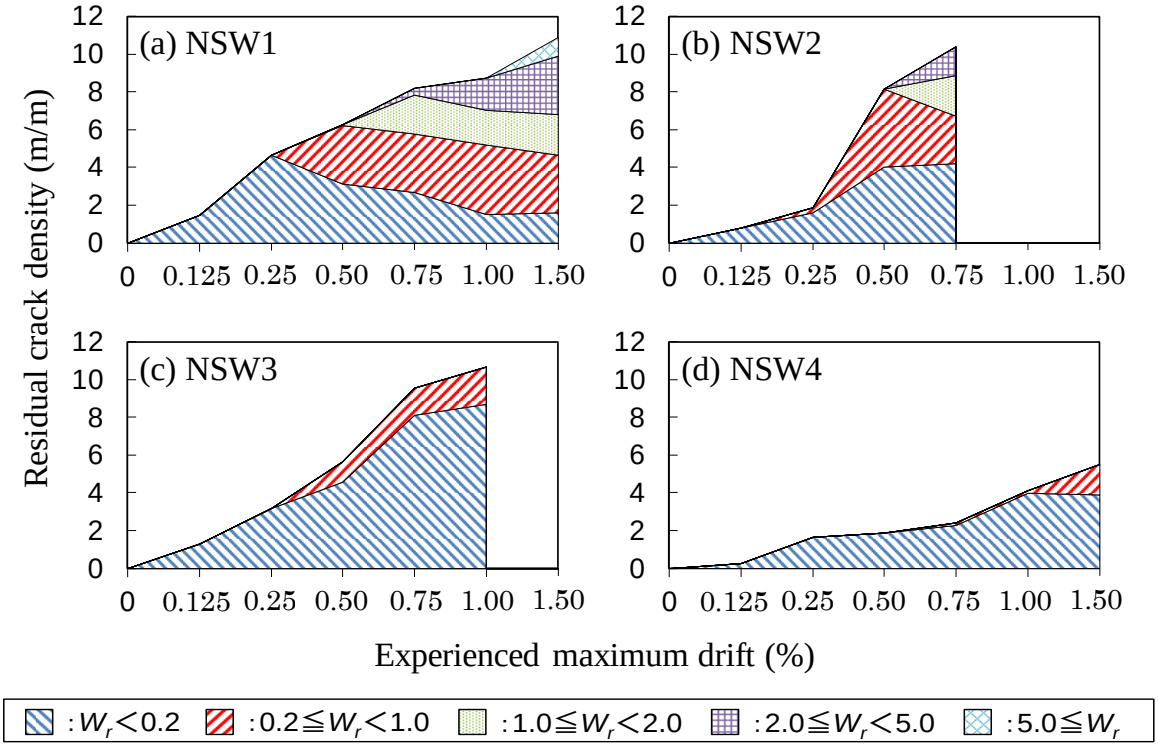

Figure 4-19 Residual crack density

4.5.1.3 Ratio of concrete spalling area

Ratio of concrete spalling area for all specimens after the second cycle of negative loading is shown in Figure 4-20. The ratio of concrete spalling area is defined as the area of concrete spalling due to either flexure or shear deformation divided by the area of front surface. Similar to the residual crack density in Figure 4-19, the ratio of spalling area also increased with increasing the drift. The ratio of spalling area for NSW1 and NSW4 were similar until R= 1.00%. Then, the ratio of spalling area increased drastically at R= 1.50% and R= 2.00% for NSW1 and NSW4, respectively. It is noted that concrete crushed at the upper and lower tips for NSW1, while for NSW4 spalling only occurred in the lower tip since it is cantilever type loading. The ratio of spalling area for NSW2 and NSW3 were similar until R= 0.50%. Then, the ratio of spalling area of NSW2 increased rapidly after R= 0.50% where concrete spalling occurred mostly at the central part

due to shear deformation. For NSW3, the concrete spalling took place at the wall tips. Concrete spalling in NSW2 and NSW3 occurred at different location because NSW3 had double amount of horizontal reinforcement compared to that of NSW2 so that shear crack did not develop to cause spalling at the central part.

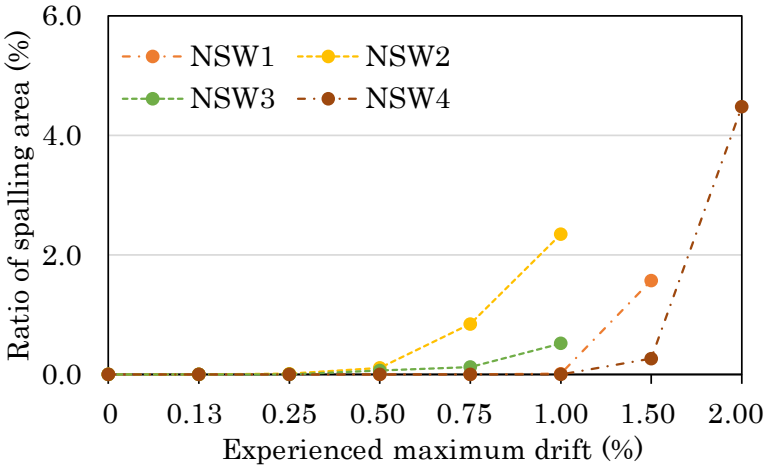

Figure 4-20 Ratio of concrete spalling area

4.5.2 Limit state and damage level

2004 AIJ Draft Guidelines [30] tabulate a relation of limit states and damage levels of members as shown in Table 4-8. Since the limit for each damage state is not defined in terms of measured quantity, quantitative criteria for each limit state is restated in Table 4-9 considering criteria proposed in the 2015 AIJ Draft [70] for prestressed concrete members. Based on Table 4-9, the limit states were determined for each specimen as shown in Table 4-11 and Figure 4-21(a). Dashed green, blue, and yellow lines in Figure 4-21 are serviceability limit state, reparability limit state I, and reparability limit state II, respectively.

Except for NSW1, the serviceability limit state of all specimens was reached by concrete since the stress of concrete at the extreme fiber reached two-third of its compressive strength. For NSW1, the serviceability limit state I was reached by yielding of vertical reinforcement at R= 0.16%. This is probably because NSW1 was tested under no axial load, so that the extreme fiber reached two-third of its compressive strength in higher drift (R= 0.29%). For NSW1, reparability limit state I occurred at R= 0.49% since strain of longitudinal reinforcement reached 2.00%. Although the lateral load carrying capacity of NSW1 did not significantly decrease after the peak, reparability limit state II occurred at R= 0.75% since the residual crack width became 2 mm. For NSW2, the reparability limit state I was reached since the strain of longitudinal reinforcement became 2.00% at R= 0.35%, while both concrete and residual crack width reached the reparability limit state II at R= 0.75%. For NSW3, longitudinal reinforcement reached the reparability limit state I at R= 0.35%, and cover concrete spalled at R= 1.00% to reach the reparability limit state II. For NSW4,

reparability limit state I was reached by all criteria at R= 1.50%, while reparability limit state I was reached by combination of buckling of longitudinal reinforcement, spalling of cover concrete, and residual drift > 0.25% at R= 2.00%, respectively.

Considering the total amount of damage (crack length and spalling area) as explained in Section 4.5.1, criteria at Table 4-9 work well to capture damage level of lightly RC walls. However, visual judgement from photos for concrete to determine minor crushing (reparability limit state I) is an important issue. It would be very subjective depending on a person who observes it. In addition, limit of $2/3f'_c$ for concrete is too strict for serviceability limit state since it is still in the range of immature elastic state as shown in Figure 4-21(a). The stress level may be taken larger than $2/3f'_c$ for the serviceability limit. By evaluating a limited experimental data, the stress of $0.8f'_c$ was proposed as serviceability limit for concrete. From Section 4.5.1.3, ratio of concrete spalling area can be also used as an indicator of concrete structures damage. Therefore, it was proposed as additional damage state criteria. Since lightly RC walls have single curtain of reinforcement, they would less likely reach high displacement ductility before the shear failure occurs. Based on experimental result of 26 wall specimens that failed in shear by Hidalgo et al. [27], the average ultimate drift, Ru, (which is defined as the lateral drift corresponding to the lateral load dropped of 80% peak value) was 0.73%. Therefore, the limit of residual drift for safety was proposed R< 1.00%.

The proposed criteria for limit and damage states is tabulated in Table 4-10, which the blue color indicates the proposed criteria. The limit states of all specimens were re-evaluated using the proposed criteria and shown in Table 4-12 and Figure 4-21(b). Limit of $0.8f'_c$ was more realistic for serviceability limit state of concrete. Although the limit state of damage did not change, it was also governed by the new criteria of ratio of concrete spalling area especially for walls that failed in flexure.

Table 4-8 Relation of limit states and damage levels (AIJ Guidelines, 2004)

Limit state	Damage state	Damage level	Damage state		
			Longitudinal reinforcement	Concrete	Residual crack width
	Continuous usage	I	Elastic	Nearly elastic	< 0.2 mm
Serviceability	Easily repaired	II	Yielding	Healty	0.2 - 1.0 mm
Reparability I	Reparable	III	Buckling	Core concrete is healthy	1.0 - 2.0 mm
Reparability II	Veritical load can be sustained	IV	No fracture	Core concrete has not crushed	
Safety	Lateral load capacity degrade	V	Fracture	Crushing of core concrete	

Table 4-9 Criteria used to categorize into four damage states

Limit state	Damage state			
	Longitudinal reinforcement	Concrete	Residual crack width	Residual drift
Serviceability	Yielding	Stess < $2/3f'_c$ (check axial strain at extreme fiber)	< 0.2 mm	R < 0.10%
Reparability I	Yielding is allowed to some extend (strain = 2.0%)	Minor crushing of cover (visual judgement from photos)	0.2 - 1.0 mm	R < 0.25%
Reparability II	Buckling (visual judgement from photos)	Cover spalling	1.0 - 2.0 mm	R < 0.50%
Safety	Fracture (from photos)	Crushing of core concrete (from photos)	> 2.0 mm	R = 4.00%

Table 4-10 Proposed criteria of limit states and damage levels of lightly RC walls

Limit state	Damage state				
	Longitudinal reinforcement	Concrete	Residual crack width	Residual drift	Ratio of Concrete Spalling Area
Serviceability	Yielding	Stess < $0.8f'_c$ (check axial strain at extreme fiber)	< 0.2 mm	R < 0.10%	= 0.0%
Reparability I	Yielding is allowed to some extend (strain = 2.0%)	Minor crushing of cover (visual judgement from photos)	0.2 - 1.0 mm	R < 0.25%	< 1.0%
Reparability II	Buckling (visual judgement from photos)	Cover spalling	1.0 - 2.0 mm	R < 0.50%	< 5.0%
Safety	Fracture (from photos)	Crushing of core concrete (from photos)	> 2.0 mm	R < 1.00%	> 5.0%

Table 4-11 Limit state and damage level of all specimens based on Table 4-9

Criteria			Limit state	Specimen							
				NSW1		NSW2		NSW3		NSW4	
Reinforcement	RB	Yielding	Serviceability limit state	0.16		0.31		0.17		0.24	
		Tensile strain ≤ 2.0%	Reparability limit state I	0.49		0.35		0.35		1.50	
		Buckling of longitudinal reinforcement	Reparability limit state II	1.50		1.00		1.50		2.00	
		Fracture of longitudinal reinforcement	Safety limit state	-		-		-		-	
Concrete	CO	Concrete stress ≤ 2/3f'c	Serviceability limit state	0.29		0.13		0.10		0.10	
		Minor spalling of cover concrete	Reparability limit state I	1.00		0.51		0.75		1.50	
		Spalling of cover concrete	Reparability limit state II	1.50		0.75		1.00		2.00	
		Crushing of core concrete	Safety limit state	1.50		1.00		1.50		2.00	
Residual crack	CR	< 0.2 mm	Serviceability limit state	0.25		-		0.50		0.50	
		0.2 - 1.0 mm	Reparability limit state I	0.50		0.50		1.00		1.50	
		1.0 - 2.0 mm	Reparability limit state II	0.75		0.75		-		-	
		> 2.0 mm	Safety limit state	0.75		0.75		-		-	
Residual drift	DR	R < 0.10%	Serviceability limit state	0.25		0.50		0.50		1.00	
		R < 0.25%	Reparability limit state I	0.75		1.00		1.00		1.50	
		R < 0.50%	Reparability limit state II	1.00		-		-		2.00	
		R = 4.00%	Safety limit state	-		-		-		-	
Governed drift (%)			Serviceability limit state	0.16	RB	0.13	CO	0.10	CO	0.10	CO
			Reparability limit state I	0.49	RB	0.35	RB	0.35	RB	1.50	ALL
			Reparability limit state II	0.75	CR	0.75	CO, CR	1.00	CO	2.00	RB, CO, DR
			Safety limit state	0.75	CR	0.75	CR	1.50	CO	2.00	CO

Table 4-12 Limit state and damage level of all specimens based on Table 4-10

Criteria			Limit state	Specimen							
				NSW1		NSW2		NSW3		NSW4	
Reinforcement	RB	Yielding	Serviceability limit state	0.16		0.31		0.17		0.24	
		Tensile strain ≤ 2.0%	Reparability limit state I	0.49		0.35		0.35		1.50	
		Buckling of longitudinal reinforcement	Reparability limit state II	1.50		1.00		1.50		2.00	
		Fracture of longitudinal reinforcement	Safety limit state	-		-		-		-	
Concrete	CO	Concrete stress ≤ 0.8f'c	Serviceability limit state	0.40		0.17		0.16		0.18	
		Minor spalling of cover concrete	Reparability limit state I	1.00		0.51		0.75		1.50	
		Spalling of cover concrete	Reparability limit state II	1.50		0.75		1.00		2.00	
		Crushing of core concrete	Safety limit state	1.50		1.00		1.50		2.00	
Residual crack	CR	< 0.2 mm	Serviceability limit state	0.25		-		0.50		0.50	
		0.2 - 1.0 mm	Reparability limit state I	0.50		0.50		1.00		1.50	
		1.0 - 2.0 mm	Reparability limit state II	0.75		0.75		-		-	
		> 2.0 mm	Safety limit state	0.75		0.75		-		-	
Residual drift	DR	R < 0.10%	Serviceability limit state	0.25		0.50		0.50		1.00	
		R < 0.25%	Reparability limit state I	0.75		1.00		1.00		1.50	
		R < 0.50%	Reparability limit state II	1.00		-		-		2.00	
		R < 1.00%	Safety limit state	-		-		-		-	
Ratio of Concrete Spalling Area	SP	≈ 0.0%	Serviceability limit state	0.75		0.25		0.25		1.00	
		< 1.0%	Reparability limit state I	1.00		0.75		1.00		1.50	
		< 5.0%	Reparability limit state II	1.50		1.00		-		2.00	
		> 5.0%	Safety limit state	-		-		-		-	
Governed drift (%)			Serviceability limit state	0.16	RB	0.17	CO	0.16	CO	0.18	CO
			Reparability limit state I	0.49	RB	0.35	RB	0.35	RB	1.50	ALL
			Reparability limit state II	0.75	CR	0.75	CO, CR	1.00	CO	2.00	RB, CO, DR, SP
			Safety limit state	0.75	CR	0.75	CR	1.50	CO	2.00	CO

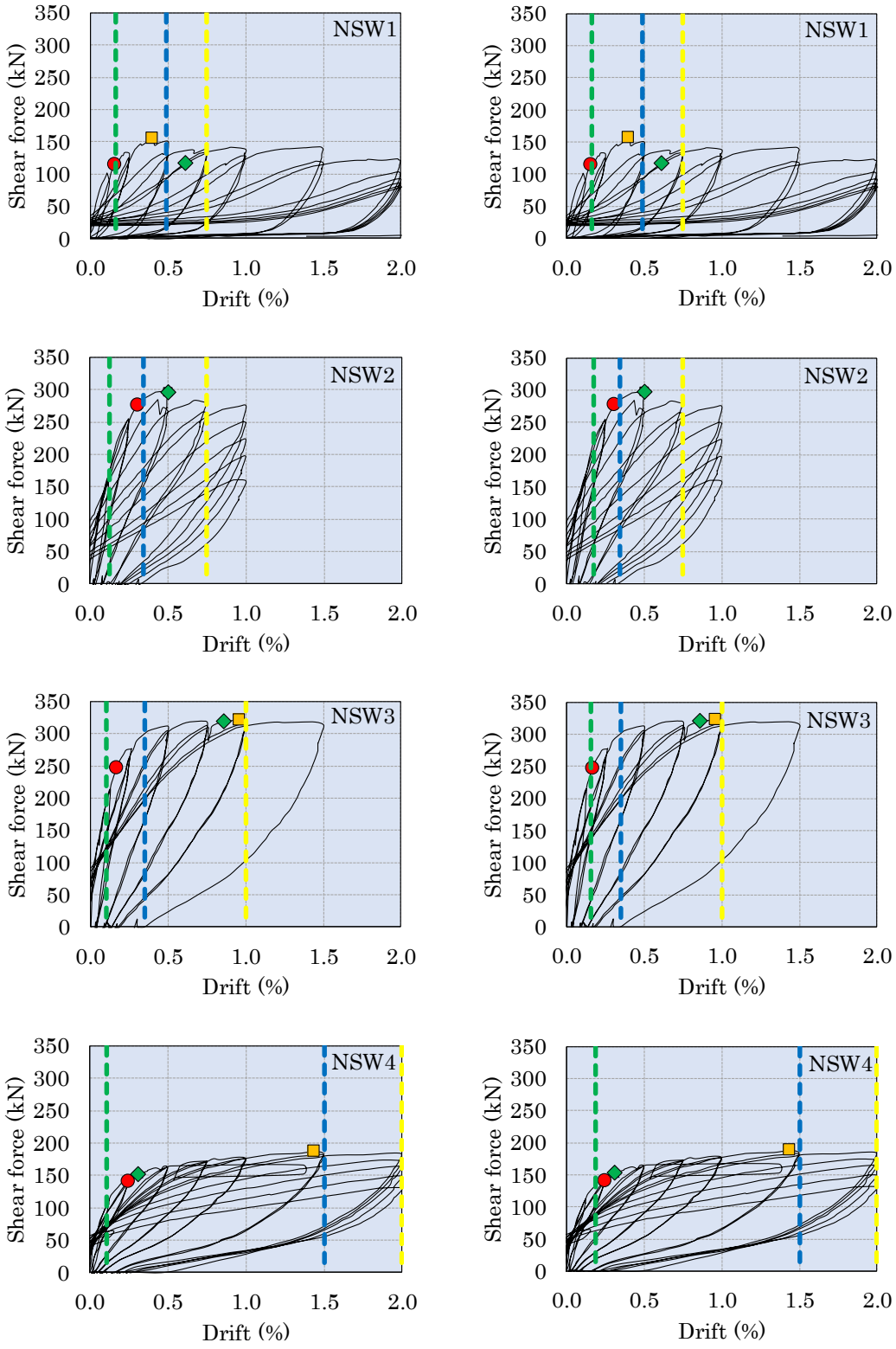

(a) Based on Table 4-10 (b) Based on proposed criteria

Yield of vertical reinforcement, Yield of horizontal reinforcement, Max. lateral load capacity

Figure 4-21 Evolution of limit states for all specimens

4.6 Conclusions

An experimental test was conducted on four lightly RC walls with single layer of reinforcement and with no confinement in their end regions to study their seismic behaviors such as hysteresis characteristics with load and displacement capacities, damage progress and failure modes. In addition, their damages were evaluated in terms of crack width, crack length, and concrete spalling area at different drift levels to see damage progress of RC walls. The damage level was assessed using the 2004 AIJ Guidelines [30] to study its validity for lightly RC walls and some modifications have been proposed. The findings of this study are summarized in the following paragraphs.

1) NSW1 and NSW4 showed ductile and stable behavior with less damage compared with NSW2 and NSW3. The maximum lateral load capacities of NSW2 and NSW3 were higher than those of NSW1 and NSW4. However, NSW1 and NSW4 had larger drift capacities compared to NSW2 and NSW3. The maximum lateral load and drift capacities depended on the axial load ratio and shear span to wall length ratio. Experimental results showed that higher axial load ratio and lower shear span to wall length ratio resulted in higher lateral load capacity but smaller drift capacity. In addition, the study also showed that increasing the amount of horizontal reinforcement increased the lateral load capacity slightly but increased the drift capacity significantly.
2) Shear type damage was observed for three specimens (NSW1, NSW2, and NSW3), which were tested under double curvature loading, while NSW4 failed in a compression controlled flexure mode. Axial load ratio, shear span to wall length ratio, and the amount of horizontal reinforcement affected to damage process and failure mode. Specimen with axial load tends to fail in a brittle manner. Lightly RC walls with large shear span to wall length ratio are less susceptible to brittle shear failure than walls with smaller shear span to wall length ratio. In addition, increasing the amount of horizontal reinforcement and providing 180-degree hook anchorage improved the seismic behavior and prevented the opening of shear cracks.
3) The sequence of observed damage was similar among all specimens: concrete cracking, yielding of the longitudinal reinforcement, initial spalling of the concrete cover, final spalling of the concrete cover, buckling of the longitudinal reinforcement, and no fracture of the longitudinal reinforcement was observed.
4) The maximum crack width and maximum residual crack width increase globally with the increase in specimen drift. With the rapid accumulation of damage, the deterioration of the crack closing ability of most specimens was observed after the yielding of the longitudinal reinforcement. The axial load ratio seems to be the most important factor affecting crack behavior. An increase in the axial load ratio can significantly reduce the maximum crack width and effectively promote crack closing during unloading.
5) Considering the total amount of damage (crack length and spalling area), the criteria of the

2004 AIJ Guidelines worked reasonably well to capture damage levels of lightly RC walls. However, limit of $2/3f'_c$ for concrete is too strict for serviceability limit state since it is still in the range of immature elastic state. The limit stress level of $0.8f'_c$ was proposed and provided more realistic estimate for serviceability limit state of concrete. In addition, the ratio of concrete spalling area was also proposed as damage state criteria to determine limit state of lightly RC walls.

5 EXPERIMENTAL 2: SEISMIC BEHAVIOR OF RETROFITTED LIGHTLY REINFORCED CONCRETE WALLS

5.1 Introduction

The National Institute for Land and Infrastructure Management (NILIM) and the Building Research Institute (BRI) reported that many perimeter lightly reinforced concrete (RC) walls with opening (spandrel, wall pier, wing wall) in residential and government office buildings had severe damage during the 2011 off the Pacific coast of Tohoku Earthquake [2] shown in Figure 5-1. Most damages to these walls were due to shear cracking or failure. Such damages did not affect safety of buildings but suspended the continuity of the building functions. In Japan, these walls are structurally connected to the surrounding beams or columns. They are not primary structural components and are often treated as secondary structural components which attract less attention in design [60]. A common design practice sometimes neglects their contributions to the lateral load carrying capacities. Lightly RC walls are typically 120 to 200 mm thick, and have a single curtain of reinforcement in two directions with a few additional boundary vertical reinforcing bars at section ends. In many cases, horizontal reinforcement has no hook anchorage and boundary region has no confinement. Hence, the current design practice makes lightly RC walls intrinsically vulnerable to earthquake damages. In order to avoid these damages, it is very important to have proper upgrading schemes to improve the seismic performance of lightly RC walls.

Figure 5-1 Damage of lightly RC walls after the 2011 Tohoku Earthquake [2]

This section presents an experimental study on four full-scale lightly RC walls with or without upgrading. The goal of the upgrading was to improve the seismic behavior of lightly RC walls by enhancing both shear and ultimate drift capacities. A prototype wall (NSW2), which was already

explained in Chapter 4, failed prematurely in shear reproducing the failure mode observed in condominiums in the 2011 off the Pacific coast of Tohoku Earthquake. Two specimens were upgraded by placing additional wall panel and the other specimen was upgraded by improving the reinforcement details. Experimental observations on four walls are reported in terms of lateral load carrying capacity, energy dissipation (ductility), damage process, and failure mode.

5.2 Experimental Program

5.2.1 Specimen description and materials

The experiment included four wall specimens as listed in Table 5-1. The prototype specimen, NSW2, was included for comparison. It was designed following the typical Japanese design practice for infill walls and loaded laterally under the axial load of 15% of axial load capacity. The specimen failed in shear as observed in the 2011 off the Pacific coast of Tohoku Earthquake. The detail should be referred in Chapter 4. The remaining three specimens were upgraded version of NSW2 to prevent shear failure. Figure 5-2 shows the details of four specimens. NSW2 was 2100 mm tall with a cross section of 120 mm x 1050 mm. Two D13 reinforcing bars were provided as vertical reinforcement at the both end of sections, while a single curtain of D10 bars were provided at 250 mm spacing as both vertical and horizontal reinforcement as shown in Figure 5-2(a) and (h).

The upgraded specimens (NSW2A, NSW2B, and NSW5) had higher shear capacity and NSW5 had even enhanced flexural ductility by confining boundary regions. NSW2A and NSW2B consisted of two portions, original and additional wall panels. The original wall panels are identical to that of NSW2 and an additional concrete wall panel was installed. The additional wall panel of NSW2A was 80 mm thick reinforced concrete as shown in Figure 5-2(e). Pre-installed 18-M16 high-strength bolts were used as dowels to prevent relative slip. The bolts were embedded with length of 80 mm in the original panel and 50 mm in the additional wall panel as shown in Figure 5-2(l). The 18 bolts with long nuts were installed from the beginning as a part of the original panel. Vertical reinforcement of additional wall panel was not anchored to either of the upper and lower blocks to avoid the increase of flexure capacity. A single curtain of D10@250 was placed on the upper surface of the laid specimen as both vertical and horizontal reinforcement and concrete was cast directly on the original panel. No gap was placed at the interface of the upper and lower concrete blocks. The additional wall panel of NSW2B was an ultra-high strength fiber reinforced concrete (UFC) panel with a thickness of 60 mm as shown in Figure 5-2(f) and (j). The UFC panel was placed on the upper surface of the laid specimen with 10 mm thick epoxy resin with no mechanical anchorage. Ten millimeter wide gaps at the interface of concrete blocks were also filled with epoxy resin. NSW2A and NSW2B consisting of two panels (original and additional panels) was located at the center of the concrete blocks without any eccentricity. NSW5 had the same dimension with NSW2 but enhanced reinforcement details. Deformed steel bars of D10@60 (p_{wh}= 1.0%) were provided as horizontal reinforcement with 180-degree hook anchorage, while deformed

steel bars of 4-D13 were provided as vertical reinforcement with D6@60 closed hoops at boundary regions. It is noted that the upgrading method of NSW2A and NSW2B are intended for existing walls, while that of NSW5 is intended for new construction to improve the current common practice. Mechanical properties of concrete and reinforcing bars are shown in Table 5-2 and Table 5-3, respectively.

Table 5-1 Specification of specimens

Specification		Specimen			
		NSW2	NSW2A	NSW2B	NSW5
Original wall panel	Wall thickness(mm)	120	120	120	120
	Wall length (mm)	1050	1050	1050	1050
	Wall height (mm)	2100	2100	2100	2100
	Vertical reinf. at boundary	2-D13	2-D13	2-D13	4-D13
	Confinement at boundary region	-	-	-	D6@60
	Vertical reinforcement	D10@250	D10@250	D10@250	D10@250
	Horizontal reinforcement	D10@250	D10@250	D10@250	D10@60
		(p_{wh}[1] =0.24%)	(p_{wh} =0.24%)	(p_{wh} =0.24%)	(p_{wh} =1.00%)
Additional wall panel	Wall thickness(mm)	-	80[2]	60[2, 3]	-
	Wall length (mm)	-	1050	1050	-
	Wall height (mm)	-	2100	2100	-
	Vertical reinforcement	-	D10@250	-	-
	Horizontal reinforcement	-	D10@250	-	-
Total wall thickness (mm)		120	200	190[4]	120
Loading conditions	Shear span (mm)	1050	1050	1050	1050
	M/Vl_w[5]	1.0	1.0	1.0	1.0
	Axial force, N (kN)	458	419	419	419
	P/f'_cA_g[6]	0.15	0.15	0.15	0.15

[1]Horizontal reinforcement ratio.

[2]Additional walls are RC and UFC panels for NSW2A and NSW2B, respectively.

[3]Fiber properties for UFC: diameter = 0.22 mm, length = 15.23 mm, weight ratio = 6.20%.

[4]UFC panel was placed using an adhesive with 10 mm thick.

[5]Shear-span to wall length ratio.

[6]f'_c: concrete compressive strength, A_g: gross cross-sectional area of wall (original wall for NSW2A and NSW2B)

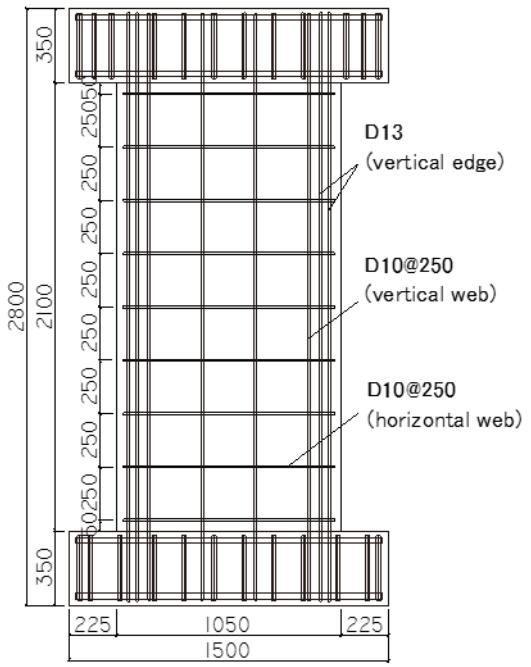

(a) NSW2, NSW2A, NSW2B (original wall)

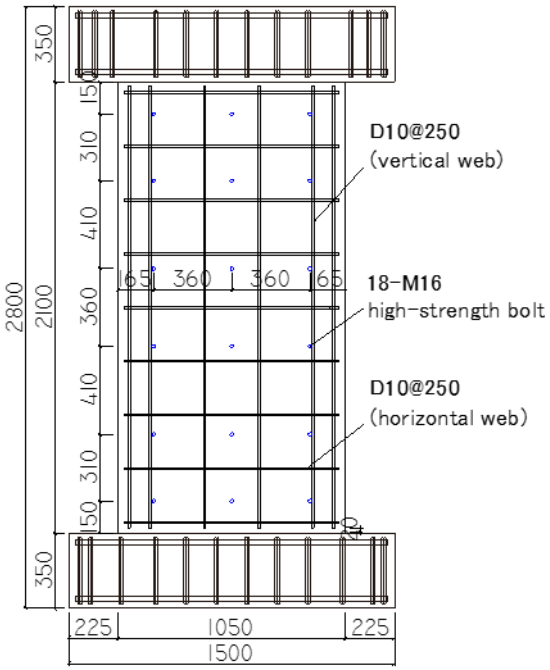

(b) NSW2A(additional wall)

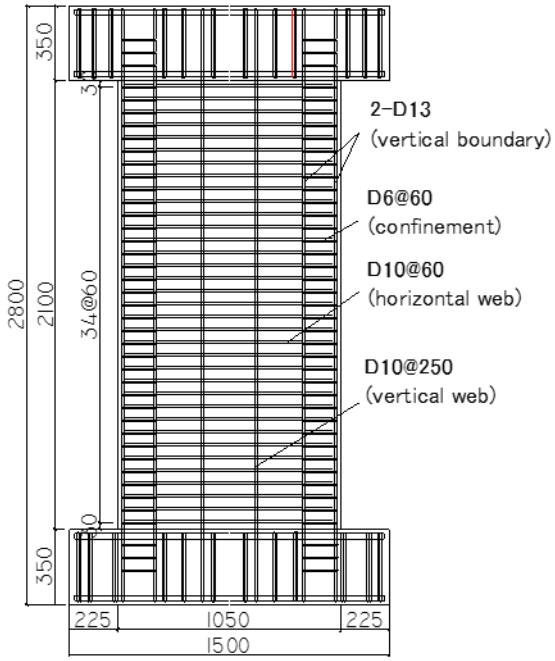

(c) NSW5

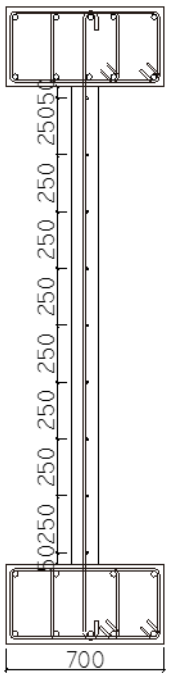

(d) NSW2

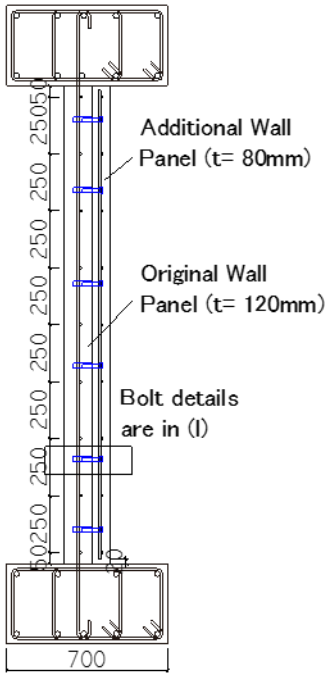

(e) NSW2A

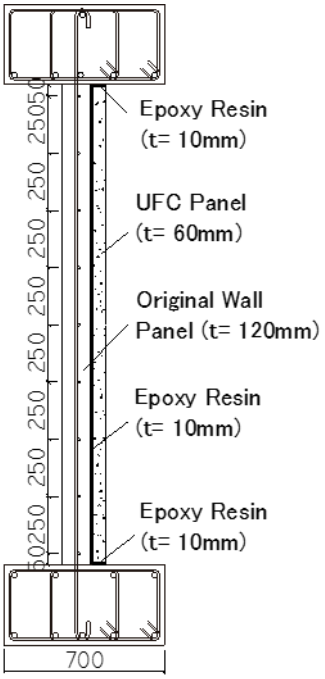

(f) NSW2B

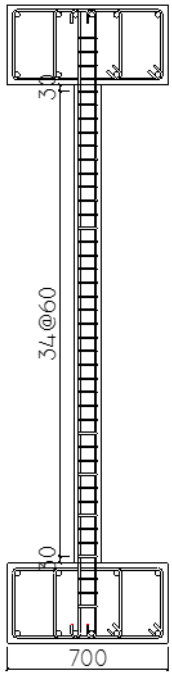

(g) NSW5

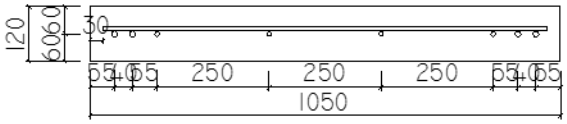

(h) Cross section of NSW2

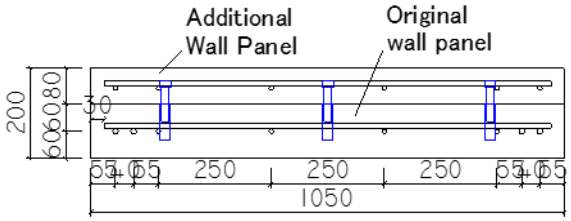

(i) Cross section of NSW2A

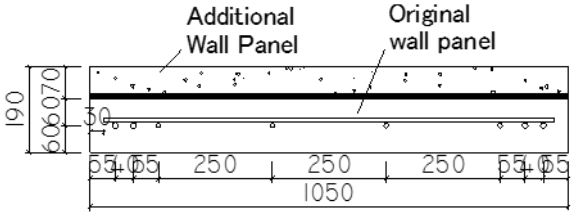

(j) Cross section of NSW2B

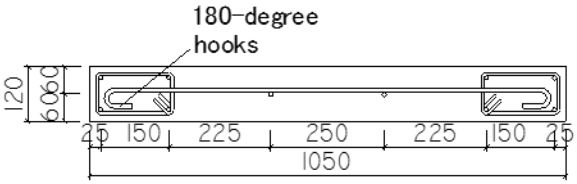

(k) Cross section of NSW5

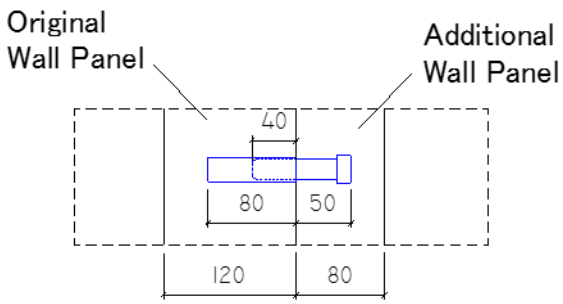

(l) Bolt details of NSW2A

Figure 5-2 Dimension and reinforcing detail of specimens (unit: mm)

Table 5-2 Mechanical properties of concrete

Member		Specimen	f'_c	E_c	ε_c	f_t
			(N/mm^2)	(kN/mm^2)	(%)	(N/mm^2)
Original wall panel		NSW2	24.2	26.3	0.182	2.46
		NSW2A, 2B, 5	22.2	24.9	0.170	2.16
Additional panel	RC	NSW2A	23.6	24.7	0.196	2.51
	UFC	NSW2B	192.5	-	-	-

f'_c: compressive strength, E_c: Young's modulus, ε_c: strain at peak, f_t: splitting tensile strength

Table 5-3 Mechanical properties of steel reinforcing bars

Location of reinforcement	Specimen	Diameter (mm)	f_y	f_u	E_s	ε_y
			(N/mm^2)	(N/mm^2)	(kN/mm^2)	(%)
Vertical and horizontal web	NSW2	D10	347	484	190	0.183
	NSW2A, 2B, 5	D10	380	506	172	0.282
Vertical boundary	NSW2	D13	360	527	190	0.189
	NSW2A, 2B, 5	D13	354	481	180	0.193
Confinement	NSW5	D6	376	504	185	0.403

f_y: yield strength, f_u: tensile strength, E_s: Young's modulus, ε_y: strain at yield strength

5.2.2 Design of specimens

All upgraded wall specimens were designed to fail in flexure by increasing their shear capacity. To achieve flexure failure, shear safety factor, *z*, which is the ratio of shear capacity to flexure capacity, was set higher than 1.0. Considering the maximum aggregate size of 20 mm and a sufficient thickness of cover concrete, an 80 mm RC wall thickness was selected as the additional wall panel for NSW2A. The thickness of additional panel for NSW2B was determined based on the experimental result of half-scale RC column retrofitted by precast UFC wing walls to improve its lateral load carrying capacity and ductility [71]. In this experiment, 50 mm thick UFC panels were placed as wing walls aside the existing column. No buckling was observed. A 60 mm thick UFC panel was adopted for additional wall panel of NSW2B to enhance shear capacity.

In order to ensure the contribution of additional wall panel, it is necessary to have a good bond between the new and old panels. In this study, eighteen M16 high-strength bolts were used for dowel bars in NSW2A. Based on ACI 318M-14 [23], the required area of shear-friction reinforcement, A_{vf} is calculated using the formula as expressed in Eq. (5-1).

$$A_{vf} = \frac{V_u}{\phi f_y \mu} \tag{5-1}$$

where V_u is factored shear force at section, ϕ is strength reduction factor (= 0.75 for shear), f_y is yield strength of reinforcement or bolt (maximum value of f_y permitted for design calculation is

420 MPa), and μ is the coefficient of friction (=0.6λ for concrete placed against hardened concrete that is clean, free of laitance, and not intentionally roughened, where λ = 1.0 for normal weight concrete). In addition, based on section 22.9.4.4 ACI 318M-14, the value of V_n across the assumed shear plane shall not exceed either minimum of $0.2f'_cA_c$ or $5.5A_c$, where A_c is area of concrete section resisting shear transfer. Since NSW2A is designed to fail in flexure, the computed flexure capacity of 318 kN was used for V_u in Eq. (5-1) and 9-M16 bolts were required for each shear span. For NSW2B, a 10 mm thick epoxy adhesive was used for the UFC panel. The epoxy had compressive strength 71 N/mm^2, Young's modulus 5.1 kN/mm^2, tensile lap-shear strength 20 N/mm^2, and bond strength to concrete surface 5.1 N/mm^2.

The Commentary of Japanese Building Code for Structural Safety [72] has a simplified wall equation of flexure capacity, Q_{mu} and empirical equation of shear capacity, Q_{su} as expressed in Eqs. (5-2) and (5-3). In addition, the 1999 AIJ Guidelines [60] provides an equation to calculate shear cracking capacity of rectangular column, Q_{sc} as shown in Eq. (5-4). Equation (5-4) is the cracking capacity when the principle tensile stress reaches the tensile strength.

$$Q_{mu} = \left(a_t f_y l_w + 0.5 a_{wv} f_{wv} l_w + 0.5 N l_w\right) / a \tag{5-2}$$

$$Q_{su} = \left\{ \frac{0.068 p_{te}^{\ 0.23} \left(f'_c + 18\right)}{\sqrt{M/(QD) + 0.12}} + 0.85\sqrt{f_{wh} p_{wh}} + 0.1\sigma_0 \right\} t_e j \tag{5-3}$$

$$Q_{sc} = \phi\left(\sqrt{{\sigma_T}^2 + \sigma_T \sigma_0}\right) t_e D \Big/ \kappa \tag{5-4}$$

where, a_t, f_y: area and yield strength of longitudinal reinforcement in the wall boundary area, a_{wv}, f_{wv}: area and yield strength of longitudinal web reinforcement, l_w: length between the centers of boundary columns (0.9D for rectangular cross-section), N: axial load, a: shear span length, p_{te}: equivalent tensile reinforcement ratio (%) (=100a_t/t_ed), d: effective length of wall (=0.95D), f'_c: concrete compressive strength, $M/(QD)$: shear span to wall length ratio ($1 \le M/(QD) \le 3$), f_{wh}: yield strength of horizontal web reinforcement, p_{wh}: horizontal web reinforcement ratio, σ_0: average axial stress for gross cross-sectional area, t_e: equivalent wall thickness, j: lever arm length (=7/8d), ϕ: capacity reduction coefficient to consider scatter of experimental data (=1.0 was used to derive the mean value), σ_T: concrete tensile strength ($=0.33\sqrt{f'_c}$), D: wall length, κ: shape coefficient (=1.5 for rectangular section).

Since the vertical reinforcement of the additional wall panel for NSW2A was not anchored to the blocks, its contribution was not accounted in Eq. (5-2). Therefore, Q_{mu} of NSW2A and NSW2B were same. The Q_{su} of the original and additional wall panels for NSW2A and NSW2B were calculated separately. Equation (5-3) was used to calculate Q_{su} of the original wall panel, while for Q_{su} of additional wall panel was calculated based on AIJ Design Guidelines 1999 [60] as follow.

$$Q_{su} = 0.5 f'_c bD \tan\theta \quad (5\text{-}5)$$

where, f'_c: concrete compressive strength, b: wall thickness, D: wall length, θ: angle of compression strut of arch mechanism, $tan\theta = 0.9D/2L$, and L: wall height. Equation (5-5) was used for additional wall panel of NSW2A to calculate shear capacity since the vertical reinforcement was not anchored to the blocks, and there was no reinforcement at UFC panel for NSW2B. The truss mechanism did not contribute to the shear capacity of additional panels. The shear capacity of NSW2A or NSW2B was assumed as summation of Q_{su}'s of the original and additional wall panels. Although two shear resisting mechanisms in the original and additional wall panels are not necessarily compatible, it is easy and useful to obtain the shear capacity by adding their capacities. Since NSW2B consisted of two different materials (concrete and UFC), Q_{sc} was calculated by considering their axial stiffness, EA to obtain the axial load portion at the original and additional wall panels. Young's modulus, E was calculated using the AIJ Standard 2010 [73] as follows.

$$E = 3.35x10^4 \left(\frac{\gamma}{24}\right)^2 \left(\frac{F_c}{60}\right)^{\frac{1}{3}} \quad (5\text{-}6)$$

where, γ: specific weight of concrete (kN/m^3) and F_c: concrete cylinder compressive strength (N/mm^2). Table 5-4 summarizes Q_{mu}, Q_{su}, Q_{sc}, and z of all specimens. For all upgraded specimens, Q_{mu} is less than Q_{su} and their failure mode is supposed to be flexure. In addition, it is expected no shear crack will occur in NSW2A and NSW2B since their Q_{sc} is greater than Q_{cal}.

Table 5-4 Calculated capacity of specimens

Specimen	Q_{mu} (kN)	Q_{su} (kN)	Q_{sc} (kN)	Q_{cal} [1] (kN)	z [2]
NSW2	333	318	221	318	0.95
NSW2A	318	535	329	318	1.68
NSW2B	318	1676	376	318	5.27
NSW5	374	429	231	374	1.15

[1] $Q_{cal} = \min(Q_{mu}, \max(Q_{su}, Q_{sc}))$,

[2] Shear safety factor ($z = Q_{su}/Q_{mu}$).

5.2.3 Test setup and loading method

The test setup is shown in Figure 4-4. Two vertical hydraulic jacks were controlled so that the axial compression load of $0.15f'_cA_g$ was constant (458 kN for NSW2 and 419 kN for the remaining walls) and the upper block was parallel to the lower block. All specimens were tested under double curvature with shear-span to depth ratio of 1.0. The lateral load was controlled by drift R, which is defined as the ratio of the horizontal displacement to the clear height of the wall panel (2100 mm). The loading protocol consisted of one cycle of R= ±0.125% followed by two cycles of ±0.25%, ±0.50%, ±0.75%, ±1.00%, ±1.50%, ±2.00%, ±3.00%, and the load was increased monotonically to

R= +5.00%. Since the lateral load capacity of NSW2 decreased quickly after the peak, five cycles were imposed at *R*= 1.00% to study the degree of degradation. NSW5 failed due to sliding shear during the first cycle of *R*= +3.00% and the loading was terminated.

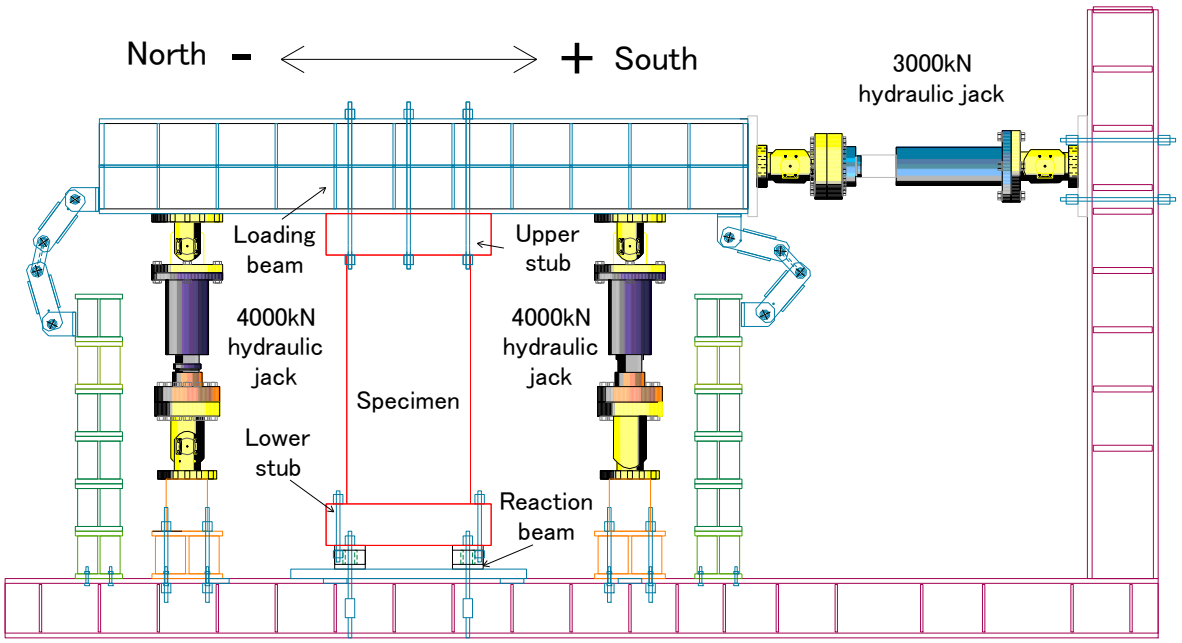

Figure 5-3 Test setup (unit in mm)

5.2.4 Instrumentation and measurement

Figure 5-4 and Figure 5-5 shows the location of displacement and strain gauges of all upgraded specimens. Four displacement transducers were mounted vertically at four zones of 0-550 mm from the lower end of wall panel (Z1), 550-1050 mm (Z2), 1050-1550 mm (Z3), and 1550-2100 mm (Z4) for both north and south sides in order to measure flexural deformation. Displacement transducers were also mounted vertically to the additional wall panel for NSW2A and NSW2B as shown in Figure 5-4(b) and (d). Eight displacement transducers were mounted diagonally in order to measure shear deformation. The gap opening and sliding between the wall panel and blocks were measured using eight (ten transducers for NSW2) displacement transducers at the interface. Out-of-plane deformation was measured using three displacement transducers which were mounted to a reference frame as shown in Figure 4-6. The lateral drift was measured using two methods, i.e. (1) by using transducer mounted to a reference frame parallel to the upper stub of the specimen as shown in Figure 4-6 and Figure 4-7, and (2) by using transducers mounted at the wall panel. Strain gauges were placed on steel reinforcing bars at critical locations as shown in Figure 5-8 - Figure 5-10.

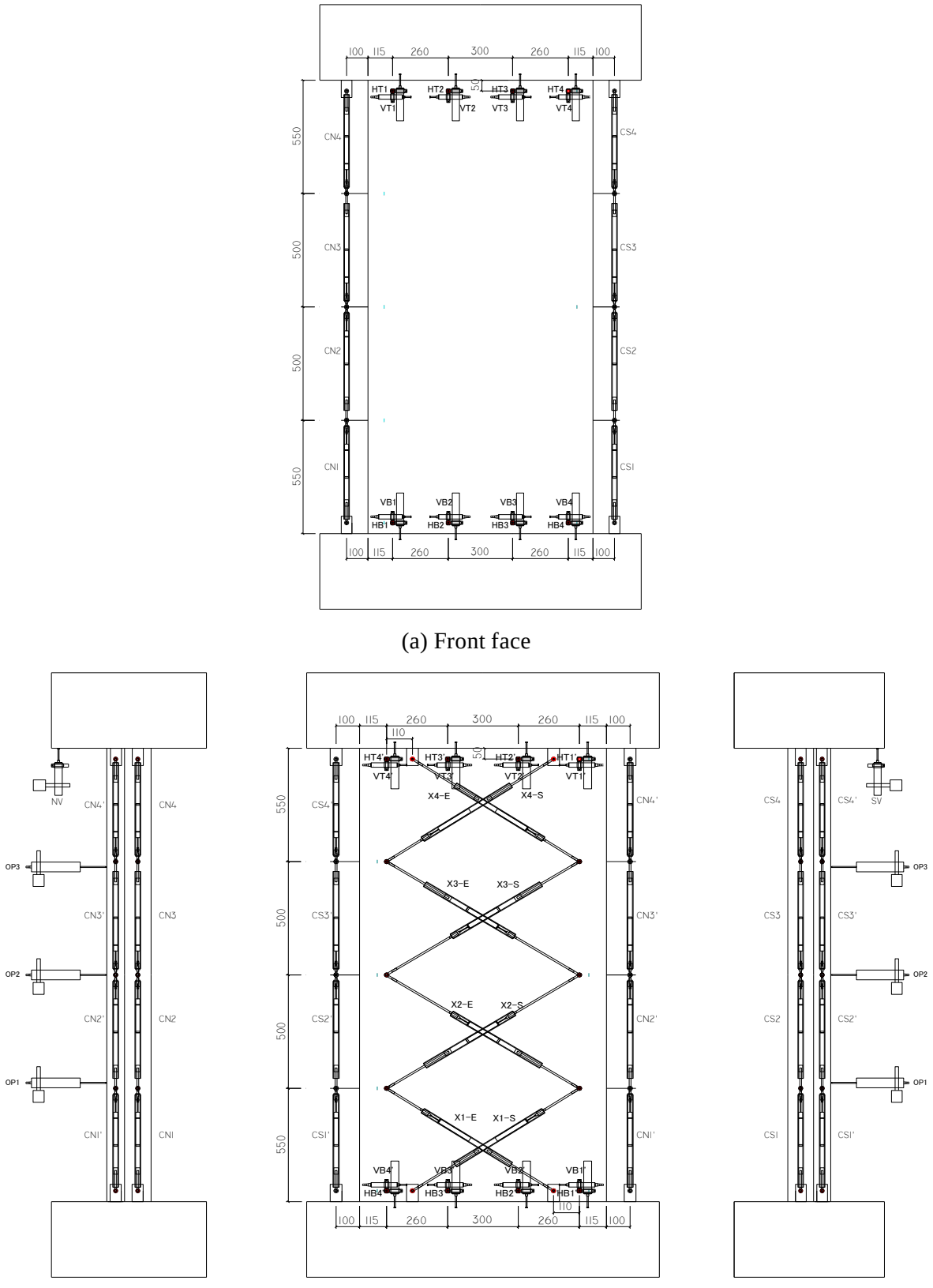

(a) Front face

(b) North side (c) Back face (d) South side

Figure 5-4 Displacement transducers location for NSW2A and NSW2B

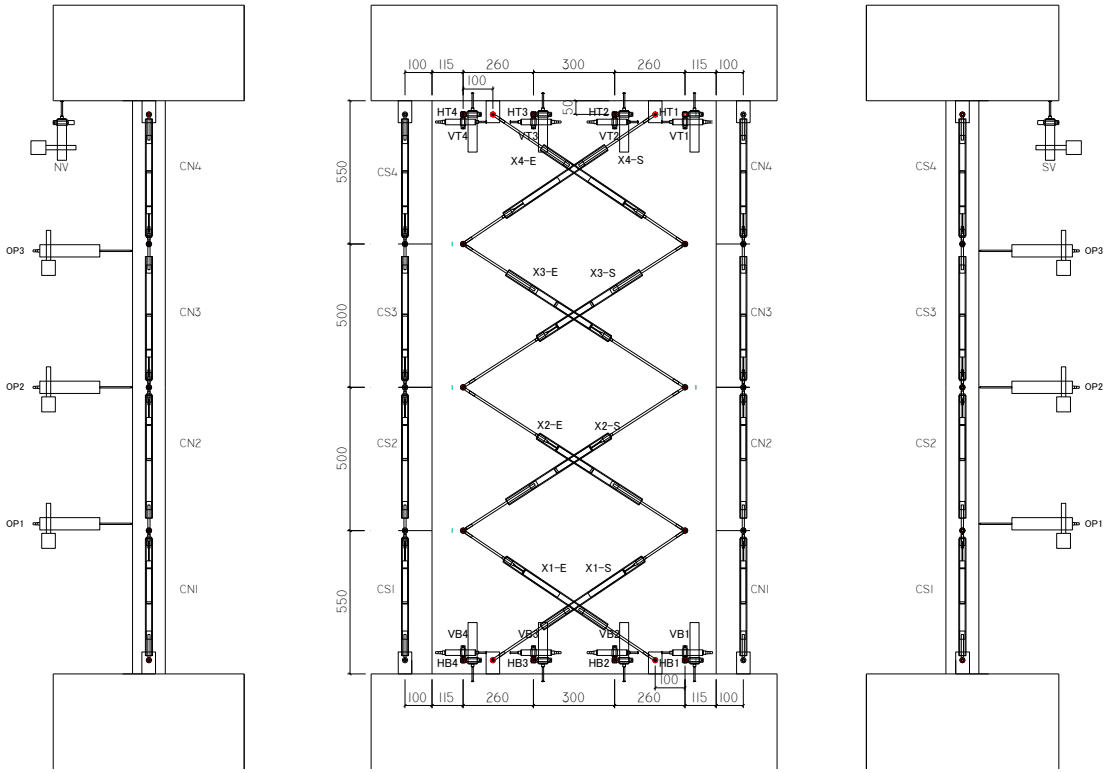

(a) North side (b) Back face (c) South side

Figure 5-5 Displacement transducers location for NSW5

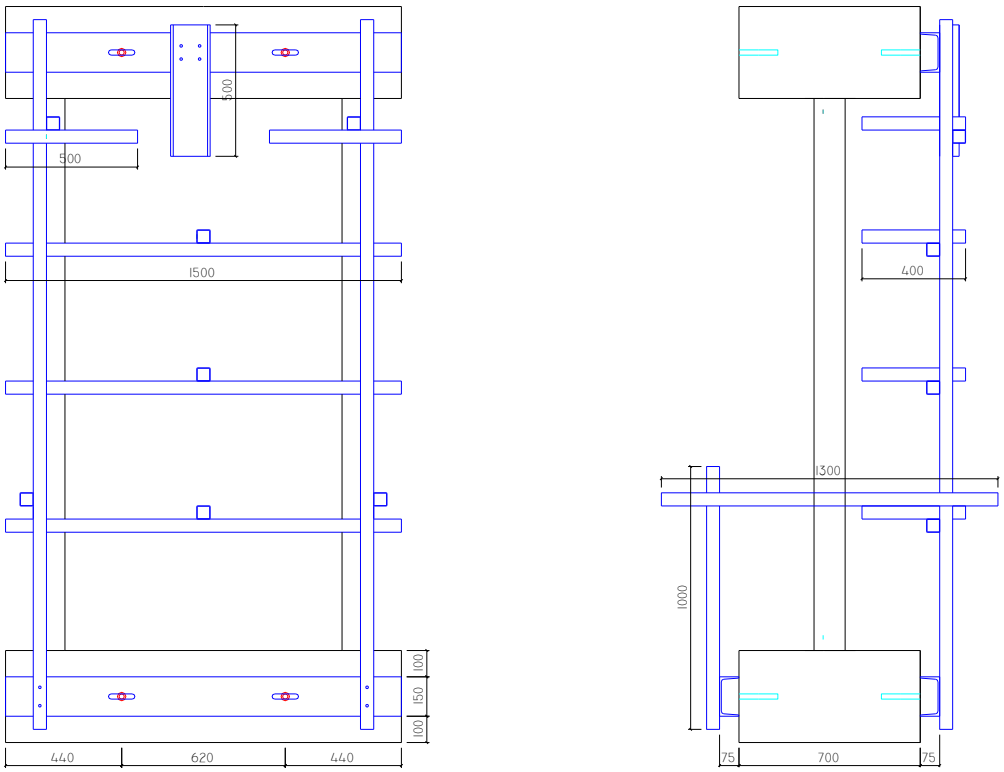

(a) Back face (b) South side

Figure 5-6 Reference frame

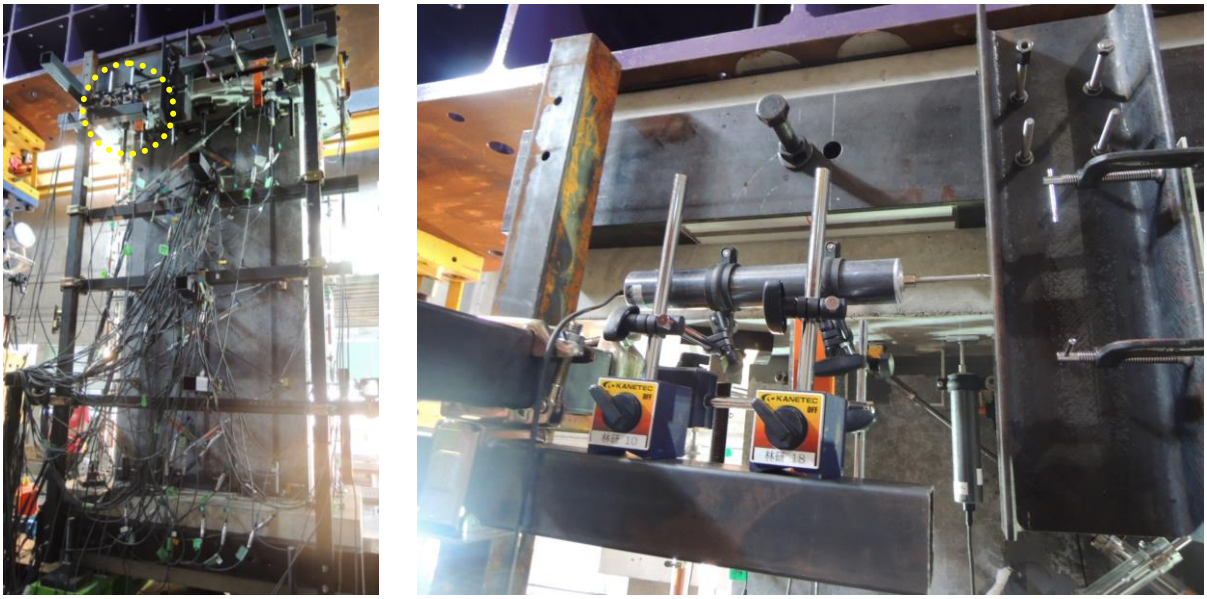

(a) Reference frame (b) displacement transducer

Figure 5-7 Displacement transducer to measure lateral drift

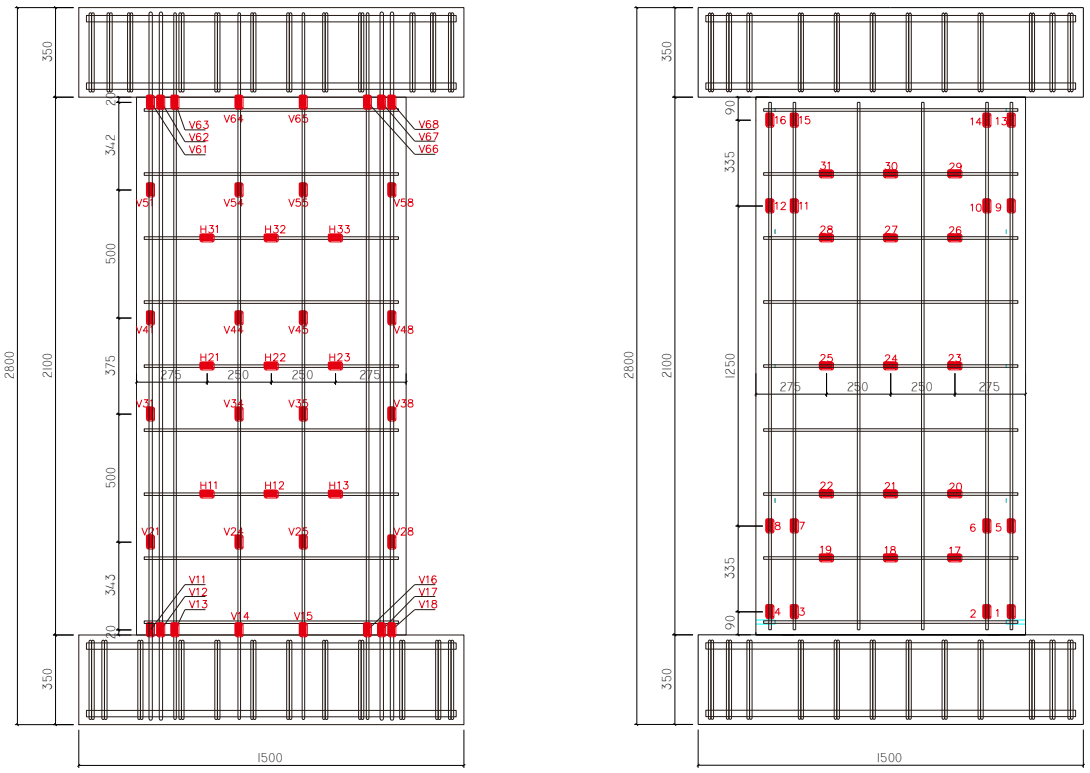

(a) Original part (North – South) (b) Additional part (North – South)

Figure 5-8 Strain gauges location for NSW2A

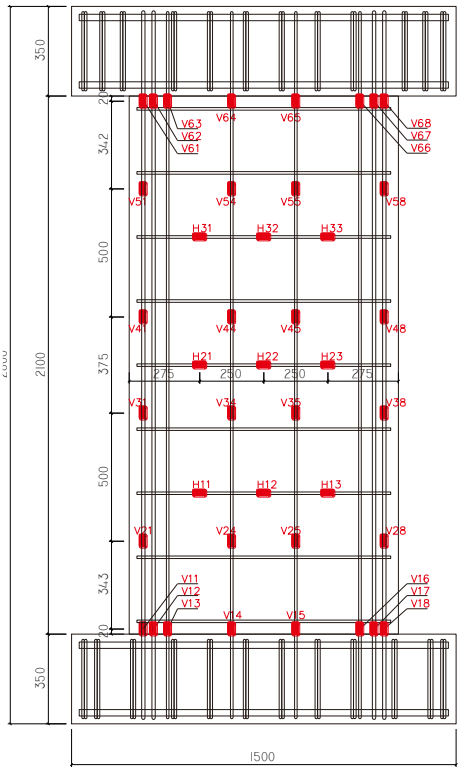

Figure 5-9 Strain gauges location for NSW2B

Figure 5-10 Strain gauges location for NSW5

5.3 Experimental Results

5.3.1 Shear force – drift relations

Shear force and lateral drift relations are shown in Figure 5-11, where Q_{mu} and Q_{su} are computed flexure and shear capacities using Eqs. (5-2) and (5-3), respectively. Table 5-5 summarizes the maximum lateral load capacity, Q_{max}, the lateral load at the first cracking, Q_{cr}, the lateral load of vertical reinforcement yielding, Q_{yv}, the lateral load of horizontal reinforcement yielding, Q_{yh}, and the corresponding drifts, R. The table also shows the ultimate drift capacity, R_u, which is defined as the measured lateral drift when the lateral load capacity decreased to 80% of the peak value.

For NSW2, yielding of the vertical reinforcement occurred at R= 0.31% and R= -0.21%. Horizontal reinforcement yielded before reaching the maximum capacity. During the first cycle of R= +0.50% and R= +0.75%, the maximum lateral load capacities were reached at 297 kN and -282 kN. A significant drop of lateral load capacity was observed during the second cycle of R= ±0.75%. Then five full cycles of R= ±1.00% were imposed to study the load capacity degradation process before the loading was terminated. The lateral load capacity decreased approximately 45% at the end of the fifth cycle from the maximum capacity because severe concrete spalling occurred in the upper region.

For NSW2A, flexure cracking initiated around R= ±0.04% drift in both of positive and negative directions. Yielding of vertical reinforcement occurred at R= 0.17% and R= -0.14%. No yielding was captured by the strain gauges in horizontal reinforcement until R= 5.00% for both original and additional wall panels. The maximum lateral capacities were reached at 334 kN and -345 kN during the first cycle of R= ±1.50%. NSW2A maintained the lateral load capacity up to R=5.00% with small post-peak degradation.

For NSW2B, the first flexural crack appeared at approximately R= 0.05% and developed to the epoxy at R= 0.07% for both of positive and negative loadings. Yielding of vertical reinforcement occurred at R= 0.12% and R= -0.16%. No yielding was captured by the strain gauges in horizontal reinforcement until R= 5.00%. The maximum lateral capacities were reached at 339 kN and -348 kN during the first cycle of R= ±1.50%. NSW2B maintained the lateral load capacity up to R= 5.00% and the post-peak degradation was gentler than that of NSW2A.

For NSW5, flexure cracking initiated at approximately R= 0.06% and R= -0.02%. Yielding of vertical reinforcement occurred at R= 0.29% and R= -0.28%. No yielding was captured by the strain gauges in horizontal and confining reinforcements until the specimen failed. NSW5 showed a stable behavior until R= ±2.00% where it reached the maximum lateral capacity. During the first cycle of R= 3.00%, sliding shear occurred suddenly along the upper block at approximately R= 2.75% and the loading was terminated.

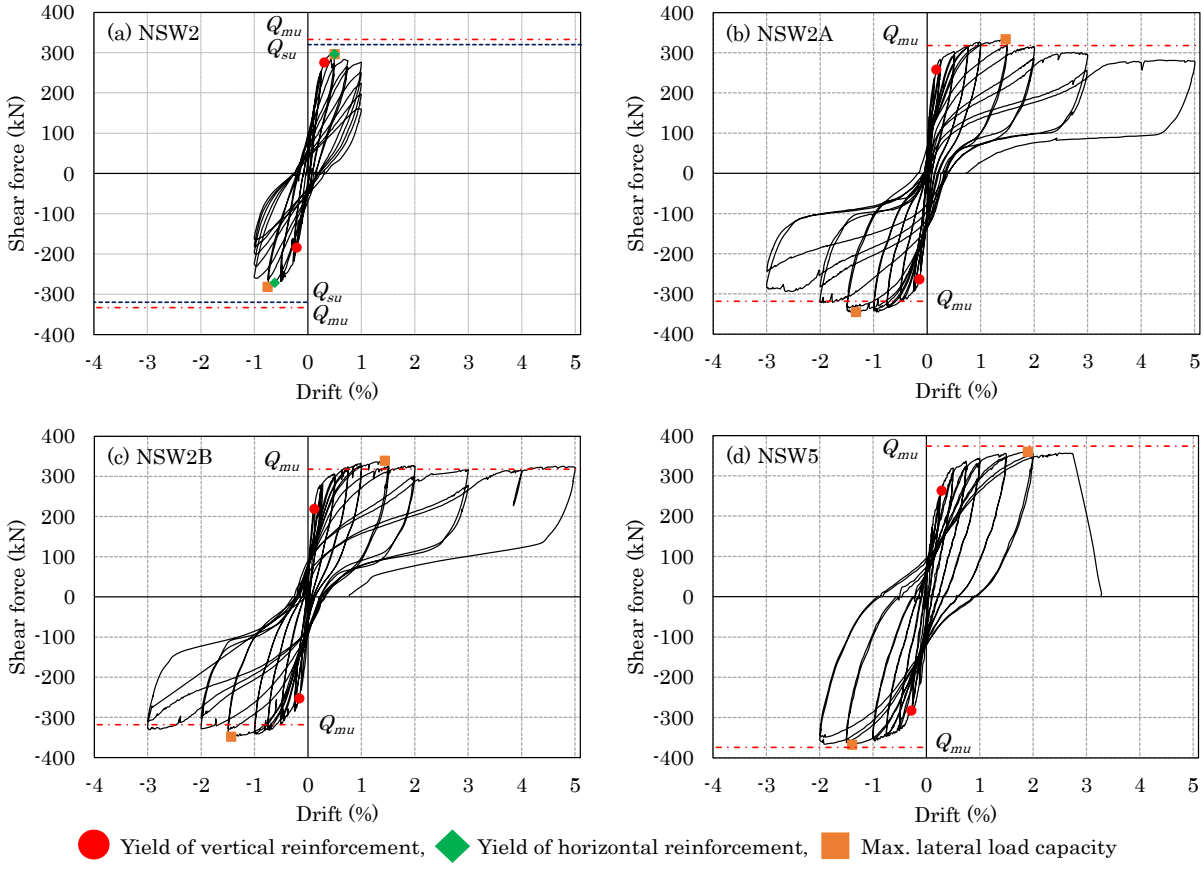

Figure 5-11 Shear force – drift relations

Table 5-5 Shear force and drift of characteristic points (unit: Q in kN and R in %)

Specimen	Q_{max} (R_{max})		Q_{cr} (R_{cr})		Q_{yv} (R_{yv})		Q_{yh} (R_{yh})		R_u	
	+	-	+	-	+	-	+	-	+	-
NSW2	297	-282	-	-	276	-184	297	-271	1.00	-1.00
	(0.50)	(-0.75)			(0.31)	(-0.21)	(0.50)	(-0.62)		
NSW2A	334	-345	140	-155	258	-264	-	-	>5.01*	>3.00*
	(1.47)	(-1.33)	(0.04)	(-0.04)	(0.17)	(-0.14)				
NSW2B	339	-348	150	-160	219	-253	-	-	>5.01*	>3.00*
	(1.44)	(-1.44)	(0.05)	(-0.05)	(0.12)	(-0.16)				
NSW5	360	-368	120	-119	263	-283	-	-	2.75	-2.00*
	(1.90)	(-1.39)	(0.06)	(-0.02)	(0.29)	(-0.28)				

*Maximum lateral load capacity did not drop to 80%.

5.3.2 Damage process and failure modes

Figure 5-12 shows residual crack patterns after the second cycle of each drift. Blue and red lines show cracks in positive and negative loadings, respectively. Black line in Figure 5-12(a) indicates the cracks which formed initially due to the loading system trouble. For NSW2, a web-shear crack appeared during the first cycle of R= ±0.50%. Concrete crushed around the intersection of shear cracks at the upper portion of the wall during R= ±0.75% and developed to the

central part of wall during *R*= ±1.00%. Severe spalling of cover concrete occurred at the second cycle of *R*= 1.00% since the horizontal reinforcement was simply curtailed at the end and not properly anchored to the concrete. During unloading of the fifth cycle of *R*= +1.00%, severe concrete spalling occurred in the upper south corner of the wall followed by buckling of vertical reinforcement at the end region. The ultimate failure mode is considered as shear-compression failure as shown in Figure 5-13(a). Since the computed flexural and shear capacities are close to each other, the degradation after the peak load took place as expected considering the inadequate anchorage of horizontal reinforcement. For NSW2A, the cracking started to appear during *R*= +0.125%. The crack not only occurred on the original wall but also on the additional RC panel. As increasing the drift angle, new cracks appeared and existing cracks extended and widened. The cracking was limited at the lower and upper portion as shown in Figure 5-12(b). The spalling of cover concrete occurred during the second cycle of *R*= -0.50%. Concrete crushed at the wall tips at *R*=±1.50% followed by buckling of vertical reinforcing bars. NSW2A failed in compression-controlled flexure as shown in Figure 5-13(b) which shows the original concrete face. NWS2B had similar damage process and failure mode to NSW2A, but crushing of concrete occurred only on the original wall panel, while UFC panel did not crush due to its high strength as shown in Figure 5-12(c) and Figure 5-13(c). For NSW5, the cracking started to appear during *R*= +0.125%. At *R*= ±0.25%, flexure-shear cracks spread along the height of the wall. Spalling of cover concrete was observed during the second cycle of *R*= -0.75% and concrete crushed at the tip of walls at the first cycle of *R*= -1.50%. The vertical reinforcement at the boundary regions buckled at the second cycle of *R*= +2.00%. Crack width at the top portion of the wall became larger prior to a sudden sliding shear failure at *R*= 2.75% as shown in Figure 5-13(d).

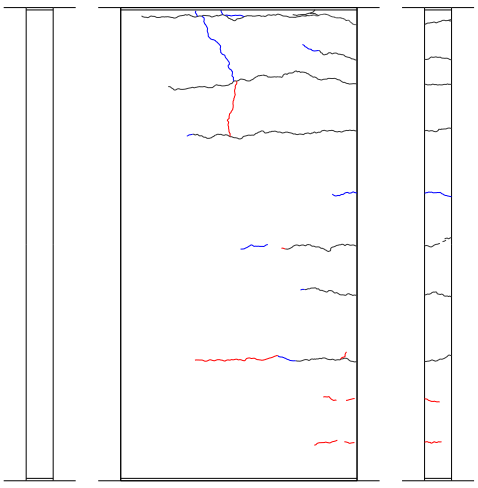

R= ±0.125%

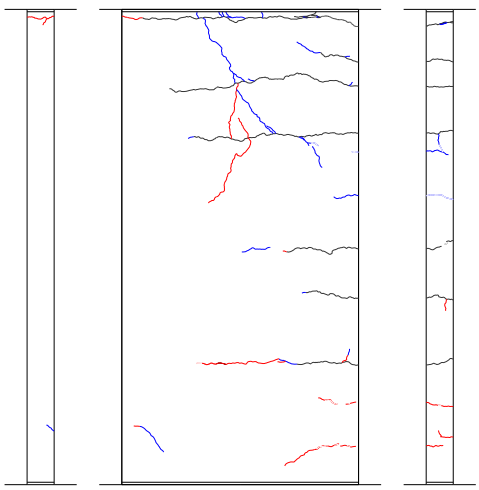

R= ±0.25%(2)

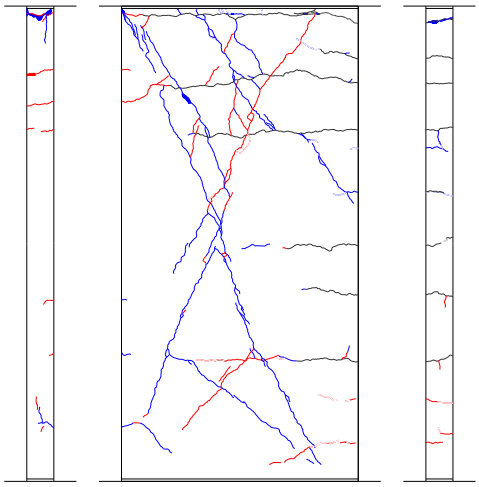

R= ±0.50%(2)

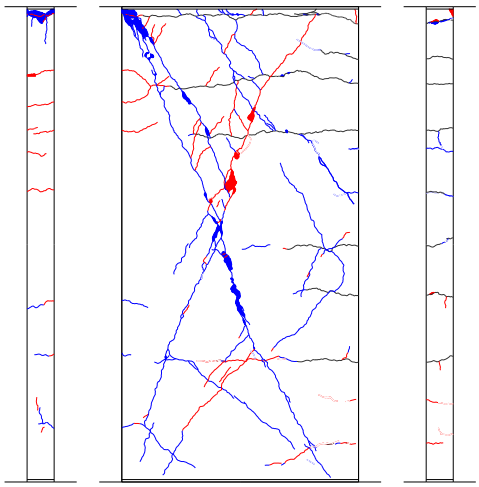

R= ±0.75%(2)

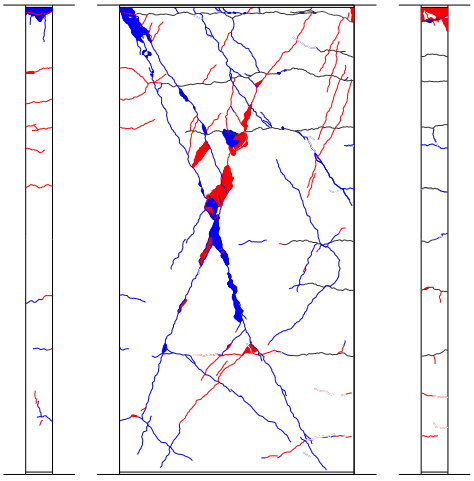

R= ±1.00% (2)

(a) NSW2

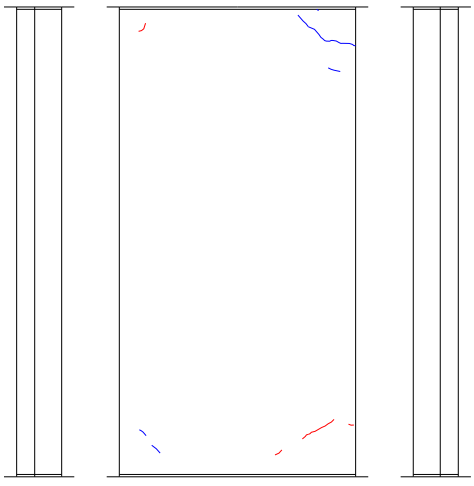

R=-1/800

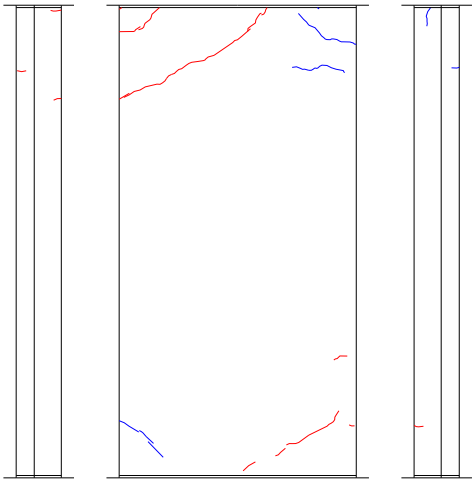

R=-1/400(2)

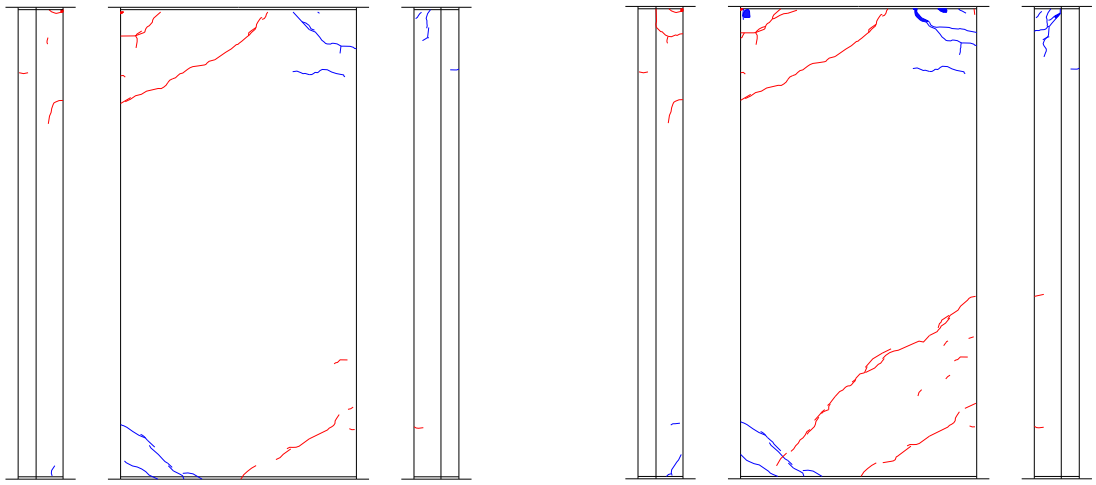

R=-1/200(2)

R=-133(2)

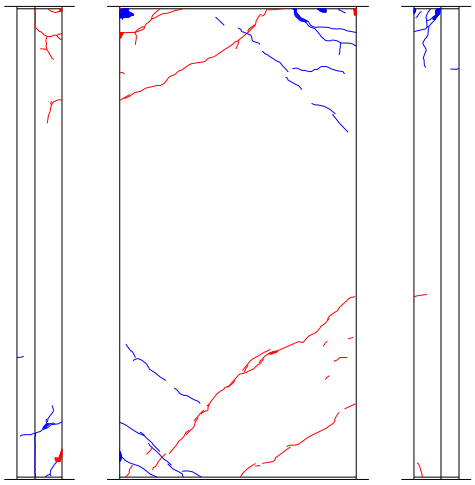

R=-1/100(2)

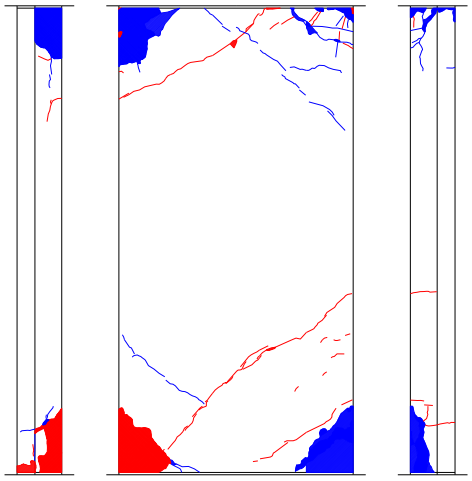

R=-1/67(2)

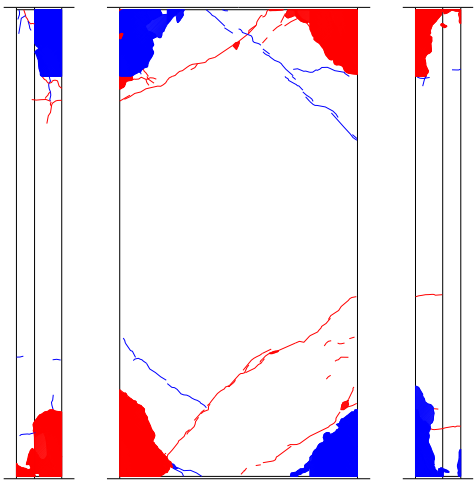

R=-1/50(2)

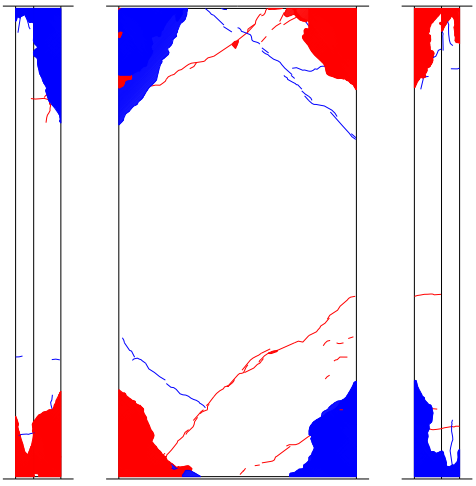

R=-1/33(2)

(b) NSW2A (original concrete face)

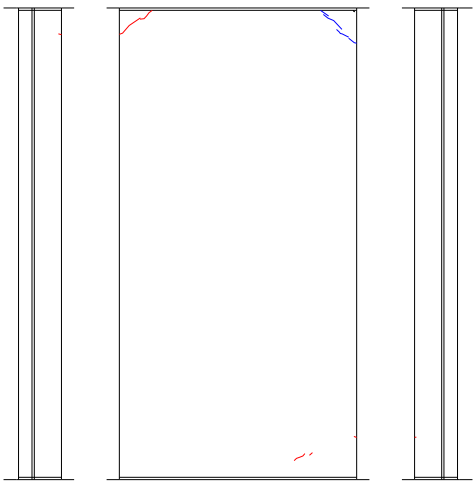

R=-1/800

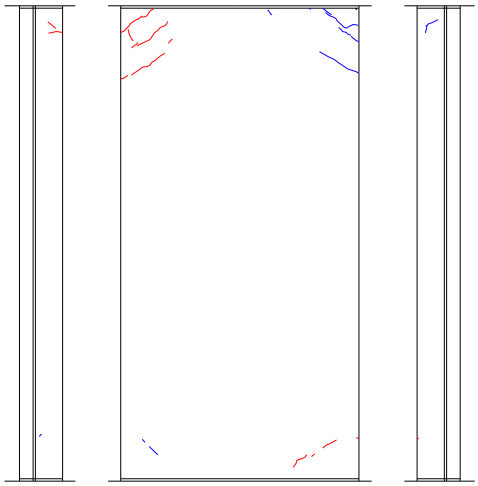

R=-1/400(2)

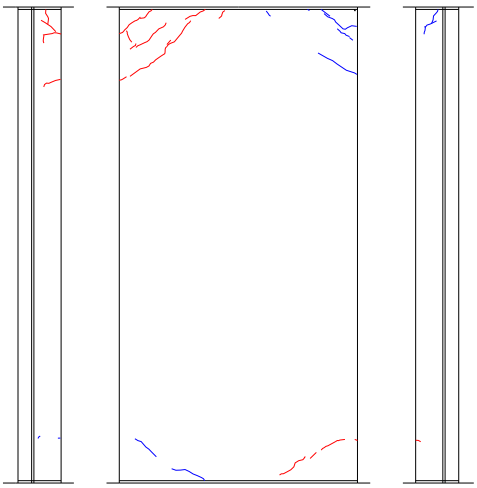

R=-1/200(2)

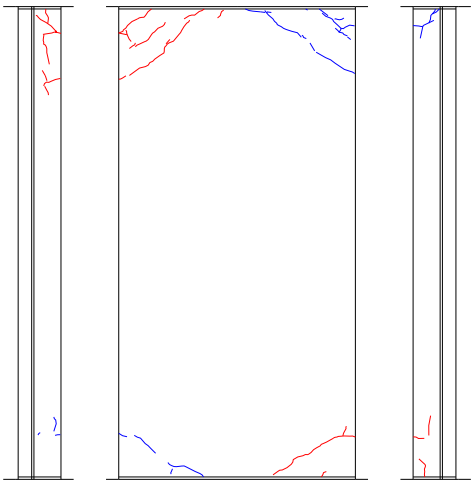

R=-133(2)

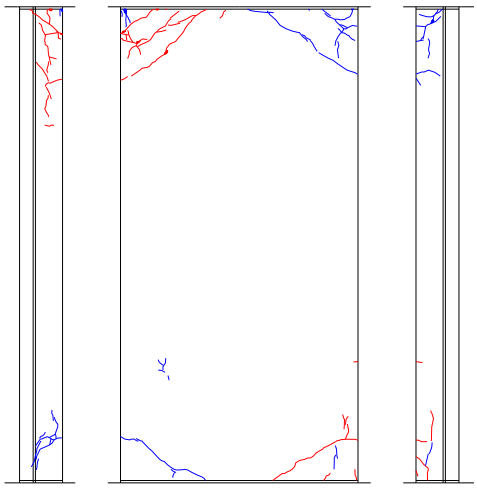

R=-1/100(2)

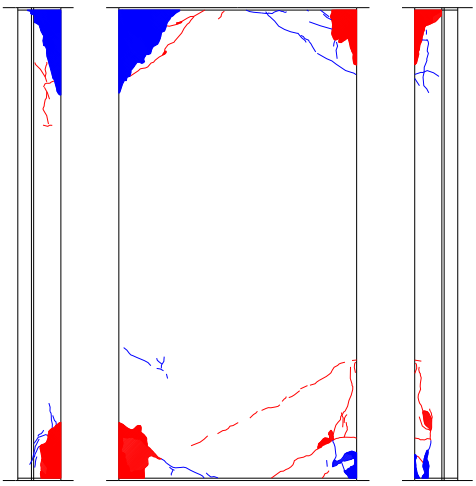

R=-1/67(2)

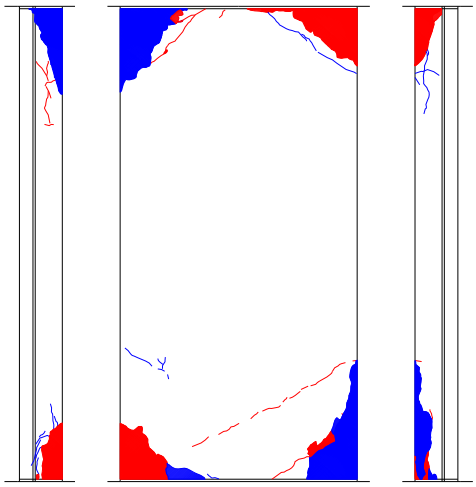

R=-1/50(2)

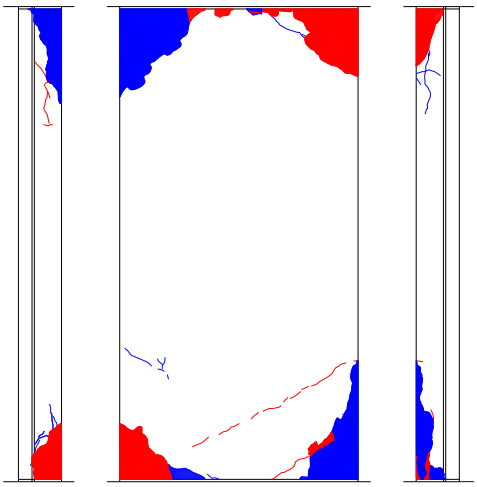

R=-1/33(2)

(c) NSW2B (original concrete face)

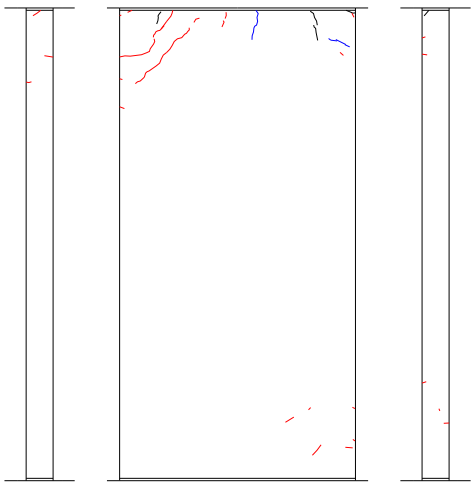

R=-1/800

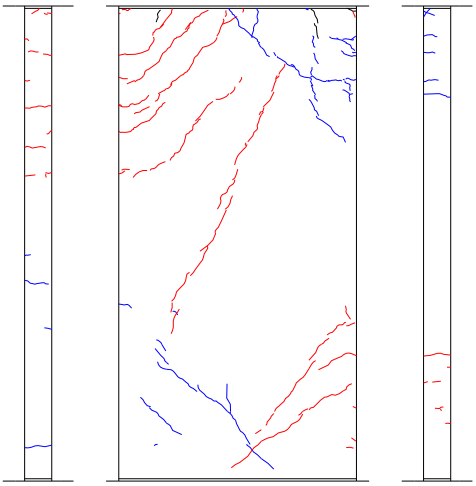

R=-1/400(2)

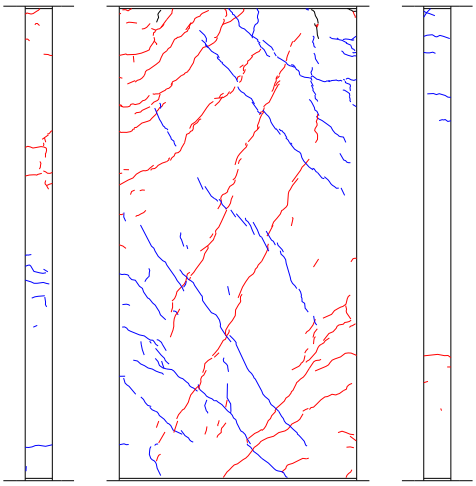

R=-1/200(2)

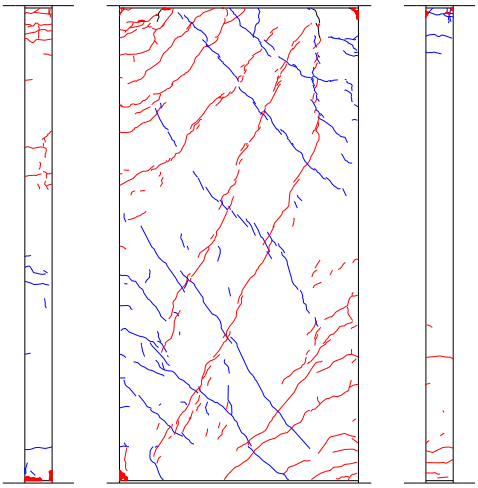

R=-133(2)

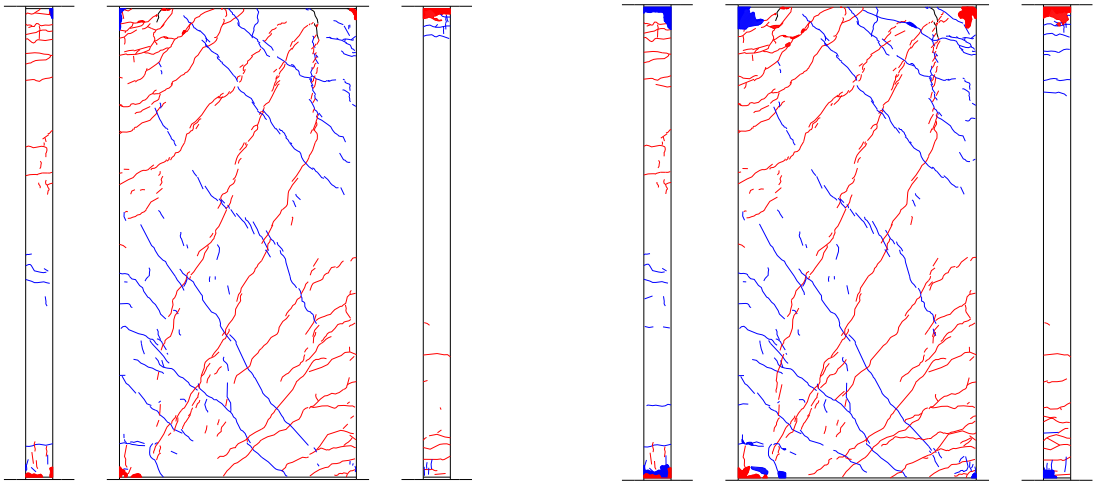

R=-1/100(2) R=-1/67(2)

(d) NSW5

Figure 5-12 Residual cracks of all specimens after the second cycle of each drift

Upper North side

Upper South side

Lower North side

Front face

Lower South side

(a) NSW2

Front face

Back face

Upper North side

Upper South side

Lower North side

Lower South side

(b) NSW2A

Front face

Back face

Upper North side

Upper South side

Lower North side

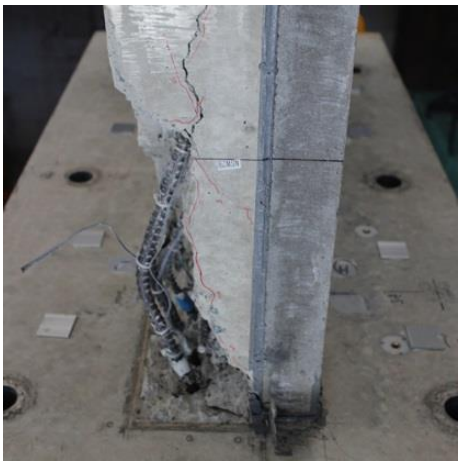

Lower South side

(c) NSW2B

Front face

Back face

Upper North side

Upper South side

Lower North side

Lower South side

(d) NSW5

Figure 5-13 Final damage of specimens (left is north)

5.4 Discussion of Test Results

5.4.1 Strength and stiffness of specimens

Response envelopes for all specimens are shown in Figure 4-11. The lateral load carrying capacity of upgraded specimens increased about 17.3%, 18.7%, and 25.7% for NSW2A, NSW2B, and NSW5, respectively compared to that of the prototype specimen (NSW2). NSW2A and NSW2B reached their flexural capacity followed by gradual post-peak degradation. As expected, NSW5 had higher maximum lateral load capacity than the other specimens. This is because there were additional vertical reinforcements on the boundary regions of NSW5. However, during the first cycle of R= +3.00%, sliding shear along the upper block occurred suddenly since amount of vertical reinforcement was not enough. Therefore, in order to prevent such damage, it is required to increase the amount of vertical reinforcement.

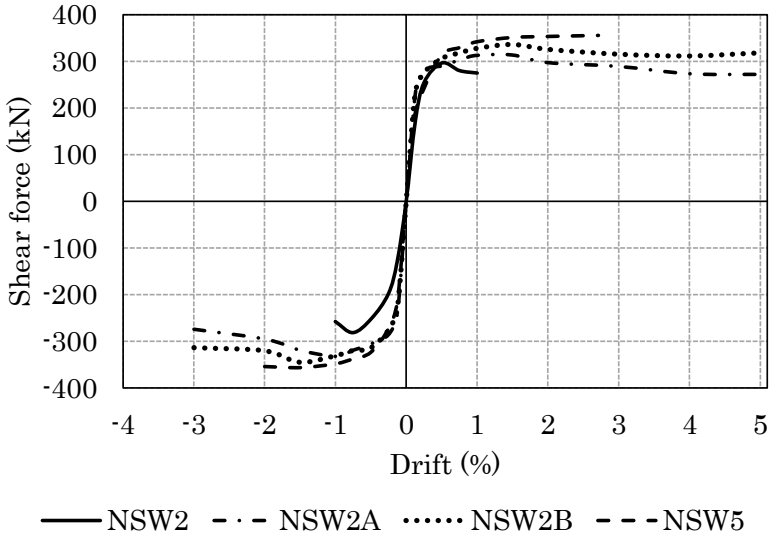

Figure 5-14 Response envelopes of specimens

The experimental flexural capacity of NSW2A and NSW2B was about 8.9% higher compared to that of calculated value. It indicates that the flexural capacity can be computed in a good accuracy by neglecting the contribution of additional wall panel. As mentioned in Section 5.2.2, since the vertical reinforcement of additional wall panel for NSW2A was not anchored to the blocks and no reinforcement was placed in the additional panel of NSW2B, the contribution of the additional walls was not accounted into flexural capacity calculation. For NSW5, its calculated flexural capacity was slightly higher than the experiment. This is because the distance between the centers of boundary columns (l_w) was assumed 0.9 of the wall length, which is overestimated. In case of the real l_w value is used in calculating flexural capacity, the experimental value was conservative, which was 7.4% higher than the calculated value.

The variation of the secant stiffness with shear force for all specimens is illustrated in Figure 4-12. NSW2A and NSW2B had higher initial stiffness than NSW2 and NSW5 due to its additional

wall panel. For NSW2, the initial cracking occurred due to the loading system trouble and initial stiffness decreased. Although the initial stiffness of specimen was different, its secant stiffness was similar at the first crack. It was about 83.8 kN/mm and 291.8 kN/mm for NSW2, NSW5 and NSW2A, NSW2B, respectively. At the maximum lateral load, the secant stiffness was 28.1 kN/mm for NSW2 and about 10.2 kN/mm in average for upgraded specimens (NSW2A, NSW2B, and NSW5). Increasing the maximum displacement of the loading cycle increases stiffness deterioration (see Figure 5-11). Furthermore, after a number of cycles, the decrease in secant stiffness is smaller than the decay occurring during the first few cycles.

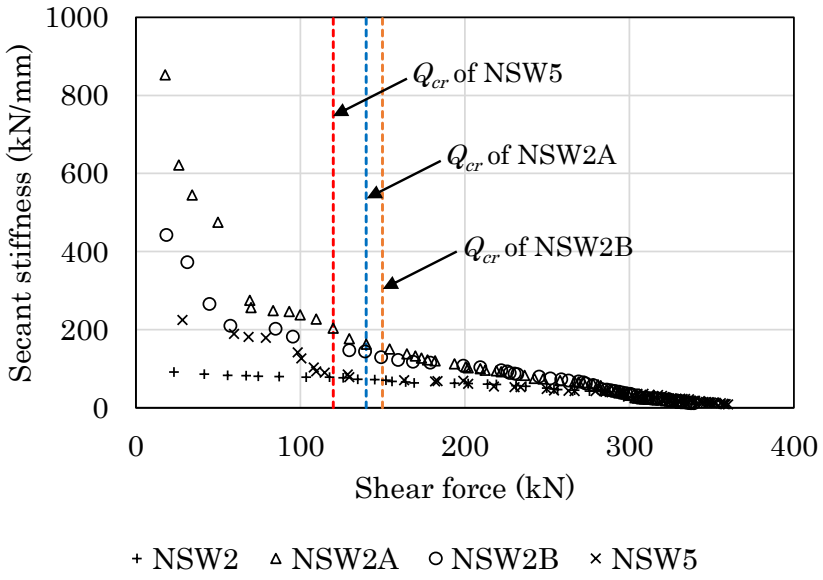

Figure 5-15 Secant stiffness variation of specimens (Q_{cr} is lateral load at the first cracking)

5.4.2 Drift capacity and energy dissipation

The ultimate drift of all specimens is presented in Table 5-5, which is defined as the lateral drift corresponding to the lateral load dropped to 80% of peak value. The ultimate drift of NSW2 was reached at 1.00% due to excessive concrete crushing around the intersection of shear cracks at the central part. All upgraded specimens had larger ultimate drift compared to NSW2. NSW2A and NSW2B maintained the lateral load capacity up to 5.00% drift with small post-peak degradation. Both additional RC and UFC walls restrained the dilation of the original walls by preventing crack propagation, and NSW2A and NSW2B developed its flexural capacity in a ductile manner. NSW2A and NSW2B reached its ultimate drift at R= 5.00% where the lateral load dropped to 0.84% and 0.95%. It is noted that although the original wall of NSW2B crushed at the wall toes, the UFC panel did not crush due to its high strength and carried most of the lateral load after R= 3.00%. As a result, NSW2B maintained its lateral load capacity with small deterioration after the peak. NSW5 reached its ultimate drift at R= 2.75% prior to the sliding shear failure.

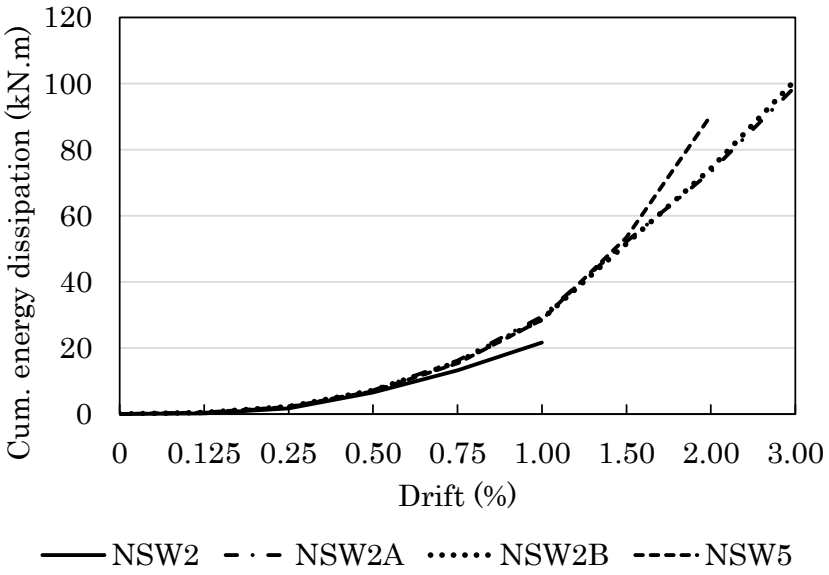

Figure 5-16 Cumulative energy dissipation of specimens

Figure 4-13 shows the cumulative energy dissipation of specimen at each level of drift. For each specimen, energy dissipation was determined by calculating the areas inside the hysteretic loops for each cycle. The cumulative energy dissipation was defined as the summation of the areas enclosed by all previous hysteresis loops. For all specimens, the energy dissipation during the first cycle was larger than the amount energy dissipated during the second cycle at the same drift level. The energy dissipated during the second cycle was about 83% of the energy dissipated during the first cycle. The experimental data also show that the amount of energy dissipation increased considerably with the drift level of the cyclic loading. The cumulative energy dissipation of NSW2 was similar to that of upgraded specimens up to R= 0.50%. Although the cumulative energy dissipation of NSW2 still increased after R= 0.50%, it was smaller than that of the upgraded specimens. This can be explained basically by lateral load capacity dropped due to shear cracks propagation at the central part. At R= 1.50%, the cumulative energy dissipation of upgraded specimens was about 52.4 kNm in average. The energy dissipation of NSW2A and NSW2B was associated with concrete crushing and reinforcement buckling, while for NSW5 dissipated energy through the yielding of tensile bars and the concrete cracking. It is noted that NSW2A and NSW2B exhibited pinched hysteresis loops due to reinforcement pull-out and bond-slip at the wall block joint accompanying the shear slip along the joint planes between wall and blocks. It caused NSW2A and NSW2B dissipated less amount of energy than that of NSW5 at R= 2.00%.

5.4.3 Drift components

This section provides lateral drift component measurements based on experimental result. Displacements of a shear wall subjected to a lateral load are illustrated in Figure 4-14(a). It is assumed that these displacements can be represented by two components, i.e. flexural deformation

and shear deformation. The vertical displacement transducers were used to measure flexural deformation (U_f) and can be calculated as:

$$U_f = \theta h = \frac{(V_L - V_R)}{L} h \tag{5-7}$$

where θ is the rotation over the height h, V_L and V_R are the vertical displacements along the wall edge (measurements of the two vertical displacement transducers), and L is the horizontal between V_L and V_R, as shown in Figure 4-14(a). The diagonal displacement transducers were used to measure shear deformation (U_s), which was estimated from changes in their length as expressed in Eq. (5-8).

$$U_s = \frac{(d_1' - d)d - (d_2' - d)d}{2L} \tag{5-8}$$

where d_1' and d_2' are the deformed length of diagonal, d is the original diagonal length, and L is the horizontal distance between gauges, as shown in Figure 4-14(a). However, the shear deformation given by Eq. (5-8) contains flexural deformation because of the existence of a moment gradient along the height of the shear walls [66]. Therefore, the shear deformation given by Eq. (5-8) should be corrected and can be expressed as follows [67]:

$$U_{s\_corrected} = U_s - (\alpha - 0.5)\theta h \tag{5-9}$$

Hiraishi [67] suggested that the factor α is estimated based on the rotation (θ), as it is the ratio of the shaded area to the rectangular surrounded by solid lines shown in Figure 4-14(c), giving same results for α when calculated as the ratio of curvature centroid to panel height as shown in Figure 4-14(b). Massone and Wallace [68] set α to 0.67, assuming a triangle curvature distribution. By using this assumption, the drift components of wall at the first cycle for each drift level are illustrated in Figure 4-15.

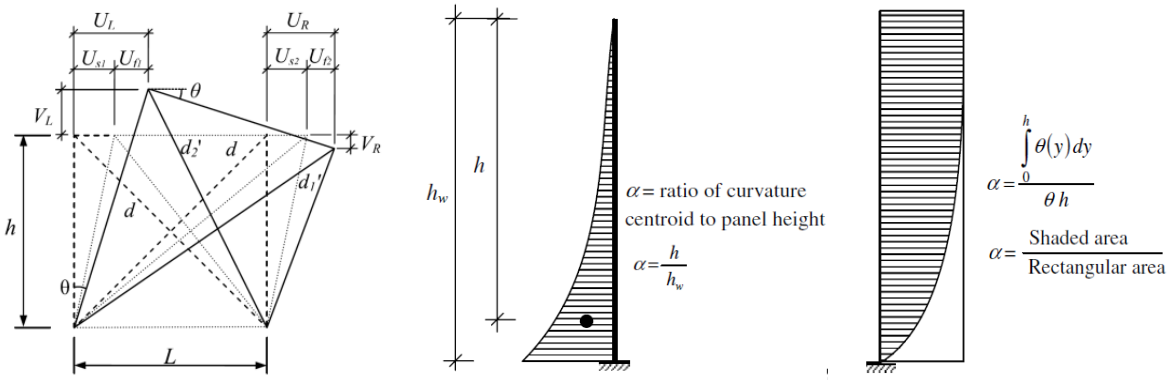

(a) Flexure and shear deformations accounting for vertical displacement

(b) Estimating α based on curvature profile

(c) Estimating α based on rotation profile

Figure 5-17 Drift components [66]

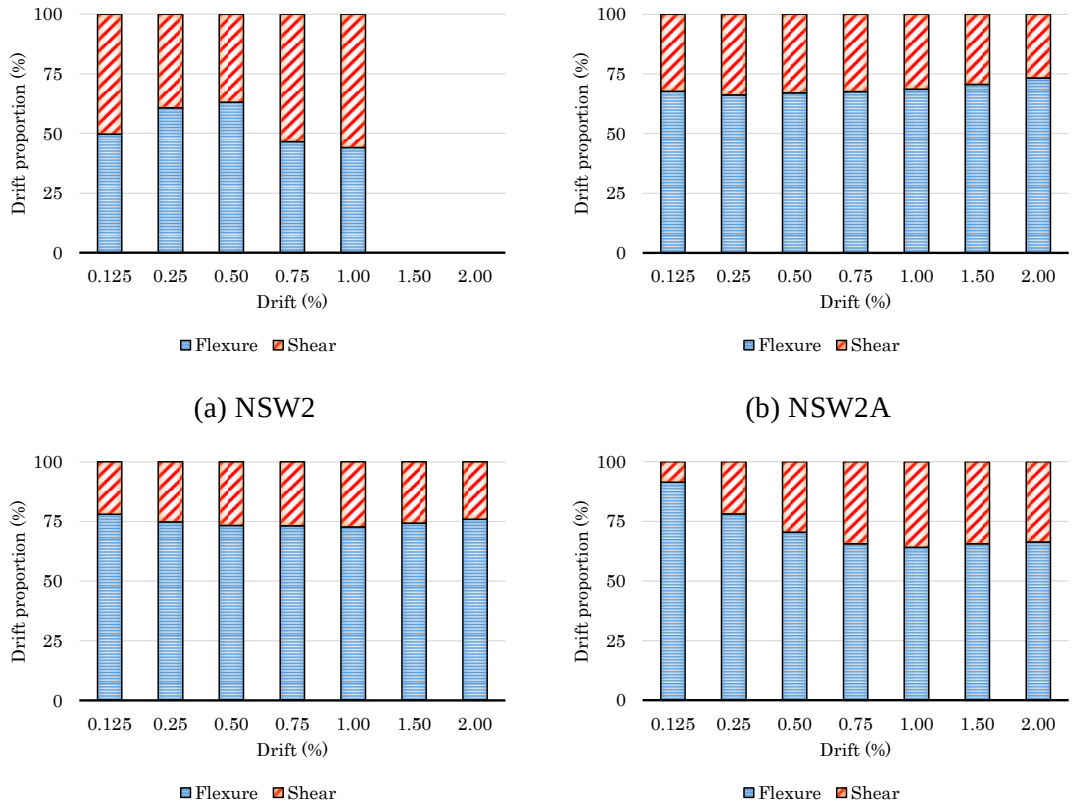

(a) NSW2

(b) NSW2A

(c) NSW2B

(d) NSW5

Figure 5-18 Drift components of specimens

It is clear from Figure 4-15 that the relative contribution of each mode varied with the level of lateral drift. For NSW2, flexural deformations dominated the response (more than 50% of the total deformation) up to *R*= 0.50%. However, at higher level of drift, the shear deformation became significantly pronounced and the contribution of flexural deformation decreased to 45% of the total deformation. This is corresponding to concrete crushing around the intersection of shear cracks at

the central part. For NSW2A and NSW2B, although the contribution of each deformation varied, the flexural deformations dominated the response for all drift levels. The flexural deformations were 69% and 75% of the total deformation in average for NSW2A and NSW2B, respectively. It was interesting that the flexural contributions were relatively constant up to *R*= 2.00%. Instead of new cracks, the existing cracks extended and widened, and these cracks were limited at the lower and upper portions. Initially, flexural deformations dominated the response of NSW5. For example, the flexural deformations account for about 91% and 78% at *R*= 0.125% and *R*= 0.25%, respectively. As the load increased, the contribution of flexural deformations decreased to 70% at *R*= 0.50%, and this change correspond to flexure-shear crack formation at the central part. The flexural contributions dropped slightly to 65% from *R*= 0.75% up to *R*= 2.00%. At *R*= 2.00% the specimen had concrete crushing and buckling of vertical reinforcing bars. The result demonstrated the coupling of inelastic shear and flexure, that is, inelastic flexural deformations appear to have led to inelastic shear deformations.

5.5 Damage Assessment

Post-earthquake assessment of damaged structures is a critical and complex problem. In the immediate aftermath of an earthquake, it is the engineer's responsibility to judge, if a structure is safe enough to keep using. In the subsequent phase, the responsibility to identify the most cost effective repair actions for the damaged structure belongs to the engineer. Evaluating the effects of the damage on the structural properties and expected future seismic performance is pivotal in this respect.

The objective of this study is to develop a post-earthquake seismic evaluation method for lightly reinforced concrete (RC) walls. For this purpose, damage evaluation in terms of crack width, crack length, and concrete spalling area was carried out at different drift levels to see damage progress of lightly RC walls. Then, the damage level was assessed using the 2004 AIJ Guidelines [30] to study its validity for lightly RC walls. Some modifications were proposed and the recommendations of this study can help the inspector in estimating the current limit state or performance level of the wall.

5.5.1 Concrete cracking and spalling area

The crack width is accepted as an important index for evaluating the damage level of structural components affected by earthquakes. The residual crack width, closely related to the retrofit method and cost, has been used as a damage indicator in some standards [30][69]. In this study, the intensity of observed damage of specimens was evaluated in terms of crack width, crack length, and concrete spalling area. The measurement was carried out on three faces of the wall; front face and both north and south side faces. Crack width was measured using an imprinted crack scale card with 0.05 mm intervals as shown in Figure 4-16(a). The crack width measurement was

conducted at the second cycle of negative peak drift and unloading for each drift level (except for R= 0.125% at the first cycle). Each visible residual crack at the first cycle of R= -0.125% and the second cycle of -0.25%, -0.50%, -0.75%, -1.00%, -1.50%, and -2.00% was traced on transparencies (overhead projector sheets) as shown in Figure 4-16(b). The numbering system on the transparencies and the wall panel is shown in Figure 4-17 -Figure 5-22. Each individual crack was labeled and the maximum width along its length was measured. In this measurement, if the crack was visible but the crack width was less than 0.05mm (minimum measurable crack width with the crack scale), the crack width was expressed as 0.00mm. These transparencies were scanned and all cracks were traced digitally on a computer CAD program so that location and length of cracks were digitalized later. Each residual crack was classified based on the maximum width along the crack. In this study, the residual crack width, ${}_rW_{cr}$ was classified as ${}_rW_{cr} < 0.2$ mm, $0.2 \text{ mm} \le {}_rW_{cr} < 1.0$ mm, $1.0 \text{ mm} \le {}_rW_{cr} < 2.0$ mm, $2.0 \text{ mm} \le {}_rW_{cr} < 5.0$ mm, ${}_rW_{cr} \ge 5.0$ mm.

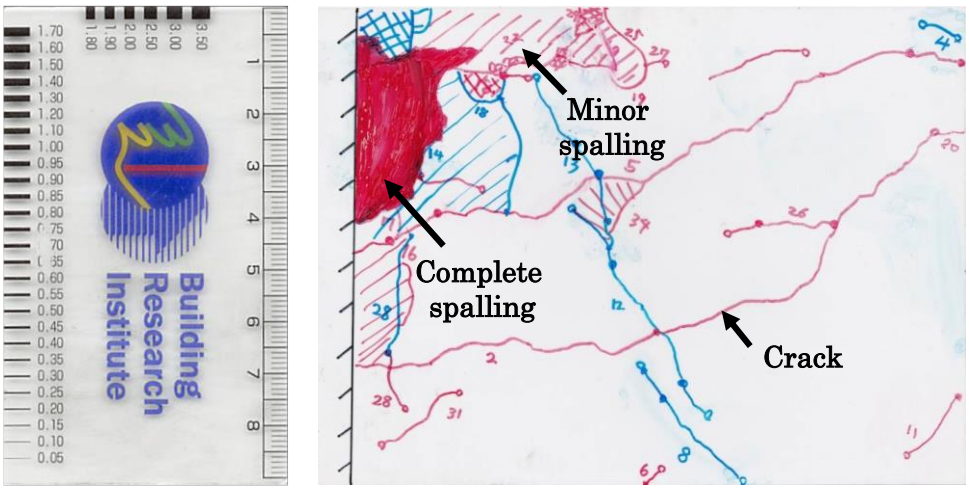

(a) Crack gauge card (b) Sample of transparency

Figure 5-19 Tracing cracking and spalling on a transparency

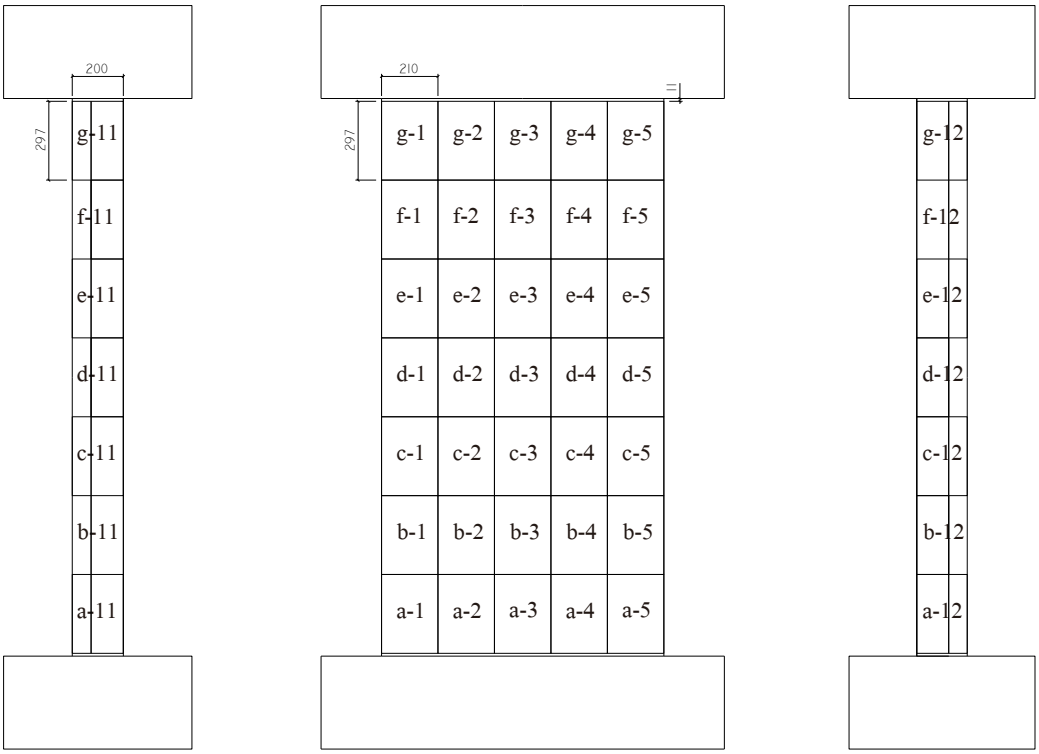

(a) North side (b) Front face (c) South side

Figure 5-20 Numbering system of crack measurement NSW2A

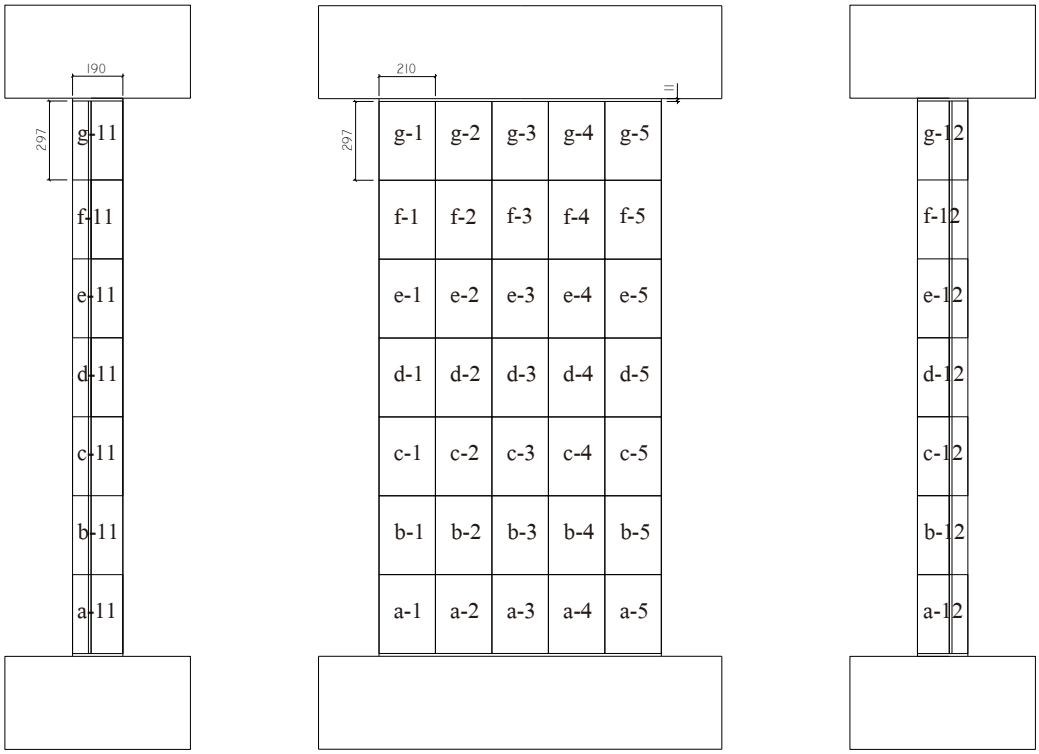

(a) North side (b) Front face (c) South side

Figure 5-21 Numbering system of crack measurement for NSW2B

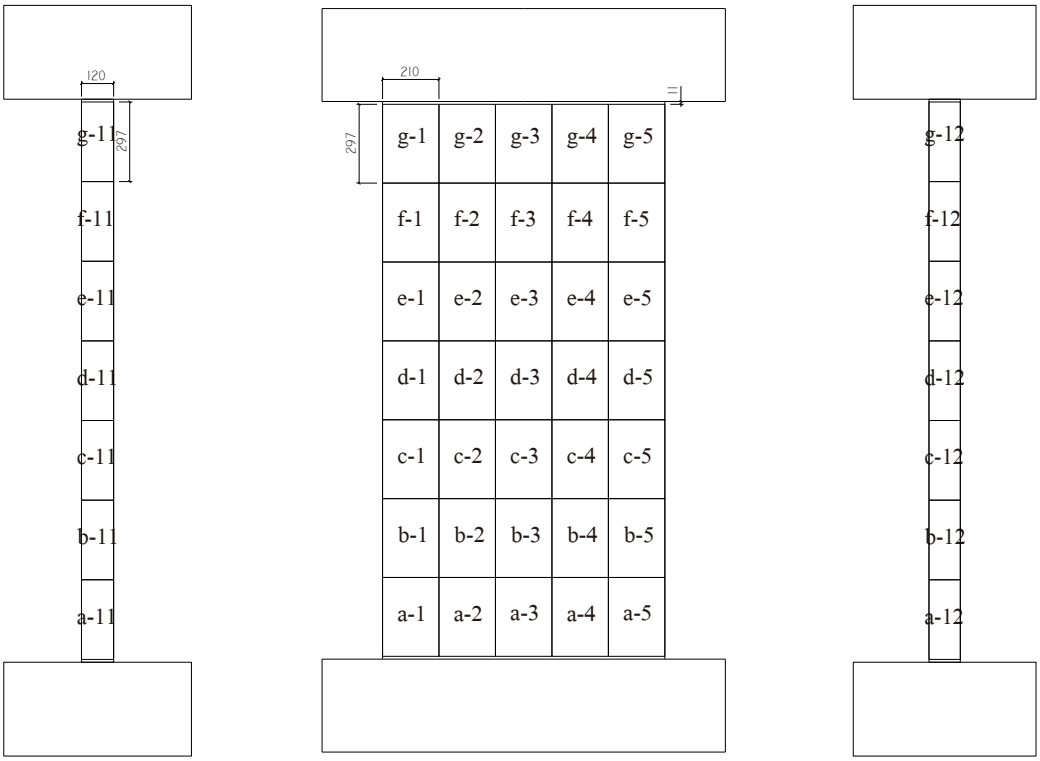

(a) North side (b) Front face (c) South side

Figure 5-22 Numbering system of crack measurement for NSW2 and NSW5

5.5.1.1 Maximum crack width

The transition of maximum peak and residual crack widths for NSW2A, NSW2B, and NSW5 together with NSW2 are illustrated in Figure 5-23. The maximum peak crack width ($_pW_{cr\text{-}max}$) is defined as the maximum width of all visible cracks at the peak point of the cycle. The maximum residual crack width ($_rW_{cr\text{-}max}$) is defined as the maximum width of all visible cracks when the lateral load is completely removed from the peak point. It is noted that $_pW_{cr\text{-}max}$ and $_rW_{cr\text{-}max}$ were not necessarily measured at the same point. In actual earthquake condition, smaller earthquake shakings after the maximum shaking make the residual drift smaller. Therefore, this study considers the worst scenario for residual crack width. Although $_pW_{cr\text{-}max}$ of NSW2 and NSW5 was similar up to R= 1.00%, $_rW_{cr\text{-}max}$ of NSW5 was smaller than NSW2, especially after R= 0.50%. This is because shear cracks are dominant in NSW2 after R= 0.50%. These shear cracks did not close when unloaded probably because the sliding took place with opening and cracked concrete surface was not able to return to the original position. The additional RC and UFC walls in NSW2A and NSW2B restrained the original wall to prevent crack propagation. In consequence, the cracks were limited to stay in the lower and upper portions and their width became larger. Therefore, $_pW_{cr\text{-}max}$ of NSW2A and NSW2B was greater than that of other specimens. However, flexural cracks were dominant in NSW2A and NSW2B. Flexural cracks are able to return to the original position relatively easily. The maximum residual crack width ($_rW_{cr\text{-}max}$) of all upgraded specimens was

smaller than that of NSW2 for each drift level and it was less than 2.0 mm up to *R*=1.00%.

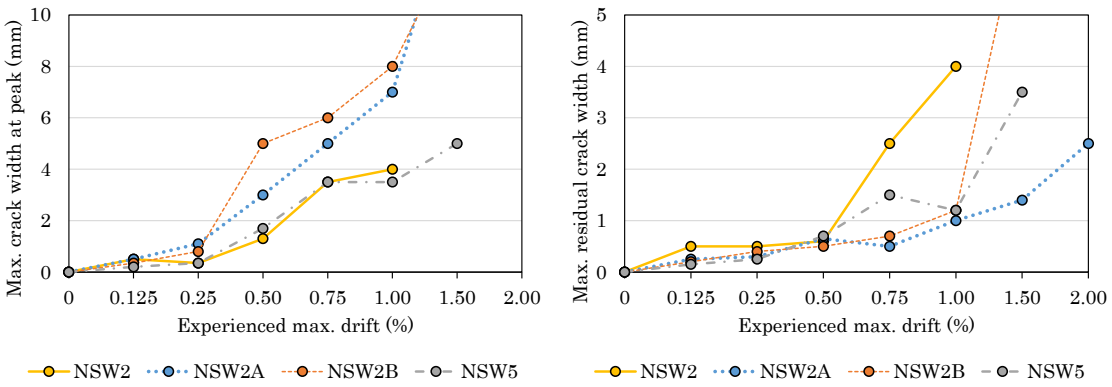

(a) Peak (b) Residual

Figure 5-23 Maximum peak and residual crack widths

5.5.1.2 Residual crack density

Figure 5-24 shows the variation of residual crack density of NSW2A, NSW2B, and NSW5 together with NSW2 after the second cycle of negative loading. The residual crack density is defined as the total residual crack length per square root area. Each labeled crack was classified depending on its representative crack width and its length was summed to obtain the total length of that classification. The total length was divided by the square root area of front surface. The residual crack density of NSW2 was similar with NSW2A and NSW2B up to *R*= 0.25%. However, it started to increase rapidly after *R*= 0.25% and exceeded NSW2A and NSW2B at *R*= 0.50%. At *R*= 0.75%, NSW2 had residual crack wider than 2.0 mm. Since cracks only occurred at the lower and upper portions, NSW2A and NSW2B had smaller residual crack density than NSW5. The residual crack density of NSW2A and NSW2B dropped at *R*= 1.50% due to spalling of cracked concrete. For NSW5, the residual crack density was greater than NSW2. However, crack width of most cracks were less than 0.2 mm. It indicates that increasing the amount of horizontal reinforcement with anchorage suppressed the opening of crack width.

5.5.1.3 Ratio of concrete spalling area

Ratio of concrete spalling area for NSW2A, NSW2B, and NSW5 together with NSW2 after the second cycle of negative loading is shown in Figure 5-25. The ratio of concrete spalling area is defined as the area of concrete spalling due to either flexure or shear deformation divided by the area of front surface. Similar to the residual crack density, the ratio of spalling area also increased with increasing the drift. The ratio of spalling area for all specimens was similar up to *R*= 0.50%. However, the ratio of spalling area of NSW2 increased rapidly at *R*= 0.75%, while for all upgraded specimens tended constant up to *R*= 1.00%. At *R*= 1.50%, excessive crushing occurred at the wall tips of NSW2A and NSW2B, and its ratio of spalling area increased quickly. Concrete crushing

took place at the wall tips for all upgraded specimens, but UFC panel did not crush due to its high strength. For NSW2, concrete spalling occurred mostly at the central part due to insufficient horizontal web reinforcement.

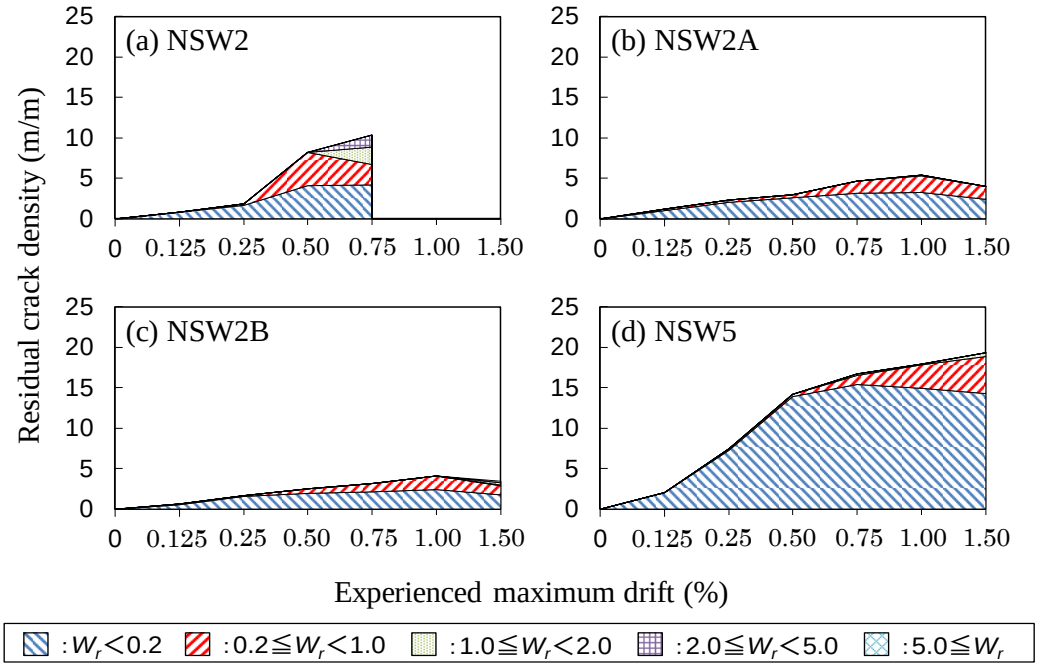

Figure 5-24 Residual crack density

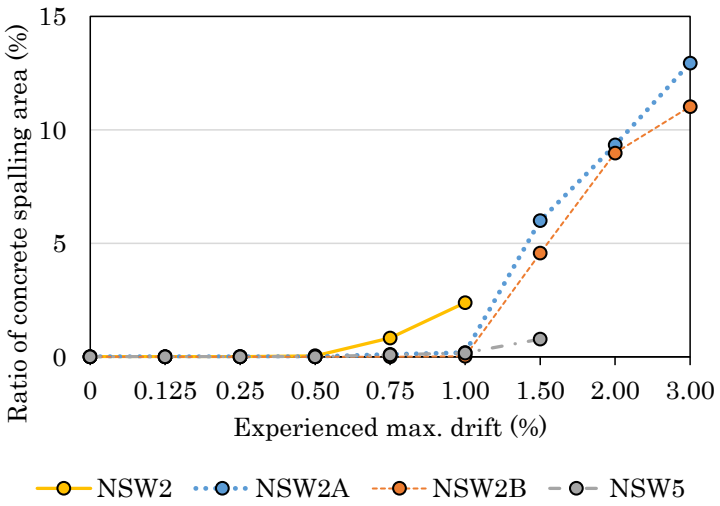

Figure 5-25 Ratio of concrete spalling area

5.5.2 Limit state and damage level

2004 AIJ Draft Guidelines [30] tabulate a relation of limit states and damage levels of members as shown in Table 4-8. Since the limit for each damage state is not defined in terms of measured quantity, quantitative criteria for each limit state is restated in Table 4-9 considering

criteria proposed in the 2015 AIJ Draft [70] for prestressed concrete members. Based on Table 4-9, the limit states were determined for each specimen as shown in Table 4-11 and Figure 4-21(a). Dashed green, blue, and yellow lines in Figure 4-21 are serviceability limit state, reparability limit state I, and reparability limit state II, respectively.

For NSW2A, NSW2B, and NSW5, the stress of concrete at the extreme fiber reached two-third of its compressive strength at drift less than 0.10%. This is probably due to additional walls and confinement in boundary regions for NSW2A and NSW2B, and NSW5, respectively. For NSW2A and NSW2B, the serviceability limit state I was reached by yielding of vertical reinforcement at R= 0.36% and R= 0.46%, respectively, while the serviceability limit state II was reached at R= 1.50%. It is noted that the residual drift of NSW2B was less than 0.25% after R= 1.50% due to no crushing at the additional wall. For NSW5, most of the damage states were controlled by concrete criteria.

Considering the total amount of damage (crack length and spalling area) as explained in Section 5.5.1, criteria at Table 4-9 work well to capture damage level of lightly RC walls. However, visual judgement from photos for concrete to determine minor crushing (reparability limit state I) is an important issue. It would be very subjective depending on a person who observes it. In addition, limit of $2/3f'_c$ for concrete is too strict for serviceability limit state since it is still in the range of immature elastic state as shown in Figure 4-21(a). The stress level may be taken larger than $2/3f'_c$ for the serviceability limit. By evaluating a limited experimental data, the stress of $0.8f'_c$ was proposed as serviceability limit for concrete. From Section 5.5.1.3, ratio of concrete spalling area can be also used as an indicator of concrete structures damage. Therefore, it was proposed as additional damage state criteria. Since lightly RC walls have single curtain of reinforcement, they would less likely reach high displacement ductility before the shear failure occurs. Based on experimental result of 26 wall specimens that failed in shear by Hidalgo et al. [27], the average ultimate drift, Ru, (which is defined as the lateral drift corresponding to the lateral load dropped of 80% peak value) was 0.73%. Therefore, the limit of residual drift for safety was proposed R< 1.00%.

The proposed criteria for limit and damage states is tabulated in Table 4-10, which the blue color indicates the proposed criteria. The limit states of all specimens were re-evaluated using the proposed criteria and shown in Table 4-12 and Figure 4-21(b). Limit of $0.8f'_c$ was more realistic for serviceability limit state of concrete. Although the limit state of damage did not change, it was also governed by the new criteria of ratio of concrete spalling area especially for walls that failed in flexure.

Table 5-6 Relation of limit states and damage levels (AIJ Guidelines, 2004)

Limit state	Damage state	Damage level	Damage state		
			Longitudinal reinforcement	Concrete	Residual crack width
Serviceability	Continuous usage	I	Elastic	Nearly elastic	< 0.2 mm
Reparability I	Easily repaired	II	Yielding	Healty	0.2 - 1.0 mm
Reparability II	Reparable	III	Buckling	Core concrete is healthy	1.0 - 2.0 mm
Safety	Veritical load can be sustained	IV	No fracture	Core concrete has not crushed	
	Lateral load capacity degrade	V	Fracture	Crushing of core concrete	

Table 5-7 Criteria used to categorize into four damage states

Limit state	Damage state			
	Longitudinal reinforcement	Concrete	Residual crack width	Residual drift
Serviceability	Yielding	Stess < $2/3f'_c$ (check axial strain at extreme fiber)	< 0.2 mm	R < 0.10%
Reparability I	Yielding is allowed to some extend (strain = 2.0%)	Minor crushing of cover (visual judgement from photos)	0.2 - 1.0 mm	R < 0.25%
Reparability II	Buckling (visual judgement from photos)	Cover spalling	1.0 - 2.0 mm	R < 0.50%
Safety	Fracture (from photos)	Crushing of core concrete (from photos)	> 2.0 mm	R = 4.00%

Table 5-8 Proposed criteria of limit states and damage levels of lightly RC walls

Limit state	Damage state				
	Longitudinal reinforcement	Concrete	Residual crack width	Residual drift	Ratio of Concrete Spalling Area
Serviceability	Yielding	Stess < $0.8f'_c$ (check axial strain at extreme fiber)	< 0.2 mm	R < 0.10%	= 0.0%
Reparability I	Yielding is allowed to some extend (strain = 2.0%)	Minor crushing of cover (visual judgement from photos)	0.2 - 1.0 mm	R < 0.25%	< 1.0%
Reparability II	Buckling (visual judgement from photos)	Cover spalling	1.0 - 2.0 mm	R < 0.50%	< 5.0%
Safety	Fracture (from photos)	Crushing of core concrete (from photos)	> 2.0 mm	R < 1.00%	> 5.0%

Table 5-9 Limit state and damage level of all specimens based on Table 4-9

Criteria			Limit state	Specimen							
				NSW2		NSW2A		NSW2B		NSW5	
Reinforcement	RB	Yielding	Serviceability limit state	0.31		0.17		0.12		0.29	
		Tensile strain ≤ 2.0%	Reparability limit state I	0.35		0.36		0.46		1.50	
		Buckling of longitudinal reinforcement	Reparability limit state II	1.00		1.50		1.50		2.00	
		Fracture of longitudinal reinforcement	Safety limit state	-		-		-		-	
Concrete	CO	Concrete stress ≤ 2/3f'c	Serviceability limit state	0.13		0.06		0.08		0.09	
		Minor spalling of cover concrete	Reparability limit state I	0.51		0.75		1.00		0.75	
		Spalling of cover concrete	Reparability limit state II	0.75		1.50		1.50		1.50	
		Crushing of core concrete	Safety limit state	1.00		1.50		1.50		1.50	
Residual crack	CR	< 0.2 mm	Serviceability limit state	-		-		-		0.50	
		0.2 - 1.0 mm	Reparability limit state I	0.50		1.00		0.75		0.75	
		1.0 - 2.0 mm	Reparability limit state II	0.75		1.50		1.50		1.50	
		> 2.0 mm	Safety limit state	0.75		1.50		1.50		-	
Residual drift	DR	R < 0.10%	Serviceability limit state	0.50		0.75		1.00		0.50	
		R < 0.25%	Reparability limit state I	1.00		1.50		1.50		1.00	
		R < 0.50%	Reparability limit state II	-		1.50		-		1.50	
		R = 4.00%	Safety limit state	-		-		-		-	
Governed drift (%)			Serviceability limit state	0.13	CO	0.06	CO	0.08	CO	0.09	CO
			Reparability limit state I	0.35	RB	0.36	RB	0.46	RB	0.75	CO, CR
			Reparability limit state II	0.75	CO, CR	1.50	ALL	1.50	RB, CO, CR	1.50	CO, CR, DR
			Safety limit state	0.75	CR	1.50	CO, CR	1.50	CO, CR	1.50	CO

Table 5-10 Limit state and damage level of all specimens based on Table 4-10

Criteria			Limit state	Specimen							
				NSW2		NSW2A		NSW2B		NSW5	
Reinforcement	RB	Yielding	Serviceability limit state	0.31		0.17		0.12		0.29	
		Tensile strain ≤ 2.0%	Reparability limit state I	0.35		0.36		0.46		1.50	
		Buckling of longitudinal reinforcement	Reparability limit state II	1.00		1.50		1.50		2.00	
		Fracture of longitudinal reinforcement	Safety limit state	-		-		-		-	
Concrete	CO	Concrete stress ≤ 0.8f'c	Serviceability limit state	0.17		0.07		0.09		0.11	
		Minor spalling of cover concrete	Reparability limit state I	0.51		0.75		1.00		0.75	
		Spalling of cover concrete	Reparability limit state II	0.75		1.50		1.50		1.50	
		Crushing of core concrete	Safety limit state	1.00		1.50		1.50		1.50	
Residual crack	CR	< 0.2 mm	Serviceability limit state	-		-		-		0.50	
		0.2 - 1.0 mm	Reparability limit state I	0.50		1.00		0.75		0.75	
		1.0 - 2.0 mm	Reparability limit state II	0.75		1.50		1.50		1.50	
		> 2.0 mm	Safety limit state	0.75		1.50		1.50		-	
Residual drift	DR	R < 0.10%	Serviceability limit state	0.50		0.75		1.00		0.50	
		R < 0.25%	Reparability limit state I	1.00		1.50		1.50		1.00	
		R < 0.50%	Reparability limit state II	-		1.50		-		1.50	
		R < 1.00%	Safety limit state	-		-		-		-	
Ratio of Concrete Spalling Area	SP	≈ 0.0%	Serviceability limit state	0.25		0.50		0.50		0.50	
		< 1.0%	Reparability limit state I	0.75		1.00		1.00		1.00	
		< 5.0%	Reparability limit state II	1.00		-		-		1.50	
		> 5.0%	Safety limit state	-		1.50		1.50		-	
Governed drift (%)			Serviceability limit state	0.17	CO	0.07	CO	0.09	CO	0.11	CO
			Reparability limit state I	0.35	RB	0.36	RB	0.46	RB	0.75	CO, CR
			Reparability limit state II	0.75	CO, CR	1.50	RB, CO, CR, DR	1.50	RB, CO, CR	1.50	CO, CR, DR, SP
			Safety limit state	0.75	CR	1.50	CO, CR, SP	1.50	CO, CR, SP	1.50	CO

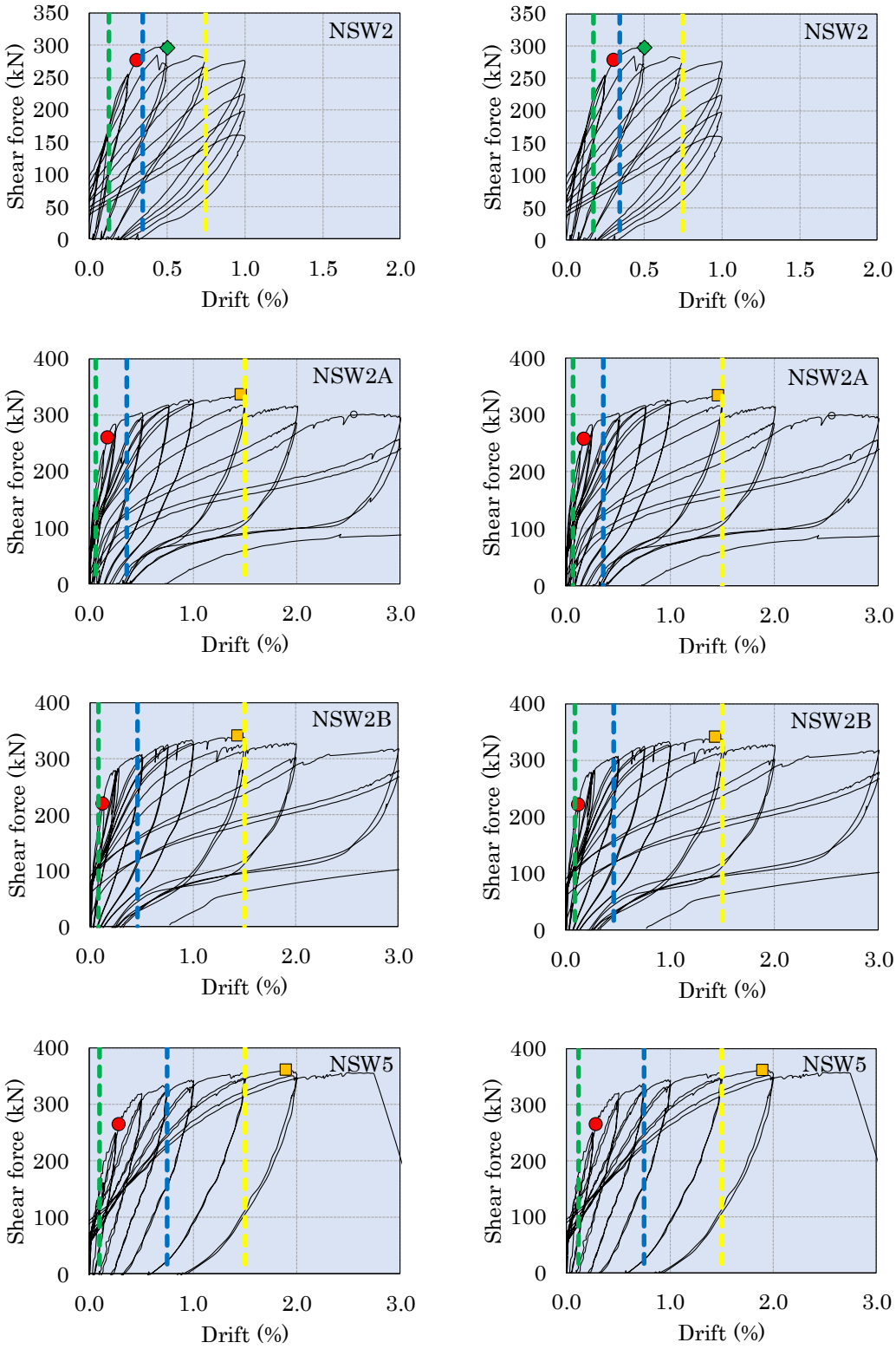

Figure 5-26 Evolution of limit states for all specimens

5.6 Conclusions

An experimental test was carried out on four full-scale wall specimens, three of which were upgraded with various schemes to improve the seismic behavior of shear-type damage of lightly RC walls. Two specimens were upgraded using additional RC panel (NSW2A) and ultra-high strength fiber reinforced concrete (UFC) panel (NSW2B) to prevent shear failure. The other specimen had upgraded reinforcement details to increase shear capacity and flexural ductility (NSW5). Behavior characteristics of walls, such as lateral load carrying capacity, ductility, and failure mode of wall specimens were investigated. From this study, the following conclusions were drawn.

1) The lateral load carrying capacity of upgraded specimens increased about 17.3%, 18.7%, and 25.7% for NSW2A, NSW2B, and NSW5, respectively compared to that of the prototype specimen (NSW2). All the upgraded specimens reached their flexure capacity with small post-peak degradation. The ultimate drift of NSW2A and NSW2B were reached at R= 5.00% where the maximum lateral load dropped to 0.84% and 0.95%. NSW5 reached its ultimate drift at R= 2.75% prior to the sliding shear failure. The increase in strengths is well explained by using equations for flexural and shear capacities introduced in the text.
2) All upgraded specimens showed less damage compared with the prototype specimen (NSW2). For NSW2A and NSW2B, cracks appeared only in the upper and lower portions of the wall panel. In contrast, cracks spread over the wall height in NSW5. All upgraded specimens exhibited flexural failure. Adding RC and UFC panels improved the behavior of lightly RC wall and prevented crack formation at the central part of the wall panel. Increasing the amount of horizontal reinforcement and providing 180-degree hook anchorage decreased the crack width. The increased confinement of the boundary regions delayed the concrete crushing in compression and allowed the full utilization of the vertical reinforcement in tension due to the increased strength of the compressive zone.
3) Upgrading method of NSW2A and NSW2B can be applied for an existing wall, while NSW5 is intended for the new lightly RC walls to decrease shear type damage. Upgrading walls with an additional panel (NSW2A and NSW2B) can be applied on one side of the members, and this allows the continuous use of the building. The construction process of NSW2B may easier than NSW2A, since it does not need post-installed mechanical anchors, installing formwork, and casting concrete. However, both upgrading methods proved to be effective and improved the shear strength and ductility for lightly RC walls as compared to the prototype wall (NSW2).
4) As a drawback, however, the upgrading of the existing lightly RC walls using additional wall panel results in increasing of gravity load as well as shear forces that to be transferred to the foundations, and it may need to be checked.

6 PARAMETRIC STUDY OF LIGHTLY REINFORCED CONCRETE WALLS USING FINITE ELEMENT ANALYSIS

6.1 Introduction

In this chapter, finite element (FE) analysis was conducted to simulate the damage progress as well as hysteresis curve of the tested specimens explained in Chapter 4. Additional FE analysis with 210 case studies was conducted in order to investigate the effects of axial force (P/f'_cA_g), horizontal reinforcement ratio (ρ_{wh}), and shear span to wall length ratio (M/Vl_w) on damage process and maximum lateral load capacity of lightly reinforced concrete walls.

6.2 Finite Element Model

6.2.1 Mesh

To simulate the hysteretic characteristics of lateral load – drift relations with damage process of the tested specimens, a numerical analysis was carried out using three-dimensional (3D) nonlinear FE analysis. The specimens were modeled with hexahedral elements using a commercial nonlinear finite element analysis software (FINAL [74]) as shown in Figure 6-1(a). The vertical reinforcing bars were modeled as beam elements with bond link to account for bond-slip effects while the horizontal reinforcing bars were modeled with perfect bond. A 180-degree hook anchorage of horizontal reinforcement for NSW3 and NSW4 was not modeled in this analysis. Nodes at the bottom face of lower stub were fixed for all degrees of freedom. Translational degrees of freedom (DOF) at the top surface of the upper stub were forced to follow those of the central master node for NSW1, NSW2, and NSW3, while they are free for NSW4 in order to achieve the boundary conditions explained in Section 2.2.2. A constant axial load of 458 kN (equivalent with $0.15f'_cA_g$) was applied at the master node for NSW2, NSW3, and NSW4. For all specimens, the lateral displacement was applied at the master node as shown in Figure 6-1(b). Analysis was conducted following the loading protocol of the experiment. The drift was defined as relative horizontal displacement between the upper and lower stubs divided by clear span of wall specimen (2100 mm).

6.2.2 Constitutive models

Mechanical properties of materials in

Table 6-1 and Table 6-2 were used in the analysis, which ones are from Section 4.2.1. The modified Ahmad model [75] and Nakamura model [76] were adopted for the envelope compressive stress-strain relation of concrete for ascending and descending branches, respectively, with no reduction on compressive strength after cracking. The analysis employed Ottosen's four-parameter model [77] to define the failure criterion of concrete. In the tension zone, the stress-strain relationship is assumed to be linear up to cracking, while the tension stiffening after cracking,

Izumo model [78] was used with coefficient *c* of 1.0 for NSW1, NSW2, and NSW3 and Naganuma model [79] was adopted for NSW4. Since NSW4 had concentrated cracks at the bottom part due to cantilever type loading, when Izumo model was applied, a significant drop of lateral load capacity occurred after peak and Naganuma model was adapted for a better result. The smeared crack model with a fixed angle concept was used to express cracking of concrete. The minimum crack angle between a new crack and an existing crack was assumed 20 degrees. Naganuma model [80] was adopted to model internal loop of stress-strain relations of concrete under cyclic load as shown in Figure 6-2(a). Menegotto-Pinto model [81] in Figure 6-2(b) was used for the stress-strain relation of steel reinforcement. Shear transfer model after cracking employed Naganuma model [82] as shown in Figure 6-2(c). To model bond behavior between concrete and vertical reinforcement, the bond stress-slip relation followed Naganuma model [80] as shown in Figure 6-2(d). The peak of bond stress, σ_b was defined by Eq. (3-1).

$$\sigma_b = \frac{F_{\max}}{\pi LD} \tag{6-1}$$

where σ_b is the maximum bonding stress (MPa), F_{max} is the maximum pull-out load (N) and assumed as $f_y A_s$ in this study, f_y and A_s are the yield strength (MPa) and section area of vertical steel bars (mm^2), respectively, L is the bond length and taken as development length of vertical reinforcement to the stub of 300 mm, and D is the diameter of vertical steel bars (mm).

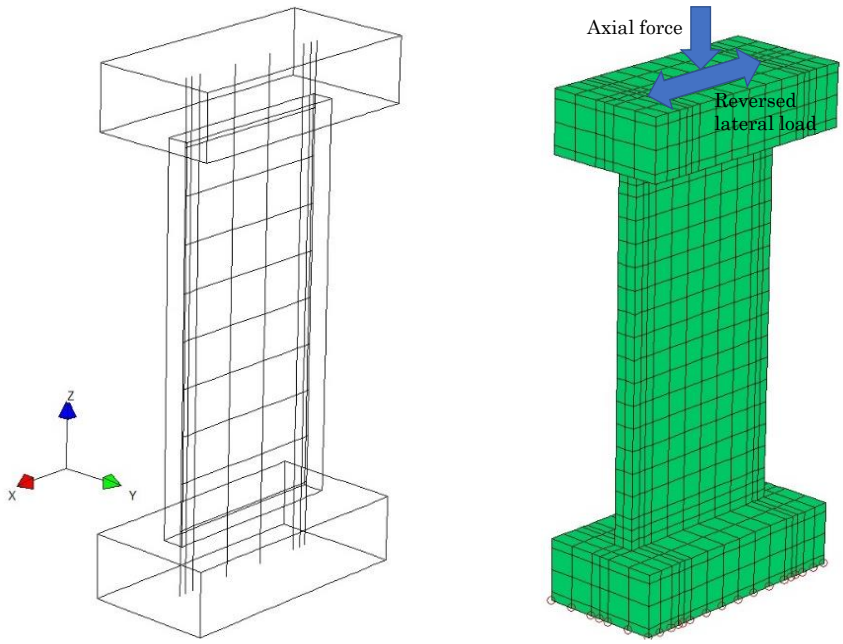

(a) Steel reinforcement in the FE model (b) Input of axial and lateral load

Figure 6-1 Finite element mesh (for NSW2)

Table 6-1 Mechanical properties of concrete

f'_c	ε_c	E_c	f_t
(N/mm^2)	(%)	(kN/mm^2)	(N/mm^2)
24.2	0.182	26.3	2.46

f'_c: compressive strength of concrete cylinders,

ε_c: strain at compressive strength,

E_c: Young's modulus, f_t: splitting tensile strength

Table 6-2 Mechanical properties of steel reinforcing bars

Diameter (mm)	f_y	f_u	E_s	ε_y
	(N/mm^2)	(N/mm^2)	(kN/mm^2)	(%)
D10 (SD295A)	347	484	190	0.183
D13 (SD345)	360	527	190	0.189

f_y: yield strength, f_u: tensile strength,

E_s: Young's modulus, ε_y: yield strain

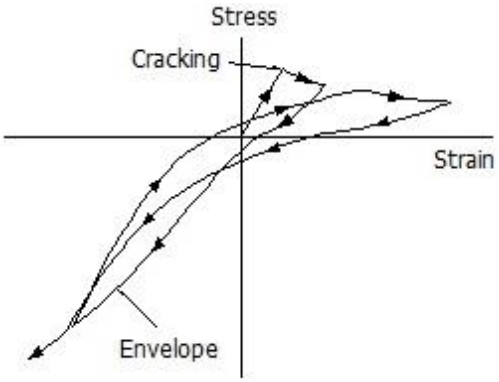

(a) Naganuma model for concrete axial behavior [80]

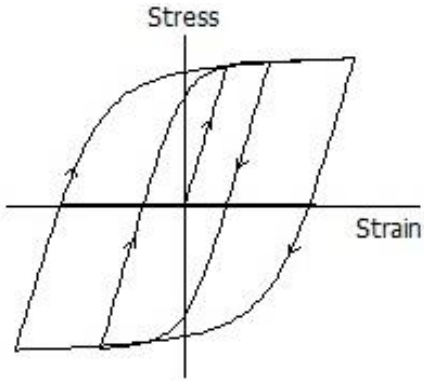

(b) Menegotto-Pinto model for steel [81]

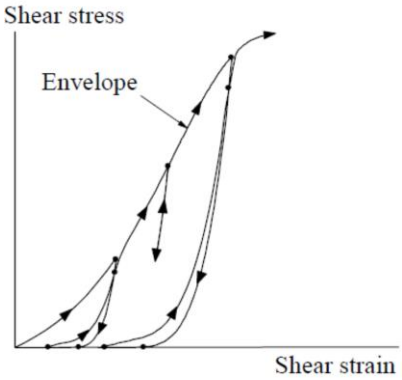

(c) Naganuma model for concrete shear [82]

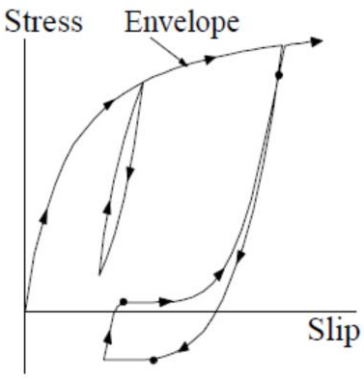

(d) Naganuma model for bond-slip [80]

Figure 6-2 Constitutive models for FE analysis

6.2.3 Validation of models using Experimental 1 (capacities and damage)

Figure 6-3 shows shear force-drift relations of experimental and analytical results. Analytical capacities are shown in Table 6-3. For NSW1, the computed peak load is 154 kN, which agrees well with experimental peak load of 155 kN in positive loading. In negative loading, the computed peak load is 30% higher than that of experimental value. The analytical load-drift relations agree with experimental one where the analytical hysteresis loop is similar to that of experiment up to R= 0.75%. It should be noted that the finite element analysis could not capture sliding shear observed in NSW1. For NSW2, the initial stiffness of analysis is quite higher compared to the experiment. This is because the initial cracking occurred due to the loading system trouble and initial stiffness decreased in experiment. This stiffness degradation was not modeled in FE analysis. The computed peak loads are 315 kN and -289 kN in positive and negative loadings, respectively. These values agree well with experimental peak load of 297 kN and -282 kN in positive and negative loadings, respectively. The analysis also shows dropping of lateral load capacity after reaching its maximum value due to diagonal shear cracks. Widening of those cracks resulted in decrease of shear capacity. Figure 6-5 shows the crack propagation, principal stress, and maximum shear stress of NSW2. Shear cracking is expected at any point in a shear wall where the principle tensile stress exceeds the tensile strength of the concrete (note: concrete tensile strength of specimens, f_t= 2.46 MPa). Once shear cracks occur, the maximum shear stress decreases as shown in Figure 6-5(b) to Figure 6-5(d). In consequence, the lateral load capacity also decreases. For NSW3, the computed peak load agrees well with experimental peak load of approximately 320 kN for both positive and negative loadings. The initial stiffness of analysis is slightly higher than experimental one. Similar to NSW2, a noticeable drop also occurred during the second cycle of each drift due to concrete spalling at the wall tips. For NSW4, the analysis tends to simulate slightly higher initial stiffness. However, the analytical backbone curve agrees well with the experimental one, especially in negative loading direction. The computed peak loads are 169 kN and -164 kN in positive and negative loadings, respectively. It is slightly lower than experimental peak load of 187 kN in positive loading direction, and it agrees well with experimental peak load of -162 kN in negative loading.

Figure 6-4 shows the residual crack and compressive damage distribution of experiment and FE analysis at the second cycle of R= -0.25%, -0.50%, and -1.00%. For FE analysis, black lines and red colored elements represent crack and compression softening of concrete, respectively. For NSW1, flexural cracks appeared at 45 kN and -25 kN. Unlike the experiment, crack started to appear in the central part of wall at R= 0.50%. New crack appeared at the central part during R= 0.75% and concrete crushed at the wall tips. NSW1 failed under compression-controlled flexure. For NSW2, flexural cracks appeared at 126 kN and -94 kN. Although concrete spalling occurred at the wall tips which was not observed in the experiment during the first cycle of R= ±0.50%, crack appeared at the central part similar to that of experiment. Concrete crushed at the central part

during R= ±0.75% and failed due to shear-compression failure at R=1.00% similar to that of experiment. For NSW3, flexural cracks appeared at 119 kN and -87 kN. Unlike the experiment, concrete spalling occurred at the wall tip during R= ±0.25%. Crack appeared at the central part during R= ±0.50% and this is similar to the experiment. Compression at bottom and top parts due to a combination of flexure and shear led to the ultimate failure. This is different with the experiment, which failed due to sliding along the flexure-shear crack. For NSW4, flexure crack appeared during R= ±0.125% at the lower portion. Unlike the experiment, concrete crushed at the wall base during R= ±0.50%. NSW4 failed in compression controlled flexure at R= 2.00% that similar to the experiment.

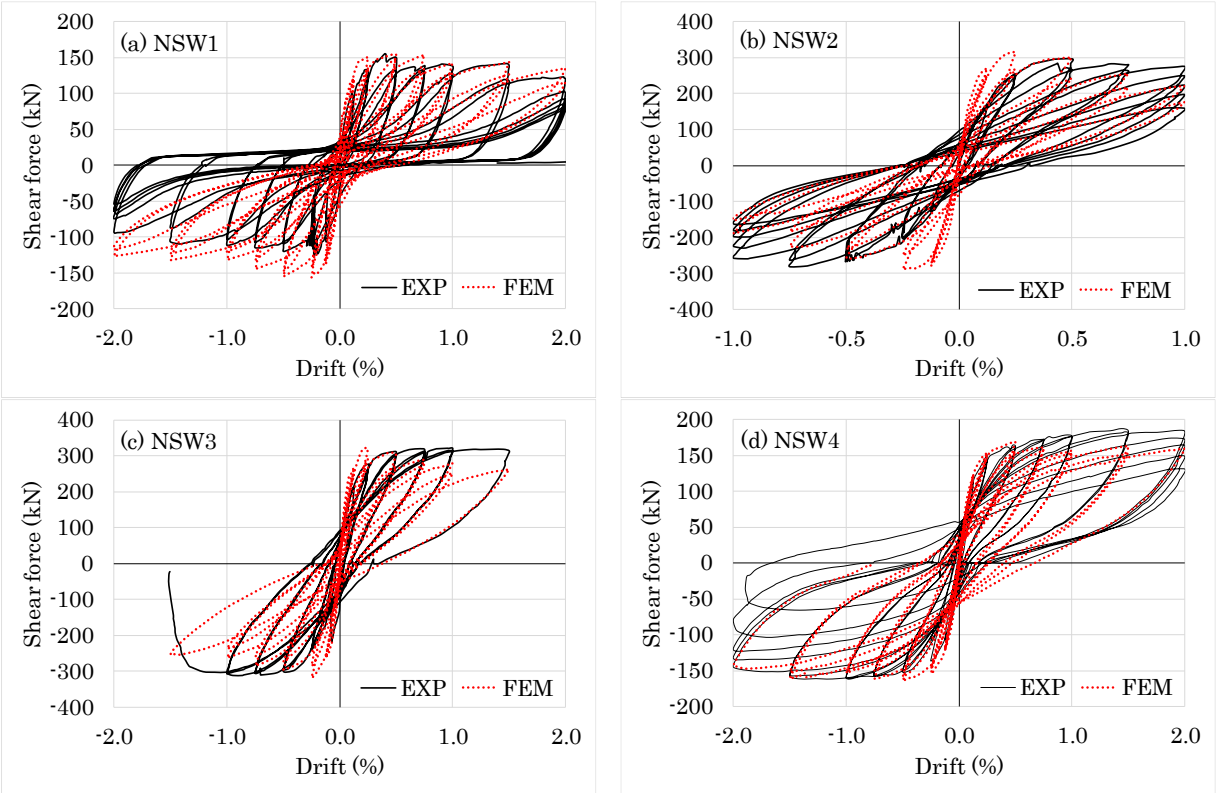

Figure 6-3 Shear force-drift relations of experimental test and FE analysis

Table 6-3 Capacities of specimens (Q in kN and R in %)

Spec.	Cal. based on Eqs. (2-1) - (2-3)					Experiment			FE Analysis				
	$_cQ_{mu}$	$_cQ_{su}$	$_cQ_{sc}$	z	Q_{CAL} *1	Q_{max} (R_{max}) +	Q_{max} (R_{max}) -	Q_{EXP} *2	Q_{FEM} (R_{FEM}) +	Q_{FEM} (R_{FEM}) -	Q_{FEM} *2	Q_{EXP}/Q_{CAL}	Q_{EXP}/Q_{FEM}
NSW1	127	282	136	2.22	127	155 (0.40)	-120 (-0.50)	155	154 (0.48)	-156 (-0.25)	156	1.22	0.99
NSW2	333	320	245	0.96	320	297 (0.50)	-282 (-0.75)	297	315 (0.23)	-289 (-0.25)	315	0.93	0.94
NSW3	333	352	245	1.06	333	321 (0.96)	-312 (-0.86)	321	322 (0.23)	-318 (-0.25)	322	0.96	1.00
NSW4	166	298	245	1.80	166	187 (1.44)	-162 (-1.37)	187	169 (0.50)	-164 (-0.50)	169	1.13	1.11

*1 $Q_{cal} = \min(_cQ_{mu}, \max(_cQ_{su}, _cQ_{sc}))$,

*2 Q_{EXP} *and* Q_{FEM} *are* taken as the maximum shear force in negative and positive directions.

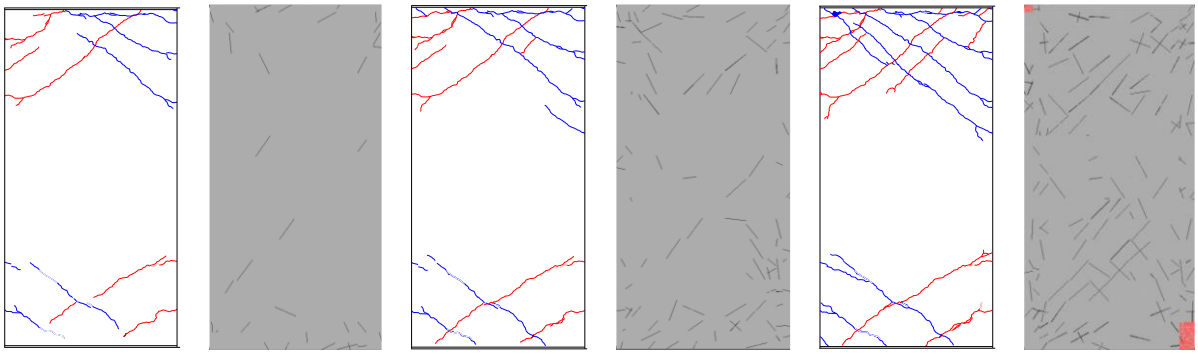

Experiment FEA Experiment FEA Experiment FEA

R= -0.25%(2) *R*= -0.50%(2) *R*= -1.00%(2)

(a) NSW1

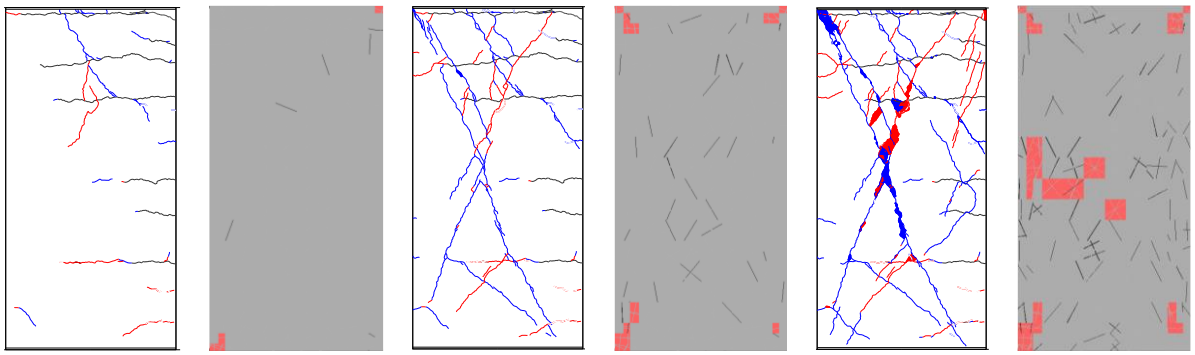

Experiment FEA Experiment FEA Experiment FEA

R= -0.25%(2) *R*= -0.50%(2) *R*= -1.00%(2)

(b) NSW2

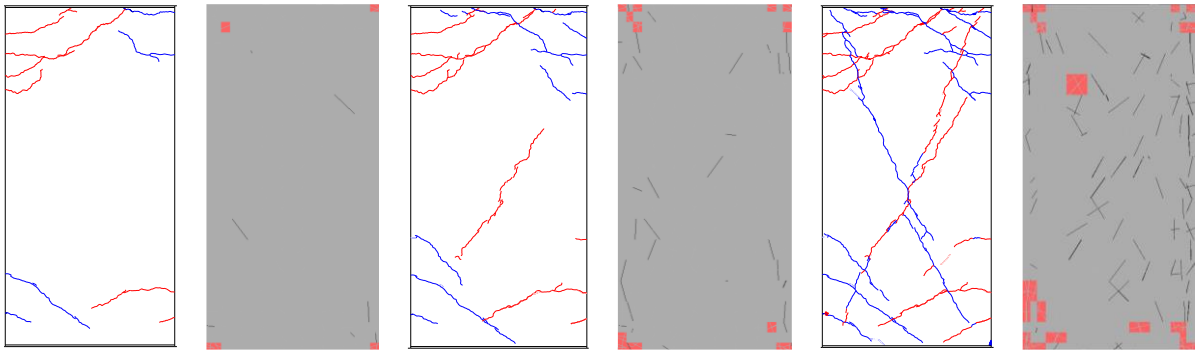

Experiment FEA Experiment FEA Experiment FEA

R= -0.25%(2) *R*= -0.50%(2) *R*= -1.00%(2)

(c) NSW3

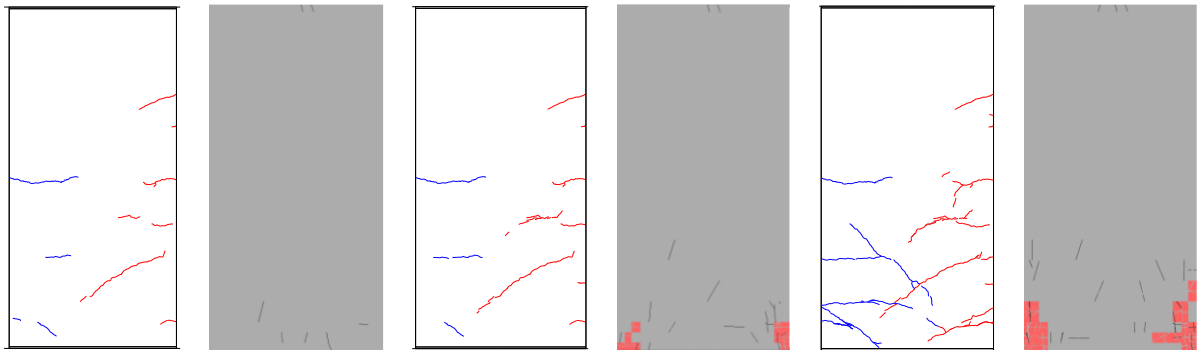

Experiment FEA Experiment FEA Experiment FEA

R= -0.25%(2) *R*= -0.50%(2) *R*= -1.00%(2)

(d) NSW4

Figure 6-4 Residual crack and compressive damage distribution of experiment and FE analysis

Drift (%)	Concrete crack propagation	Principal stress (MPa)	Maximum shear stress (MPa)
(a) 0.25	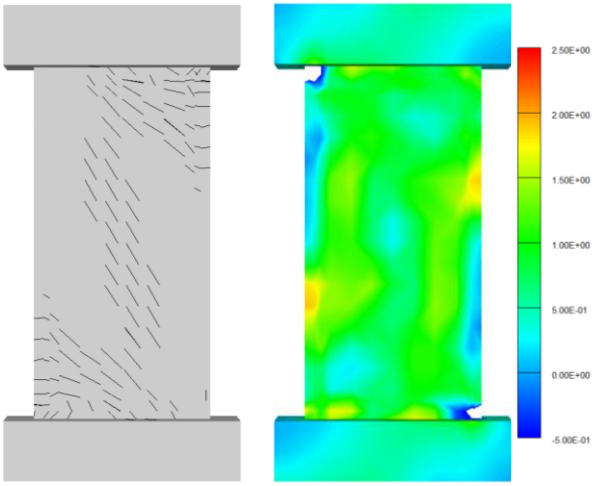		

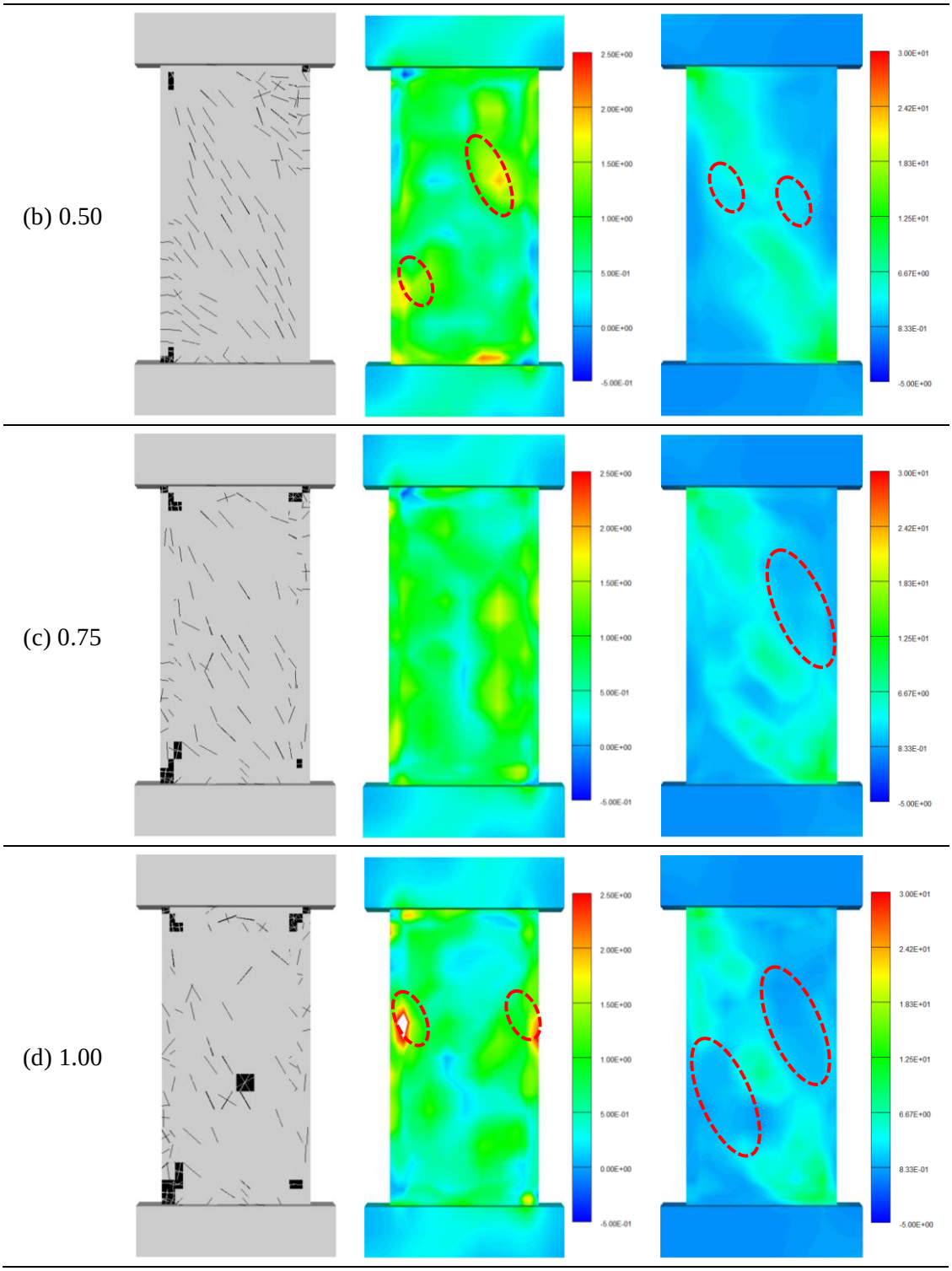

Figure 6-5 Crack propagation, principal stress, and maximum shear stress of NSW2

6.3 Parametric Study

In order to find the effects of axial force (N/f'_cA_g), horizontal reinforcement ratio (ρ_{wh}), and shear span to wall length ratio (a/d) on damage process and maximum lateral load capacity of lightly RC walls, a parametric study was conducted using finite element (FE) analysis. In the end, the process of predicting the failure modes and maximum lateral load capacity explained in Section 2.2.3 is validated. As shown in Table 6-4, a total of 210 cases were analyzed by combining seven axial load levels (N/f'_cA_g), six shear reinforcement ratios (ρ_{wh}), and five shear span to wall length ratio (a/d), while wall length (l_w), wall thickness (t_w), and vertical reinforcement ratio (ρ_v) were kept constant. Yuen and Kuang [83] compared the limit of axial load ratio for reinforced concrete walls from three codes as shown in Table 6-5. It is worthy to mention here that United States' concrete design code ACI 318-11 does not introduce similar limits on the axial compression ratios for RC columns and walls. Nevertheless, a standard for seismic rehabilitation of buildings ASCE/SEI 41-06 has stated that RC walls with axial loads greater than 35% of nominal axial load strength shall be considered not effective in resisting seismic forces. Therefore, in this study the limit of axial load ratio for parametric study was 0.3. As explained in Chapter 4, NSW4 had shear span ratio of 2.0 and failed in flexure. Since this study focuses on shear behavior of lightly RC walls, the limit shear span ratio of 1.50 was used in this parametric study. The range of N/f'_cA_g was 0.00 – 0.30, while the range of ρ_{wh} and a/l_w was 0.00% - 0.85% and 0.29 – 1.48, respectively. The thickness and length were same to those of specimens in Chapter 4 (120 mm and 1050 mm, respectively). In addition, the arrangement and vertical reinforcement ratio were identical to those of experiments. The constitutive models for concrete and steel followed models explained in Section 6.2.2 by employing the mechanical properties in Table 6-1 and Table 6-2.

Table 6-4 Constants and variables of parametric study

Parameters			
Constants	Variables		
l_w = 1050 mm t_w = 120 mm ρ_v = 0.63% Material properties in Table 2 and 3	Seven cases of axial load ratio (N/f'_cA_g) (0.00, 0.02, 0.05, 0.10, 0.15, 0.20, 0.30)	Six cases of shear reinforcement ratio (ρ_{wh}) (0.00%, 0.06%, 0.11%, 0.25%, 0.45%, 0.85%)	Five cases of shear span to wall length ratio (M/Vl_w) (0.29, 0.52, 0.76, 1.00, 1.48)

Table 6-5 Comparisons of codes provisions on axial load ratios for RC walls [83]

	CoP-SUC 2013	GB50011-2010*	EN 1998-1:2004
Original definition of ACRs	$\frac{N_{W,HK}}{0.45 f_{cu} A_c}$	$\frac{N_{W,C}}{f_c' A_c}$	$\frac{N_{ED,EC}}{f_{cd} A_c}$
Limit(s)	≤ 0.75	$\leq \begin{cases} 0.4 & \text{Grade I, Intensity 9} \\ 0.5 & \text{Grade I, Intensity 7 or 8} \\ 0.6 & \text{Grade II or III} \\ - & \text{Grade IV} \end{cases}$	$\leq \begin{cases} 0.35 & \text{DCH} \\ 0.4 & \text{DCM} \\ - & \text{DCL} \end{cases}$
Seismic/lateral forces effects	×	×	✓
Variable load reduction	×	✓	✓
Renormalised ACRs limits wrt f_c	$\frac{N_{W,HK}}{f_c A_c} \leq 0.42$	$\frac{N_{W,C}}{f_c A_c} \leq \begin{cases} 0.22 & \text{Grade I, Intensity 9} \\ 0.28 & \text{Grade I, Intensity 7 or 8} \\ 0.34 & \text{Grade II or III} \\ - & \text{Grade IV} \end{cases}$	$\frac{N_{ED,EC}}{f_c A_c} \leq \begin{cases} 0.23 & \text{DCH} \\ 0.26 & \text{DCM} \\ - & \text{DCL} \end{cases}$

* Limits for grades I, II and III short pier RC shear walls ($4 < H/B \leq 8$) are 0.45, 0.50 and 0.55 respectively.

ACRs: axial compression ratio; fcu: the characteristic tube strength of concrete under uniaxial compression at 28 days with safety factor of 1.5; f'_c: the design axial compressive strength of concrete under uniaxial compression at 28 days, which is equal to the characteristic axial strength of concrete f'_{ck} (is determined by 150 x 150 x 300 mm prism compression test) divided by the safety factor 1.4; f_{cd}: the design (factored with safety factor 1.5) cylinder strength of concrete under uniaxial compression at 28 days; f_c: compressive strength of concrete cylinder; Grade I: structure have high drift ductility; Grade II and III: structures have moderate to high drift ductility; Grade IV: structures have relatively low drift ductility; DCH, DCM, and DCL: ductility class high, moderate, and low, respectively.

6.3.1 Damage process

Figure 6-6 shows the crack propagation of cases for different level of axial force with ρ_{wh}= 0.25% and *a/d*= 1.00. For cases without or with low axial force ratio [Figure 6-6(a) and (b)], flexural cracks were dominant up to *R*= 0.25%. As increasing the lateral drift, cracks appeared at the middle and the flexural cracks near the base became wider similar to NSW1. Concrete crushing occurred at the wall tips at *R*= 1.00% and *R*= 0.50% for N/f'_cA_g= 0.00 and 0.05, respectively. For N/f'_cA_g= 0.15 [Figure 6-6(d)], cracks appeared at the middle height for *R*= 0.25% and those cracks became larger as the lateral load increased. The wall failed at *R*= 1.25% due to concrete crushing. For high axial force ratio [Figure 6-6(e) and (f)], diagonal cracks appeared during *R*= 0.25% and followed by concrete crushing at *R*= 0.50%. Both cases failed due to diagonal compression crushing of concrete before *R*= 1.00%. It is concluded that the axial force ratio significantly affected the damage process and the lateral drift capacity. A case with high axial load ratio tended to fail in brittle manner and resulted in lower lateral drift capacity.

N/f'_cA_g	R= 0.25%	R= 0.50%	R= 1.00%
(a) 0.00		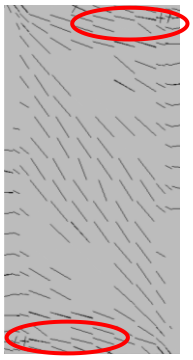	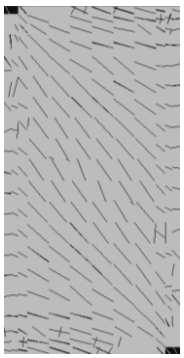
(b) 0.05	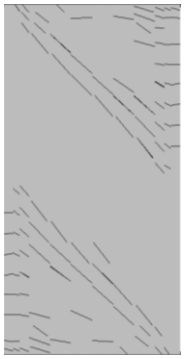	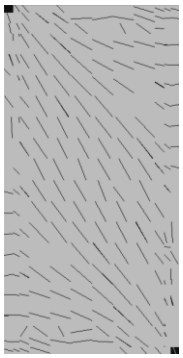	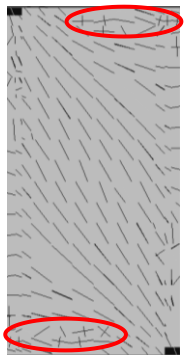
(c) 0.10	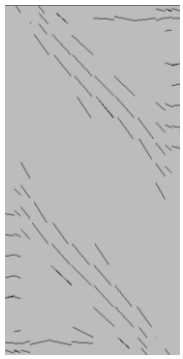	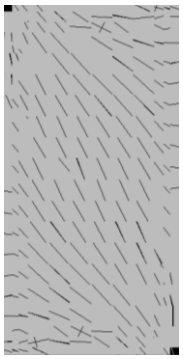	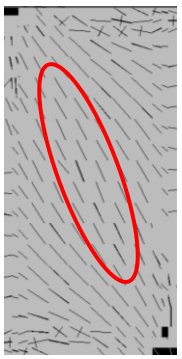
(d) 0.15		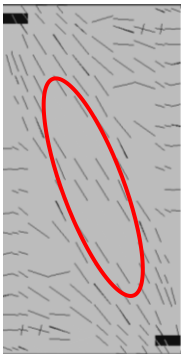	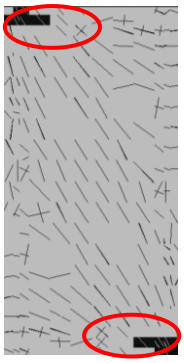

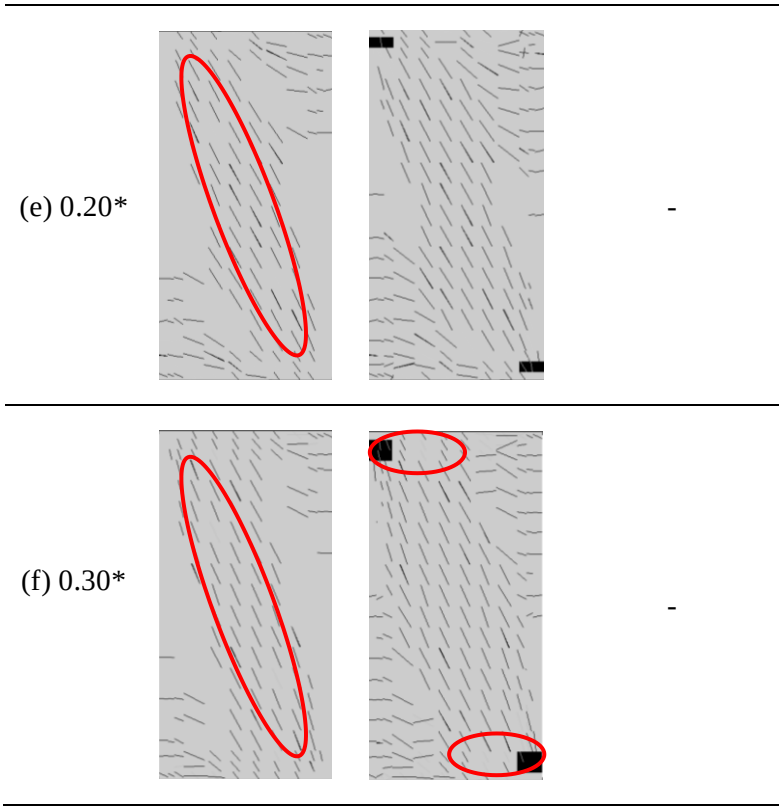

Figure 6-6 Crack propagation for different axial force level. All cases had ρ_{wh}= 0.25% and *a/d*= 1.00. Mark * in (e) and (f) indicates that specimen failed before reaching *R*= 1.00%

Figure 6-7 shows crack propagation for different amount of horizontal reinforcement with N/f'_cA_g= 0.15 and M/Vl_w= 1.00. For low amount of horizontal reinforcement [Figure 6-7(a), (b), and (c)], diagonal cracks occurred at *R*= 0.25% and those cracks became larger as the drift increased. The diagonal cracks were more intense for lesser horizontal reinforcement ratio. Concrete crushing occurred at the wall tips at *R*= 0.50%. All cases failed due to diagonal tension crushing of concrete. For ρ_{wh}= 0.25%, 0.45%, and 0.85% [Figure 6-7(d), (e), and (f)], flexural cracks were dominant up to *R*= 0.25%. As the drift increased, cracks spread along the height of wall panels and concrete crushed at the wall tips. The case with ρ_{wh}= 0.25% failed due to compression at the mid-height and wall tips. Other cases failed due to concrete crushing at wall tips in a ductile manner. It is concluded that the amount of horizontal reinforcement ratio affected the damage process and the lateral drift capacity. A case with low amount of horizontal reinforcement tended to fail in diagonal tension crushing of concrete and lead to lower drift capacity.

ρ_{wh}	R= 0.25%	R= 0.50%	R= 1.00%
(a) 0.00%	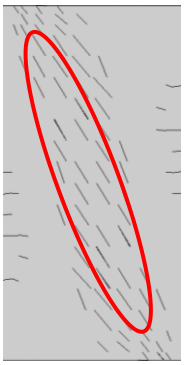		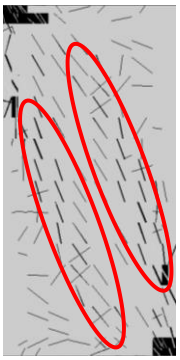
(b) 0.06%	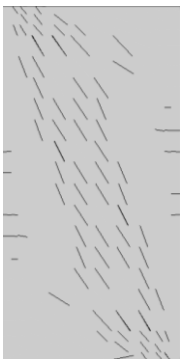	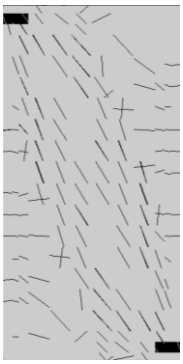	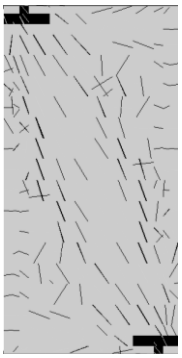
(c) 0.11%		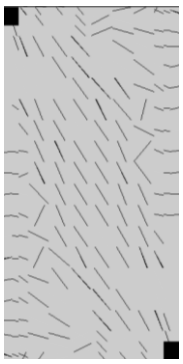	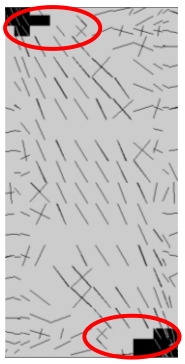
(d) 0.25%	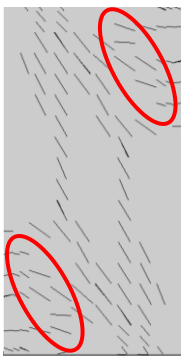	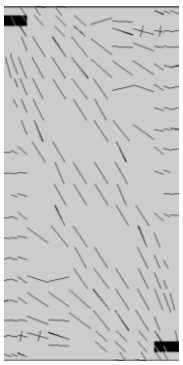	

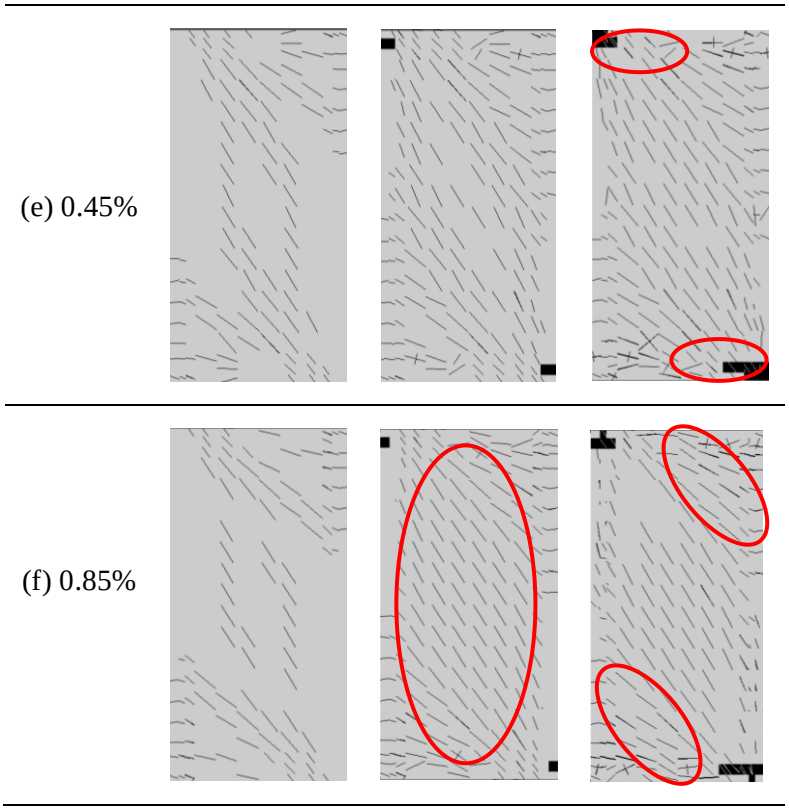

Figure 6-7 Crack propagation for different amount of horizontal reinforcement ratio. All cases had N/f'_cA_g= 0.15 and a/d= 1.00

Figure 6-8 shows the crack propagation for different shear span to wall length ratio with N/f'_cA_g= 0.15 and ρ_{wh}= 0.25%. For M/Vl_w= 0.29 [Figure 6-8(a)], diagonal cracks appeared during R= 0.25%. As increasing the drift, those diagonal cracks became larger. However, no concrete crushing occurred up to R= 1.00% since the wall was very short and axial load ratio of N/f'_cA_g= 0.15 was relatively high. The wall failed due to diagonal tension crushing of concrete. For M/Vl_w= 0.52 to 1.00 [Figure 6-8(b), (c), and (d)], flexural and diagonal cracks appeared at R= 0.25%. Concrete crushing occurred at the wall tips during R= 0.50% and the diagonal cracks became larger. As increasing the drift, concrete crushing became severe and walls failed due to diagonal compression crushing of concrete. For M/Vl_w = 1.48 [Figure 6-8(e)], flexural cracks were dominant up to R= 0.50%. As the drift increased, the flexural cracks became larger and concrete crushing occurred at the wall tips. The wall failed due to a compression-controlled flexure mode which was similar to the failure mode of NSW4. It is concluded that the shear span to wall length ratio affected the propagation of the cracks. Higher shear span to wall length ratio ($M/Vl_w > 1.0$) lead to flexure dominant deformation, while low shear span to wall length ratio ($M/Vl_w \leq 1.0$) resulted in shear dominant deformation with multiple diagonal cracks.

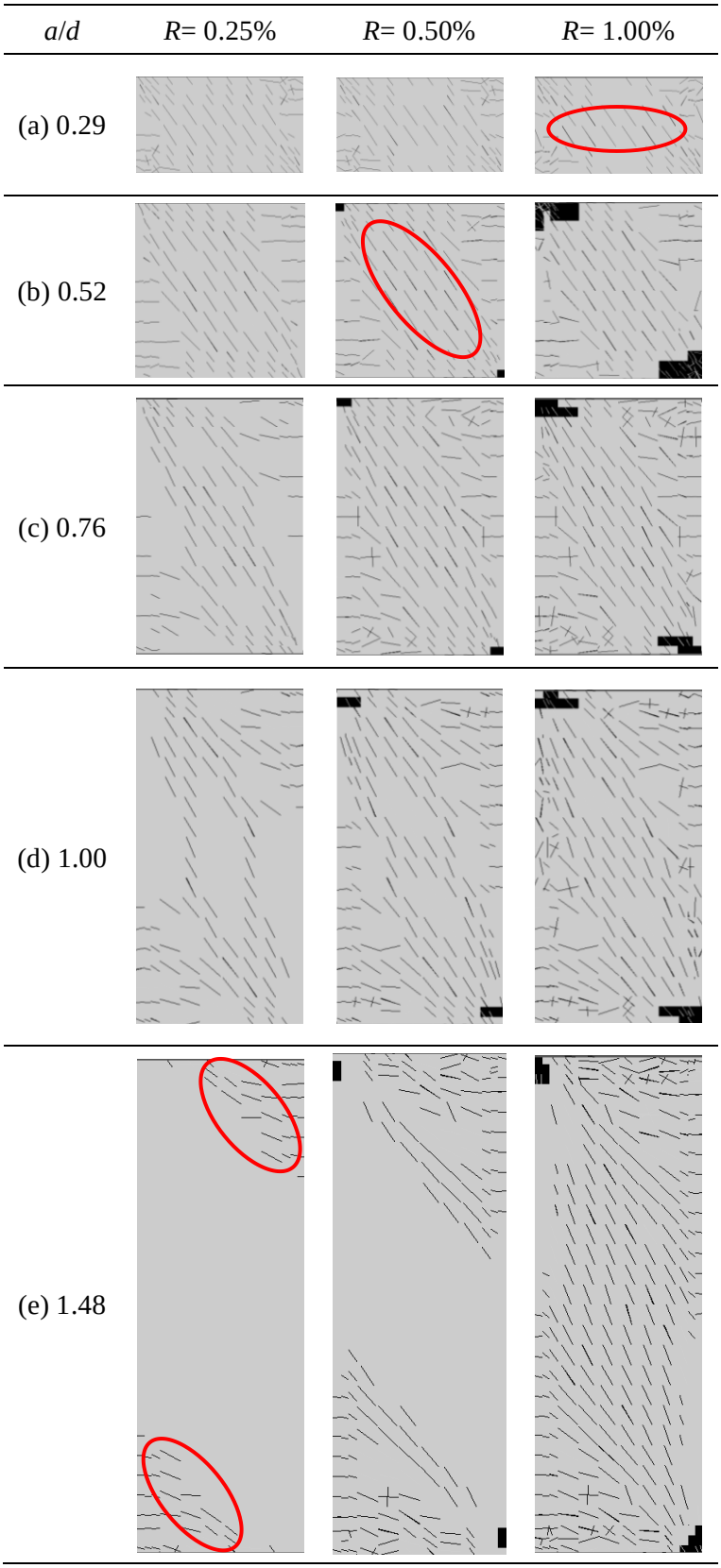

Figure 6-8 Crack propagation of cases for different shear span to wall length ratio. All cases had N/f'_cA_g= 0.15 and ρ_{wh}= 0.25%

6.3.2 Maximum lateral load capacity and failure mode

Figure 6-9 shows Q_{FEM} and ρ_{wh} relations for different N/f'_cA_g and a/d. Q_{FEM} is the maximum lateral load capacity from finite element analysis. Two kinds of failure modes (shear and flexure) are separated by the red line. As increasing axial force and amount of horizontal reinforcement ratio, the maximum lateral load capacity increases. It was interesting that the effect of horizontal reinforcement ratio is not very significant compared to the effect of the axial force, especially for a case with larger shear span to wall length ratio ($M/Vl_w > 1.0$) as shown in Figure 6-9(e). The failure mode was determined based on the cracking and concrete crushing. The level of axial force and shear span to wall length ratio significantly affected the failure mode. Higher axial force and lower shear span to wall length ratio caused walls fail in shear. However, a case with high amount of horizontal reinforcement ratio ($\rho_{wh} \geq 0.25\%$) prevented shear failure and caused flexural failure as shown in Figure 6-9(c), (d), and (e).

The maximum lateral load capacities simulated with FE analysis (Q_{FEM}) are compared to the shear capacity ($_cQ_{su}$) in Eq. (2) as shown in Figure 6-10. Both quantities (Q_{FEM} and cQ_{su}) are normalized with the flexural capacity ($_cQ_{mu}$) in Eq. (1) so that the simulated failure modes can be also seen from the figure. If $_cQ_{su}/_cQ_{mu}$ is smaller than 1.0, the maximum lateral load capacity is controlled by shear mode. Otherwise, the maximum lateral load capacity is controlled by flexure mode. Most markers stay near or above the line, the procedure in Section 2.2.3 works fine although it is slightly conservative. Blue and red markers in Figure 6-10 indicate shear and flexural failure, respectively based on finite element analysis. The flexure and shear strength design equations in Section 2.2.3 were not very precise to simulate failure modes for 210 finite element analysis cases.

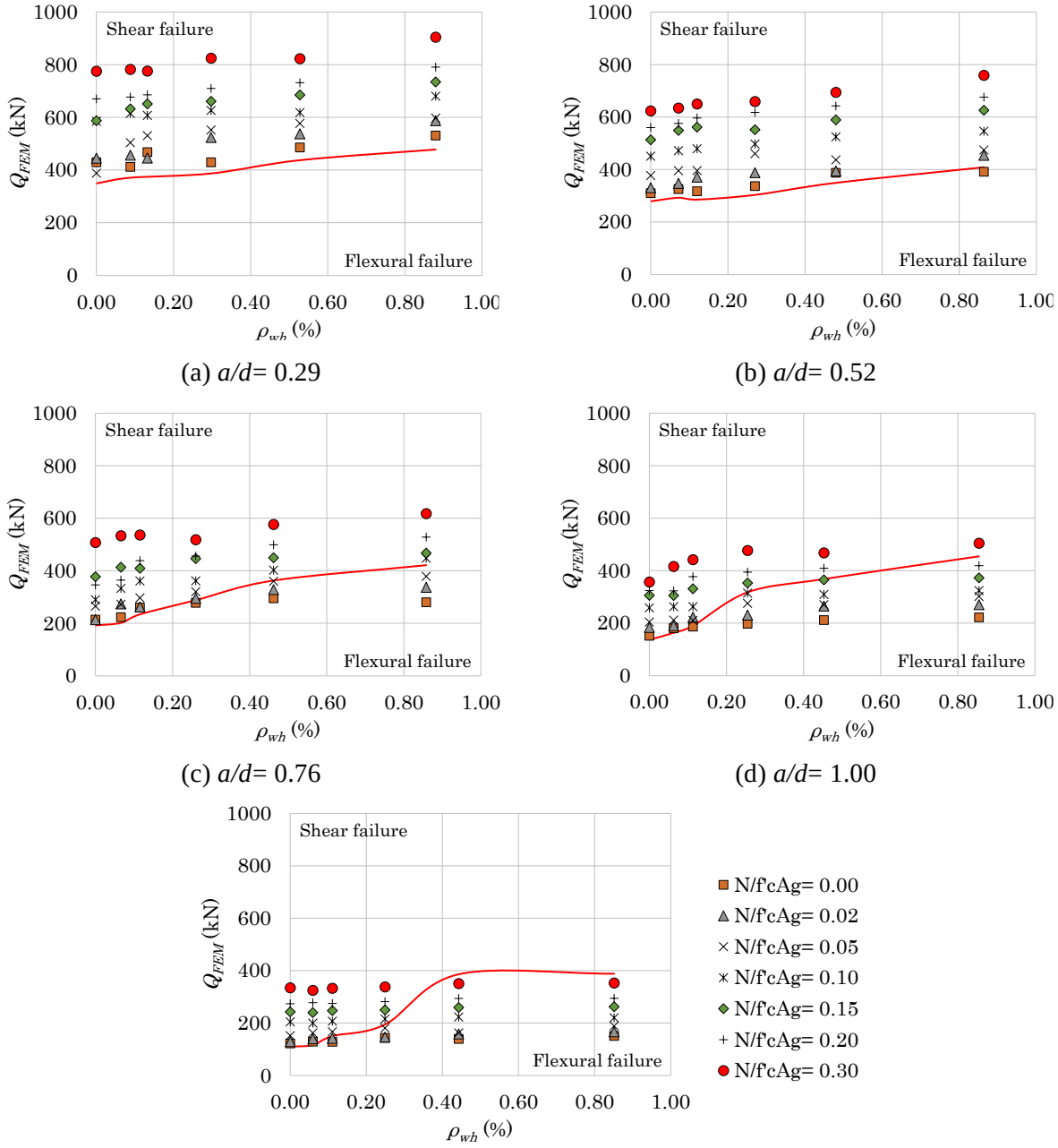

(a) a/d= 0.29

(b) a/d= 0.52

(c) a/d= 0.76

(d) a/d= 1.00

(e) a/d= 1.48

Figure 6-9 Q_{FEM} and ρ_{wh} relations for different N/f'_cA_g and a/d

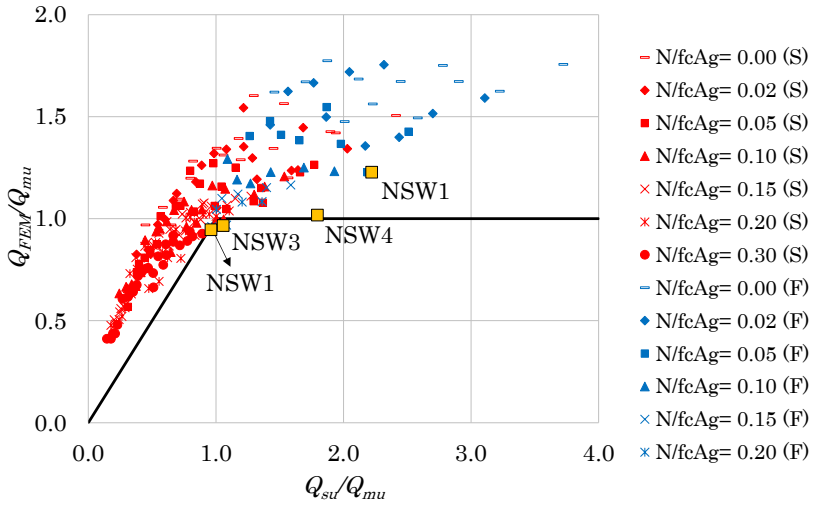

(a) Classification based on N/f'_cA_g

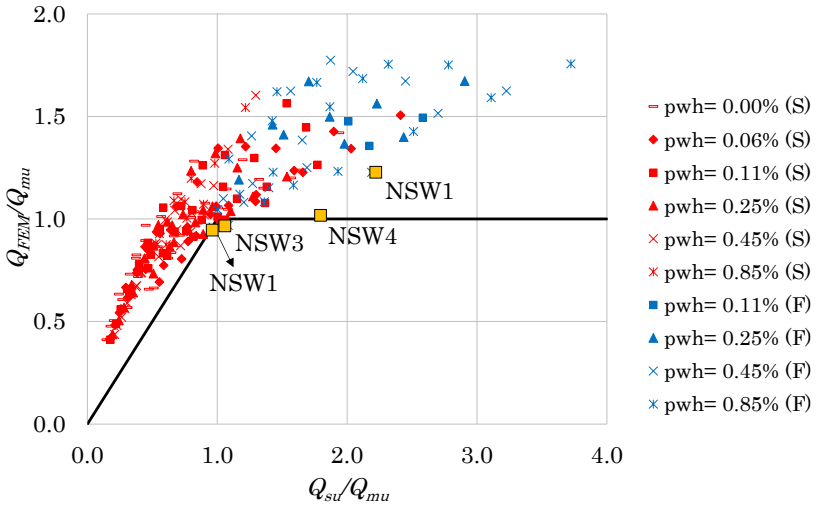

(b) Classification based on ρ_{wh}

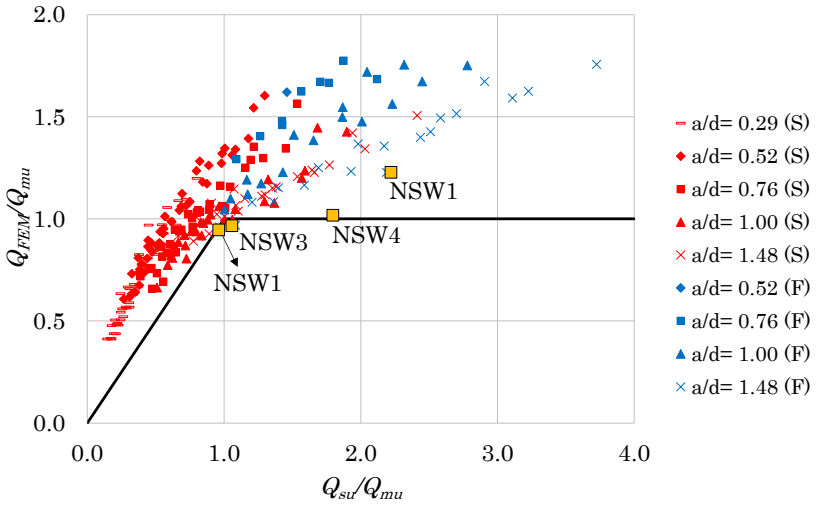

(c) Classification based on *a/d*

Figure 6-10 Comparison of lateral load capacities simulated by the procedure in Chapter 4 Section 4.2.2 and finite element analysis

6.4 Conclusions

A finite element analysis was conducted on four tested lightly RC walls with single layer of reinforcement and with no confinement in their end regions to simulate the hysteretic characteristics of lateral load – drift relations with damage process. In addition, a parametric study was conducted to provide insight into the effects of axial load, horizontal reinforcement ratio, and shear span to wall length ratio on damage process and maximum lateral load capacity of lightly RC walls. The findings of this study are summarized in the following paragraphs.

1) The finite element analysis model was confirmed by comparing with experimental results of four specimens in Chapter 2. The model is found to be able to reasonably capture the lateral load versus drift response of the specimens and predict most of the experimentally observed failure mechanisms of lightly RC walls except shear sliding. The damage process and the crack distribution also reasonably agreed with experimental observations.
2) From the parametric study of 210 cases, finite element analysis simulated different failure mode and maximum lateral load capacities. Similar to that of experimental test, axial load and shear span ratio had significant effect to lateral load capacity of lightly RC walls, while amount of horizontal reinforcement is less sensitive to lateral load capacity but significant effect to the drift capacity. Axial load ratio, shear span to wall length ratio, and amount of shear reinforcement affected to damage progress and failure mode. It was confirmed that lightly RC walls with high axial load and low shear span to wall length ratio tended to fail in a brittle manner. Increasing the amount of horizontal reinforcement improved the seismic behavior and prevented the opening of shear cracks.
3) The flexure and shear strength equations in Chapter 4 Section 4.2.2 simulated the lateral load capacity conservatively as they are intended. However, simulated failure mode based on equations were not very precise for 210 finite element analysis cases although were good for four tested specimens. It is required to revise the shear strength formula in Chapter 4 Section 4.2.2 which takes into account the degradation of concrete shear strength due to increasing the ductility.

7 SUMMARY AND CONCLUSIONS

7.1 Conclusions

In this study, a performance based backbone model was developed to predict the seismic behavior of lightly RC walls. The selected tri-linear model is associated with three limit state: diagonal cracking, peak shear strength, and ultimate deformation was proposed. The proposed shear strength model was formulated using an experimental database of rectangular walls and combined with parametric study using finite element analysis. In addition, two series of experimental on as-built and retrofitted lightly RC walls were carried out to investigate the seismic behavior of lightly RC walls. A quantitative seismic damage evaluation in terms of crack width, crack length, and concrete spalling area was carried out to investigate the correlation between seismic damage and lateral drift. The major conclusions of this research are summarized in this chapter.

1) A new shear strength model has been proposed by modifying revised UCSD shear model for RC walls. An experimental database of 39 rectangular walls is used in the formulation of the proposed shear model and to test the accuracy of the model. The available database was selected with the following criteria: (1) Rectangular wall, (2) the specimen failed in flexure-shear or shear, (3) the wall had a single curtain of reinforcement and additional boundary vertical reinforcing bars at section ends, and (4) there was no confinement in boundary region. Attempts have been made in the formulation of the proposed shear model to improve the calculation of the primary components contributing to the shear resistance of lightly RC walls. The focus of the proposed changes to the revised UCSD shear model for RC walls are on the contribution of the axial load and concrete shear resisting mechanisms. The recommended changes improve the concrete contribution to shear resistance by modifying the variable α and β, reduce the upper limit of displacement ductility, introduce parameter λ and ω to modify the calculated axial load contribution to shear resistance, which the factor λ accounts for the shear span ratio of wall, and factor ω is a modifier that accounts for increasing the depth of compression zone due to axial load. Based on the analysis, the proposed shear model results in a closer average ratio of experimental to predicted shear strength and improves the dispersion of the results from Krolicki et al.'s model. In addition, the proposed shear model is found to correctly predict shear failures and flexure-shear failure for all specimens of the collected database. Based on these results the proposed shear model is recommended for the calculation of the shear strength of lightly RC walls. It is envisioned that the proposed shear model can be used as a new tool for the assessment or design of lightly reinforced concrete walls in existing buildings or in the design of new structures. In addition, proposed shear model was suggested to use as peak strength for the backbone curve. The modification provided a good estimate to the wall database force-drift response.

2) The experimental test of four lightly RC walls with different level of axial load, amount of shear reinforcement, and shear span ratio showed that the maximum lateral load and drift capacities depended on the axial load ratio and shear span to wall length ratio. Experimental results showed that higher axial load ratio and lower shear span to wall length ratio resulted in higher lateral load capacity but smaller drift capacity. In addition, the study also showed that increasing the amount of horizontal reinforcement increased the lateral load capacity slightly but increased the drift capacity significantly. Axial load ratio, shear span to wall length ratio, and the amount of horizontal reinforcement affected to damage process and failure mode. Specimen with axial load tends to fail in a brittle manner. Lightly RC walls with large shear span to wall length ratio are less susceptible to brittle shear failure than walls with smaller shear span to wall length ratio. In addition, increasing the amount of horizontal reinforcement and providing 180-degree hook anchorage improved the seismic behavior and prevented the opening of shear cracks. Considering the total amount of damage (crack length and spalling area), the criteria of the 2004 AIJ Guidelines worked reasonably well to capture damage levels of lightly RC walls. However, limit of $2/3f'_c$ for concrete is too strict for serviceability limit state since it is still in the range of immature elastic state. The limit stress level of $0.8f'_c$ has been proposed and provided more realistic estimate for serviceability limit state of concrete. In addition, the ratio of concrete spalling area was also proposed as damage state criteria to determine limit state of lightly RC walls.
3) The experimental test of three lightly RC walls with seismic upgrading showed that all upgraded specimens experienced less damage compared with the prototype specimen (NSW2). For two specimens with additional walls, cracks appeared only in the upper and lower portions of the wall panel. In contrast, cracks spread over the wall height in specimen with improving reinforcement details. All upgraded specimens exhibited flexural failure. Adding RC and UFC panels improved the behavior of lightly RC wall and prevented crack formation at the central part of the wall panel. Increasing the amount of horizontal reinforcement and providing 180-degree hook anchorage decreased the crack width. The increased confinement of the boundary regions delayed the concrete crushing in compression and allowed the full utilization of the vertical reinforcement in tension due to the increased strength of the compressive zone. Upgrading walls with an additional panel can be applied on one side of the members, and this allows the continuous use of the building. All upgrading methods proved to be effective and improved the shear strength and ductility for lightly RC walls as compared to the prototype wall (NSW2).
4) The experimental test results were confirmed by the finite element analysis. The model is found to be able to reasonably capture the lateral load versus drift response of the specimens and predict most of the experimentally observed failure mechanisms of lightly RC walls except shear sliding. The damage process and the crack distribution also reasonably agreed with

experimental observations. From the parametric study of 210 cases, finite element analysis simulated different failure mode and maximum lateral load capacities. Similar to that of experimental test, axial load and shear span ratio had significant effect to lateral load capacity of lightly RC walls, while amount of horizontal reinforcement is less sensitive to lateral load capacity but significant effect to the drift capacity. Axial load ratio, shear span to wall length ratio, and amount of shear reinforcement affected to damage progress and failure mode. Lightly RC wall with high axial load and low shear span to wall length ratio tended to fail in a brittle manner. Increasing the amount of horizontal reinforcement improved the seismic behavior and prevented the opening of shear cracks. The flexure and shear strength equations in Chapter 4 Section 4.2.2 simulated the lateral load capacity conservatively as they are intended. However, simulated failure mode based on equations were not very precise for 210 finite element analysis cases although were good for four tested specimens. It is required to revise the shear strength formula in Chapter 4 Section 4.2.4 which takes into account the degradation of concrete shear strength due to increasing the ductility.

7.2 Suggestions for Future Research

The following are some suggestions for future research of lightly reinforced concrete walls:

1) To evaluate the contribution of lightly RC walls to the frame and the whole building system in terms of stiffness and lateral load.
2) To investigate the effects of strengthening schemes to the frame and whole building system, especially effects of additional lateral load capacity.

REFERENCES

[1] Federal Emergency Management Agency, “Evaluation of Earthquake Damaged Concrete and Masonry Wall Buildings: Basic Procedures Manual,” FEMA 306, 1998, Washington, D. C.

[2] National Institute for Land and Infrastructure Management (NILIM) and Building Research Institute (BRI), “Summary of the Field Survey and Research on the 2011 off the Pacific coast of Tohoku Earthquake (the Great East Japan Earthquake),” Technical Note NILIM, 647, BRI Research Paper, 150, 2011.

[3] National Institute for Land and Infrastructure Management (NILIM) and Building Research Institute (BRI), “Quick Report of the Field Survey on the Building Damage by the 2016 Kumamoto Earthquake,” Technical Note NILIM, 929, Building Research Data, 173, 2016.

[4] Federal Emergency Management Agency, “NEHRP Commentary on the Guidelines for the Seismic Rehabilitation of Buildings,” FEMA 274, 1997, Washington, D. C.

[5] Greifenhagen, C. and Lestuzzi, P., “Static Cyclic Tests on Lightly Reinforced Concrete Shear Walls”, Engineering Structures, 2005, pp. 1703-1712.

[6] Gabreyohaness, A. S., Clifton, G. C., Butterworth, J. W., “Experimental Investigation on the In-plane Behavior of Non-ductile RC Walls”, Proceedings of the 9th Pacific Conference on Earthquake Engineering, Auckland, New Zealand, April 14-16, 2011.

[7] Orakcal, K., Massone, L. M., Wallace, J. W., “Shear Strength of Lightly Reinforced Wall Piers and Spandrels”, ACI Structural Journal, 2009, No. 106-S43, pp. 455-465.

[8] Sugiyama, T., Uemura, M., Fukuyama, H., Nakano, K., Matsuzaki, Y., Experimental Study on the Performance of the RC Frame Infilled Cast-in-place Non-structural RC Walls Retrofitted by using Carbon Fiber Sheets”, The 12th World Conference on Earthquake Engineering, Auckland, New Zealand, Jan 30 – Feb 4, 2000.

[9] Yoon, R., Sanada, Y., Suzuki, S., Akahori, T., Kuramoto, H., “Structural Experiments of One-story One-bay RC Moment Resisting Frames with Non-structural Walls”, The 16th Japan-Taiwan-Korea Joint Seminar on Earthquake Engineering for Building structures, Seoul, Korea, Sep 19-20, 2014, pp. 249-256.

[10] Sanada, Y. and Ojio, Y., “Effects of Secondary Walls on Damage to a Concrete Building Attacked by the 2011 Tohoku, Japan Earthquake”, The 2nd European Conference on Earthquake Engineering and Seismology, Istanbul, Turkey, August 25-29, 2014.

[11] Krolicki, J., Maffei, J., Calvi, G. M., “Shear Strength of Reinforced Concrete Walls Subjected to Cyclic Loading,” Journal of Earthquake Engineering, 2011, 15:S1, pp. 30-71.

[12] American Society of Civil Engineers (ASCE), “Seismic Evaluation and Retrofit of Existing Building,” ASCE/SEI 41, 2013, Reston, VA.

[13] Wallace J. W., “Lightly Reinforced Wall Segments, in: New Information on the Seismic Performance of Existing Concrete Buildings Seminar Notes,” 2006, Earthquake Engineering Research Institute, Oakland, CA.

[14] Federal Emergency Management Agency, “Design for Earthquake: A Manual for Architects,” FEMA 454, 2006, Washington, D. C.

[15] Applied Technology Council, “Guidelines and Commentary for Seismic Rehabilitation of Building,” ATC-33,

1995, Redwood City, California.

[16] Structural Engineers Association of California, “Vision 2000: A Framework for Performance Based Design”, SEAOC, 1995, Sacramento, California.

[17] Barda F., Hanson J. M., and Corley W. G., “Shear Strength of Low-Rise Walls with Boundary Elements.”, ACI Special Publications, Reinforced Concrete in Seismic Zones, SP-53-8, 1977, pp.149-202. (Also, Research and Development Bulletin, No. RD043.01D, Portland Cement Association.)

[18] Aktan A. E., and Bertero V. V., “RC Structural Walls: Seismic Design for Shear.”, Journal of Structural Engineering, Vol. 111, No. 8, August 1985, pp. 1775-1791.

[19] Wood, S. L., “Minimum Tensile Reinforcement Requirements in Walls,” ACI Structural Journal, Vol. 86, No. 5, September-October 1989, pp. 582-591.

[20] Wood S. L., “Shear Strength of Low-Rise Reinforced Concrete Walls,” ACI Structural Journal, Vol. 87, No. 1, January-February 1990, pp. 99-107.

[21] Collins, M. and Mitchell. D., “A Rational Approach to Shear Design: The 1984 Canadian Code Provisions,” ACI Journal, 1986, Vol. 83, pp. 925-933.

[22] Aoyama, H., “Design Philosophy for Shear in Earthquake Resistance in Japan,” International Workshop on Concrete in Earthquake, University of Houston, Houston, Texas, 1991.

[23] ACI Committee 318, “Building Code Requirements for Structural Concrete (ACI 318M-14) and Commentary”, American Concrete Institute, Farmington Hills, MI, 2014.

[24] The Japan Building Disaster Prevention Association, “Standard for Seismic Evaluation of Existing Reinforced Concrete Buildings”, Tokyo, 2001.

[25] Priestley, M. J. N., Verma, R., Xiao, Y., “Seismic Shear Strength of Reinforced Concrete Column,” Journal of structural Engineering, ASCE, 1994, Vol. 120, No. 8, pp. 2320-2329.

[26] Kowalsky, M. J. and Priestley M. J. N., “Improved Analytical Model for Shear Strength of Circular Reinforced Concrete Columns in Seismic Regions,” ACI Structural Journal, 2000, Vol. 97, No. 3, pp. 388-396.

[27] Hidalgo, P. A., Ledezma, C. A., and Jordan, R. M., “Seismic Behavior of Squat Reinforced Concrete Shear Walls,” Earthquake Spectra, 2002, Vol. 18, No. 2, pp. 287-308.

[28] Beko, A., Rosko, P., Wenzel, H., Pegon, P., Markovic, D., Molina, F. J., “RC Shear Walls: Full-scale Cyclic Test, Insights and Derived Analytical Model”, 2015, Vol. 102, pp. 120-131.

[29] Lopes, M. S., “Experimental Shear-dominated Response of RC Walls: Part I Objectives, Methodology and Results”, Engineering Structures, 2001, 23(3), pp. 229-239.

[30] Architectural Institute of Japan, “Draft of Guidelines for Performance Evaluation of Earthquake Resistant Reinforced Concrete Buildings”, AIJ, 2004.

[31] Alcocer, S. M., Ruiz, J., Pineda, J. A., Zepeda, J. A., “Retrofitting of Confined Masonry Walls with Welded Wire Mesh”, The 11th World Conference on Earthquake Engineering, Acapulco, Mexico, 1996, Paper No.1471.

[32] Penazzi, D., Valluzzi, M.R., Saisi, A., Binda, L., Modena, C., “Repair and Strengthening of Historic Masonry Buildings in Seismic Areas”, International Millennium Congress: More than Two Thousand Years in the History of Architecture Safeguarding the Structure of our Architectural Heritage, Bethlehem, Palestine, 2001.

[33] ElGawady, M., Lestuzzi, P., Badoux, M., “A Review of Conventional Seismic Retrofitting Techniques for URM”, The 13th International Brick and Block Masonry Conference, Amsterdam, Netherlands, 2004.

[34] Yardim, Y. and Lalaj, O., “Shear Strengthening of Unreinforced Masonry Wall with Different Fiber Reinforced Mortar Jacketing”, Construction and Building Materials, 2016, Vol. 2, pp. 149-154.

[35] Marini, A. and Meda, A., “Retrofitting of R/C Shear Walls by means of High Performance Jackets”, Engineering Structures, 2009, No. 31, pp. 3059-3064.

[36] Altin, S., Kopraman, Y., Baran, M., “Strengthening of RC Walls using Externally Bonding of Steel Strips”, Engineering Structures, 2013, No. 49, pp. 686-695.

[37] Liao, W. I., Effendy, E., Song, G., Mo, Y. L., Hsu, T. T. C., Loh, C. H., “Effect of SMA Bars on Cyclic Behavior of Low-rise Shear Walls”, Smart Structures and Materials: Sensors and Smart Structures Technologies for Civil, Mechanical, and Aerospace Systems, 2006, Proceedings of SPIE, 6174: 1-8, San Diego, CA, USA.

[38] Khalil, A. and Ghobarah, A., “Behavior of Rehabilitated Structural Walls”, Journal of Earthquake Engineering, 2005, Vol. 9, No. 3, pp. 371-391.

[39] El-Sokkary, H. and Galal, K., “Cyclic Test on FRP-Retrofitted RC Shear Wall Panels”, The 15th World Conference on Earthquake Engineering, Lisbon, Portugal, September 24-28, 2012.

[40] Altin, S., Anil, O., Kopraman, Y., Kara, M. E., “Hysteretic Behavior of RC Shear Walls Strengthened with CFRP Strips”, Composites: Part B, 2013, No. 44, pp. 321-329.

[41] Lau, D. T. and Cruz-Noguez, C. A., “Developments on Seismic Retrofit of RC Shear Walls with FRP”, The 5th International Conference on Advances in Experimental Structural Engineering, Taipei, Taiwan, November 8-9, 2013.

[42] Galal, K. and El-Sokkary, H., “Recent Advancements in Retrofit of RC Walls”, The 14th World Conference on Earthquake Engineering, Beijing, China, October 12-17, 2008.

[43] Yamaguchi, H. and Nomura, S., "Analysis of RC Walls by Plastic-Fracturing Theory," Structural Design, Analysis and Testing, Proceedings of the Sessions Related to Design, Analysis and Testing at Structures Congress' 89, ASCE, May 1989, pp. 204-213.

[44] Bazant, Z. P. and Kim, S., "Plastic-Fracturing Theory of Concrete," Journal of the Engineering Mechanics Division, ASCE, Vol. 105, No. EM3, June 1979, pp. 407-478.

[45] Ueda, M. and Kawai, T., "Discrete Limit Analysis of RC Shear Walls," Finite Element of Reinforced Concrete Structures, ASCE, May 1985, pp. 277-287.

[46] Sotomura, K. and Murazumi, Y., "Nonlinear Analysis of Shear Walls with Numerous Small Openings," Finite Element of Reinforced Concrete Structures, ASCE, May 1985, pp. 300-307.

[47] Inoue, N., Koshika, N., Suzuki, N., "Analysis of Shear Wall Based on Collins Panel Test," Finite Element of Reinforced Concrete Structures, ASCE, May 1985, pp. 288-299.

[48] Vecchio, F. J. and Collins, M. P., "The Response of Reinforced Concrete to In-plane Shear and Normal Stresses," Publication No. 82-03, Department of Civil Engineering, University of Toronto, March 1982.

[49] Federal Emergency Management Agency, “Next-generation Performance-based Seismic Design Guidelines,” FEMA 445, 2006, Washington, D. C.

[50] Tall Buildings Initiative, “Guidelines for Performance-based Seismic Design of Tall Buildings,” Pacific Earthquake Engineering Research Center, 2010, Berkeley, California.

[51] Kono, S., Arai, M. Watanabe, H., Taleb, R., Yuniarsyah, E., Obara, T., “Seismic Performance and Its Assessment of RC Structural Walls,” Structural Engineering Frontier Conference (SEFC), Tokyo Institute of Technology, Yokohama, Japan, March 18-19, 2015.

[52] Aaleti, S., Dai, H., Sritharan, S., “Ductile Design of Slender Reinforced Concrete Structural Walls,” Proceedings of the 10th National Conference in Earthquake Engineering, Earthquake Engineering Research Institute, Anchorage, AK, July 21-25, 2014.

[53] Kono, S., Tani, M., Mukai, T., Fukuyama, H., Taleb, R., Sakashita, M., “Seismic Behavior of Reinforced Concrete Walls for a Performance Based Design.” The 2nd European Conference on Earthquake Engineering and Seismology, Istanbul, Turkey, Aug 25-29, 2014, ID #1471.

[54] Beyer, K., Dazio, A., Priestley, M. J. N., “Shear Deformations of Slender Reinforced Concrete Walls under Seismic Loading,” ACI Structural Journal, 2011, Vol. 108, No. 2, pp. 167-177.

[55] Kent, D. C., and Park, R., "Flexural Members with Confined Concrete," Journal of the Structural Division, Proc. of the American Society of Civil Engineers, 1971, Vol.97, Issue 7, pp. 1969-1990.

[56] Priestley, M. J. N., Calvi, G. M., Kowalsky, M. J., “Displacement Based Seismic Design of Structures,” IUSS Press, 2007, Pavia, Italy.

[57] Priestley, M. J. N. and Kowalsky M. J., “Aspects of Drift and Ductility Capacity of Rectangular Cantilever Structural Walls,” Bulletin of the New Zealand National Society for Earthquake Engineering, 1998, 31(2), pp. 73-85.

[58] Pujol, S. and Fick, D., “The Test of a Full-scale Three-story RC Structure with Masonry Infill Walls”, Engineering Structures, 2010, 32(10), pp. 3112-3121.

[59] Basha, S. H. and Kaushik, H. B., “Behavior and Failure Mechanisms of Masonry-infilled RC Frames (in Low-rise Buildings) Subject to Lateral Loading”, Engineering Structures, 2016, Vol. 111, pp. 233-245.

[60] Architectural Institute of Japan, “Design Guidelines for Earthquake Resistant Reinforced Concrete Buildings Based on Inelastic Displacement Concept”, AIJ, 1999. (In Japanese)

[61] National Institute for Land and Infrastructure Management (NILIM) and Building Research Institute (BRI), “Report on Field Surveys and Subsequent Investigations of Building Damage Following the 2011 Pacific Coast of Tohoku Earthquake”, Technical Note NILIM, 674, Building Research Data, 136, 2012. (In Japanese)

[62] Ojio, Y., Oo, T., Sanada, Y., “FEM Analyses of Non-structural Walls Constructed Monolithically with RC Moment Resisting Frames”, Summaries of Technical Papers of Annual Meeting, AIJ, 2013, D-2, 33-34. (In Japanese)

[63] Mizutani, H., Ichinose, T., Oishi, T., Kato, M., “Effect of Bars End Details on Shear Strength of RC Wall”, Proceedings of the Japan Concrete Institute, 17(2), 1995, pp. 523-528. (in Japanese)

[64] Japanese Standards Association, “JIS G 3112: Steel Bars for Concrete Reinforcement”, Japanese Industrial Standard, 2004.

[65] National Institute for Land and Infrastructure Management, “Commentary of Structural Technique Standard for

Buildings", Tokyo, 2015.

[66] Mohamed, N., Farghaly, A. S., Benmokrane, B., Neale, K. W., "Flexure and Shear Deformation of GFRP Reinforced Shear Walls", Journal of Composites for Construction, ASCE, 2013, Vol. 18(2): 04013044.

[67] Hiraishi, H., "Evaluation of Shear and Flexural Deformations of Flexural Type Shear Wall", Bulletin of the New Zealand National Society for Earthquake Engineering, 1984, Vol. 17(2), pp. 135-144.

[68] Massone, L. M. and Wallace, J. W., "Load Deformation Responses of Slender Reinforced Concrete Walls", ACI Structural Journal, 2004, Vol. 101(1), pp. 103-113.

[69] Federal Emergency Management Agency, "Prestandard and Commentary for the Seismic Rehabilitation of Buildings," FEMA 356, 2000, Washington, D. C.

[70] Architectural Institute of Japan, "Draft of Guidelines for Structural Design and Construction of Prestressed Concrete Building Based on Performance Evaluation Concept", AIJ, 2015. (In Japanese)

[71] Mukai, T., Fukuyama, H., Suwada, H., Shirai, K., Kinugasa, H., "Ultimate Strength of RC Column Retrofitted by Precast Wing Walls with Ultra High Strength Fiber Reinforced Concrete", Journal of Structural and Construction Engineering, AIJ, 2015, Vol. 80, No. 710, pp. 637-645. (In Japanese)

[72] Building Guidance Division, Housing Bureau, Ministry of Land, Infrastructure, Transport and Tourism (MLIT), et al., "Commentary of Japanese Building Code for Structural Safety", Tokyo, 2007. (In Japanese)

[73] Architectural Institute of Japan, "AIJ Standard for Structural Calculation of Reinforced Concrete Structures", AIJ, 2010. (In Japanese)

[74] Itochu Techno Solutions Corporation, "FINAL V.11 User's Manual", 2012. (In Japanese)

[75] Naganuma, K., "Stress-Strain Relationship for Concrete under Triaxial Compression", Journal of Structural and Construction Engineering, 1995, No. 474, pp. 163-170. (In Japanese)

[76] Nakamura, H. and Higai, T., "Compressive Fracture Energy and Fracture Zone Length of Concrete", Seminar on Post-peak Behavior of RC Structures Subjected to Seismic Load, 1999, JCI-C51E, Vol.2, pp.259-272. (In Japanese)

[77] Ottosen, N. S., "A Failure Criterion for Concrete", Journal Engineering Mechanics, ASCE, 1977, 103(EM4), pp. 527-535.

[78] Izumo, J., "Analysis Model for A Reinforced Concrete Panel Element Subjected to Reversed Cyclic In-plane Stress", Journal of Structural Mechanics and Earthquake Engineering, JSCE, 1989, No. 408, pp. 51-60. (In Japanese)

[79] Naganuma, K. and Yamaguchi, T., "Tension Stiffening Model under In-plane Shear Stress", Summaries of Technical Papers of Annual Meeting, AIJ, 1990, pp. 649-650. (In Japanese)

[80] Naganuma, K., Yonezawa, K., Kurimoto, O., Eto, H., "Simulation of Nonlinear Dynamic Response of Reinforced Concrete Scaled Model using Three-Dimensional Finite Element Method", The 13th World Conference on Earthquake Engineering, Vancouver, Canada, Aug 1-6, 2004, No. 586.

[81] Ciampi, V., Eligehausen, R., Bertero, V., Popov, E. P., "Analytical Model for Concrete Anchorages of Reinforcing Bars under Generalized Excitations", Report No. UCB/EERC-82/23, Univ. of California, Berkeley, Nov, 1982.

[82] Naganuma, K., “Nonlinear Analytical Model for Reinforced Concrete Panels under In-plane Stresses (Part 1: Study on Nonlinear Analytical Method for Concrete Wall Structures)”, Journal of Structural and Construction Engineering, 1991, No. 421, pp. 39-48. (In Japanese)

[83] Yuen, Y. P. and Kuang, J. S., “Axial Compression Effect on Ductility Design of RC Structural Walls,” the 2nd European Conference on Earthquake Engineering and Seismology, 2014, Istanbul, Turkey, August 25-29.